The Herpes Simplex Virus 1 Transcription Activator ICP4 Modulates Histone Dynamics

by

Rebecca Leigh Gibeault

A thesis submitted in partial fulfillment of the requirements for the degree of

Doctor of Philosophy

Department of Biochemistry

University of Alberta

Abstract

Herpes simplex virus 1 (HSV-1) is a nuclear-replicating, double-stranded (ds) DNA virus. HSV-1 genes are expressed in a coordinate manner. The tegument protein VP16 first activates expression of the five immediate-early (IE) genes. Two IE proteins, ICP4 and ICP0, then activate early (E) and late (L) gene expression. The mechanisms whereby VP16 activate IE gene expression are so well characterized that VP16 is used as a tool to study gene expression in general. In contrast, the mechanisms whereby ICP4 and ICP0 activate gene expression are not fully understood. ICP4 is the only essential HSV-1 transcription activator.

HSV-1 genomes are not chromatinized in the virion, but are chromatinized in the nucleus. The basic unit of chromatin is the nucleosome, composed of two each of the core histone dimers H2A-H2B and H3-H4 wrapped by 146 base pairs of dsDNA. Chromatin is dynamic, as histones disassemble from nucleosomes, diffuse through the free pool bound by chaperones, and reassemble nucleosomes at different sites. HSV-1 chromatin is more dynamic than cellular chromatin.

Cellular chromatin dynamics are altered by the incorporation of variant histones in place of canonical ones. Variant H3.3 is enriched in nucleosomes assembled with DNA of transcribed genes or telomeres, and nucleosomes containing H3.3 are more dynamic than those assembled with H3.1. Variants macroH2A and H2A.B are preferentially enriched in nucleosomes assembled with DNA of silenced or transcribed genes, respectively. MacroH2A assembles less dynamic nucleosomes than canonical H2A, whereas H2A.B assembles more dynamic ones.

Upon nuclear entry of HSV-1 genomes, the total amount of nuclear DNA increases and histone synthesis is inhibited. As the number of histone binding sites increases but the amount of histones does not, we would expect the histone free pools to decrease in HSV-1-infected cells. However, it increased. Nuclear entry of HSV-1 genomes is required to enhance histone free pools, but HSV-1 DNA replication is not. We proposed a **model** in which a cellular defense mechanism chromatinizes HSV-1 genomes to silence HSV-1 gene expression. To counteract silencing, HSV-1 evolved proteins that prevent or disrupt the stable chromatinization of their genomes. My **hypothesis** is that these proteins are HSV-1 transcription activators.

In this thesis, I show that HSV-1 VP16 and ICP0 mutants still enhanced histone dynamics, though less so than the wild type virus, whereas ICP4 mutants barely enhanced them. To test whether ICP4 enhanced histone dynamics directly, I evaluated histone dynamics in cells co-expressing fluorescently tagged histones and full length or truncated, transcriptionally inactive, ICP4. The dynamics of H2B and H4, which have no variants and thus represent the H2A-H2B and H3-H4 dimers, were enhanced in cells expressing detectable levels of full length, but not truncated, ICP4. The dynamics of H3.1 and H3.3, which assemble less or more dynamic nucleosomes, respectively, were both enhanced in ICP4-expressing cells. Whereas H3.1 had granular distribution in cells expressing undetectable levels of ICP4, consistent with the incorporation of H3.1 in chromatin, it was diffusely distributed in ICP4-expressing cells. H3.3 distribution was not affected by ICP4. The dynamics of H2A, macroH2A, H2A.X, or H2A.Z did not change in ICP4-expressing cells, but

those of H2A.B were enhanced. The distribution of H2A.B was altered in ICP4-expressing cells, with greater H2A.B enrichment at the nucleolus, where ICP4 itself localized. Histones in the nucleolus are more dynamic than those in the cellular chromatin. The increased dynamics of H2A.B in ICP4-expressing cells may thus be a result of the greater amount of H2A.B in the most dynamic population. The nucleolus is disassembled in HSV-1-infected cells. Whereas H2A, macroH2A, and H2A.X are mostly depleted from the replication compartments, H2A.B was less so. The dynamics of all H2A variants except for H2A.B increased in HSV-1-infected cells. In cells infected with an HSV-1 mutant encoding truncated ICP4, n12, the replication compartments do not form and the nucleoli are fragmented. H2A.B is displaced from the fragmented nucleoli in n12-infected cells, but its dynamics do not decrease. Functional ICP4 is thus not required to displace H2A.B from the nucleolus, but is required to decrease H2A.B dynamics.

In this thesis, I show that ICP4 is the major HSV-1 modulator of histone dynamics. I suggest a model in which ICP4 activates transcription by maintaining the HSV-1 genomes in a most dynamically chromatinized and transcriptionally competent state.

Preface

Chapter 3 of my thesis has been modified from a paper published as R.L. Gibeault, K.L. Conn, M.D. Bildersheim, and L.M.S. Schang, "*An Essential Viral Transcription Activator Modulates Chromatin Dynamics*," PLoS Pathogens, e1005842. The data from Figures 1-3 and 9 was obtained and analyzed by K.L. Conn. The data from Figure 10 was obtained and analyzed by M.D. Bildersheim. I was responsible for the data collection and analysis of all other figures. I wrote the manuscript, with contribution from K.L. Conn and M.D. Bildersheim and editing by L.M.Schang.

Appendix 1 of my thesis has been modified from a paper published as K. Tsai, L. Chan, R. Gibeault, K. Conn, J. Dheekollu, J. Domsic, R. Marmorstein, L.M. Schang, and P.M. Lieberman, "*Viral Reprogramming of the Daxx-Histone H3.3 Chaperone during EBV Early Infection*", Journal of Virology, volume 88, issue 24, pages 14350-63. I obtained and analyzed the data from Figure 4, as well as wrote the results section corresponding to the figure, with editing by L.M. Schang.

Table of Contents

List of Tables

List of Figures and Illustrations

Chapter 1:

Chapter 3:

Chapter 4:

Chapter 5:

Appendix 1:

List of Abbreviations

ASF1: anti-silencing function protein 1
ATM: ataxia telangiectasia mutated serine/threonine kinase
ATP: adenosine triphosphate
ATR: ataxia telangiectasia and Rad3-related protein
BAF: BRG1 associated factors
bp: base pair
BRG1: Brahma related gene 1
BRE: TFIIB recognition element
BRM: Brahma
CAF-1: chromatin-assembly factor 1
cAMP: cyclic adenosine monophosphate
CATD: CENP-A targeting domain
CENP-A: centromeric protein A
CHD: chromodomain
CHRAC: chromatin-accessibility complex
CPSF: cleavage and polyadenylation specificity factor
CTCF: CCCTC binding protein
CTD: carboxy-terminal domain
CTEA: chromatin transcription-enabling activity
CVSC: capsid vertex-specific component
DAXX: death domain associated protein 6
DNA: deoxyribonucleic acid
DNA-PK: DNA-dependent protein kinase
DPE: downstream promoter elements
ds: double-stranded
E: early
E1: ubiquitin-activating enzyme
E2: ubiquitin-conjugating enzyme
E3: ubiquitin-protein isopeptide ligase
EBV: Epstein-Barr Virus
FACT: facilitates chromatin transcription
FAD: flavin adenine dinucleotide
FRAP: fluorescence recovery after photobleaching
FRET: fluorescence resonance energy transfer
g: glycoprotein; ex. glycoprotein B, gB
GFP: green fluorescent protein
H: histone; ex. histone 1, H1
HAT: histone acetyltransferase
HCF-1: host cell factor 1
HCMV: human cytomegalovirus
HDAC(1-2): histone deacetylase (1-2)
HDMT: histone demethyltransferase
HHV: human herpesvirus
HIRA: histone regulator A

HJURP: holliday junction-recognizing protein
HMG: high mobility group
HMT: histone methyltransferase
HP1: heterochromatin protein 1
hpi: hours post infection
HSC: heat shock cognate
HSP: heat shock protein
HSV: herpes simplex virus
ICP: infected-cell polypeptide; ex. infected cell polypeptide 4, ICP4
IE: immediate-early
INM: inner nuclear membrane
INR: initiator
kbp: kilo base pairs
KCl: potassium chloride
KM110: ICP0 and VP16 truncation mutant
KSHV: Kaposi's sarcoma-associated virus
L: late
LAT: latency-associated transcript
LSD1: lysine-specific demethyltransferase
MCN: micrococcal nuclease
moi: multiplicity of infection
mRNA: messenger ribonucleic acid
n12: ICP4 truncation mutant
n212: ICP0 truncation mutant
NaCl: sodium chloride
NAP1: nucleosome assembly protein 1
NASP: nuclear autoantiogenic sperm protein
ND10: nuclear domain 10
NEC: nuclear egress complex
NGF: nerve growth factor
NHEJ: non-homologous end-joining pathway
OCT-1: octamer-binding protein
OriL: origin L
OriS: origin S
PBAF: polybromo associated factors
PCNA: proliferating cell nuclear antigen
PFU: plaque-forming unit
PHD: plant homeodomain
PIC: pre-initiation complex
PML: promyelocytic leukemia protein
Pol II: RNA polymerase II
PRMT: protein arginine N-methyltransferase
PTM: post-translational modifications
RFP: red fluorescent protein
RING: really interesting new gene
RL: repeat long

RNA: ribonucleic acid
RS: repeat short
RSC: remodels the structure of chromatin
SET: Su(var)3-9, enhancer of zeste and thithorax
SWI/SNF: SWItch/Sucrose Non Fermentable
TAF: TBP-associated factor
TBP: TATA-box binding protein
TF: transcription factor
TSA: trichostatin A
TSS: transcription start site
UL: unique long
US: unique short
VZV: Varicella zoster virus
VP: virion protein; ex. virion protein 16, VP16
wt: wild-type

Chapter 1: Literature Review

1.0 Herpesviridae

The herpesviridae are a family of nuclear-replicating, enveloped, double-stranded (ds) DNA viruses. There are 8 herpesviridae that infect humans, classified into three subfamilies based on replication cycle and host ranges, alpha, beta, and gamma herpesviridae. All herpesviridae establish latent infections. In contrast to lytic infections when all viral genes are expressed and viral DNA is replicated, viral gene expression is restricted and viral DNA is not replicated during latent infections. Latent infections persist for life, with periodic reactivation.

The alpha herpesviruses, which include herpes simplex virus 1 (HSV-1), HSV-2 and Varicella Zoster Virus (VZV), have the shortest replication cycle and the broadest host range. Alpha herpeviruses establish lytic and latent infections in epithelial cells and neurons of sensory ganglia, respectively. Beta herpesviruses, including cytomegalovirus (CMV), human herpesvirus 6 (HHV-6) and HHV-7, have a long replication cycle and a restricted host range. CMV establishes lytic and latent infections in cells of the salivary glands and immune system, respectively. HHV-6 and -7 establish lytic infections in T lymphocytes. The sites of HHV-6 and HHV-7 latency are not yet determined, but may be blood monocytes. Gamma herpesviruses, including Epstein-Barr virus (EBV) and Kaposi's sarcoma virus (KSHV), have a long replication cycle and a single host. EBV and KSHV appear to establish lytic infections in the oral epithelial cells or the B cells of tonsils, respectively. Both establish latency in lymphocytes.

1.0.1 HSV-1 Pathology

The most common signs of lytic HSV-1 infection are epithelial lesions. HSV-1 infection usually produces lesions on the lips, called herpes labialis, whereas HSV-2 infection usually produces lesions on the genital area, called herpes genitalis (1, 2). However, genital lesions caused by HSV-1 and mouth lesions caused by HSV-2 are becoming increasingly common (3). HSV-1 also produces lesions on the fingers, called herpes whitlow, or on the torso, called herpes gladiatorum, a common infection among wrestlers (4, 5). In most people with competent immune systems,

these lesions are often of little consequence. Though the lesions heal, HSV-1 remains dormant in sensory ganglia (6, 7). At any time, HSV-1 reactivates, produces new infectious virions that re-infect the epithelial cells, resulting in a recurrence of symptoms. The main cause of HSV-1 reactivation is stress, whether internal, such as anxiety, or external, such as trauma, UV light, or cold exposure (8, 9).

HSV-1 may also cause serious disease. HSV-1 infection of the eyes may lead to herpes stromal keratitis, which is the leading cause of infectious corneal blindness in the developed world (10). HSV-1 infection may also lead to encephalitis, which often results in brain damage or death (11–13). Neonatal HSV-1 exposure results in either disseminated (25% of cases), CNS (30% of cases), or skin, eye, and mouth disease (14). Disseminated or CNS disease may cause encephalitis, respiratory failure, or hepatic failure. Approximately 29 or 4% of neonates with disseminated or CNS disease, respectively, will die from the disease (14).

1.0.2 HSV-1 Epidemiology and Treatment

HSV-1 or -2 are transmitted through physical contact of the epithelial or mucosal cells of an uninfected patient with the infectious virions shed from an infected patient. HSV-1 or -2 infectious virions are most often shed in the absence of symptoms, meaning that transmission often goes unnoticed. Approximately 67% of the global population is infected with HSV-1 (15). Twenty-seven percent of the global population is infected before five years of age, and 79% of the global population is infected by 50 years of age (15). Infection rates are highest in Africa, and lowest in the Americas. However, infection rate in women living in the Americas is still 50%. Approximately 46 or 19% of Canadians tested positive for antibodies against HSV-1 or -2, respectively (16).

There is currently no cure or vaccine for HSV-1 or -2. The drugs acyclivoir, famciclivoir, or vacyclivoir, used to treat HSV-1 infection are nucleoside analogues that differ slightly in chemical structure. They are prodrugs that become only active drugs in HSV-1 infected cells, as they must be phosphorylated by HSV-1 thymidine kinase (17, 18). The HSV-1 DNA polymerase incorporates the phosphorylated

nucleoside analogue in replicating DNA strands, causing chain termination, and inhibiting HSV-1 replication. Mutations within the HSV-1 genome may confer resistance to nucleoside analogues (19–21).

1.1 Structure of HSV-1

All herpesviruses have a lipid bilayer envelope acquired from the cell during egress. Embedded in the HSV-1 envelope are thirteen glycoproteins, four of which (gH/gL, gB and gD) are essential for HSV-1 entry (22). The HSV-1 tegument contains approximately twenty-three proteins, which are classified as either inner or outer tegument proteins (22). The inner tegument proteins, such as UL36 and UL37, are most strongly associated with the capsid, whereas the outer ones, such as VP16, VP13/14, and VP22, are most strongly associated with the envelope (23). The outer tegument proteins are typically present in larger amounts (over 600 copies each of VP16, VP13/14, and VP22) than the inner tegument proteins (under 200 copies each of UL36, and UL37) (24).

The HSV-1 genome is held within a capsid, with a T=16 icosahedral lattice (25, 26). Pentamers of capsid protein VP5 arrange on eleven of the twelve vertices. The twelfth vertice is a dodecameric UL6 portal, which serves as the site of entry for HSV-1 DNA into the capsid. The linear, dsDNA HSV-1 genomes in the capsid interact with no histones (27). Instead, the negative charge of HSV-1 DNA is partially neutralized with spermine (28).

The HSV-1 genome consists of approximately 152 kilo base pairs (kbp) which encode approximately 84 proteins. The linear HSV-1 genome is divided into unique long (UL) and unique short (US) domains, of 108 kbp and 13 kbp, respectively. Short repeat (RS) domains of 6.6 kbp flank the US region, and long repeat (RL) domains of 9 kbp flank the UL region. Genes encoded within the RS and RL domains, including those for the transcription activators ICP0 and ICP4, are thus encoded twice within each genome. Homologous recombination between the repeat domains results in four HSV-1 genome isomers, which differ only in the orientation of UL and US relative to each other (Figure 1.1.). The four isomers, termed P

(prototype), IL (inverted long), IS (inverted short), and ILS (inverted long and short), are usually present in equimolar amounts (29).

1.2 Chromatin

1.2.1 Chromatin structure

Each human cell contains over 3 billion base pairs (bp) of dsDNA. The nuclear dsDNA is organized in chromatin. The basic unit of chromatin is the core nucleosome, composed of two each of the core histone dimers H2A-H2B and H3-H4 wrapped 1.65 times by 147 bp of dsDNA (30). Linker histone H1 further binds dsDNA at the exit and entry points of the core nucleosome. Chromatin is compacted to form chromosomes during mitosis.

Chromatin is classified as either euchromatin or heterochromatin based on whether it fully decondenses at the end of mitosis or not, respectively. Euchromatin is more accessible to nucleases, and DNA-binding proteins, than heterochromatin (31). The DNA in euchromatin is transcribed to higher levels than that in heterochromatin (31, 32). Approximately 94% of the human genome is euchromatin (33). Constitutive heterochromatin is constitutively condensed, whereas facultative heterochromatin decondenses at particular points, such as during differentiation or a certain points in the cell cycle.

1.2.2 Replication-dependent chromatin assembly

During the S (synthesis) phase of the cell cycle, DNA is replicated and canonical histones are synthesized (34). Newly synthesized histones are folded with the assistance of chaperones. Heat shock cognate 70 kDa protein (HSC70) and heat shock protein 90 (HSP90) assist in the folding of canonical H3.1 in the cytoplasm (35). NASP (nuclear autoantiogenic sperm protein) binds to a dimer of H3.1 and H4 and stabilizes it in a cytoplasmic reservoir ready for assembly (35, 36). ASF1 (anti-silencing factor 1) then binds to a dimer of H3.1-H4 (37), and the complex associates with importin-4 to translocate into the nucleus (38).

Chromatin assembly factor 1 (CAF-1) is a complex of three sub units; p60, p150, and RbAp48. ASF1 interacts with the p60 subunit, and transfers the H3.1-H4

dimer to CAF-1 (39). CAF-1 binds a second H3.1-H4 dimer to form a H3.1-H4 tetramer (40). The p150 subunit interacts with PCNA (proliferating cell nuclear antigen) at the DNA replication fork. (41). CAF-1 then deposits the H3-H4 tetramer on the DNA of the newly synthesized dsDNA (42). Nucleosome assembly protein 1 (NAP-1) binds to H2A-H2B dimers in the cytoplasm, and shuttles them into the nucleus by interacting with the importin protein Kap114p (43). NAP1 then deposits two H2A-H2B dimers onto the H3-H4 tetramer.

1.2.3 Replication-independent chromatin assembly

Nucleosomes are displaced during transcription, and nucleosomes are then reassembled behind the transcription complex via DNA-replication-independent mechanisms (44). Nucleosomes assembled with transcribed DNA are enriched in histone variant H3.3 instead of canonical H3.1 (45, 46). ASF1a-H3.3-H4 translocates into the nucleus. ASF1a, but not ASF1b, interacts with HIRA, which deposits an H3.3-H4 tetramer on DNA of transcribed genes (47, 48).

H2A encodes many variants, such as H2A.X and H2A.Z (described in 1.4.3 and 1.4.6, respectively), which differ in sequence and have specific roles. These H2A variants are exchanged with canonical H2A by different mechanisms. NAP1 binds to a dimer of H2A.Z-H2B in the cytoplasm and the complex translocate into the nucleus (49). H2A.Z-H2B is there transferred to CHZ1, and then to SWR1 for assembly (49, 50). H2A-H2B is replaced with H2A.Z-H2B by the SWR1 chromatin remodeling complex (51). NAP1 exchanges H2A.B-H2B with H2A-H2B (52), whereas FACT exchanges H2A.X-H2B with H2A-H2B (53). The mechanisms of H2A variant incorporation are still not entirely understood.

1.2.4 Chromatin remodeling

Chromatin remodeling occurs during transcription, replication, or DNA repair. There are four known classes of ATP-dependent chromatin remodelers, SWI/SNF, NuRD (or CHD), ISWI, and INO80. The SWI/SNF multi-subunit complex was the first ATP-dependent chromatin remodeler identified, in yeast (54). RSC (remodels the structure of chromatin) was later identified as a second member of the SWI/SNF

family of chromatin remodelers, also in yeast (55). In humans, these two complexes are BAF (BRG1 associated factors) and PBAF (polybromo associated factors), which contain BRG1 or BRM as the ATPase subunits, respectively. Though closely related, BRG1 and BRM have different roles (56, 57). In addition to the ATPase domain, BRG1 (also called SMARCA4) and BRM also have a HAS (post-SANT) and a bromo-domain. The HAS domain binds ARP, another subunit of the SWI/SNF complex, whereas the bromodomain binds to acetylated lysine residues on histone tails (58, 59). BRG1 and BRM bind with the greatest affinity to H3K14ac (60, 61). Histone acetylation enhances the efficiency of RSC promotion of the passage of Pol II through nucleosomes (62). SWI/SNF complexes disassemble nucleosomes (63), but also unwrap approximately 50 bp from around the nucleosomes and slide the nucleosomes down the DNA (64).

The NuRD complex is a multi-subunit complex, consisting of one of the ATPases CHD3 or CHD4, the histone deacetylases HDAC1 and/or HDAC2, and more than ten other proteins. Whereas SWI/SNF knockdown inhibits transcription, NuRD knockdown stimulates it (65). CHD4 contains two PHD fingers, two chromodomains and one ATPase domain. The PHD fingers of CHD4 interact with the N-terminal tail of H3 (66, 67). Methylation of H3K9 enhances the affinity of CHD4 for H3 (66). The chromodomains, which bind to DNA, are required for NuRD activity (68). The ATPase activity of CHD4 is stimulated by nucleosomes, but not by free DNA or histones (69). The NuRD complex slides nucleosomes at the gene promoters, from positions that permit to positions that impede transcription (70, 71).

Humans encode two ISWI ATPases, Snf2H and Snf2L, which are orthologues of yeast Isw1 and Isw2, respectively. In addition to an ATPase domain in the N-terminus, ISWI proteins contain HAND, SANT (Swi3 Ada2 N-CoR TFIIB), and SLIDE (SANT-like ISWI) domains at their C-termini. Both the N-terminus and C-terminus of ISWI proteins contribute to nucleosome binding in vitro (72). The N-terminus, which contains the ATPase domain, cannot remodel chromatin in the absence of the C-terminus, suggesting that nucleosome recognition by the C-terminus is required for activity (72). Snf2H and Snf2L form many different complexes, including CHRAC

and NURF, which contain different regulatory subunits and have different biological functions. Snf2H contributes to nucleosome positioning at CTCF elements (73).

The INO80 family of chromatin remodeling complexes is the most recently discovered. Whereas the yeast INO80 complex consists of eight subunits, the human INO80 consists of fourteen subunits (74). One, Ino80, contains a Snf2-like ATPase domain and a HSA domain. The INO80 complex slides nucleosomes along DNA (74).

1.2.5 Chromatin dynamics

Chromatin is dynamic. Nucleosomes are disassembled, reassembled, and remodeled. The only technique to directly evaluate histone dynamics in live cells is fluorescence recovery after photobleaching (FRAP) (75–79). For FRAP, histones are fused in frame with green fluorescent protein (GFP) or another bleachable fluorescent tag. The GFP-histones in a region of the fluorescent nucleus is irreversibly photobleached with a high intensity laser. Fluorescence within the bleached region is regained as fluorescent histones from outside of the bleached region dissociate from nucleosomes, diffuse into the bleached region, and reassemble nucleosomes, and the bleached histones dissociate from nucleosomes, diffuse outside of the bleached region, and reassemble nucleosomes.

The fluorescence in the bleached region at each time point is normalized to the total nuclear fluorescence and then to the normalized fluorescence in the same region immediately prior to photobleaching (T = 0 sec). The relative fluorescence is plotted against time, as the relative fluorescence recovery curve (Figure 1.2.). At the first time point after photobleaching, the relative fluorescence is at a minimum. This minimum relative fluorescence is a surrogate measure for the free pool of histones, as only histones not assembled in nucleosomes diffuse into and out of the bleached region during photobleaching or in the first second after photobleaching.

GFP consists of 238 amino acids, bigger than any core histone. Though GFP-histones are incorporated into chromatin, the fusion of GFP reduces the affinity of histones for DNA. GFP-histones are a tracer for endogenous ones. Histones with GFP fused to the N-terminus have greater affinity for DNA, much closer to the endogenous histones, than histones with GFP fused to the C-termimus (80, 81).

Core histones are less dynamic than linker histones. The fluorescence recovery of core histones is biphasic, resulting from two different populations of core histones (78, 82). The fast exchanging population is histones weakly assembled in chromatin, whereas the slow exchanging population is histones stably assembled in chromatin. H3 and H4, which are first deposited into the nucleosome, are less dynamic than H2B and H2A, which are deposited later (80). Consistently, H2B-H2A dimers can be exchanged without the removal of the H3-H4 tetramer (83, 84).

The dynamics of linker histones are lower than those of other nuclear proteins that interact with DNA such as the HMGN1 (non-histone chromosomal protein HMG-14) (76). Mutants of linker histones unable to bind DNA have dynamics similar to those of free GFP (76). The slow dynamics of linker histones are thus a result of their incorporation into chromatin. ATP is not required for linker histone exchange (75).

DNA methylation does not prevent linker histone binding (85, 86). The dynamics of linker histones are nonetheless decreased in cells deficient in DNA methylation (87). The numbers of linker histones bound to methylated or unmethylated DNA may be the same at any given point if the residency time of linker histones on methylated DNA is shorter, resulting in the observed faster dynamics. Chromatin dynamics are also altered by post-translational modifications (Section 1.3).

1.2.6 Nucleolar chromatin

Nucleoli are membrane-less nuclear organellas around the ribosomal DNA (rDNA) genes. The rDNA genes are clustered head-to-tail on five different chromosomes (in humans) (88). rDNA is transcribed by RNA polymerase I (Pol I) into the 47S ribosomal RNA (rRNA) precursor. The 47S rRNA is cleaved into the 28S, 18S, and 5.8S mature rRNAs. The 28S and 5.8S rRNAs then form the 60S ribosomal subunit along with the 5S rRNA (which is transcribed in the general nucleus by RNA polymerase III) and ribosomal proteins. The 18S rRNA, with ribosomal proteins,

forms the 40S ribosomal subunit. The assembled 40S and 60S subunits translocate to the cytoplasm where they then translate mRNA.

The nucleolus is subdivided into three regions called fibrillar centres (FCs), dense fibrillar components (DFCs), and granular components (GCs). Pol I is enriched in the FCs, where rDNA transcription occurs at the periphery. The rRNAs are processed in the DFCs, and the ribosomal subunits are assembled in the GCs, where the ribosomal proteins localize. The nucleolus contains less DNA, but more RNA and protein than the general nucleus (89, 90).

Not all rDNA clusters are transcribed at any given time. Electron microscopy shows that the transcriptionally active nucleolar chromatin is not associated with nucleosomes, whereas the transcriptionally inactive chromatin is (88). Many RNA fibrils extend from active rDNA clusters as a result of a single rDNA gene being transcribed into multiple rRNA by multiple Pol I at the same time (88). "Spacer" DNA between two copies of the rDNA genes appears to be naked or assembled in nucleosomes (88). The appearance of the active nucleolar chromatin or spacer DNA as naked is likely due to the increased dynamics of nucleosomes on their DNA, as the nuclease digestion of active rDNA genes results in protection to nucleasomal patterns (91, 92). However, the DNA bands are fainter and broader than those produced by digestion of inactive rDNA genes or other cellular chromatin, suggesting that the active rDNA genes are assembled into highly dynamic chromatin (93). Post-translational modifications to histones in the rDNA nucleosomes may contribute to the increased rDNA chromatin dynamics (94).

Pol I is unable to transcribe through chromatin, suggesting that Pol I by itself does not disrupt chromatinization of rDNA genes (95). Chromatin remodeling complexes, such as nucleolin or FACT, promote transcription by Pol I through chromatinized templates (95). The more dynamic chromatin of active rDNA genes may promote transcription, whereas the less dynamic chromatin of inactive rDNA prevents it. Alternatively, active and inactive rDNA clusters may be determined by a yet undiscovered cellular mechanism, and the dynamics of rDNA chromatin may be a consequence of the high transcription rate.

1.3 Histone modifications

Core histones are mostly globular, with unstructured N-terminal, and sometimes C-terminal, domains (30). The N-terminal domains extend from the core nucleosome and interact with DNA and other proteins, to increase the stability of the nucleosome or to promote higher order chromatin folding (96). Histones are modified post-translationally extensively, especially on their N-terminal domains, which are enriched in lysine and serine residues. These post-translational modifications (PTMs), including acetylation, methylation, phosphorylation, and ubiquitination, regulate the recruitment of proteins, the stability of the nucleosome and, ultimately, the transcription levels (Figure 1.3.) (97–103).

1.3.1 Histone acetylation

A family of enzymes called histone acetyltransferases (HAT) transfers acetyl groups ($O=C-CH_3$) from acetyl CoA to histone lysine residues. HATs are broadly grouped into two categories based on subcellular localization. Type A HATs acetylate histones in the nucleus, whereas Type B HATs acetylate histones in the cytoplasm. The 30 known human HATs are further classified into families based on structural and catalytic similarities. The Gcn5 N-acetyltransferase (GNAT) family of HATs includes Gcn5 and PCAF, among others. The MYST family of HATs is named for the founding members Morf, Ybf2, Sas2, and Tip60. Other HATs, such as p300/CBP or SRC/NCoA, which do not contain consensus HAT domains, are referred to as orphans.

Humans encode 18 histone deacetylases (HDAC), enzymes that remove acetyl residues from histones. HDACs are broadly categorized into two families, classical or sirtuin. The classical HDACs require a zinc ion to remove an acetyl group, whereas the sirtuins require NAD^+. Together, HATs and HDACs regulate the acetylation status of histones.

As DNA is negatively charged, the positively charged lysine residues of histones strengthen the interactions between histones and DNA. The interactions between histones and DNA are disrupted at higher concentrations of salt. Hyperacetylated nucleosomes are disrupted at lower salt concentrations than native

nucleosomes (104). It was classically believed that histone acetylation just weakened this interaction.

DNA that is assembled in more stable nucleosomes is less accessible to nuclease digestion than DNA assembled in less stable ones. The nuclease sensitive regions of the chicken embryo erythrocyte beta globin locus contain acetylated histones, whereas the nuclease insensitive regions contain non-acetylated histones (105). Chromatin assembled in vitro with linker histones and hyperacetylated histones was more accessible to nucleases than chromatin assembled with regularly acetylated histones (106). Chromatin assembled with hyperacetylated histones was also more flexible than that assembled with regularly acetylated histones (106), suggesting that the DNA entry and exit sites of the core nucleosome are looser. Chromatin assembled in vitro with hyperacetylated histones but without linker histones resulted in a less condensed structure than when assembled with regularly acetylated histones (107). The inhibition of higher order folding by histone acetylation results in greater levels of transcription (108). Mutating lysine to glutamine residues mimics acetylation of lysine residues by removing the positive charge. Glutamine substitutions of N-terminal histone tails reduces the formation of higher order chromatin, with substitutions within H2B and H4 N-terminal tails being the most effective (109). More recently, nucleosome dynamics have been evaluated by FRET (fluorescence resonance energy transfer). DNA is labeled on either side of the dyad axis with either a donor or acceptor fluorophore. When the nucleosome is folded normally, the donor and acceptor fluorophores are in proximity, and the donor fluorophore transfers energy to the acceptor fluorophore. The fluorescence released from the acceptor fluorophore is then quantitated. As DNA unwinds from the nucleosome, however, the donor and acceptor fluorophores are too far apart for the energy transfer. As a result, less fluorescence is produced by the acceptor fluorophore. Nucleosomes containing hyperacetylated H3 release less fluorescence than those containing non-acetylated H3 (99). These results are consistent with the model proposing that acetylation of H3 reduces nucleosome stability.

DNA that is assembled with hyperacetylated histones is transcribed more efficiently than that assembled with native histones (110). An antibody against hyperacetylated H4 was used to show that in chicken embryo erythrocytes the transcribed alpha D globin gene is enriched in H4 acetylation, whereas the silenced ovalbumin gene is not (111). Acetylation of histones, and the resulting destabilization of nucleosomes, is thus associated with high levels of transcription.

Although PTMs of the N-terminal tails are perhaps the most studied histone PTMs, PTMs also occur on their globular domain. H3 is acetylated at K56 by Gcn5, for example (112). The H3K56 side chain is pointed towards the major groove of DNA. Acetylation of this residue was thus expected to weaken the interaction between histones and DNA. Acetylation of H3K56 was shown to indeed particularly reduce nucleosome stability (113).

Acetylation of histones also recruits proteins, such as those involved in transcription or DNA damage repair. This recruitment is mediated by specific interactions with certain protein domains. Bromodomains, for example, recognize acetylated lysine residues. A bromodomain in the chromatin remodeling complex RSC recognizes H3K14ac (114).

1.3.2 Histone methylation

Whereas histone acetylation almost uniformly destabilizes nucleosomes, histone methylation can destabilize or stabilize nucleosomes depending on site and degree of methylation. A family of enzymes called histone methyltransferases (HMT) catalyze the transfer of methyl groups from S-adenosyl methionine to lysine or arginine residues, most often in H3 or H4. Lysine residues can be mono, di-, or tri-methylated, whereas arginine residues are monomethylated, or asymmetrically or symmetrically dimethylated. There are three main types of HMTs, SET domain-containing lysine-specific, non-SET domain-containing lysine specific, or arginine-specific.

There are 9 identified protein arginine N-methyltransferase (PRMT) in humans, 6 of which are HMTs. The transcriptional coactivator PRMT1 preferentially methylates H4K3 (115). Consistently, H4K3 methylation is generally associated

with transcribed genes (116). In contrast, PRMT6 transfers a second methyl group to H3K2 to produce dimethylated H3K2, which is associated with silenced genes (117).

Humans encode one non-SET domain containing lysine specific methyltransferase, DOT1L, which belongs to the DOT1 HMT family (118). DOT1L methylates H3K79 (118). H3K79 methylation is completely abrogated in DOT1 knockout cells. DOT1L is thus the only HMT that methylates that residue (119). Knockout of DOT1 results in embryonic lethality, indicating that methylation of H3K79 is essential for viability (119). H3K79 is hypomethylated in heterochromatin, including telomeres (120). DOT1 is also required for the establishment of other heterochromatin marks at telomeres (119).

There are seven families of SET-domain containing lysine specific methyltransferases, organized by the sequence similarity surrounding the SET domain. Set1, of the Set1 family, di- or tri-methylates H3K4 (121, 122). H3K4 di- or tri-methylation is generally associated with transcription (121, 122). In contrast, SUV39HI, of the SUV39 family, di- or tri-methylates H3K9, PTMs associated with silencing (123). Methylated residues recruit proteins with chromodomains. The chromodomain of HP1 (heterochromatin protein 1), for example, recognizes methylated H3K9 (124).

Histone methylation is reversed by histone demethylases (HDMTs). The first HDMT discovered was lysine-specific demethylase 1 (LSD1), which was also a transcriptional corepressor (125). LSD1 demethylates dimethylated H3K4, which is a marker of active chromatin, but not H3K9, which is a marker of repressed chromatin. LSD1 acts by an amine oxidation reaction that requires flavin adenine dinucleotide (FAD) (125). As amine oxidation reactions require protonated nitrogens, LSD1 demethylates monomethylated but not trimethylated H3K4 (125). Trimethylated H3K4 was proposed to be removed by either histone turnover or by other HDMTs.

JHDMA1 demethylates mono- and di-methylated H3K36 (126). Unlike LSD1, JHDMA1 activity requires no FAD, but requires Fe2+ and alpha ketoglutarate instead. It thus represents another class of histone demethylases (126). H3K36

trimethylation was later found to be removed by a related protein JMJD2A (127). JMJD2A and closely related JMJD2C also remove H3K9 trimethylation (127, 128).

1.3.3 Histone phosphorylation

As another important histone PTM, serine or threonine histone residues are phosphorylated by protein kinases and dephosphorylated by phosphatases. Linker histone H1 is phosphorylated by DNA-PK in vitro, which reduces the binding affinity of H1 for DNA (129). CDK2 also phosphorylates H1 and increases its dynamics (130). The phosphorylation of H1 likely promotes repair of dsDNA breaks, in that linker histones block dsDNA break ligation by the non-homologous end-joining pathway (NHEJ) in vitro (129).

The H2A variant H2A.X is also phosphorylated in response to dsDNA breaks. ATM, ATR, and DNA-PK phosphorylate H2A.X at S139, and to a lesser extent T136 (97, 131). Phosphorylated H2A.X is less stable than unphosphorylated H2A.X. Moreover, when H2A.X is phosphorylated, H1 binds to linker DNA regions between core nucleosomes less efficiently (97).

Other sites of histone phosphorylation include H3S10 and H3S28 (132, 133). Phosphorylation at either of these sites increased H3 acetylation and gene transcription (132, 133). H3S10 phosphorylation also regulates chromatin structure. The condensed chromatin during mitosis is enriched in H3S10 phosphorylation (134, 135).

1.3.4 Histone ubiquitination

Ubiquitination is a three-step process that conjugates ubiquitin, a 76 amino acid protein, to the ε amino group on lysine residues. First, a ubiquitin-activating enzyme (E1) catalyzes ATP to conjugate ubiquitin to a cysteine residue of ubiquitin-conjugating enzyme (E2) via a thioester bond. An ubiquitin-protein isopeptide ligase (E3) then catalyzes the transfer of the ubiquitin from the E2 to the lysine residue of the target substrate. Polyubiquitinylated chains are formed through the conjugation of additional ubiquitins to the substrate-conjugated ubiquitins on lysine 48 or 63, or, less commonly to lysines 6, 11, 27, 29, or 33. Whereas lysine-48-linked

polyubiquitin chains typically target the substrate for degradation by the proteasome, lysine-63-linked polyubiquitin chains usually regulates other cellular processes.

Ubiquitinated histones were initially discovered as preferentially incorporated in nucleosomes on transcribed genes. MCN digested chromatin was incubated with increasing concentrations of salt to destabilize the nucleosomes. Ubiquitinated H2A or H2B was enriched in the extracts with the lowest salt concentration and depleted from the ones with the highest salt concentration (136). Nucleosomes containing ubiquitinated H2A or H2B are thus likely more dynamic than non-ubiquitinated ones. Chromatin containing transcribed genes was enriched in extracts at the lowest salt concentrations, leading to the conclusion that ubiquitinated H2A and H2B were enriched in transcribed genes (136). However, the low-salt fraction was later found to also contain silenced genes (137). Ubiquitinated histones thus did not necessarily fractionate with transcribed genes (137). In another study, DNA was nicked and repaired using biotin-tagged nucleotides. The biotinylated, or accessible, chromatin was fractionated from the nonbiotinylated, less accessible, chromatin. Ubiquitinated H2A or H2B were equally enriched in the more or less accessible fractions, suggesting that ubiquitinated histones do not preferentially associate with soluble DNA (138).

Nucleosomes containing ubiquitinated H2A or H2B are more dynamic than those containing non-ubiquitinated histones (139). However, not all sites of ubiquitination destabilize the nucleosome. H2B is predominately ubiquitinated by the E3 ligase Rad6 at K123 in yeast or by RNF20 at K120 in humans. H2B K123 or K120 ubiquitination stabilizes nucleosomes (140, 141).

The core histones H3 and H4 and the linker histone H1 are also ubiquitinated. Ubiquitination of CENP-A, a H3 variant, at K124 by the E3 ligase CUL4A-RBX1 is required for the incorporation of CENP-A in centromeric nucleosomes, possibly by promoting the interaction with HJURP (142). CUL4A also ubiquitinates H3 and H4 in response to DNA damage, which results in increased nucleosome stability (143). Monoubiquitination of H4K31, in contrast, destabilizes the nucleosome (141).

1.4 Histone variants

The genes encoding canonical histones contain no introns, and the resulting mRNA are not poly-adenylated. In contrast, the genes encoding variant histones may contain introns, and their mRNA may be polyadenylated. Whereas canonical histones are assembled during S phase of the cell cycle and are assembled in nucleosomes with newly synthesized DNA via replication-dependent mechanisms (Section 1.2.3), variant histones are assembled in nucleosomes independently of the cell cycle via replication-independent mechanisms (Section 1.2.4). H2B and H4 encode no variants in somatic cells, whereas H2A and H3 do. The incorporation of histone variants into nucleosomes often affects nucleosome stability.

1.4.1 H3.3

Canonical H3.1 is encoded by ten genes clustered on chromosome 6. In constrast, variant H3.3 is encoded by two genes on chromosome 1 and 17. Human H3.1 and H3.3 are 132 amino acids long and have only five differences between them (Figure 1.4.). However, H3.3 has functions that cannot be performed by H3.1, as mice knocked out for both H3.3 genes are not viable (144).

The five amino acids different between H3.1 and H3.3 cause them to be recognized by different chaperones and assembled in nucleosomes by different pathways. H3.1-H4 or H3.3-H4 dimers interact with the closely related chaperones ASF1a and ASF1b (40, 145). However, only H3.1-H4 are bound by the chaperone CAF-1, and only H3.3-H4 by HIRA (40). DAXX is another specific H3.3 chaperone (146, 147). CAF-1 assembles H3.1 in nucleosomes via replication-dependent mechanisms. HIRA or DAXX assemble H3.3 in nucleosomes with DNA of transcribed genes or telomeres, respectively (45, 146, 147).

Total nuclear H3.3 is enriched in PTMs marking active chromatin in comparison to H3.1 (148). Nonetheless, H3.3 assembled in telomeric chromatin is enriched is K9 trimethylation, a marker of silenced chromatin (149). H3.3 assembled in nucleosomes with telomeric DNA is less dynamic than H3.3 assembled in nucleosomes with transcribed DNA (150). However, all nucleosomes assembled

with H3.3 in vitro are more dynamic than those assembled with H3.1, and nucleosomes assembled with hypoacetylated H3.3 were still more dynamic (151). H3.3-containing nucleosomes are thus more dynamic not only due to the abundance in PTMs.

1.4.2 CENP-A

The gene encoding the 140 amino acid long CENP-A is located on chromosome 2. The histone fold domain of CENP-A has approximately 60% homology to that of H3.1, but CENP-A has unique N- and C-terminal domains (Figure 1.4.) (152). CENP-A was first identified as a 17 kDa constitutive protein of the kinetochore (153). CENP-A only eluted from the nuclei at high salt concentrations (2M NaCl), very much like core histones, and was purified from chromatin (154), leading to the discovery that CENP-A is a H3 variant. CENP-A knockout mice are embryonic lethal, which is not surprising considering that CENP-A is required for chromosome segregation (155).

CAF-1, HIRA, or ASF1 do not purify CENP-A, suggesting that none of them is a CENP-A chaperone (156). CENP-A, but not H3.1 or H3.3, assemble a complex with HJURP (Holliday Junction-Recognizing Protein) (156). CENP-A is not assembled in centromeric chromatin in cells knocked down for HJURP, suggesting that HJURP is a CENP-A specific chaperone (156). HJURP recognizes a unique CENP-A domain, termed the CENP-A targeting domain (CATD) (157). A mutant H3.1 containing the CATD is recognized by HJURP, although this recognition is not sufficient for incorporation in centromeric nucleosomes (157). CENP-A nucleosomes have been described to form octamers or hemisomes (one dimer each of CENP-A-H4 and H2A-H2B) (158, 159). Disruption of the interaction between two CENP-A molecules prevents the assembly of CENP-A in centromeric nucleosomes (157). Only heterotetramers of CENP-A-H4 thus appear to assemble in centromeric nucleosomes, suggesting that centromeric nucleosomes are indeed octamers and not hemisomes.

Nucleosomes containing CENP-A have been reported to be less or more dynamic than those containing canonical H3.1 (160, 161). However, CENP-A-

containing octameric nucleosomes are less tightly bound by dsDNA at the exit and entry sites than canonical nucleosomes (162, 163).

1.4.3 H2A.X

The variant H2A.X has approximately 80% homology to canonical H2A (Figure 1.5.). Most of the divergence is on the C-terminal tail, which is 13 amino acids longer for H2A.X than for canonical H2A (164). H2A.X is synthesized from a single gene, independently of the cell cycle (34). Like the canonical H2A genes, the H2A.X gene is intronless. However, H2A.X is transcribed into two alternate transcripts. One of the transcripts is terminated by a stem-loop structure, like canonical H2A, whereas the other is polyadenylated like the vast majority of human transcripts (164).

H2A.X is not necessary for mouse viability, but mice knocked out for both copies of the gene encoding H2A.X are sterile (165). All H2A.X knockout mice die in 11 days after radiation exposure to a dose that is only lethal for 20% of wild type mice (165). Lethality is a consequence of the role that H2A.X plays in DNA damage repair. H2A.X is phosphorylated on serine 139 in response to dsDNA breaks, such as those induced by radiation (131). ATM, ATR, and DNA-PK have all been found to phosphorylate H2A.X on serine 139 (166, 167). MDC1 (mediator of DNA damage checkpoint 1) is recruited to the phosphorylated H2A.X, and in turn recruits the other proteins required to repair the DNA damage (98).

Nucleosomes containing H2A.X are more sensitive to salt than those containing canonical H2A, especially when phosphorylated, suggesting that they are less stable in vitro (97). However, FRAP experiments have shown that H2A.X is less dynamic than H2A in vivo (81).

1.4.4 MacroH2A

Whereas canonical histones range from 12 to 14 kDa, macroH2A is a 42 kDa protein (168). The gene encoding macroH2A1 is located on chromosome 5 and contains 11 exons (169). Two isoforms of macroH2A, named macroH2A1.1 and macroH2A1.2, are transcribed from this gene and then alternatively spliced (170). The gene encoding macroH2A2 is located on chromosome 10, and is structurally

similar to that of macroH2A1, with the absence of an alternate splicing site within exon 5 (169).

The histone fold of macroH2A is approximately 60% similar to that of canonical H2A (Figure 1.5.). However, macroH2A also contains an extended C-terminal domain, termed the macro domain. MacroH2A localize to the inactive X chromosome, also called the Barr body (169, 171). Truncated macroH2A1 or macroH2A2 containing only the histone fold domain still localizes to Barr bodies (172). The fusion of the C-terminal macro domain to H2A or H2B also resulted in their localization to Barr bodies (172). Thus, both domains of macroH2A target it to Barr bodies. Mice knocked out for macroH2A1 and macroH2A2 genes are still viable (173)

Nucleosomes containing macroH2A are less dynamic than those containing canonical H2A due to the stronger interaction between the macroH2A molecules in the nucleosome (174–176). The macro domain of macroH2A also interacts with HDAC1, contributing to the increased stability of macroH2A-containing nucleosomes (174). The genes assembled in nucleosomes containing macroH2A are generally silenced (177). The incorporation of macroH2A into nucleosomes prevents remodeling by SWI/SNF (178). This inhibition of remodeling likely inhibits transcription.

1.4.5 H2A.Z

Human H2A.Z has approximately 60% sequence similarity to human canonical H2A (Figure 1.5.) (179). Humans encode a single gene for H2A.Z, which contains five exons (180). H2A.Z is synthesized independently of the cell cycle and represents approximately 5% of the total cellular H2A (179). The sequence of H2A.Z is at least 90% similar between different organisms, suggesting a uniquely important (but yet identified) role in the cell. Consistently, truncation mutations within the H2A.Z gene are lethal in *Drosophilia* (181), and mouse embryos knocked out for H2A.Z do not survive to term (182).

H2A.Z is assembled in nucleosomes located upstream from genes, independently of transcription (183, 184). H2A.Z is assembled in nucleosomes by

the Swr1 remodeling complex, which exchanges H2A-H2B dimers for H2A.Z-H2B ones (51, 185). Ino80 has the reverse role, as it replaces H2A.Z-H2B dimers with H2A-H2B ones (186).

Nucleosomes containing H2A.Z are less stable than those containing H2A (184). H2A.Z assembles less stable dimers with H2B than H2A (187). However, the crystal structure of a nucleosome containing H2A.Z revealed little differences in interactions between H2A or H2A.Z with H2B and DNA (188). Fewer hydrogen bonds form in between the two dimers of H2A.Z-H2B relative to H2A-H2B, which likely destabilizes the nucleosome (188). H2A.Z-H2B also forms three fewer hydrogen bonds with H3-H4 than H2A-H2B (188).

1.4.6 H2A.B

H2A.B (previously called H2A.Bbd for Barr body deficient) has 48% homology to canonical H2A (Figure 1.5.) (189). H2A.B is encoded in three intronless genes located on chromosome X (189). H2A.B has a longer N-terminal tail than canonical H2A, but lacks all of the N-terminus lysine residues that are post-translationally modified in H2A. Instead, H2A.B has a stretch of six arginine residues in its N-terminal tail, resulting in a less basic protein. H2A.B also lacks the C-terminal tail of H2A, resulting in a shorter protein of 115 amino acids, and has a docking domain that is highly divergent from H2A.

Nucleosomes containing H2A.B are less stable than those containing canonical H2A, and H2A.B is more dynamic than H2A (190, 191). The C-terminal and docking domains of H2A stabilize its interaction with H3 in the core nucleosome (30). H2A.B-containing nucleosomes were thus expected to be more dynamic because H2A.B lacks a C-terminal tail and has a highly divergent docking domain. The docking domain, but not the C-terminal tail, affected nucleosome dynamics (192).

The DNA in nucleosomes containing H2A.B is less restrained than the DNA in nucleosomes containing H2A (192). Whereas 146 bp of DNA wraps stably around nucleosomes containing H2A, only 118 – 132 bp of DNA wraps stably around nucleosomes containing H2A.B (192, 193). The angle between the DNA entering

and exiting the nucleosomes is wider in H2A.B-containing nucleosomes, suggesting that the exit and entry DNA interact less strongly with H2A.B-containing nucleosomes than the canonical ones (193). The fusion of the H2A docking domain and C-terminus to H2A.B increased the length of DNA stably wrapped around nucleosomes (193). Conversely, the length of DNA stably wrapped around nucleosomes decreased when the docking domain of H2A was replaced with that of H2A.B (193). The docking domain of H2A.B therefore confers its unusually unstable properties.

The docking domain of H2A is also required for the binding of H1 to the linker DNA in between core nucleosomes and for nucleosome remodeling by RSC (194). As a result, H2A.B-containing nucleosomes bind less H1 than H2A-containing nucleosomes, and H2A.B-containing nucleosomes are not remodeled by RSC (194).

H2A.B is expressed to lower levels than the other H2A variants, and endogenous H2A.B is not detectable by antibodies. The subnuclear distribution of H2A.B can therefore only be evaluated from exogenous H2A.B. Inactive X chromosomes are often depleted of H2A.B, whereas nucleoli are often enriched in H2A.B (189, 195). Consistently, ChIP studies show that H2A.B is depleted from silenced genes, and enriched in transcribed genes (177). The chaperones that assemble H2A.B in nucleosomes have not been identified.

1.5 Transcription by RNA polymerase II

1.5.1 Structure of cellular genes

The promoters of cellular genes are categorized into two groups, focused or dispersed. Unlike focused promoters, which contain core promoter elements spanning from approximately 40 base pairs (bp) upstream to 40 bp downstream of the transcription start site (TSS), dispersed promoters lack core promoter elements and contain multiple TSS. Although only approximately one third of mammalian promoters are focused, all HSV-1 promoters are.

Core promoter elements are specific DNA sequences that recruit specific transcription factors (Figure 1.6.). The TATA box is, for example, located between 80 bp upstream to 80 bp downstream of the TSS in 24% of human genes (196).

TATA boxes are most commonly found approximately 30 bp upstream from the TSS, and are bound by the TATA box binding protein (TBP), a subunit of the transcription factor (TF) IID complex. The initiator element (INR) is also located between 80 bp upstream or downstream of the TSS in 15% of human genes. INR are most commonly located on the TSS and are bound by TBP associated factors (TAF) 1 and 2, subunits of the TFIID complex (196). 30% of genes have an INR but no TATA box, and 46% of genes have neither a TATA box nor an INR (196).

TFIIB recognition elements (BRE) are located beside TATA boxes, and are bound by TFIIB (197). Downstream promoter elements (DPE), located approximately 30 bp downstream from the TSS, are bound by the TAF6 and TAF9 subunits of the TFIID complex (198, 199). Approximately 25% of human genes have a DPE or BRE (200). BRE is found more commonly in promoters without a TATA box, whereas DPE has no preference.

1.5.2 Pre-initiation complex formation

The pre-initiation complex (PIC) is composed of Pol II and the general transcription factors (GTFs) TFIIA, TFIIB, TFIID, TFIIE, TFIIF, and TFIIH. TFIIB is a monomer, whereas the other TFs are multi-subunit proteins. TFIID contains TBP, which binds to the TATA box, and several TBP-associated factor (TAF) proteins. TAFs are not required to initiate transcription in vitro. Instead, TAFs provide promoter selectivity. The PIC is suggested to then assemble in a step-wise manner. TFIIB binds TFIID, while also interacting with the DNA. TFIIF and Pol II are recruited, followed by TFIIE and TFIIH, completing the formation of the PIC (201–204).

The mediator complex is a multi-subunit protein complex required for transcription (205, 206). The mediator complex is associated with PICs, and enhances the recruitment of TFIID to promoters (207, 208). Though TFIID is still recruited to promoters in the absence of the mediator complex, TFIIF and TFIIH are not (209). Crystal structures revealed that the mediator complex cradles TFIIH and Pol II, likely stabilizing them (210).

1.5.3 Transcription elongation

TFIIE and TFIIH unwind and separate the dsDNA strands at the promoter (211). TFIIH consists of nine subunits that assemble a ring, two of which have helicase activity (212). TFIIH utilizes the energy from ATP hydrolysis to unwind the DNA at the TSS (213).

Pol II contains twelve different subunits. The carboxy-terminal domain (CTD) of RPB1, the largest subunit of Pol II, has 52 repeats of the consensus sequence YSPTSPS. CDK7, the kinase subunit of TFIIH, phosphorylates the CTD at Ser 5 (214). Ser 5 phosphorylation induces promoter escape by Pol II (215). The PIC dissociates after initiation, such that only TFIIF remains associated with Pol II during elongation (216). As elongation progresses, Ser 2 also becomes phosphorylated by CDK9 (217, 218).

1.5.4 Transcription termination

Pol II transcription termination is coupled to mRNA 3' end processing. The cleavage and polyadenylation specificity factor (CPSF) and the cleavage stimulatory factor (CsfF) bind to the CTD of Pol II (219). CPSF consists of five subunits, CPSF-30, CPSF-73, CPSF-100, CPSF-160, and Fip1. CPSF-160 binds to the polyadenylation signal (PAS; AAUAAA) at the 3' end of the transcript (220). CsfF consists of 3 subunits, CsfF-50, CsfF-64, and CsfF-77. CsfF-64 binds to the U/GU-rich region approximately 30 nucleotides downstream of the cleavage site (221). CPSF-73 is the endonuclease that cleaves the mRNA transcript 10-30 nucleotides downstream of the polyadenylation signal (PAS; AAUAAA) (222). The polyadenylate polymerase (PAP) is recruited to the cleavage site by CPSF, where it adds the poly-A tail to the mRNA transcript (223). The 5' to 3' exonuclease XRN5 degrades the downstream transcript (224). The torpedo model of transcription termination suggests that when XRN5 reaches Pol II, it triggers the release of Pol II from the DNA template. Alternatively, the allosteric model suggests that after transcribing the PAS, a conformational change or destabilization of Pol II causes its release.

1.5.5 Transcription regulation

In vitro, DNA that is not assembled in nucleosomes is transcribed more efficiently by Pol II than DNA that is assembled in nucleosomes (44, 225). In vitro, Pol II is able to displace an H2A-H2B dimer from the nucleosome to transcribe through histone hexamers (226). However, most often, Pol II pauses on DNA and backtracks upon reaching a nucleosome (227). The complex CTEA (chromatin transcription-enabling activity) then promotes the passage of Pol II through the nucleosome (228). TFIIS, a component of CTEA, is sufficient to promote passage of Pol II by itself, but the entire CTEA complex is more efficient (227). Other cellular factors promote the passage of Pol II by disassembling or remodeling nucleosomes. Like TFIIS, FACT promotes the passage of Pol II through nucleosomes (229). Unlike TFIIS, FACT acts as a histone chaperone, binding to an H2A-H2B dimer after its removal from the core nucleosome (83).

Histones assembled in nucleosomes with DNA of transcribed genes are enriched in histone acetylation. Chromatin remodelers, such as SWI/SNF and RSC, contain bromo-domains that recognize and bind acetylated lysine residues on histone tails (60, 61) (See 1.6.2). Through ATP hydrolysis, SWI/SNF and RSC promote transcription through chromatinized templates (62). Though SWI/SNF is able to disassemble nucleosomes *in vitro*, SWI/SNF is also able to remodel nucleosomes when the histone dimers are cross-linked, indicating that SWI/SNF does not have to disassemble nucleosomes for its activity (63, 64). SWI/SNF unwraps up to 50 bp of DNA from around the nucleosome, and slides the nucleosome down the DNA template (64).

Insulators are DNA sequences bound by CTCF that block *cis*-acting elements, such as enhancers or repressors, from affecting neighbouring genes (230). CTCF contains eleven zinc-finger domains, of which only four are required to bind DNA (230, 231). CTCF binds to unmethylated GC-rich DNA with the consensus sequence CCGCGNGGNGGCAG, where N is any nucleotide (231, 232). CTCF recruits the transcriptional repressor Sin3A, which in turn recruits HDAC (233).

High mobility group (HMG) chromosomal proteins are grouped into three sub-families, HMGA, HMGB, and HMGN. The AT-hook domains of HMGA proteins and the HMG-box domains of HMGB proteins both bind DNA. In contrast, HMGN

proteins, such as HMG14 and HMG17, bind to nucleosomes. HMG14 and HMG17 both promote Pol II transcription through chromatinized templates (234, 235)

1.6 Lytic life cycle of HSV-1

1.6.1 Cell entry

HSV-1 first establishes lytic infections in epithelial cells. HSV-1 is internalized into epithelial cells by three mechanisms; pH-independent cell fusion, pH-independent endocytosis, or pH-dependent endocytosis. The main method of HSV-1 entry in Vero cells is to pH-independent cell fusion. HSV-1 has five glycoproteins that mediate membrane fusion; gB, gC, gD, gH, and gL. gC first binds to heparan sulfate on the cell surface (236, 237). However, gC or heparan sulfate are not required for HSV-1 entry (236). gD then binds to herpesvirus-entry mediator (HVEM), nectin-1 (previously called HveC), or 3-O-sulfated heparan sulfate (238–240). Knockout of either HVEM or nectin-1 in mice attenuated the establishment of HSV-1 infections, whereas the double knockout of both receptors had a synergistic effect (241).

Upon binding to its receptors, gD undergoes a conformational change to an open position (242). This open position is believed to promote the interaction of gD with the gH/gL heterodimer and the viral fusogen gB (243). The cytotail of gH activates gB, perhaps by causing a conformational change in gB that exposes the fusogenic domain (244). However, the mechanisms whereby HSV-1 fuses to the cell membrane are not yet fully elucidated.

1.6.2 Temporal regulation of gene expression

The more than 80 HSV-1 genes are classified into three classes, based on their requirements for expression. Immediate-early (IE) genes are expressed first, as they do not require any de novo protein synthesis. In contrast, expression of early (E) genes requires prior de novo HSV-1 protein synthesis. Late (L) genes are expressed only after HSV-1 DNA replication. In contrast to cellular genes, the promoters of mostly all HSV-1 genes have TATA boxes. The promoters of IE genes also contain TAATGARAT sequences, which are recognized by the cellular protein

OCT-1 in complex with VP16. E and L genes do not have TAATGARAT sequences. Instead, L genes have Inr sequences, which are recognized by TFIID, and E genes have GC and CCAAT boxes (Figure 1.7.).

Upon fusion of the envelope to the cell membrane, the tegument proteins are released into the cytoplasm, including the transcription transactivator VP16. VP16 binds to the cellular protein host cell factor 1 (HCF-1) and the complex translocates into the nucleus. The promoters of IE genes contain TAATGARAT sequences which are recognized and bound by the cellular protein OCT-1. OCT-1 recruits VP16 and HCF-1, which in turn recruit several chromatin modifying proteins (Section 1.4). IE genes are then transcribed by Pol II. Two of the IE proteins, ICP0 and ICP4, then activate transcription of the E genes, by mechanisms which remain mostly unknown. The E genes encode the proteins required for HSV-1 DNA replication, among others. L genes are transcribed after HSV-1 DNA replication starts, and their expression is activated by ICP0 and ICP4. L genes encode the proteins required for virion assembly and egress.

1.6.3 HSV-1 DNA replication

HSV-1 has three distinct origins of replication. OriL is encoded near the center of the UL region, whereas OriS is encoded in the repeat region of IRS and TRS (245). OriL is not required for HSV-1 replication in cell culture, or for reactivation in a murine model (246). The OriS sequences are also not required for HSV-1 replicatiom, suggesting that only one origin is needed (247). OriS and OriL both have palindromic sequences. OriS has a 45 bp palindromic sequence (248), whereas OriL has a 144 bp palindromic sequence (249), which form hairpin secondary structures.

Seven HSV-1 proteins are required for HSV-1 DNA replication, UL9, ICP8, UL30, UL42, UL5, UL8, and UL52 (250). OriS has three binding sites for UL9 (also called the origin binding protein or OBP), called box I, box II, and box III (251, 252). A dimer of UL9 binds to each box of OriS (253). The dimers interact, resulting in the distortion of DNA and the formation of a stem-loop structure between either box I and II or box I and III (252, 254).

ICP8 (also called the single-strand DNA binding protein or SSB) interacts with UL9 and, in an ATP-dependent process. Together, they unwind and distort the DNA at the origin (255–257). The helicase/primase complex consisting of UL5, UL8, and UL52 binds to ssDNA (258). A minimum of six nucleotides of ssDNA is required for binding of UL5/UL8/UL52 (258). UL5/UL8/UL52 synthesizes the RNA primers (259).

The HSV-1 polymerase consists of UL30, the catalytic subunit, and UL42, the processivity subunit. The C-terminus of UL30 is required for its interaction with UL42 and for activity (260). Recruitment of the HSV-1 DNA polymerase to the origin requires an active primase (259). UL30 interacts with UL8, whereas UL42 binds to UL9 (261). Once recruited, the HSV-1 polymerase synthesizes the new leading and lagging DNA strands.

1.6.4 Egress

HSV-1 form three types of capsids, A, B and C (25). All types of capsids have the same outer shell, lying on a T=16 icosahedral lattice (25, 26). The 12 pentons, which form the vertices, are connected by 150 hexons, 320 triplexes, and a capsid floor layer (26). Eleven of the pentons are identical, whereas the twelvth is different and serves as the portal for DNA packaging (262). VP5 is the most abundant capsid protein, forming all of the hexons and eleven of the pentons (263). The distal hexons also contain six molecules of VP26 (263). The 320 triplexes are each formed with one molecule of VP19C and two of VP23 (263). The portal is formed with twelve copies of UL6, which form a cylinder around an axial channel of about 5 nm in diameter (262). These five major proteins form the A capsid. B capsids contain a core of mostly cleaved scaffolding protein VP22a (264). C capsids are the only ones that contain DNA, and are therefore the infectious ones.

Six proteins are required for cleaving and packaging the HSV-1 genome into the procapsid, UL15, UL17, UL25, UL28, UL32, and UL33. The terminase complex is composed of UL15, UL28, and UL33. The terminase complex interacts with UL6 at the portal, but the mechanisms by which it translocates the HSV-1 DNA into the capsid are not yet fully understood (265). UL28 binds to specific DNA sequences

required for cleavage called *pac1* and *pac2* (266, 267). UL15 contains Walker A and B boxes, which bind to, and hydrolyze, ATP (268). Mutation to the Walker A box inhibited the ability of a plasmid encoding UL15 to support a UL15-null mutant virus, suggesting that UL15 provides the catalytic energy to translocate the HSV-1 DNA into the procapsid (268). The function of UL33 is not yet known.

UL17 and UL25 are part of the capsid vertex-specific component (CVSC), along with UL36. The CVSC binds to the triplexes adjacent to the 11 pentons. In the absence of functional UL25, HSV-1 DNA is still cleaved at the proximal and distal end (269). The distal HSV-1 DNA cleavage that normally occurs after a full genome, however, occurs prematurely (269). UL25 may thus stabilize the capsid during DNA packaging, allowing the entry of the full genome. UL17 is required for both cleaving and packaging HSV-1 DNA.

HSV-1 capsids bud twice, first from the inner nuclear membrane (INM), and second from the trans-golgi network (TGN). Egress from the INM requires the L proteins UL31 and UL34, which form the nuclear egress complex (NEC). UL34 has a C-terminal transmembrane helix that anchors it to the INM (270). UL31 is recruited to the INM by UL34 (270). UL31 and UL34 oligomerize, forming a hexagonal scaffold on the inside of the membrane bud (271). The CVSC is believed to interact with UL31 to attach the capsid to the envelope (272). The enveloped capsid buds into the perinuclear space, then fuses with the outer nuclear membrane, which releases the capsid into the cytoplasm.

HSV-1 glycoproteins are synthesized on the endoplasmic reticulum (ER) and transported through the golgi network (GN) (273, 274). The capsid acquires its envelope with glycoproteins from the TGN (275, 276). UL37, a inner tegument protein, interacts with the cytoplasmic domain of gK, directing the capsid to the TGN (277). The mechanisms of secondary envelopment are not yet fully understood, but the glycoproteins gB, gD, and gE appear to be required (278, 279). The enveloped virus is transported inside a vesicle to the plasma membrane for egress, most likely by a cellular exocytosis pathway (280).

1.7 Latency

1.7.1 Establishment and maintenance of latency

After the primary infection of epithelial cells, HSV-1 travels to the sensory neurons that innervate the primary site. HSV-1 then establishes latency in the ganglia of these sensory neurons, during which the majority of HSV-1 genes are not expressed, no infectious virions are produced, and therefore there are no signs or symptoms of disease. The mechanisms by which HSV-1 establishes latent instead of lytic infections are not yet fully understood, but most likely involve both viral and cellular factors.

HSV-1 mutants in the three transcription activators VP16, ICP0, or ICP4, are able to establish latent infection, despite not being able to establish lytic infections (281–283). HSV-1 mutants in thymidine kinase are also able to establish latent infections (284). Though HSV-1 mutants in thymidine kinase establish latency less efficiently than wild-type virus, they are still able to establish latent sites with multiple copies of the HSV-1 genome (285).

Most HSV-1 genes are not expressed during latent infection, with the exception of the latency-associated transcripts (LAT). The LATs were first detected as HSV-1 transcripts of approximately 2.0 and 1.5 kb in the trigeminal ganglia of latently infected mice and rabbits (286, 287). Unlike lytic transcripts, which peak at 4 days post infection, the LAT transcripts are only detected after 4 days of infection, and increase in amount up to 60 days post infection (288).

The LATs are not required for establishment of latency, but enhance the efficiency of latency establishment (289–292). The LATs are transcribed from the IRL, antisense to ICP0 (286, 287), and encode no protein products (293). HSV-1 replication in a cell line stably expressing LATs was inhibited at low mois but not affected at high mois (294). The amount of IE mRNA, including ICP0, is also reduced in cells lines expressing LATs infected with HSV-1 (294). Six miRNAs (miR-H2 to miR-H7) are encoded within the LAT, two of which overlap with the ICP34.5 gene (miR-H3 and miR-H4) and one of which overlaps with the ICP0 gene (miR-H2) (295). HSV-1 mutants lacking miR-H2 or miR-H4 had greater expression of ICP0 or ICP34.5, respectively (296, 297). However, the deletion of miR-H2, miR-H3, or miR-

H4 had no effect on viral replication, and the deletion of miR-H2 had no effect on the establishment of latency (296, 297).

1.7.2 Reactivation from latency

By definition, latent HSV-1 genomes have the ability to reactivate and reestablish lytic infections. Just like mechanisms by which HSV-1 establish latency, the mechanisms by which HSV-1 reactivate are also not fully understood. In infected humans, HSV-1 is reactivated by physiological stress, such as extreme cold or heat, or by psychological stress, such as anxiety.

In cell cultures, HSV-1 is reactivated by physical or chemical stressors. The exposure of latently-infected cells to temperatures of 42˚C reactivates HSV-1 (298). The deprivation of nerve growth factor (NGF) or the blocking of the NGF signaling cascade also reactivate HSV-1 (299). Trichostatin A (TSA), an inhibitor of HDACI/II, induces reactivation of HSV-1 (300). Stimulation of the cyclic AMP (cAMP) pathway with either chlorophenylthio-cAMP (CPT-cAMP), an analog of cAMP, or forskolin, an activator of adenylate cyclase, induces reactivation of HSV-1 (301).

HCF-1 is localized in the cytoplasm of latently-infected cells, but becomes enriched in the nucleus during reactivation (302). De novo HSV-1 protein synthesis was not required to translocate HCF-1 to the nucleus, suggesting that HCF-1 nuclear recruitment is an early step in reactivation (302). HCF-1 enhances the expression of IE genes, suggesting that expression of the transcription activators ICP0 or ICP4, which are IE proteins, may be required for reactivation (303). Consistently, HSV-1 mutants in ICP0 or ICP4 were deficient in their ability to reactivate (304, 305). An HSV-1 mutant in VP16, which activates IE gene expression, was also deficient in its ability to reactivate (305). The expression of any of the three HSV-1 transcription activators, ICP0, ICP4, or VP16, from adenovirus vectors induces the reactivation of latent HSV-1 (305).

Reactivation of HSV-1 is suggested to be biphasic (306). The first phase of reactivation involves the expression of all HSV-1 genes, regardless of kinetic class. The amount of HSV-1 mRNA peaks at 20 hpi. By 25 hours after reactivation, the mRNA levels are not significantly different from those in latent cells. HSV-1 genes

are expressed in a temporal manner in the second phase of reactivation, as they are during lytic infection. Though VP16 is expressed at both phases, it is only nuclear during phase II (306). Consistently, expression of VP16 only enhances the expression of HSV-1 genes in phase II (306).

Expression of LAT is also required for efficient HSV-1 reactivation (290, 307–309). LAT thus enhances the efficiency of both latency establishment and reactivation.

1.8 HSV-1 transcription activators

1.8.1 VP16

The mechanisms by which VP16 activates IE gene transcription are well characterized. VP16 is an outer tegument protein. Upon fusion of the HSV-1 lipid envelope to the cell membrane, VP16 is released into the cytoplasm, where it interacts with cellular HCF-1 (310, 311). IE promoters have TAATGARAT sequences, which are recognized by cellular OCT-1 (312). VP16 and HCF-1 translocate into the nucleus and interact with OCT-1 (312). VP16 binds to OCT-1 directly, but the presence of HCF-1 stabilizes the interaction (313, 314).

VP16 and HCF-1 then recruit cellular chromatin modifying proteins. VP16 recruits the HATs GCN5, PCAF, and CBP/p300 as well as the chromatin remodeling chromatin SWI/SNF (315). In the absence of the C-terminal activation domain of VP16, the HATs, SWI/SNF, and Pol II complex are underrepresented on IE promoters (316). In contrast, H3 is enriched on IE promoters in the absence of the C-terminal activation domain of VP16 (316, 317). VP16 may thus activate IE gene expression by recruiting cellular chromatin modifying proteins that prevent the formation of stable nucleosomes on IE promoters. The knockdown of GCN5, PCAF, and CBP/p300, or the ATPase subunits of SWI/SNF prior to HSV-1 infection does not inhibit HSV-1 gene expression (318). However, knockdown of these factors may result in nucleosomes not being disassembled from cellular chromatin or assembled onto the incoming HSV-1 genomes, maintaining HSV-1 genomes in a transcriptionally active, as opposed to a transcriptionally inactive, state.

The histone demethyltransferase LSD1 is recruited by VP16 to IE promoters, whereas the histone methyltransferase Set1 is recruited by HCF-1 (319, 320). LSD1 demethylates H3K9, a marker of inactive chromatin, whereas Set1 methylates H3K4, a marker of active chromatin (121, 122, 321). The knockdown or inhibition of LSD1 reduces IE gene expression (319, 322). Set1 knockdown also reduces IE gene expression (323).

VP16 is a potent transactivator, and can be modified to activate any gene of interest by fusing the C-terminal activation domain of VP16 to the DNA-binding domain of another protein. The Gal4-VP16 fusion protein contains the DNA-binding domain of Gal4 and the activation domain of VP16 (324). Gal4-VP16 was 100-fold more potent than wild-type Gal4 at activating genes with Gal4 DNA-binding sequences in their promoters. Gal4-VP16 was able to activate transcription even when bound to DNA over 1000 bp upstream or downstream from the TSS. VP16 can thus be modified and used as a tool to study chromatin in general. For example, the lac-VP16 fusion protein, containing the DNA-binding domain of the lac repressor protein and the activation domain of VP16, was shown to cause chromatin global decondensation (325).

1.8.2 ICP0

ICP0 activates expression of the E and L genes by mechanisms that are not yet fully understood. ICP0 is not essential, as HSV-1 mutants encoding no functional ICP0 still replicate in cells, though the efficiency is somewhat dependent on the multiplicity of infection in certain cell lines (326, 327). ICP0 enhances the transactivation abilities of ICP4 on the gD promoter (328). ICP0 also enhances the expression of some genes, such as the E gene TK, in the absence of any other HSV-1 protein (329), but not all (328). Other transcription factors, such as BMAL1, are likely required for ICP0 activity in the absence of ICP4 (330).

ICP0 is 775 amino acid residues long. Amino acid residues 537 to 613 of ICP0 have sequence homology to the amino-terminus of CoREST (331). CoREST forms a silencing complex with REST and HDAC1. During infection with wt HSV-1, ICP0 interacts with CoREST, displacing HDAC1 (331). In the absence of functional

ICP0, HDAC1 remains in complexes with CoREST during infection (331). Both ICP0, via residues 668-718, and HDAC1 bind to the amino-terminus of CoREST (332). The disruption of the CoREST-HDAC1 interaction enhances the replication of ΔICP0 HSV-1 mutants at low multiplicities of infection, suggesting that this disruption of the CoREST-HDAC1 promotes HSV-1 replication (332).

Displacement of HDAC1 from HSV-1 promoters would be expected to increase the acetylated H3 in nucleosomes assembled with HSV-1 genomes. As nucleosomes containing acetylated H3 are more dynamic than those containing deacetylated H3, promoters would also be expected to be stably associated with more total H3. Consistently, HDAC1 is not displaced from HSV-1 promoters in cells infected with an HSV-1 mutant encoding no functional ICP0. HSV-1 genes are stably associated with more acetylated H3 or total H3 in cells infected with an ICP0 mutant than in cells infected with wt HSV-1 (333, 334).

Upon nuclear entry, HSV-1 genomes localize next to ND10 (nuclear domain 10, also called PML bodies), nuclear domains that contain predominantly PML (promyelocytic leukemia protein) among other proteins. In the absence of functional ICP0, PML inhibits HSV-1 replication (335). Whereas infection with wt HSV-1 induced the loss of certain isoforms of PML, infection with an HSV-1 mutant encoding no functional ICP0 did not (336). ICP0 has a RING finger domain between amino acid residues 116 and 156. A mutant strain of HSV-1 encoding ICP0 with the deletion of the RING finger domain did not induce PML loss either, suggesting that the RING finger of ICP0 induces PML degradation (336). Inhibition of the proteasome prevented PML loss during HSV-1 infection, suggesting that PML is degraded by the ubiquitin pathway (336). Consistently, ICP0 stimulated the ubiquitination activity of the E2 ligases UBE2R1, UBE2R5a, and UBE2R6 in vitro (337, 338). Residues 77 to 211 of ICP0, which includes the RING-finger domain, was sufficient to stimulate the E2 ligases (338). ICP0 is thus an E3 ubiquitin ligase. ICP0 also targets other cellular proteins for degradation including the centromeric H3 variant CENP-A (339) and the catalytic subunit of the DNA-dependent protein kinase (340).

1.8.3 ICP4

1.8.3.1 Structure and biochemical features of ICP4

ICP4 is 1298 amino acid residues long, with a predicted molecular mass of 133 kDa. Extensive post-translational modifications including phosphorylation, acetylation, and ADP-ribosylation result in 175 kDa (341). ICP4 has an elongated structure, with a stokes radius of approximately 90 angstroms (342). The C-terminus and DNA-binding domains are predicted to have globular structures, whereas the N-terminus is predicted to be unstructured (343).

ICP4 is a homodimer of approximately 350 kDa in solution (344). Amino acids 343 to 376 are essential for dimerization (Figure 1.8.) (345, 346). Only one molecule of the heterodimer has to be functional for it to activate transcription (347).

ICP4 binds to the DNA sequence RTCGTCNNYNYSG, where R is a purine, Y is a pyrimidine, S is a C or G and N is any base (348). ICP4 binds to its own promoter and to the promoters of other IE genes to inhibit transcription (349–351). The DNA binding domain of ICP4 is from amino acids 258 to 487 (352). Residues 258 to 289, 415 to 427, and 455 to 457, establish most of the interactions with DNA (352). ICP4 does not bind to specific DNA sequences in order to activate transcription. ICP4 mutants that cannot bind to DNA but retain the ability to dimerize activate transcription (353).

ICP4 has a major serine tract, which has 19 serine residues, between amino acids 173 and 210. This region is extensively phosphorylated by PKA and perhaps CDK2 (354–357). The serine-rich region of ICP4 is not required for HSV-1 replication in cell culture (354, 358). However, mutants of HSV-1 encoding an ICP4 lacking the serine-rich region replicate less efficiently than wt HSV-1 in the eyes of mice, and even less efficiently in their ganglia (354). This mutant also reactivates less efficiently (354). The serine-rich region of ICP4 is not required for binding to the specific DNA consensus sequence (358). However, phosphorylated ICP4 has greater affinity for E and L promoters than unphosphorylated ICP4 (359).

1.8.3.2 ICP4 interacting proteins

ICP4 interacts with a larger number of viral and cellular proteins during infection. Full length ICP4 interacts with 82, 141, or 215 proteins in HSV-1 infected cells at 3, 6, or 12 hpi, respectively, as analyzed by mass spectrometry (360). The n208 mutant contains only the N-terminal 775 amino acid residues of ICP4 and activates E but not L gene expression (361). n208 interacts with 188 proteins in infected cells at 6 hpi (360).

ICP4 activates HSV-1 gene expression in the absence of any other HSV-1 protein (329). However, ICP0 enhances the transcription activity of ICP4 (328). ICP4 amino acid residues 1064 to 1296 directly interact with ICP0 amino acids residues 616 to 775 (362).

ICP27 is an IE protein that shuttles HSV-1 mRNA from the nucleus into the cytoplasm. ICP27 and ICP4 interact at multiple sites. ICP27 amino acid residues 27 to 103 or 179 to 403 interact with ICP4 amino acid residues 575 to 1298 (363). ICP27 amino acid residues 179 to 403 also interact with ICP4 amino acid residues 245 to 450 (363). ICP27 is not required for ICP4 to bind to DNA. However, the presence of ICP27 stabilizes the interaction of ICP4 with non-specific DNA sequences in HSV-1 infected cells (363).

All of the components of TFIID and most of the mediator proteins interact with ICP4. The levels of interaction of TAF1, TBP, and other TFIID components with ICP4 decreases from 3 to 6 hpi (360). In contrast, the levels of interaction of Med1 and other mediator components with ICP4 increases from 3 to 6 hpi. The C-terminal amino acid residues 775 to 1298 of ICP4 are required for the interaction with TBP or TAF250 (364).

Like VP16 and ICP0, ICP4 also interacts with chromatin modifying complexes. ICP4 interacts with the ATPase subunits of the chromatin remodeling complexes SWI/SNF, NURD and Ino80, as well as with the HAT CLOCK (360, 365). However, it is not yet known whether these interactions are direct or mediated by other (cellular or viral) proteins.

1.8.3.3 Transcription inhibition mechanism by ICP4

ICP4 binds to the specific DNA sequence RTCGTCNNYNYSG (where R is a purine, Y is a pyrimidine, S is a C or G and N is any base) in its own promoter and the promoters of other IE genes to inhibit transcription (348–351, 366). ICP4 then forms a repressive tripartite complex with TBP and TFIIB (367). ICP4, TBP, and TFIIB cooperatively increase each others binding to the ICP4 promoter. TBP binds to the TATA box in the ICP4 promoter with greater affinity in the presence of TFIIB (367). The presence of ICP4 further increases the affinity of TBP for the TATA box (367). Mutants of ICP4 lacking the DNA binding domain are unable to inhibit transcription (368). However, the DNA binding domain of ICP4 is not sufficient to form the tripartite complex, as amino acids 142 to 210 are also necessary (367). Mutants of ICP4 lacking amino acids 142-210 are also unable to inhibit transcription (368). The ICP4 binding site must be located less than 55 amino acids downstream from the TATA box and in the correct orientation in order for tripartite formation and transcription inhibition, suggesting that specific interaction between ICP4 and TBP is required (368, 369).

1.8.3.4 Suggested transcription activation mechanism of ICP4

ICP4 interacts with many components of the TFIID and mediator complexes, and is thus proposed to activate transcription by a 'gene-looping' mechanism (Figure 1.9.) (360). For this model, ICP4 would bind non-specifically to DNA on E or L promoters. ICP4 would recruit TFIID and the mediator complex, and together they would bridge the promoter of the E or L gene to the terminator. Pol II would transcribe the E or L gene as normal. However, Pol II would not diffuse into the nucleus after reaching the terminator element. Instead, it would dissociate from the terminator element only to be immediately recruited back to the promoter, which is close due to the gene looping. ICP4 would thus activate E or L gene transcription by increasing the rate at which Pol II is recycled on HSV-1 promoters.

The gene-looping model suggests that ICP4 must bind DNA to activate transcription. However, E and L promoters contain no specific high-affinity DNA sequences for ICP4. Mutations within the DNA-binding domain often abolish the

activity of ICP4. However, the dimerization domain overlaps the DNA-binding domain, so mutations that prevent DNA-binding often prevent dimerization. A mutant of ICP4 that is unable to bind DNA but retains the ability to dimerize activates transcription, suggesting that dimerization is required for ICP4 activity, not DNA-binding (353).

1.9 Herpesviral chromatin

1.9.1 HSV-1 chromatin

Latent HSV-1 genomes are regularly chromatinized, whereas lytic HSV-1 genomes are not (370). However, H3 is associated with HSV-1 DNA during both latent and lytic infections (316, 334, 371, 372). More recently, HSV-1 genomes were found to be chromatinized during lytic infection, in very dynamic nucleosomes (373). The dynamics of core and linker histones increase in cells infected with wild type HSV-1, consistently with the highly dynamic viral chromatin, too (82, 374, 375). Transcribed cellular genes are more accessible to nuclease digestion than silenced cellular genes, suggesting that transcribed genes are assembled in more dynamic chromatin (105, 376). Lytic HSV-1 genomes, which are transcribed to high levels, are also assembled in more dynamic chromatin than latent HSV-1 genomes, which are mostly silenced.

Histone post-translational modifications regulate the transition between the highly dynamic lytic and the stable latent HSV-1 chromatins. HSV-1 genomes are stably associated with the highest levels of total H3, H3K27me3, or H3K9me3 at early times of lytic infection (before IE gene expression), and with the lowest levels at later times (334). Likewise, most H3K9me3 is stably associated with HSV-1 genomes immediately upon induction of reactivation, and decreases later (377). During latency, the LAT promoter is approximately 7 times more enriched in H3K9K14ac than the silenced ICP0 promoter (378). In the absence of the LAT gene, the LAT promoter is still enriched in H3K9K14ac, suggesting that it is not that transcription of the LAT that induces the histone modifications (372). Acetylated H3 or H3K4me2 stable association with the LAT promoter and gene decreases with

HSV-1 reactivation, whereas the association increases on lytic HSV-1 genes (379, 380).

The knockdown or inhibition of many cellular proteins that add or remove these histone modifications affects the replication efficiency of HSV-1. The knockdown of the HDMT JMJD2 increases the levels of H3K9me3 and total H3 stably associated with IE promoters and reduces HSV-1 gene expression (381). Similarly, levels of H3K9me1, H3K9m2, or total H3 stably associated with the ICP0 promoter increased and HSV-1 gene expression decreased by knockdown or inhibition of the HDMT LSD1 (319). Whereas H3K9 trimethylation is a marker of silent chromatin, H3K4 trimethylation is a marker of active chromatin. Knockdown of HMT Set1 decreased levels of H3K4me3 stably associated with HSV-1 promoters of each kinetic class, and decreased HSV-1 gene expression (323). Knockdown of the HAT CLOCK, which acetylates H3K9 and K14, reduced HSV-1 expression, particularly of E and L genes (382).

Surprisingly, knockdown of the HATs CBP/p300, GCN5, and PCAF did not affect HSV-1 gene expression or replication (318). Knockdown of BRM and Brg1, the ATPase catalytic subunits of the SWI/SNF chromatin remodeling family, did not affect HSV-1 gene expression or replication either (318). All of these proteins were knocked down prior to HSV-1 replication. In the absence of the HATs or the SWI/SNF remodelers, histones may not have been disassembled from nucleosomes on cellular chromatin or assembled in nucleosomes with the incoming HSV-1 genomes. As a result, HSV-1 genomes may have actually been less stably chromatinized in the knockdown cells than in the wild type cells, and thus more accessible to Pol II. Knockdown of SNF2H, the ATPase catalytic subunit of the IWSI chromatin remodeling family, reduced HSV-1 IE gene expression and replication (383).

The H3/H4 chaperone Asf1, which is required for both nucleosome assembly and disassembly, has two isoforms in humans. HIRA preferentially interacts with Asf1a, over Asf1b, to deposit H3.3/H4 dimers in nucleosomes (40). Knockdown of HIRA or Asf1a inhibits HSV-1 gene expression and replication (371, 384). Unstable

chromatinization of HSV-1 genomes may help HSV-1 evade the cellular immune response, such as recognition by the foreign dsDNA sensor IFI16 (385).

1.9.2 Chromatin of other herpesviruses

HSV-1 and the other α-herpesviruses have faster replication cycles than the β- or γ-herpesviruses (approximately 18 hrs for HSV-1, 3 days for HCMV, or 4 to 5 days for EBV). The α-herpesviruses also have more dynamic chromatin than the β- or γ-herpesviruses. The highly dynamic nature of α-herpesvirus chromatin may promote higher levels of transcription and the resulting fast replication cycle.

Like HSV-1, the genomes of the β-herpesviruses HMCV are not chromatinized in the virion, but become chromatinized in the nucleus (386). However, lytic HMCV genomes are in less dynamic chromatin than lytic HSV-1 genomes (386). HCMV replication compartments are also enriched with histones, whereas those of HSV-1 are depleted of histones (374, 386). The major HCMV transcription regulator IE1 promotes histone acetylation by antagonizing HDAC3 (387). In the absence of functional IE1, HCMV genomes are more stably associated in nucleosomes (388).

The genomes of the γ-herpesvirus EBV are also chromatinized during latent and lytic infections (389, 390). During lytic infection, however, EBV genomes are assembled in more dynamic chromatin (389, 390). The transition between latent and lytic EBV appears to be modulated by histone modifications (391). However, there is no significant difference in the amount of total H3 stably associated with EBV genomes during lytic or latent infection, and lytic EBV genomes are stably associated with more H3 than lytic HSV-1 genomes (323, 391). Likewise, there is no significant difference in the amount of H3 stably associated with the genomes of another γ-herpesvirus KSHV during lytic or latent infections (392).

Herpesviruses have evolved different mechanisms to prevent the stable chromatinization of their genomes. As a result, the herpesvirus chromatin is more dynamic than the cellular chromatin. However, the α-herpesvirus chromatin is even more dynamic than the β- or γ-herpesvirus chromatin. The stable chromatinization of viral genomes is expected to prevent viral gene expression and replication. Consistent with this idea, the α-herpesviruses replicate faster than the β- or γ-

herpesviruses. The mechanisms by which α-herpesvirus chromatin is maintained in a dynamic state are not yet fully known. However, α-herpesviruses are the only herpesviruses to encode homologs of ICP4, which is the only critical HSV-1 transcription activator, and whose mechanisms of action are not known.

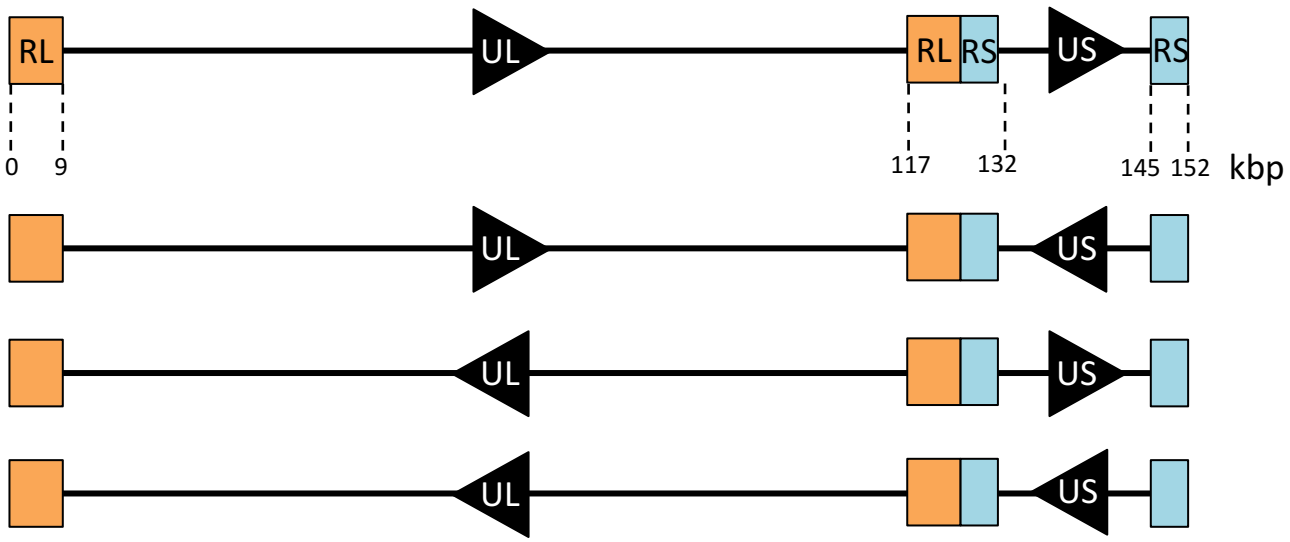

Figure 1.1. Schematic of the four isomers of the HSV-1 genomes resulting from homologous recombination of the repeat regions. RL, repeat long region; RS, repeat short region; UL, unique long region, US, unique short region.

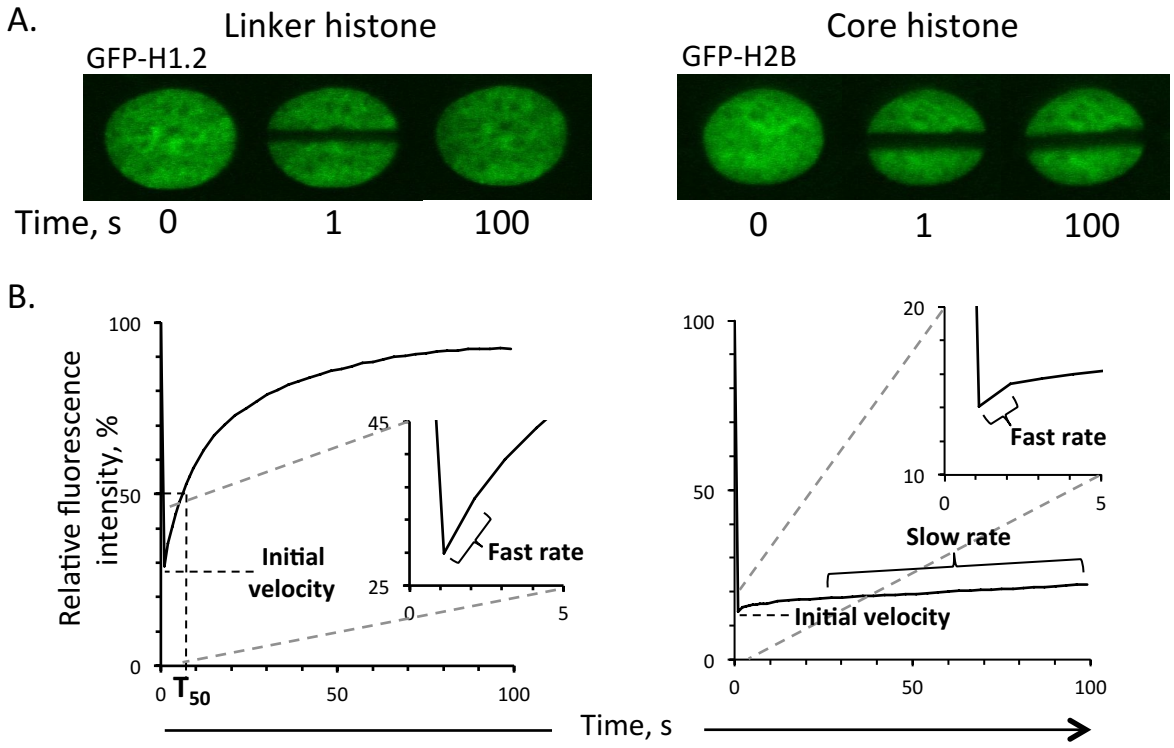

Figure 1.2. FRAP of linker and core histones. A. Fluorescent micrograph images of nuclei expressing GFP-H1.2 or GFP-H2B immediately before photobleaching (T = 0 s), immediately after photobleaching (T = 1 s), and 100 seconds after photobleaching (T = 100 s). B. Average fluorescence recovery curves of GFP-H1.2 or GFP-H2B. The relative fluorescence at T = 0 s is set as 100%. The relative fluorescence at each time point is then normalized to the relative fluorescence at T = 0 s. The relative fluorescence at T = 1 s is a surrogate measure for the histones in the free pool. The fast rate, used as a surrogate measure for the population of histones dynamically assembled in chromatin, is measured by the slope of fluorescence recovery between the first two time points after photobleaching. The time required to regain 50% of the initial fluorescence, T_{50}, is a surrogate measure for the population of linker histones assembled in less dynamic chromatin. The slow rate, used as a surrogate measure for the population of core histone assembled in less dynamic chromatin, is measured by the slope of fluorescence recovery between 25 and 100 s after photobleaching.

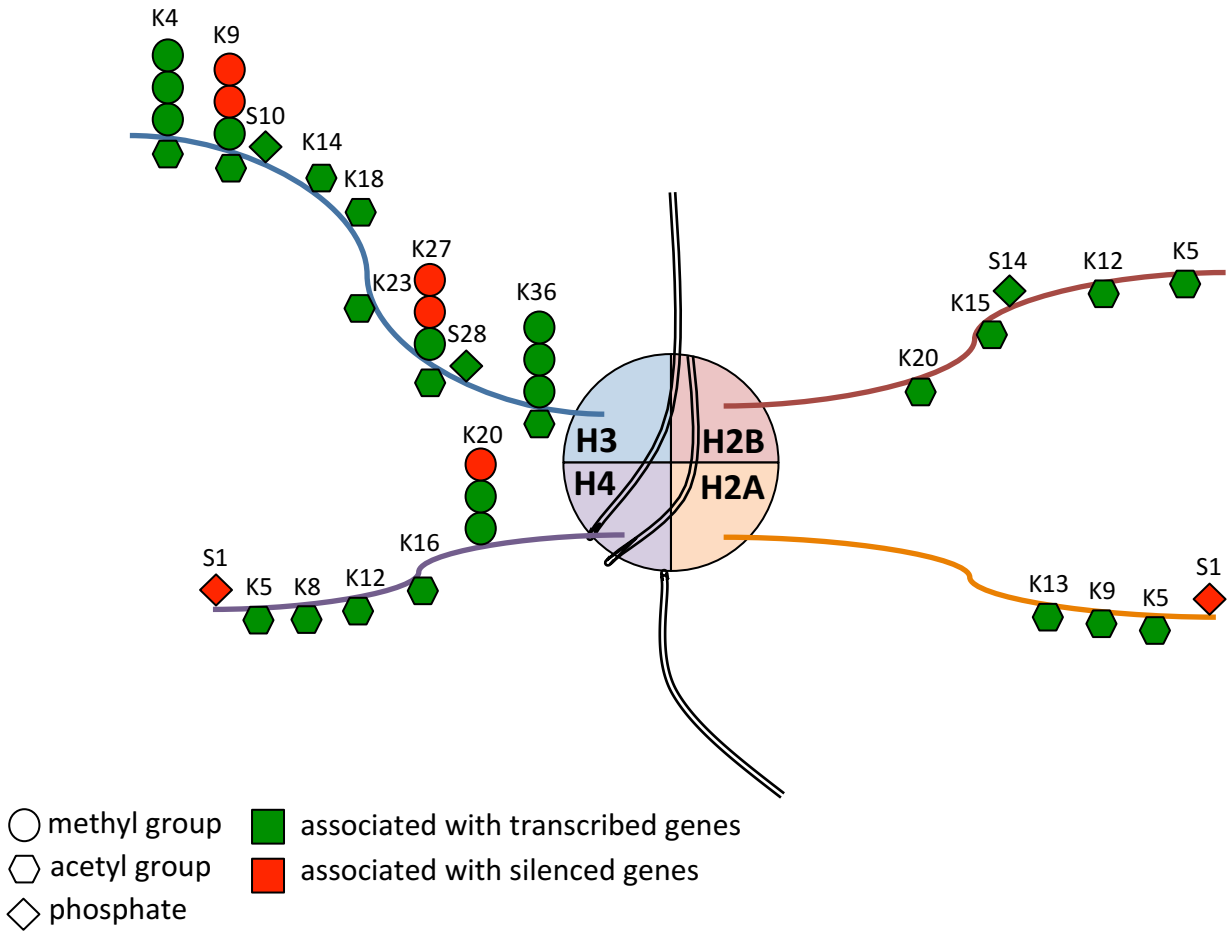

Figure 1.3. Schematic of the phosphorylation, acetylation, and lysine methylation sites of the core histone N-terminal tails that are associated with transcribed or silenced genes. K, lysine residue; S, serine residue.

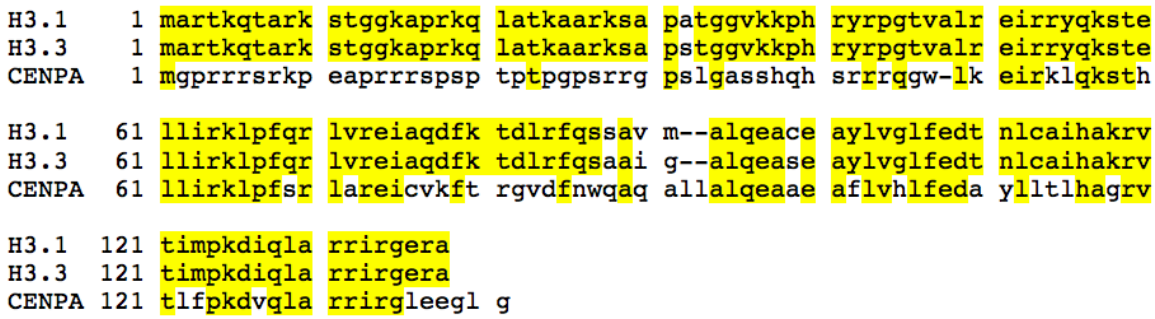

Figure 1.4. Amino acid sequence comparison of H3.1, H3.3, and CENP-A. Yellow highlight, homology to the canonical (H3.1) sequence.

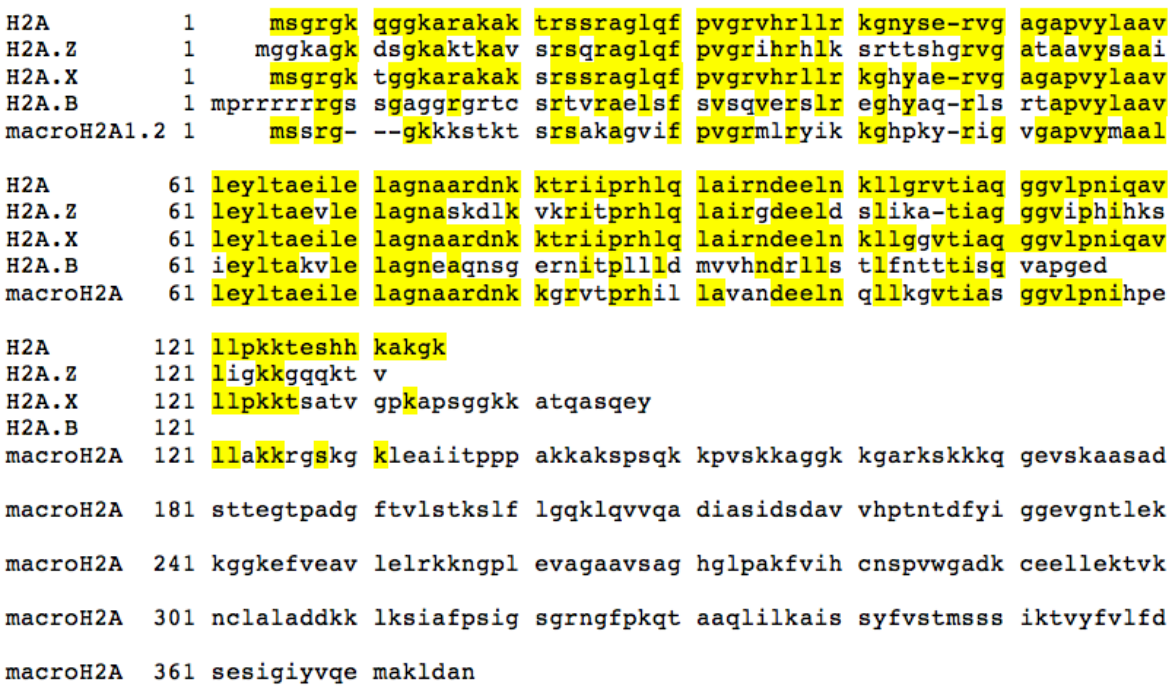

Figure 1.5. Amino acid sequence comparison of H2A variants. Yellow highlight, homology to the canonical (H2A) sequence.

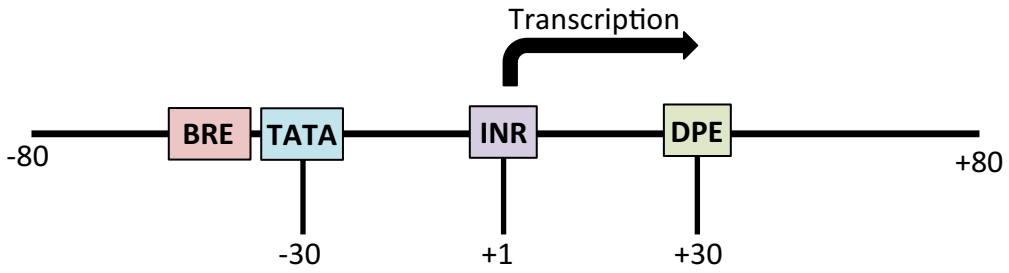

Element	Consensus Sequence
TATA-8	TATA(A/T)A(A/T)(A/G)
TATA-532	(A/T/C)(A/T)(A/T/C)(A/T)(A/T)(A/T)(A/T)(A/G)
INR	(C/T)(C/T)AN(A/T)(C/T)(C/T)
BRE	(G/C)(G/C)(A/G)CGCC
DPE	(A/G)G(A/T)CGTG

Figure 1.6. Schematic of the cellular core promoter elements. A, adenosine; T, thymidine; G, guanosine; C, cytosine; N, any nucleotide.

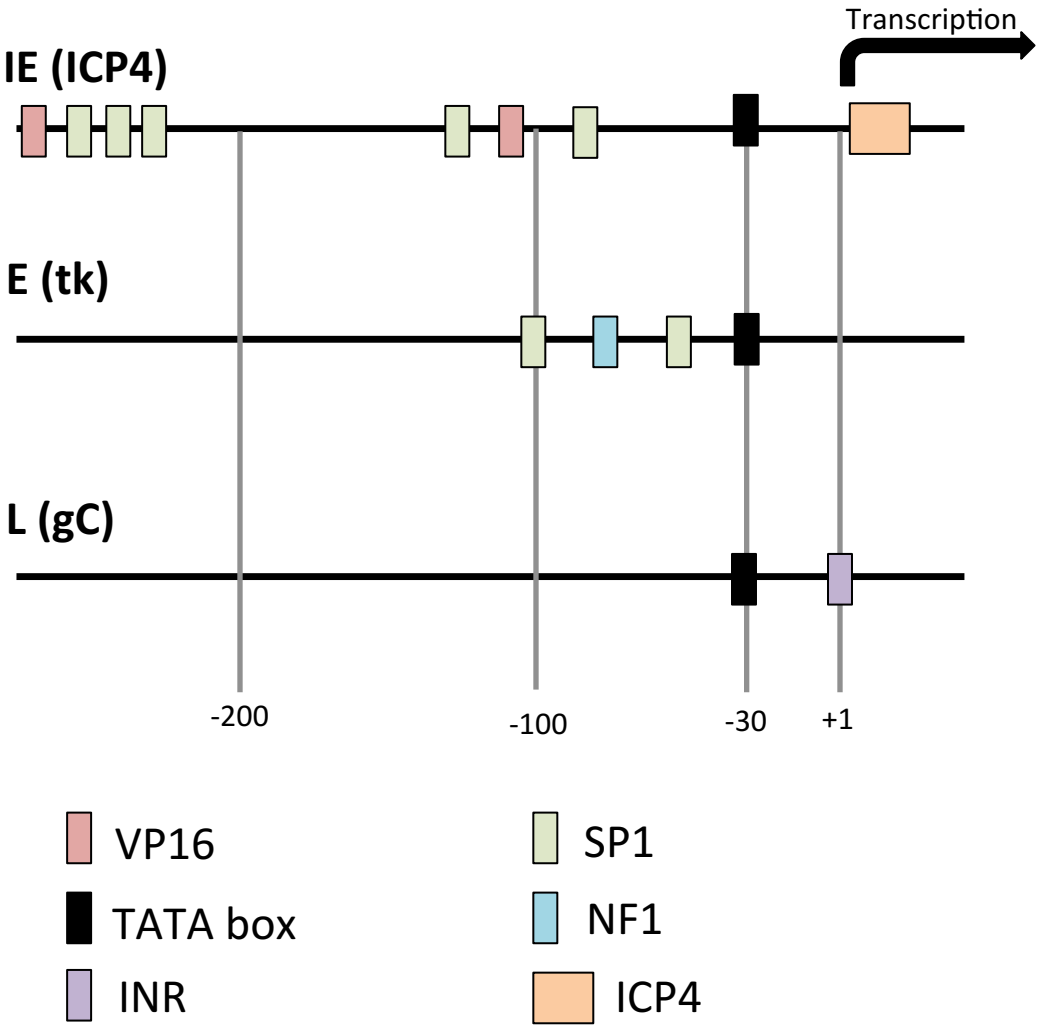

Figure 1.7. Schematic of representative promoters of HSV-1 genes of each class. IE, immediate-early; E, early; L, late.

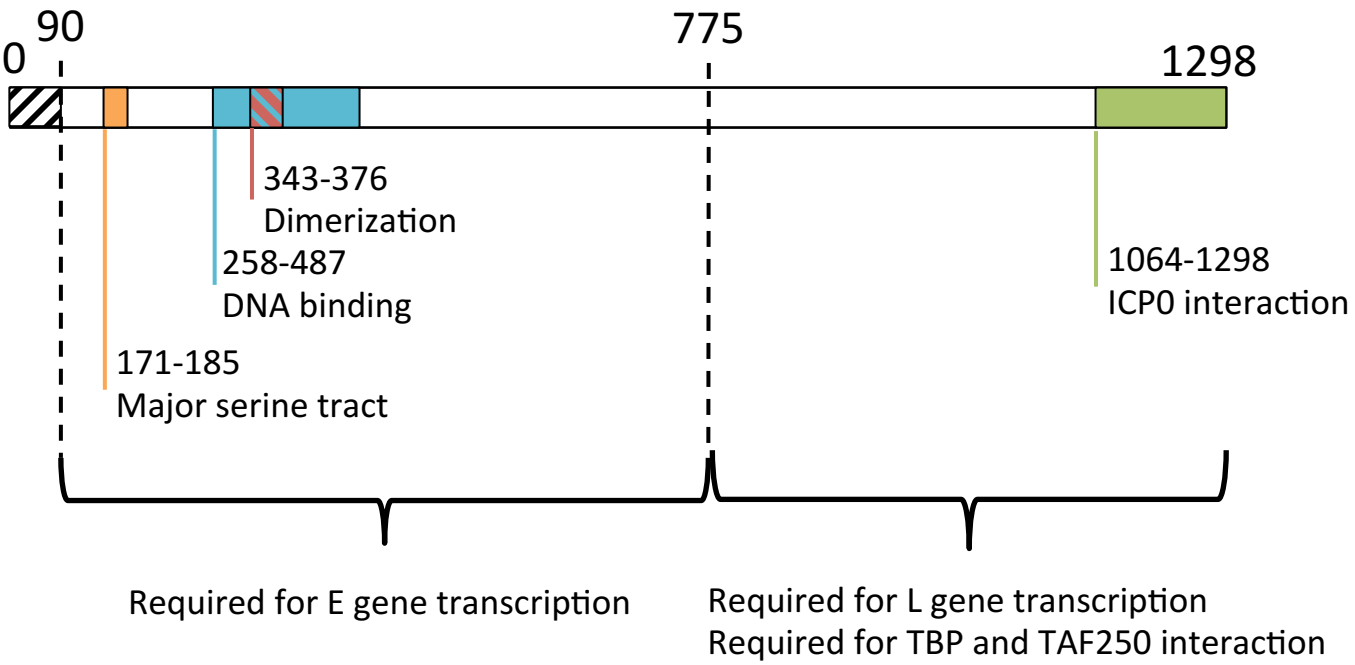

Figure 1.8. Schematic of the mapped domains of ICP4. The N-terminal 90 amino acids of ICP4 are not required for activity. The N-terminal 775 amino acids can activate early, but not late, gene expression.

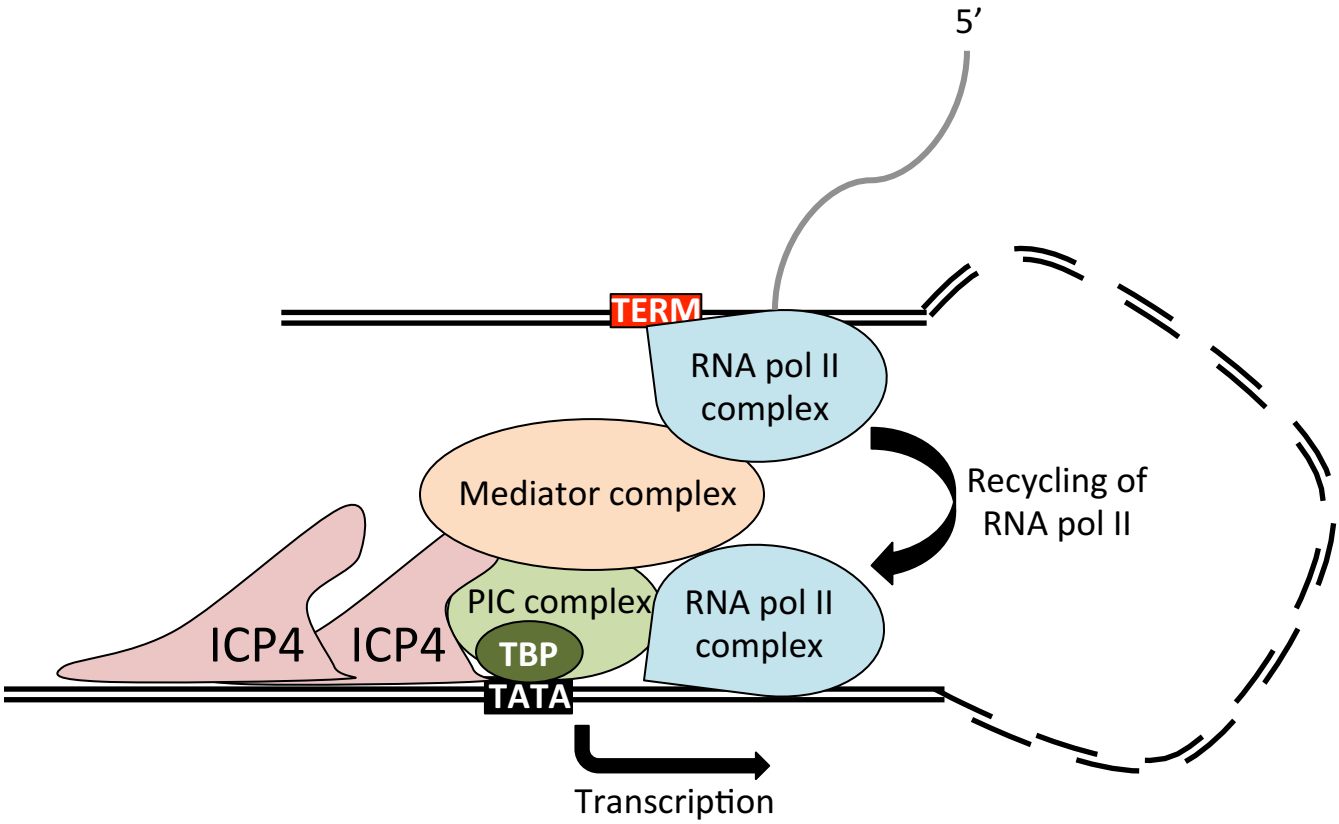

Figure 1.9. Schematic of the gene looping model by which ICP4 is suggested to activate transcription.

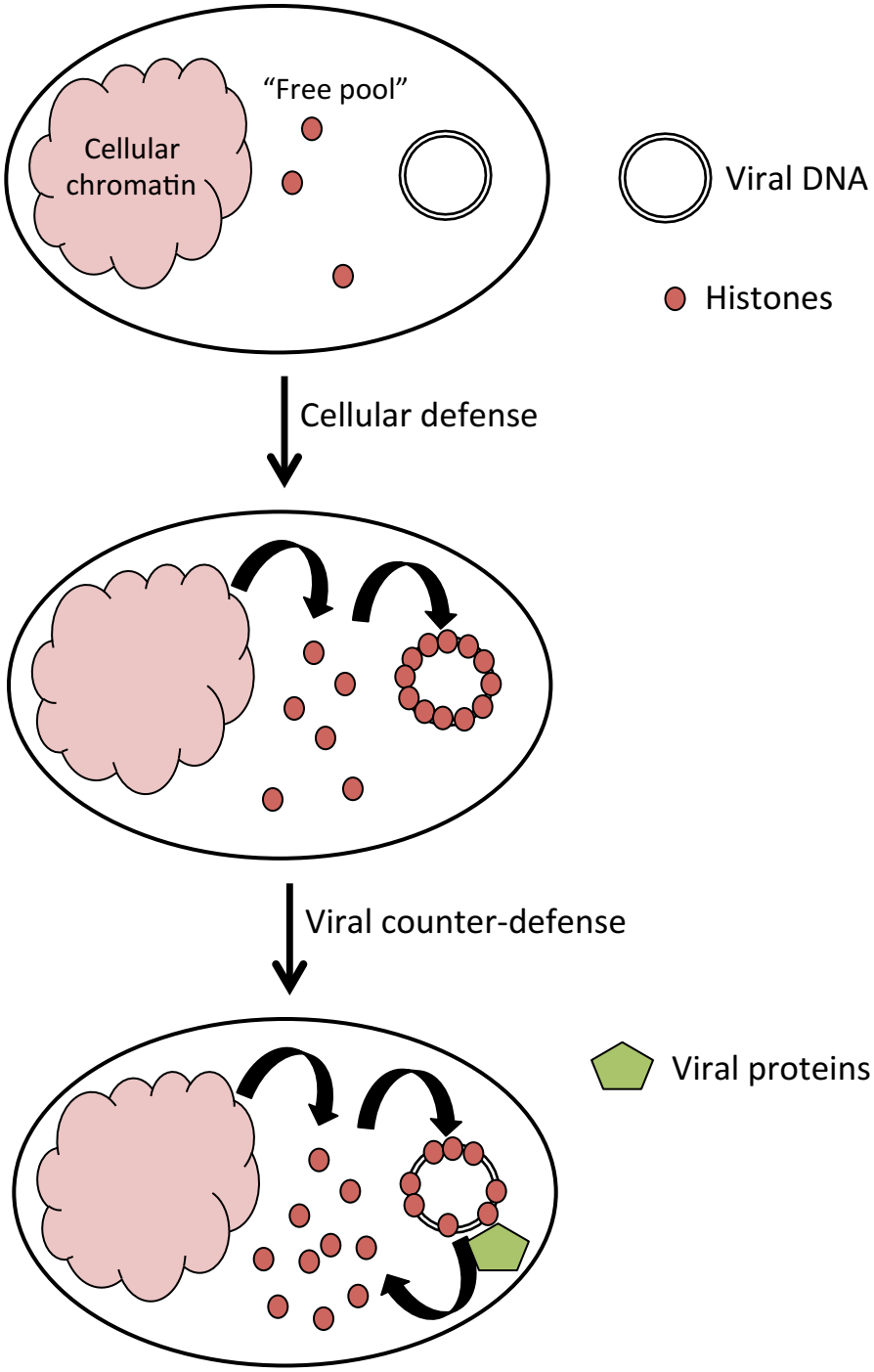

Figure 1.10. Model of the chromatinization of viral genomes. Viral genomes enter the nucleus free of histones. A cellular defense mechanism chromatinizes viral genomes to silence viral gene expression. To counteract silencing, viruses have evolved specific proteins that prevent or disrupt the stable chromatinization of viral genomes.

Chapter 2: Methods and materials

2.1 Centrifuges

A Beckman Coulter Avanti J-E centrifuge with a fixed angle JA-14 rotor (JA-14) was used for viral stock preparation. An Eppendorf centrifuge 5810R with an A-4-62 swinging bucket rotor (A-4-62) or a GE035 fixed angle rotor (GE035), or a Beckman Coulter microfuge 18 (cat# 367160) were used for all other experiments.

2.2 Cells, drugs, and reagents

African green monkey kidney Vero cells (CCL-81, ATCC, distributed by Cedarlane Laboratories Ltd., ON, CA) and n33 cells (a generous gift from the late Dr. P. Schaffer, University of Pennsylvania, Philadelphia, PA, USA), which express complementing levels of HSV-2 ICP4 from a Vero background, were maintained in Dulbecco's modified minimum Eagle's medium (DMEM, cat# 11885, Invitrogen, Burlington, ON, CA) supplemented with 5% fetal bovine serum (FBS, cat# A15-70, PAA Laboraties Inc., Etobicoke, ON, CA) at 37˚C in 5% CO_2. Human osteosarcoma U2OS cells (a generous gift from Dr. J. Smiley, University of Alberta, Edmonton, AB, CA) were maintained in DMEM supplemented with 10% FBS at 37˚C in 5% CO_2. Human embryonic kidney cells expressing the simian virus 40 (SV40) T antigen (293T) were maintained in DMEM supplemented with 10% FBS at 37˚C in 5% CO_2. Human cervical cancer HeLa cells (CCL-2, ATCC, distributed by Cedarlane Laboratories Ltd., ON, CA) were maintained in DMEM supplemented with 10% FBS at 37˚C in 5% CO_2

Kanamycin (Kan, cat# K0254, Sigma-Aldrich, Oakville, ON, CA) was stored as a stock of 50 mg/mL at 4˚C and used at a concentration of 50 µg/mL. Ampicillin (Amp, cat# 11593-027, Invitrogen, Burlington, ON, CA) was diluted in autoclaved milliQ water as a 100 mg/mL stock, sterilized through a 0.22 µm filter, and stored at -20˚C. Geneticin (cat# 11811031, Gibco, Waltham, MA, USA) was diluted in autoclaved milliQ water as a 200 mg/mL stock, sterilized through a 0.22 µm filter, and stored at -20˚C.

2.3 Viruses and virus stock preparation

HSV-1 KOS, n12, n212 (Dr. P. Schaffer, University of Pennsylvania, Phildelphia, PA, USA) and KM110 (Dr. J. Smiley, University of Alberta, Edmonton, Alberta, CA) are described (361, 393–395).

Four million Vero cells were seeded in T-150 flasks to approximately 50% confluency. Cells were inoculated with 0.1 plaque forming units (PFU) of KOS in 3 mL of 4˚C serum free media for 1 h at 37˚C in 5% CO2, rocking and rotating every 10 min. Inocula was vacuumed off and the cells were rinsed twice with 10 mL of 4˚C PBS (150 mM NaCl, l mM KH_2PO_4, 3 mM Na_2HPO_4, pH 7.4). Twelve mL of 37˚C DMEM supplemented with 10% FBS was then added and the cells were incubated at 33˚C in 5% CO2 for approximately 48 h, or until 100% cytopathic effect (CPE) was observed. The media was removed and placed in 50 mL conical tubes on ice. Attached cells were removed with a cell scraper, rinsed with 5 mL of 4˚C serum free media, and added to the 50 mL conical tubes. Cells were pelleted in the A-4-62 rotor at 3,200xg for 30 min at 4˚C. The supernatant containing the extracellular virions was removed, placed in new 50 mL conical tubes, and pelleted in the JA-14 rotor at 10,000xg for 2 h at 4˚C. The pellet containing the intracellular virions was resuspended in 100 µL of serum free DMEM. The resuspended pellet was frozen and thawed three times in a dry-ice ethanol bath and a 37˚C water bath, then sonicated three times for 30 sec each with 30 sec intervals. Cellular debris was pelleted in the A-4-62 rotor at 3,200xg for 30 min at 4˚C. Intracellular and extracellular virions were combined and stored in 100 µL aliquots at -80˚C. Titre was determined by plaque assays on Vero cells.

Preparation for n212 and KM110 stocks were similar to preparation of KOS, expect for that U2OS cells were used. Titre was determined by plaque assay on U2OS cells. Preparation for n12 used n33 cells. Titre was determined by plaque assay on n33 cells.

2.4 Plaque assay

Two hundred thousand cells were seeded in 6-well plates and incubated for 4 h at 37˚C in 5% CO_2. HSV-1 stocks were serially diluted in 15 mL snap-cap tubes. First, 3

µL of stock was added to 297 µL of serum free DMEM for a 100-fold dilution (10^{-2}). Thirty µL was then removed and added to 270 µL of serum free DMEM for a 1000-fold dilution (10^{-3}). Thirty µL was then removed from the 10^{-3} dilution and added to 270 µL of serum free DMEM for a 10000-fold dilution (10^{-4}), and so on, for a total of six 10-fold dilutions, from 10^{-2} to 10^{-7}. Media was vacuumed off from the seeded cells, and 200 µL of each dilution was added to separate wells. The 6-well plate was rocked so that the inoculum covered the entire bottom of the plate, and the wells were incubated for 1 h at 37˚C in 5% CO_2 rocking and rotating every 10 min. Inoculum was vacuumed off, the cell monolayer was rinsed with 4˚C PBS, and then overlaid with 2-3 mL of 37˚C 0.5% methylcellulose in DMEM supplemented with 10% FBS. Cells were incubated at 37˚C in 5% CO_2 for 2-3 days until plaques became visible. Crystal violet (1 g CV per 100 mL of 17% [v/v] methanol in water) was added to the cells, and plates were incubated at room temperature overnight. Crystal violet was washed off gently in room temperature water, plates were air dried, and plaques were counted.

2.5 Plasmids

2.5.1 Green fluorescent protein (GFP)-H1.1 expression plasmid

The plasmid encoding GFP-H1.1 was a generous gift from Dr. M. Hendzel, University of Alberta, Edmonton, Alberta, CA, and has been described previously (Th'ng, Sung, Ye, and Hendzel, 2005). The DNA sequence encoding the human H1.1 gene was amplified from human neuroblastoma (SK-N-SH) DNA by polymerase chain reaction (PCR), and ligated in frame into the BglII and BamHI restriction sites of the pEGFP-C1 vector (Clontech, Mountain View, CA, USA).

2.5.2 GFP-H3.3 expression plasmid

The plasmid encoding GFP-H3.3 was a generous gift from Dr. J. Th'ng, Northern Ontario School of Medicine, Thunder Bay, ON, CA. The DNA sequence encoding H3.3 was ligated in frame into the BglII and EcoRI restriction sites of the pEGFP-C1 vector (Clontech, Mountain View, CA, USA)..

2.5.3 GFP-H2A.Za and GFP-H2A.Zv expression plasmids

The plasmids expressing GFP-H2A.Za and GFP-H2A.Zv were generous gifts from Dr. J. Ausio, University of Victoria, Victoria, BC, CA. The DNA sequences encoding H2A.Za or H2A.Zv were ligated in frame into the KpnI and BamHI restriction sites of the pEGFP-N1 vector (Clontech, Mountain View, CA, USA).

2.5.4 GFP-H2A, GFP-H2B, GFP-H3.1 and GFP-H4 expression plasmids

GFP-H2A, GFP-H2B, GFP-H3.1 and GFP-H4 were constructed by Dr. K. Conn. Briefly, the DNA sequences encoding these histones were obtained from the Riken Mouse cDNA Library. The amplified DNA encoding the sequences for H2B or H4 were ligated in frame with the BglII and PstI restriction digest sites of pEGFP-C1 (Clontech). The amplified DNA encoding the sequences for H2A was ligated in frame with the BglII and SalI restriction digest sites of pEGFP-C1.

2.5.5 GFP-H2A.B expression plasmid

The DNA sequence encoding H2A.B was amplified from a plasmid generously given by Dr. Vasily Ogryzko (Institut Gustave Roussy, Villejuif, France) using the primers H2A.B F and H2A.B R (Table 1). The PCR conditions were as follows; 0.3 μM of each primer, 100 ng template, 0.3 mM dNTP, 0.5 U Platinum pfx polymerase (cat# 11708013, Invitrogen, Burlington, ON, CA), 0.5 mM $MgSO_4$ in 1X amplification buffer (200 mM Tris-HCl [pH 8.8], 100 mM $(NH_4)_2SO_4$, 100 mM KCl, 1% [v/v] Triton X-100, 1 mg/mL BSA). The reaction was incubated for 5 min at 96˚C, followed by 20 cycles of 1 min at 96˚C, 45 s at 52-60˚C, and 1.5 min at 68˚C, and a final extension of 5 min at 68˚C.

The resulting PCR fragment and the pEGFP-C1 vector (Clontech) were digested with 30 U of BglII (cat# R0144S, New England Biolabs, Ipswich, MA, USA) and 30 U of PstI (cat# R0140S, New England Biolabs, Ipswich, MA, USA) in 1X NEBuffer3.1 (100 mM NaCl, 50 mM Tris-HCl [pH 7.9], 10 mM MgCl2, 100 μg/ml BSA) for 3 h at 37˚C. The digested DNAs were extracted with an equal volume of chloroform. DNA was precipitated with 3 volumes of ethanol for 30 min at -20˚C, and pelleted at 16,000xg for 30 min at 4˚C in the GE035 rotor. The resuspended

double digested DNA was resolved on a 1% agarose gel in 1X TAE and then purified using the Gel Extraction Kit (cat# 28704, Qiagen, Toronto, ON, CA) as per the manufacturer's instructions. The double digested H2A.B PCR product was ligated with the double digested pEGFP-C1 vector with 200 U of T4 DNA ligase (cat# M0202S, New England Biolabs, Ipswich, MA, USA) in 1X T4 ligase buffer (50 mM Tris-HCl [pH 7.5], 10 mM $MgCl_2$, 1 mM ATP, 10 mM DTT) at RT overnight. The resulting ligation product was used to transform DH5α Competent E.coli cells (See 2.7 for complete details). Sequencing was performed by The Applied Genomics Core (TAGC, University of Alberta, AB, CA).

2.5.6 GFP-macroH2A expression plasmid

The DNA sequence encoding human macroH2A.2 was amplified from a plasmid generously given by Dr. Vasily Ogryzko using the primers macroH2A F and macroH2A R (Table 1). The PCR conditions were as follows; 0.3 μM of each primer, 100 ng template, 0.3 mM dNTP, 0.5 U Platinum pfx polymerase (cat# 11708013, Invitrogen, Burlington, ON, CA), 1.5 mM $MgSO_4$ in 1X amplification buffer (200 mM Tris-HCl [pH 8.8], 100 mM $(NH_4)_2SO_4$, 100 mM KCl, 1% [v/v] Triton X-100, 1 mg/mL BSA). The reaction was incubated for 5 min at 96˚C, followed by 20 cycles of 1 min at 96˚C, 45 s at 52-60˚C, and 1.5 min at 68˚C, and a final extension of 5 min at 68˚C.

The resulting PCR fragment and the pEGFP-C1 vector were digested with 30 U of BglII (cat# R0144S, New England Biolabs, Ipswich, MA, USA) and 30 U of PstI (cat# R0140S, New England Biolabs, Ipswich, MA, USA) in 1X NEBuffer3.1 (100 mM NaCl, 50 mM Tris-HCl [pH 7.9], 10 mM MgCl2, 100 μg/ml BSA) for 3 h at 37˚C. The digested DNAs were extracted with an equal volume of chloroform. DNA was precipitated with 3 volumes of ethanol for 30 min at -20˚C, and pelleted at 16,000xg for 30 min at 4˚C in the GE035 rotor. The resuspended double digested DNA was resolved on a 1% agarose gel in 1X TAE and then purified using the Gel Extraction Kit (cat# 28704, Qiagen, Toronto, ON, CA) as per the manufacturer's instructions. The double digested H2A.B PCR product was ligated with the double digested pEGFP-C1 vector with 200 U of T4 DNA ligase (cat# M0202S, New England Biolabs, Ipswich, MA, USA) in 1X T4 ligase buffer (50 mM Tris-HCl [pH 7.5], 10 mM $MgCl_2$, 1

mM ATP, 10 mM DTT) at RT overnight. The resulting ligation product was used to transform DH5α Competent E.coli cells (See 2.7 for complete details). Sequencing was performed by The Applied Genomics Core (TAGC, University of Alberta, AB, CA).

2.5.7 RFP-ICP4 expression plasmid

The SapI digestion sites of the pmCherry-C1 vector were mutated using the Quikchange Lightning Multi Site-Directed Mutagenesis Kit (cat# 210515, Agilent Technologies, Santa Clara, CA, USA), as per the manufacturer's instructions. Briefly, 50 ng of the pmCherry-C1 vector was amplified with 100 ng of each of the primers SapI 1 and SapI 2. The reaction was incubated for 2 min at 95˚C, followed by 30 cycles of 20 s at 95˚C, 30 s at 55˚C, and 2.5 min at 65˚C, and a final extension of 5 min at 65˚C. The amplified DNA was incubated with 10 U of DpnI for 5 min at 37˚C. One and a half µL of Dpn-I digested DNA was added to 45 µL of Ultracompetent XL-Gold cells in a snap cap tube. After a 30 min incubation on ice, the cells were incubated for 30 sec at 42˚C. Mutated plasmids were detected by digestion with SapI (cat# R0569S, New England Biolabs, Ipswich, MA, USA).

The amino-terminal 2300 base pairs of ICP4 were amplified from HSV-1 DNA using primers ICP4 F and ICP4 mid R (Table 1). The PCR conditions were as follows; 0.3 µM of each primer, 100 ng template, 0.3 mM dNTP, 10% glycerol, 0.5 U Platinum pfx polymerase (cat# 11708013, Invitrogen, Burlington, ON, CA), 0.5 mM $MgSO_4$ in 1X amplification buffer (200 mM Tris-HCl [pH 8.8], 100 mM $(NH_4)_2SO_4$, 100 mM KCl, 1% [v/v] Triton X-100, 1 mg/mL BSA). The reaction was incubated for 5 min at 96˚C, followed by 20 cycles of 1 min at 96˚C, 45 sec at 65-68˚C, and 5 min at 68˚C, and a final extension of 5 min at 68˚C. The PCR reaction was resolved in 1% low melting point (LMP) agarose in 1X TAE buffer (40 mM tris, 20 mM acetic acid, 1 mM EDTA). The region of the gel containing the desired fragment was excised, and the DNA was purified from the gel using phenol:chloroform extraction (Detailed protocol at 2.6). The purified PCR product or SapI mutated pmCherry-C1 vector were digested with 10 U of BglII (cat# ER0082, Invitrogen, Burlington, ON, CA) and 10 U of EcoRI (cat# ER0271, Invitrogen, Burlington, ON, CA) in 1X of REact3 buffer (50 mM Tris-HCl [pH 8.0], 10 mM $MgCl_2$, 100 mM NaCl) for 3 h at 37˚C. Digested

DNA was resolved in 1% LMP agarose, and purified using phenol:chloroform extraction. The double digested PCR product was ligated with the double digested vector with 1U of T4 DNA ligase (cat# 15224017, Invitrogen, Burlington, ON, CA) in 1X T4 ligase buffer (40 mM Tris-HCl [pH 7.8], 10 mM MgCl2, 0.5 mM ATP, 10 mM DTT) at RT overnight. The resulting ligation product was used to transform competent *dam-/dcm-* cells (See 2.7 for more details).

The carboxy-terminal 1800 base pairs of ICP4 were amplified from HSV-1 DNA using primers ICP4 mid F and ICP4 R (Table 1). The PCR conditions were as follows; 0.3 µM of each primer, 100 ng template, 0.3 mM dNTP, 10% glycerol, 0.5 U Platinum pfx polymerase (cat# 11708013, Invitrogen, Burlington, ON, CA), 1.0 mM $MgSO_4$ in 1X amplification buffer (200 mM Tris-HCl [pH 8.8], 100 mM $(NH_4)_2SO_4$, 100 mM KCl, 1% [v/v] Triton X-100, 1 mg/mL BSA). The reaction was incubated for 5 min at 96˚C, followed by 20 cycles of 1 min at 96˚C, 1 min at 60-68˚C, and 2 min at 68˚C, and a final extension of 5 min at 68˚C. The PCR reaction was resolved in 1% LMP agarose in 1X TAE buffer (40 mM tris, 20 mM acetic acid, 1 mM EDTA). The region of the gel containing the desired fragment was excised, and the DNA was purified from the gel using phenol:chloroform extraction. The purified PCR product or the pmCherry-C1 vector containing the N-terminus of ICP4 (pmCherry-N) were digested with 10 U of XbaI (cat# ER0681, Invitrogen, Burlington, ON, CA) and 30 U of SapI (cat# R0569S, New England Biolabs, Ipswich, MA, USA) in 1X of NEBuffer4.1 (20 mM tris-acetate [pH 7.9], 50 mM potassium acetate, 10 mM magnesium acetate, 1 mM DTT) for 2 h at 37˚C. Digested DNA was resolved in 1% LMP agarose, and purified using phenol:chloroform extraction. The double digested PCR product was ligated with the double digested vector with 1U of T4 DNA ligase (cat# 15224017, Invitrogen, Burlington, ON, CA) in 1X T4 ligase buffer (40 mM Tris-HCl [pH 7.8], 10 mM MgCl2, 0.5 mM ATP, 10 mM DTT) at RT overnight. The resulting ligation product was used to transform competent *dam-/dcm-* cells (See 2.7 for more details). Sequencing was performed by The Applied Genomics Core (TAGC, University of Alberta, AB, CA).

2.5.8 RFP-n12 expression plasmid

The amino-terminal 753 base pairs of ICP4, corresponding to the sequences before the stop codon introduced in HSV-1 mutant n12, were amplified from the RFP-ICP4 expression plasmid using primers ICP4 F and n12 R. The PCR conditions were as follows; 0.3 µM of each primer, 100 ng template, 0.3 mM dNTP, 10% glycerol, 0.5 U Platinum pfx polymerase (cat# 11708013, Invitrogen, Burlington, ON, CA), 1.0 mM $MgSO_4$ in 1X amplification buffer (200 mM Tris-HCl [pH 8.8], 100 mM $(NH_4)_2SO_4$, 100 mM KCl, 1% [v/v] Triton X-100, 1 mg/mL BSA). The reaction was incubated for 5 min at 96˚C, followed by 20 cycles of 1 min at 96˚C, 1 min at 66˚C, and 1 min at 68˚C, and a final extension of 5 min at 68˚C.

The resulting PCR fragment and the pmCherry-c1 vector (Clontech) were digested with 30 U of BglII (cat# R0144S, New England Biolabs, Ipswich, MA, USA) and 30 U of XbaI (cat# R0145S, New England Biolabs, Ipswich, MA, USA) in 1X NEBuffer3.1 (100 mM NaCl, 50 mM Tris-HCl [pH 7.9], 10 mM MgCl2, 100 µg/ml BSA) for 1 h at 37˚C. The digested DNAs were extracted once by an equal volume of phenol:chloroform 1:1, and twice by an equal volume of chloroform. DNA was precipitated with an equal volume of isopropanol for 30 min at -20˚C, and pelleted at 16,000xg for 30 min at 4˚C in the GE035 rotor. The resuspended digested PCR product was ligated with the resuspended digested pmCherry-C1 vector with 1U of T4 DNA ligase (cat# 15224017, Invitrogen, Burlington, ON, CA) in 1X T4 ligase buffer (40 mM Tris-HCl [pH 7.8], 10 mM MgCl2, 0.5 mM ATP, 10 mM DTT) at RT overnight. The resulting ligation product was used to transform competent DH5α cells (See 2.7 for more details).

2.6 Extraction and purification of DNA from agarose gel

The slice of 1% low melting point agarose gel containing the DNA of interest was excised and weighed in a sterile 1.5 mL Eppendorf. One µL of UltraPure buffer-saturated phenol (cat# 15513-047, Invitrogen, Burlington, ON, CA) per each µg of gel was added to the Eppendorf. The samples were subjected to three freeze and thaw cycles at -20˚C and at room temperature. Following the final thaw, the samples were centrifuged at 16,000xg for 30 min at 4˚C in the GE035 rotor. The

aqueous layer was extracted three times with chloroform. DNA was precipitated by adding an equal volume of 2-proponal and incubating at -20˚C for a minimum of 30 min. DNA was pelleted by centrifugion at 16,000xg for 30 min at 4˚C in the GE035 rotor. The supernatant was removed, and the pellet was rinsed with -20˚C 70% ethanol. The pellet was air-dried at room temperature before being resuspended in autoclaved milliQ water.

2.7 Transformations

Subcloning efficiency DH5α competent cells (cat# 18265-017, Invitrogen, Burlington, ON, CA) were thawed on ice and 50 µL was transferred to a 15 mL snap cap tube. Fifty ng (in no more than 5 µL) plasmid DNA was added to cells, and incubated on ice for 30 min with occasional gentle tapping. The sample was heated at 42˚C for exactly 20 sec, and returned to ice for 2 min, after which 950 µL of 37˚C SOC media (2% [w/v] tryptone, 0.5% [w/v] yeast extract, 10 mM NaCl, 2.5 mM KCl, 10 mM $MgCl_2$, 20 mM glucose, pH 7.4) was added. The sample was incubated for 1 h with shaking at 220 rpm at 37˚C. One hundred and fifty µL of the culture was spread on SOC agar plates containing 50 µg/mL Kan. The plates were incubated at 37˚C overnight or until a desirable number of colonies were visible. Selected colonies were inoculated into 3 mL of LB media (10 g tryptone, 5 g yeast extract, 10 g NaCl in 1 L of water; pH 7.4) containing 50 µg/mL Kan and incubated for 17 h at 37˚C shaking at 220 rpm. Plasmid DNA was purified from the resulting culture using the QIAprep Spin Miniprep Kit (cat# 27104, Qiagen, Germantown, MD, USA) as per the manufacturer's instructions.

For generation of plasmids without DNA methylation, which can block the activity of certain restriction enzymes, *dam-/dcm-* competent cells (cat# C2925I, NEB, Ipswich, MA, USA) were thawed on ice and 50 µL was transferred to a 15 mL snap cap tube. Fifty ng (in no more than 5 µL) plasmid DNA was added to cells, and incubated on ice for 30 min with occasional gentle tapping. The sample was heated at 42˚C for exactly 30 sec, and returned to ice for 5 min, after which 950 µL of 37˚C SOC media was added. The sample was incubated for 1 hour with shaking at 220 rpm at 37˚C. One hundred and fifty µL of the culture was spread on SOC agar plates

containing 50 μg/mL Kan. The plates were incubated at 37˚C overnight or until a desirable number of colonies were visible. Selected colonies were inoculated into 3 mL of LB media containing 50 μg/mL Kan and incubated for 17 h at 37˚C shaking at 220 rpm. Plasmid DNA was purified from the resulting culture using the QIAprep Spin Miniprep Kit (cat# 27104, Qiagen, Germantown, MD, USA) as per the manufacturer's instructions.

2.8 Preparation of plasmid DNA by alkaline lysis midiprep

Plasmid DNA was purified from transformed E.Coli essentially as in Molecular Cloning 3rd edition by Sambrook and Russell (Protocol 2: Preparation of Plasmid DNA by Alkaline Lysis with SDS: Midiprep).

Forty mL of LB media (10 g tryptone, 5 g yeast extract, 10 g NaCl in 1 L of water; pH 7.4) containing 50 μg/mL or 100 μg/mL of Kan or Amp, respectively, in a 250 mL Erlenmeyer flask was inoculated with transformed bacteria using a sterile pipette tip, and shaken at 220 rpm at 37˚C for 17 h. The resulting culture was separated into 4 equal parts in 15 mL snap cap tubes and the bacteria were pelleted by centrifugation at 3,200xg for 10 min at 4˚C in the A-4-64 rotor. The supernatant was removed and pellets were resuspended in 200 μL of 4˚C alkaline lysis buffer 1 (50 mM glucose, 25 mM Tris [pH 8.0], 10 mM EDTA [pH 8.0]) containing 0.1 mg/mL of ribonuclease A (cat# R-4642, Sigma-Aldrich, Oakville, ON, CA). The resuspended pellet was transferred to a 1.5 mL Eppendorf, 400 μL of freshly prepared alkaline lysis buffer 2 (0.2 N NaOH, 1% w/v SDS) was added, and the contents were mixed by inversion. Following a 2 min incubation on ice, 300 μL of 4˚C alkaline lysis buffer 3 (3 M potassium acetate, 11.5% v/v glacial acetic acid) was added, and the contents were mixed by inversion. Following a 5 min incubation on ice, cell debris was pelleted by centrifugion at 16,000xg for 5 min at 4˚C in the GE035 rotor. Six hundred μL of the supernatant was transferred to a 1.5 mL Eppendorf tube and the acqueous layer was extracted two times with an equal volume of 1:1 phenol:chloroform. The acqueous layer was then extracted twice with an equal volume of chloroform. DNA was precipitated by adding an equal volume of 2-propanol and incubating at -20˚C for a minimum of 30 min. DNA was pelleted by

centrifugation at 16,000xg for 30 min in the GE035 rotor at 4˚C. The supernatant was removed, and the pellet was rinsed with -20˚C 70% ethanol. The pellet was air-dried at room temperature before being resuspended in autoclaved milliQ water.

2.9 Transfection

2.9.1 Transfection with a single plasmid

Thirty thousand Vero or U2OS cells were seeded into each well of 6-well plates and incubated at 37˚C in 5% CO_2 for 16-19 h. For each well to be transfected, 4 µL of Lipofectamine 2000 reagent (cat# P/N 52887, Invitrogen, Burlington, ON, CA) was added to 100 µL of 4˚C serum free DMEM in a sterile 1.5 mL Eppendorf tube. For each well to be transfected, 2 µg of plasmid DNA was added to 100 µL of 4˚C serum free DMEM in a separate, sterile 1.5 mL Eppendorf tube. Following a 5 min incubation at room temperature, the contents of the Eppendorf containing Lipofectamine was added to the Eppendorf containing DNA, and gently vortexed. Following a 45 min incubation at room temperature, 800 µL of room temperature serum free DMEM was added to the DNA-Lipofectamine mix. The media on the seeded cells was vacuumed off and the contents of one Eppendorf was gently pipetted onto each well. The cells were incubated with the DNA-Lipofectamine mix for 6.5 h at 37˚C in 5% CO_2. For Vero cells, 1 mL of 37˚C DMEM supplemented with 10% FBS was added to each well, and the cells were returned to incubate at 37˚C in 5% CO_2. For U2OS cells, the media containg the DNA-Lipofectamine mix was vacuumed off and 2 mL of 37˚C DMEM supplemented with 10% FBS was added to each well, and the cells were returned to incubate at 37˚C in 5% CO_2.

2.9.2 Co-transfection with RFP-ICP4 and GFP-histones

Vero or U2OS cells ($3x10^5$) were seeded into each well of 6-well plates and incubated at 37˚C in 5% CO_2 for 16-19 h. For each well of Vero or U2OS cells to be transfected, 14 or 4 µL of Lipofectamine 2000 reagent (cat# P/N 52887, Invitrogen, Burlington, ON, CA), respectively, was added to 100 µL of 4˚C serum free DMEM in a sterile 1.5 mL Eppendorf tube. For each well of Vero cells to be transfected, 1.8 µg of RFP, RFP-n12, or RFP-ICP4 DNA and 0.2 µg of GFP-histone DNA was added to 100

μL of 4˚C serum free DMEM in a separate, sterile 1.5 mL Eppendorf tube. For each well of U2OS cells to be transfected, 1.0 μg of RFP, RFP-n12, or RFP-ICP4 DNA and 1.0 μg of GFP-histone DNA was added to 100 μL of 4˚C serum free DMEM in a separate, sterile 1.5 mL Eppendorf tube. Following a 5 min incubation at room temperature, the contents of the Eppendorf containing Lipofectamine was added to the Eppendorf containing DNA, and gently vortexed. Following a 45 min incubation at room temperature, 300 μL of room temperature serum free DMEM was added to the DNA-Lipofectamine mix. The media on the seeded cells was vacuumed off and the contents of one Eppendorf was gently pipetted onto each well. The cells were incubated with the DNA-Lipofectamine mix for 6.5 h at 37˚C in 5% CO_2. For Vero cells, 1 mL of 37˚C DMEM supplemented with 10% FBS and 0.5 mL of 37˚C serum free DMEM was added to each well, and the cells were returned to incubate at 37˚C in 5% CO_2. For U2OS cells, the media containg the DNA-Lipofectamine mix was vacuumed off and 2 mL of 37˚C DMEM supplemented with 10% FBS was added to each well, and the cells were returned to incubate at 37˚C in 5% CO_2.

2.10 Fluorescence recovery after photobleaching (FRAP)

2.10.1 FRAP with infected cells

Transfected cells ($3x10^5$) were seeded onto 18 x 18 mm coverslips (cat# 15-542A, Fisher Scientific, Ottawa, ON, CA) in each well of 6-well plates at least 4 h after transfection. Cells were incubated at 37˚C in 5% CO_2 for 4-6 h. Wild type or mutant HSV-1 stocks were diluted to the desired MOI in 4˚C serum free DMEM on ice. Two hundred μL of inocula was added to each well. For mock infections, 200 μL of 4˚C serum free media was added to the well. Cells were incubated with inocula for 1 h at 37˚C in 5% CO_2 with rocking and rotating every 10 min. Inocula was vacuumed off from the cells and cells were washed twice with 4˚C PBS before the addition of 2 mL of 37˚C DMEM containing 5 or 10% FBS for Vero or U2OS cells, respectively. Cells were incubated at 37˚C in 5% until ready for FRAP.

Slides were prepared by placing a ½" round sticker in the center of a slide. An even layer of vacuum grease was applied over the sticker on the slide, such that when the sticker was removed, there was an indentation within the grease. A small

amount of media from the well was placed within this indentation, and the cover slip was placed over the indentation with the cells facing the slide, creating a sealed enclosure for the cells. The slide was rinsed briefly with isopropanol, then immediately placed on the 37˚C stage of a Zeiss NLO 510 multiphoton microscope. Cells were viewed using a 40X F-Fluor oil immersion objective lens (NA 1.3, WD 0.12). FRAP was used using a 25 mW Argon laser (488 nm) at 95% intensity with a band pass filter of 505-530 nm and the maximum pinhole of 1000 (15 Airy units). A 1.5 μM wide region spanning the widest part of the nucleus was photobleached, with 30 or 45 iterations. Sixty images (512 x 512, 12 bit) were taken at timed intervals immediately before and for 100-200 s after photobleaching. Images were analyzed with Zeiss LSM software.

2.10.2 FRAP with co-transfected cells

Co-transfected cells were seeded onto 18 x 18 mm coverslips (cat# 15-542A, Fisher Scientific, Ottawa, ON, CA) in each well of a 6-well plates at least 4 h after transfection. Cells were incubated at 37˚C in 5% CO_2 until ready for FRAP. Slides were prepared and cells were analyzed by FRAP as with infected cells. However, before photobleaching the cells, cells were categorized as co-transfected or single transfected based on whether they expressed detectable levels of RFP in addition to GFP or not, respectively. Thus, data was compared for co-transfected and single transfected cells within each well.

2.10.3 Exclusion criteria

Nuclei of cells that were not attached to the coverslip, or of cells undergoing apoptosis or mitosis, were not analyzed. Nuclei that had blebbing or broken nuclear membranes were not analyzed. Nuclei with too little (set as gain<400) or too high (set as gain>600) fluorescence intensity were not anayzed. Nuclei with punctate distribution of GFP-histones, indicating misfolding of the GFP-histone due to overexpression, were not analyzed.

2.10.4 Statistical analysis

Statistical significance was tested using one-tailed Student's T test (for two-way comparisons) or ANOVA with Tukey's test post hoc (for multiple comparisons).

Primer	Sequence (5' to 3')
ICP4 F	AGATCTCCGGAGGATCGCCCCGCATCG
ICP4 mid R	CGTCCGAGCCGGGGGCGTCCG
ICP4 mid F	CGGCGGCCCGCGACCCCC
ICP4 R	TCTAGATCACAAGCGCCCCGCCCC
n12 R	GCAGTCTAGAGGGCTTGGGCGCGGCC
H2A.B F	GCAGAGATCTATGCCGAGGAGGAGGAG
H2A.B R	GCAGCTGCAGGTCCTCGCCAGG
macroH2A F	ATAGATCTATGTCGGGCCGGAGTGG
macroH2A R	TACTGCAGCTTGGCGTCGAGCTTG
H2A F	GCAGAGATCTATGCGCGCCAAGGCC
H2A R	GCAGGTCGACAATTTCCCCTTGGCC
H2B F	GCAGAGATCTATGCCTGAGCCAGCC
H2B R	GCAGGTCGACAACTTGGAGCTGGTG
H2A mut F	GCATGGCCGGCCTGCAGTTCCCCGTGGGCCGCGTGCACCGGCTGCTCCGCAAGGG
macroH2A mut F	GATCTATGTCGAGCCGCGGTGGGAAGAAGAAGTCCACCAAGACGTCCAGGTCTGCCAAAG
Mut R	GCATCAATTGCATTCATTTTATGTTTCAGGTTCAGGGGGAGGTG
SapI 1	CAGGATGATCTGGACGAGGAGCATCAGGGGCTCGC
SapI 2	GGCTACCCGTGATATTGCTGAGGAGCTTGGCGGCG

Table 2.1. PCR primers.

Chapter 3: An essential viral transcription activator modulates chromatin dynamics.

3.1 Introduction

The genes of the nuclear-replicating double stranded (ds) DNA virus herpes simplex virus 1 (HSV-1) are expressed in a coordinate manner. VP16, a virion protein, first activates expression of the five immediate early (IE) genes, in part through the recruitment of the histone demethylase LSD1 and histone acetyltransferase CBP/p300 to IE promoters (315, 316, 319, 322, 396). Two IE proteins, ICP0 and ICP4, then activate transcription of the early (E) genes, which encode proteins required for HSV-1 DNA replication and several other functions (328). Late (L) genes are transcribed after DNA replication. Both ICP0 and ICP4 also contribute to the activation of L gene expression.

The mechanisms whereby VP16 activates IE gene transcription are well characterized (312, 315, 316, 319, 320, 397–400). In contrast, the mechanisms whereby ICP0 and ICP4 then activate transcription of E and L genes remain only partially understood. ICP4 binds to specific DNA sequences to inhibit transcription of IE genes (401). However, it does not bind to any specific sequences to activate transcription of E or L genes (353). Over 141 proteins that interact with ICP4 at 6 h post infection (hpi) were identified by mass spectrometry analyses, including the chromatin remodeling complexes SWI/SNF, Ino80, and NuRD (360). The histone acetyltransferase CLOCK was identified as another ICP4 interactor by coimmunoprecipitation (365). ICP4 also interacts with many components of the mediator complex and may activate transcription by a gene looping mechanism (360), promoting the recycling of RNA polymerase II from the 3' end of a gene back to the transcription start sites.

Whereas HSV-1 genomes are regularly chromatinized in latent infection, HSV-1 genomes are in particularly dynamic chromatin in lytic infections (373). The basic unit of chromatin is the nucleosome, which consists of two dimers of each of the core histones H2A-H2B and H3-H4 wrapped by 146 base pairs of double stranded DNA. Linker histone H1 further binds DNA at the entry and exit sites of the core nucleosome. Chromatin is dynamic, nucleosomes disassemble and then the

released histones diffuse through the nucleus bound to chaperones and re-assemble nucleosomes at different sites. Linker histones are more dynamic than core histones, with their exchanges occurring in minutes or hours, respectively (75, 76, 80).

The dynamics of cellular nucleosomes are altered through post-translational modifications to histones and the incorporation of histone variants instead of the canonical ones, among other factors. Acetylation of histone tails by histone acetyltransferases generally destabilizes nucleosomes, whereas their methylation by histone methyltransferases destabilizes or stabilizes nucleosomes, depending on the site and the degree of methylation (113, 121, 402–408). Whereas H2B and H4 have no variants, H2A and H3 have many. Canonical histones are synthesized during S phase of the cell cycle and assembled in nucleosomes via DNA-replication dependent mechanisms. In contrast, variant histones are synthesized at any cell cycle phase and are assembled in nucleosomes via DNA-replication independent mechanisms. Histones variants destabilize or stabilize the nucleosome. Variant H3.3 differs from canonical H3.1 by only five amino acid residues. Whereas canonical H3.1 is assembled in chromatin of newly synthesized DNA by CAF1, variant H3.3 is assembled in the chromatin of transcribed genes or telomeres by HIRA or DAXX, respectively (40, 45, 146, 409–411). Salt solubility assays with purified DNA and histones show that nucleosomes containing H3.3 are more dynamic than those containing H3.1(151). H3.3 is also typically post-translationally modified with more markers of active transcription than H3.1, such as K4 and K79 methylation and K9, K14 and K23 acetylation (148). However, in vivo assays show that H3.3 assembled in nucleosomes at telomeres is more stable than H3.3 assembled in nucleosomes with transcribed genes, and that H3.3 in telomeres is enriched with post-translational modifications marking silenced chromatin (149, 150). Genes inserted to telomeric regions are not transcribed, suggesting that the chromatin is not permissive to transcription (412). H3.3 thus has two opposing roles in chromatin, depending on the genomic location of assembly.

We had found that histone dynamics increase during infection with wild type HSV-1 (82, 374, 375). Histone dynamics still increased in infected cells treated with

phosphonoacetic acid, indicating that neither HSV-1 DNA replication nor L gene expression are required, whereas they were largely unaffected by UV-inactivated HSV-1, indicating that virion attachment or entry are not sufficient. Therefore, IE or E proteins most likely affect histone dynamics.

We and others propose a model in which the chromatinization of HSV-1 DNA is a cellular defense mechanism to silence HSV-1 gene expression. To counteract this mechanism, HSV-1 would have evolved proteins that prevent or disrupt the stable chromatinization of HSV-1 genomes. This nucleosome destabilization process would increase histone dynamics and promote transcription. Under this model, one or more of the three HSV-1 transcription activators would be expected to enhance histone dynamics. Consistently, all three HSV-1 transcription activators have been reported to interact with chromatin modifying proteins.

Here we report that HSV-1 mutants encoding no functional VP16, ICP0 or ICP4 still enhance histone dynamics, but to a much lesser extent than wild type HSV-1. We further show that an HSV-1 mutant encoding no functional ICP4 is the most deficient in enhancing histone dynamics. Transient expression of ICP4 was sufficient to enhance histone dynamics in the absence of any other HSV-1 protein or DNA. ICP4 may moreover preferentially target silencing histone variants, such as H3.1. The dynamics of canonical H2A were not enhanced in cells expressing ICP4, suggesting that other H2A variants may be targeted by ICP4. During lytic infections, histones were more dynamic in the replication compartments, where ICP4 localizes, than in the cellular chromatin. Together, our results suggest a novel mechanism of transcription activation by ICP4, in which ICP4 prevents the formation of stable nucleosomes on HSV-1 genomes, or destabilizes preformed ones, to promote transcription by allowing access of the RNA polymerase II complex to the HSV-1 genes.

3.2 Results

3.2.1 Functional ICP4 or E proteins are required to enhance histone dynamics beyond a basal level.

IE or E proteins enhance linker and core histone dynamics during HSV-1 infection (82, 374, 375). To test whether the enhanced dynamics required the expression of ICP4 or any E protein, we used HSV-1 strain n12, which expresses a transactivation incompetent truncated ICP4 (361). Consequently, IE proteins other than ICP4 are expressed to high levels in the absence of any E or L protein expression or DNA replication. The levels of green-fluorescent protein (GFP)-histone fusion proteins in the free pools, and the initial rates of fluorescence recovery after photobleaching (core histones), or time to recover 50% of the relative fluorescence in the photobleached region (T_{50}; for linker histone H1.2), were evaluated to analyze histone dynamics (82, 374, 375). The fluorescence recovery of histones is biphasic (76, 79, 80). The initial, faster, phase of fluorescence recovery, analyzed by the slope of the fluorescence recovery between the first two times, reflects histones assembled in the most dynamic chromatin, such as those in rapidly transcribed genes. The later, slower, phase of fluorescence recovery, analyzed by the slope of the fluorescence recovery between 25 and 100 seconds for core histones, reflects the histones assembled in less dynamic chromatin. The relative fluorescence intensity immediately after photobleaching reflects the "free pool" of histones, as only histones not in chromatin diffuse in and out the bleached region during photobleaching. The global dynamics of linker histones are described by the T_{50}, which is the most sensitive parameter.

The levels of all free histones had unimodal normal frequency distributions throughout the population of n12 infected U2OS cells (Figure 3.1.). n12 infection of U2OS cells was not sufficient to increase the free pools of any core histone, whereas those of H1.2 were only increased to a basal degree at early times after infection (Figure 3.1A). The levels of all free histones also had unimodal normal frequency distributions throughout the population of n12 infected Vero cells (Figure 3.1B). The free pools of H3.1, H3.3, and H4 were also increased at 4 and 7 hpi in n12 infected Vero cells, although less than in KOS infected cells.

We had previously shown that the enhancement of histone dynamics in Vero cells infected with an HSV-1 mutant in ICP0 was partly impaired, such that the enhanced late increase of histone dynamics ultimately occurs (82, 374, 375). The pools of some free histones were increased to an even larger degree at 7 hpi in the absence of ICP0 (Figure 3.2.). The double ICP0 and VP16 HSV-1 mutant, which expresses little ICP4 in Vero cells (395), also enhanced histone dynamics less than wild type HSV-1 in these cells (Figure 3.2.). Vero cells infected with ICP4 mutant n12 only had a basal increase in the levels of free linker and core histones, which was not further enhanced at later times after infection (Figure 3.2.). Expression of ICP0, ICP22, ICP27, or ICP47 in the absence of functional ICP4 (and E proteins) is thus not sufficient to increase the pools of free core or linker histones to the same degree as infection with wild-type or ICP0 or VP16 mutant strains of HSV-1 (82, 374, 375)).

To test whether the inability of n12 to enhance histone dynamics above the basal degree was due to unknown mutations within this strain, histone dynamics were re-evaluated in a complementary Vero-derived cell line (n-33) that expresses HSV-2 ICP4 upon infection (413). The dynamics of core and linker histones were enhanced to approximately the same degree in n-33 cells infected with n12 or wild-type KOS (Figure 3.3.).

3.2.2 The dynamics of core histones H2B and H4 increase in cells transiently expressing ICP4.

The above results show that histones are minimally mobilized in U2OS or Vero cells infected with an HSV-1 mutant encoding no functional ICP4. ICP4 may induce the increase in histone dynamics by itself. Alternatively, the protein product of an E gene may increase histone dynamics (DNA replication or L proteins are not required (82, 375)), as the expression of E genes requires ICP4. To test these possibilities, we analyzed the effects on histone dynamics of ectopically expressed ICP4.

H4 and H2B have no major variants, and they therefore represent the entire population of H3-H4 and H2A-H2B dimers, respectively. To evaluate the dynamics of H4 and H2B in cells transiently expressing ICP4, we optimized the co-transfection of GFP-H2B or GFP-H4 with free red fluorescent protein (RFP) or RFP-ICP4 such

that approximately half of the cells expressing detectable levels of GFP also expressed detectable levels of the RFP fusion proteins (or free RFP). This approach allows us to analyze histone dynamics in cells expressing detectable or undetectable levels of the test proteins in otherwise identical conditions. GFP fluorescence within the bleached region was normalized to total nuclear fluorescence to account for differences in GFP expression. The relative fluorescence within the bleached region at each time was then normalized to the initial relative fluorescence within the same region prior to photobleaching. The results are therefore independent of the GFP-histone expression levels (82, 374, 375).

The free pools of GFP-H4 or -H2B were 22 or 12% greater, respectively, in cells expressing detectable compared to undetectable levels of RFP-ICP4 ($p<0.01$) (Figure 3.4. A,B,D,E). As expected, the free pools of GFP-H4 or -H2B were not significantly different in cells expressing detectable or undetectable levels of free RFP. The slow exchange rate of GFP-H2B, which evaluates the dynamics of the H2B molecules in low turnover nucleosomes, was 57% greater in cells expressing detectable than undetectable levels of RFP-ICP4 ($p<0.05$) (Figure 3.4.). While the slow exchange rate of GFP-H4 tended to be faster in cells expressing detectable than undetectable levels of RFP-ICP4, the difference was not significant. The slow exchange rates of GFP-H2B or -H4 were not significantly changed in cells expressing detectable levels of free RFP (Figure 3.4.C,F).

3.2.3 The dynamics of canonical H3.1 and variant H3.3 increase in cells transiently expressing ICP4.

H3.3 is initially detected in the nucleosomes assembled with HSV-1 genomes, whereas H3.1 is detected in HSV-1 nucleosomes only after the onset of HSV-1 DNA replication (371). Consistently, the dynamics of H3.1 and H3.3 are differentially affected in cells infected with wild type HSV-1 (375). Their free pools decrease between 4 and 7 hpi in Vero cells, but those of H3.1 decreases to a much greater extent (Figure 3.2.B). The free pools of H3.1 also decreased between 4 and 7 hpi in U2OS cells, whereas those of H3.3 did not (Figure 3.2.A). Whereas the free pool of H3.3 at 7 hpi is not affected by HSV-1 DNA replication, that of H3.1 is two-fold

greater when HSV-1 DNA replication is inhibited (375). The dynamics of H4 were enhanced in cells transiently expressing ICP4 (Figure 3.4.D). We therefore expected the dynamics of H3.1 or H3.3, which both form dimers with H4, to also be enhanced.

The free pool of GFP-H3.3 was 11% greater in Vero cells expressing detectable than undetectable levels of RFP-ICP4 ($p<0.05$) (Figure 3.5.B). The unimodal frequency distribution of the GFP-H3.3 free pools had its peak shifted to the right, indicating a larger free pool, in cells expressing detectable ICP4 compared to cells expressing undetectable ICP4 (Figure 3.5.E). In contrast, the frequency distribution of the GFP-H3.3 free pools was not altered in cells expressing detectable or undetectable RFP (Figure 3.5.F).

GFP-H3.1 was mobilized to a much greater extent (Figure 3.5.C). The average free pool of GFP-H3.1 was 248% greater in cells expressing detectable than undetectable levels of RFP-ICP4 (Figure 3.5.D). The frequency distribution curves of the GFP-H3.1 free pools showed moreover that the cells expressing undetectable levels of ICP4 had free pools distributed normally around 20%, whereas the cells expressing detectable ICP4 had a skewed distribution peaking at twice as large (Figure 3.5.G). Cells expressing detectable RFP or not had equally distributed free pools (Figure 3.5.H). The increased dynamics of GFP-H3.1 were also reflected by its nuclear distribution (Figure 3.5.I). GFP-H3.1 had the punctuated localization characteristic of chromatin in cells expressing undetectable levels of RFP-ICP4. In contrast, GFP-H3.1 was diffusely distributed through the nucleus in cells expressing detectable levels of RFP-ICP4, distribution which is consistent with soluble proteins (i.e., free H3.1).

The free pools of GFP-H3.3 or -H3.1 were also 22% or 40% greater, respectively, in U2OS cells expressing detectable than undetectable levels of RFP-ICP4 ($p<0.01$) (Figure 3.6.B,D). Cells expressing undetectable levels of RFP-ICP4 or RFP had equally normally distributed free pools of GFP-H3.1 (Figure 3.6.G,H). In contrast, cells expressing detectable levels of ICP4 had free pools of GFP-H3.1 with a skewed distribution with a clear shoulder at 40% (Figure 3.6.G). The increased dynamics of GFP-H3.1 were also reflected by its nuclear distribution in U2OS cells (Figure 3.6.I).

3.2.4 The dynamics of canonical H2A were not affected in cells transiently expressing ICP4.

H2B was mobilized in cells expressing ICP4, albeit its free pool increased the least of all core histones. H2B forms dimers with canonical H2A or any of its multiple variants. No H2A variant has been shown to interact with HSV-1 genomes, whereas canonical H2A has. We thus co-transfected cells with plasmids expressing GFP-H2A and RFP-ICP4. Surprisingly, the dynamics of canonical GFP-H2A were not significantly affected in cells expressing detectable levels of RFP-ICP4 (or free RFP) (Figure 3.7.A,B).

3.2.5 The dynamics of linker histone H1.2 were increased in cells transiently expressing ICP4.

All linker histones are mobilized in cells infected with wild type HSV-1 (374). Variant H1.2 was mobilized the most, with a T_{50} in infected cells 60% of that in mock infected cells. H1.2 is synthesized independently of the cell cycle stage and in all cell types that HSV-1 infects. We therefore focused on the mobilization of H1.2 in cells expressing RFP-ICP4.

The T_{50} of GFP-H1.2 in cells expressing detectable levels of RFP-ICP4 was 76% of that in cells expressing undetectable levels of RFP-ICP4 ($p<0.01$), and the free pools were 17% greater ($p<0.01$) (Figure 3.7.D,E). As expected, GFP-H1.2 T_{50}, or its free pools, were not significantly different in cells expressing detectable or undetectable levels of free RFP.

3.2.6 The truncated, transcriptionally inactive ICP4 n12 mutant does not enhance histone dynamics.

HSV-1 n12 encodes only the amino-terminal 251 amino acid residues of ICP4. This mutant is unable to activate early or late gene expression (361). The HSV-1 n12 mutant virus barely enhanced the dynamics of any histone in Vero or U2OS cells. The mutant form of ICP4 was therefore not expected to alter histone dynamics. To test this model, a plasmid encoding the n12 form of ICP4 fused in frame with red

fluorescent protein was constructed (RFP-n12). Mobilization of core and linker histones was analyzed in cells expressing RFP-n12. The dynamics of no histones were altered in Vero cells expressing detectable or undetectable levels of RFP-n12 (Figure 3.8). Free pools, fast and slow exchange, or T_{50} of no histone were affected by expression of RFP-n12. GFP-H3.1 had the expected granular localization in cells expressing detectable levels of RFP-n12, or of RFP.

3.2.7 Histone dynamics increase preferentially within HSV-1 replication compartments.

HSV-1 DNA and ICP4 localize to the HSV-1 replication compartments, where they also co-localize with a small pool of histones (Figure 3.9). There was less fluorescence in the replication compartments than in the cellular chromatin, which may indicate fewer histones in the replication compartments or that the histones within the replication compartments are more dynamic and spend less time in them than in the cellular chromatin. A fluorescent micrograph cannot distinguish between 80% fewer histones or the same amount of histones having an 80% shorter residency time in the replication compartments.

We therefore characterized next the histone dynamics in the replication compartments and the general chromatin of the same cell. The free pools of core histones H2A, -H2B, -H3.1, -H3.3, and -H4, and that of linker histone GFP-H1.2, all increased preferentially within the HSV-1 replication compartments (Figure 3.10.C). GFP-H4 and -H3.1 had the largest average relative free pools in the replication compartments, 73 or 67% greater than those in the cellular chromatin, respectively. The free pools of GFP-H2A, -H2B, and -H3.3 were 50%-56% larger in the replication compartments than in the cellular chromatin, whereas that of linker histone GFP-H1.2 had the smallest difference, 41% larger in the replication compartments than in the cellular chromatin. The free pools were consistently higher in the replication compartments than in the cellular chromatin in all cells (Figure 3.10).

The average slow exchange rates of H3.3 or H2B were 67 or 128% faster ($P<0.01$), respectively, in the replication compartments than in the cellular chromatin, whereas those of other histones were not statistically different.

3.3 Discussion

During latent infections, when most HSV-1 genes are not transcribed and no HSV-1 virions are produced, HSV-1 genomes are regularly chromatinized (370). It has only recently been agreed that HSV-1 genomes are also chromatinized during lytic infections, when most HSV-1 genes are transcribed and HSV-1 virions are produced (414–421). However, lytic HSV-1 chromatin is far more dynamic than latent HSV-1 chromatin or cellular chromatin (373). Cellular chromatin containing transcribed genes is more dynamic than that containing silenced genes (402, 422–424). The dynamics of HSV-1 chromatin are therefore consistent with the high or low rates of transcription of the viral genomes during lytic or latent infection, respectively.

A balance between cellular and viral effects may determine the unusual dynamics of HSV-1 chromatin. The assembly of nucleosomes with HSV-1 DNA may be a cellular response to inhibit HSV-1 transcription by assembling the viral genome in silenced chromatin. To counteract such silencing, HSV-1 would have evolved proteins to destabilize nucleosomes or to mobilize them away from its genome. Either mechanism would result in increased access by RNA polymerase II to the viral DNA, activating transcription. These HSV-1 proteins would thus be expected to act as transcription activators, without actually binding to specific promoter sequences.

ICP4 is one of the three HSV-1 transcription activators, and the only one required for HSV-1 replication. Though it binds to specific DNA sequences to inhibit transcription, it does not do likewise to activate it (353, 401). Its mechanism of transcription activation remains only partially understood. Here I show that ICP4 is both necessary and sufficient to increase histone dynamics. Consistent with these findings, HSV-1 genomes are less accessible to nuclease digestion in the absence of IE proteins (425), and H3 association with HSV-1 DNA appears to increase in the absence of functional ICP4 (333). The changes in H3 association with HSV-1 DNA were not statistically different in the absence or presence of functional ICP4,

perhaps due to the variability in the degree of the increased association for the ICP4 mutant virus.

We selected the histones to be evaluated based on the following criteria. H1.2 is expressed in all cell types that HSV-1 infects, and is mobilized the most of all linker histones (374). H4 and H2B have no variants, and therefore represent the two core histone dimers, whereas H3 and H2A have several variants. H3.1 and H3.3 bind to HSV-1 genomes, via DNA-replication dependent or independent mechanisms, respectively (371), and their dynamics are differentially affected in HSV-1 infected cells (375). Canonical H2A is the most prevalent H2A in nucleosomes, and no H2A variant has yet been reported to interact with HSV-1 chromatin. We analyzed histone dynamics at 4 or 7 hpi, and never beyond 8 hpi. At later times, chromatin shearing or marginalization (426) may well indirectly affect histone dynamics.

In U2OS cells, the HSV-1 n212 ICP0 mutant induced increases in the free pools of all histones except H4 larger than those induced by the wild type virus. ICP0 may induce the degradation of the histones in the free pools. Nonetheless, the HSV-1 mutant encoding a truncated non-functional ICP4 n12 was the most defective in affecting histone dynamics. This mutant either failed to enhance histone dynamics (in U2OS cells) or only enhanced them to a basal level (in Vero cells), even though it overexpresses all other IE proteins. ICP4 may therefore modulate histone dynamics by itself. Alternatively, ICP4 could indirectly affect histone dynamics through any E protein, as the expression of all E proteins requires ICP4 (DNA replication or L proteins are not required (82, 374, 375)). To test these possibilities, we constructed plasmids expressing full length or truncated forms of ICP4 fused in frame with RFP. The dynamics of all core histones except H2A increased in cells transiently expressing ICP4 but not in cells expressing the non-functional truncated n12 mutant form of ICP4.

H3.3 is initially assembled in nucleosomes with HSV-1 genomes, whereas H3.1 starts to be assembled in HSV-1 nucleosomes concomitantly with HSV-1 DNA replication (371). Nucleosomes containing H3.3 are more dynamic than those containing H3.1 in salt solubility assays (151). However, salt solubility assays are

performed with purified DNA and histones, and may not be a true representation of the stability of nucleosomes in the cell. H3.3 assembled in telomeres is less dynamic than H3.3 assembled in transcribed genes, and telomeric chromatin is silencing to transcription (150, 412). Though total nuclear H3.3 is enriched in post-translational markers of active chromatin, H3.3 assembled with nucleosomes in telomeres is enriched in post-translational markers of silenced chromatin (148, 149). HSV-1 genomes have lower levels of H3.3 when HIRA expression is knocked down (371). However, HSV-1 transcription and replication is also inhibited when HIRA expression is knocked down, suggesting that the assembly of H3.3 in nucleosomes with HSV-1 genomes via HIRA is beneficial for HSV-1 replication (371). In contrast, the replication of an HSV-1 mutant lacking ICP0 is increased when Daxx is knocked down, suggesting that the assembly of H3.3 in nucleosomes with HSV-1 genomes via Daxx is silencing to HSV-1 replication (427). Therefore, H3.1-containing nucleosomes may be more or less prone to support transcription than those containing H3.3, depending on the mechanisms of H3.3 assembly in the nucleosome. The free pools of GFP-H3.3 increased by only 11 or 22% in Vero or U2OS cells expressing ICP4, whereas those of GFP-H3.1 increased by 248 or 40% in Vero or U2OS cells, respectively. ICP4 may thus preferentially prevent the assembly of H3.1 in HSV-1 nucleosomes.

Whereas the assembly of stable nucleosomes with HSV-1 genomes is expected to inhibit HSV-1 transcription, the assembly of dynamic nucleosomes with HSV-1 genomes may well benefit it. Consistent with this model, DAXX knockdown increases HSV-1 replication, but HIRA knockdown inhibits it (371, 428).

Upon recognition of nuclear naked dsDNA, the cellular sensor IFI16 starts a signaling cascade for apoptosis (429). IFI16 localizes with HSV-1 genomes immediately upon their entry into the nucleus, but is degraded after 4 hours of infection, perhaps as a result of ICP0 activities (430–432). The expression of IFI16 inhibits HSV-1 transcription and replication (385). As IFI16 recognizes naked DNA, HSV-1 genomes assembled in nucleosomes would be better shielded from recognition by IFI16 at the early times of infection before IFI16 is degraded.

The free pool or slow exchange rate of GFP-H2B increased by 12% or 57%, respectively, in cells expressing ICP4. H2B forms dimers with canonical H2A or any one of its many variants. No H2A variant has yet been reported to bind to HSV-1 genomes. H2A was therefore expected to be mobilized in cells expressing ICP4. Surprisingly, it was not. It is thus most likely some other H2A variants are targeted by ICP4. Whereas H2A and H2A.X associate with both transcribed and silenced genes, for example, macroH2A preferentially associates with silenced ones and H2A.B with transcribed ones (177). Nucleosomes containing macroH2A or H2A.B are less or more dynamic, respectively, than those containing canonical H2A (175, 176, 193). Like its differential effects on H3.1 and H3.3, ICP4 could preferentially mobilize particular H2A variants away from HSV-1 genomes. If ICP4 mobilizes H3.1 because it assembles more stable nucleosomes than H3.3, like those in transcribed genes, we would then expect that it would target macroH2A. If ICP4 mobilizes H3.1 because it assembles more dynamic nucleosomes that H3.3, liked those in telomeres, we would then expect that it would target H2A.B.

ICP4 accumulates in replication compartments during lytic infection, but is distributed throughout the nucleus when transfected. Given its effect on chromatin, it is not surprising that transfection of ICP4 is sufficient to enhance the expression of selected human genes, including the α-globin gene, which is normally silenced without being assembled in heterochromatin (433). During lytic infection, when ICP4 accumulates in replication compartments, we would expect histone dynamics to increase preferentially in the replication compartments. Indeed, we found that the dynamics of all histones were faster in the replication compartments than in the cellular chromatin of the same nuclei. Though the free pools of all histones were greater in replication compartments, the slow exchange rates of only GFP-H2B and GFP-H3.3 were significantly greater, and that of GFP-H2B by nearly twice as much as that of GFP-H3.3. Consistently, the slow exchange rate of only GFP-H2B was also significantly greater in cells expressing detectable levels of ICP4. HSV-1, and ICP4 in particular, may preferentially affect the less dynamic nucleosomes, which affect the slow exchange rate the most, over the more dynamic ones. However, VP16 also localizes at replication compartments at early times of infection, and it also

promotes histone modifications and their weaker association with HSV-1 genomes (316, 434). Using this model, I cannot distinguish the contributions of ICP4 to the enhancement of histone dynamics in replication compartments from those of VP16, or any other protein localized at replication compartments.

All herpesviruses appear to encode proteins that regulate chromatin dynamics. These proteins are either tegument proteins, and therefore introduced into the cell with the infected virions, or expressed immediately upon nuclear entry of the viral genome. They are thus all available to remodel chromatin before the activation of generalized viral gene expression. The genomes of human cytomegalovirus (HCMV) are in much less dynamic chromatin in the absence of immediate early protein 1, for example. The Epstein-Barr virus (EBV) major tegument protein BNRF1 binds to the H3.3 chaperone DAXX, which physiologically assembles silencing H3.3-containing nucleosomes in telomeres, thus preventing silencing H3.3 incorporation into EBV chromatin (388, 435). Nonetheless, the genomes of beta- or gamma- herpesviruses are assembled in far less dynamic chromatin than those of the alpha-herpesviruses. The genomes of HCMV and EBV are consequently less accessible to MCN digestion than those of HSV-1 (386, 388, 389, 436). ChIP also co-immunoprecipitates relatively more EBV or HCMV than HSV-1 DNA, which also consistent with the EBV and HCMV chromatins being less dynamic than that of HSV-1 (377, 391, 437). Nucleosomes are also more uniformly assembled with EBV or HCMV than HSV-1 genomes (437–439), which is again consistent with less dynamic chromatin for the former. Alphaherpesviruses also have much shorter replication cycles (~18 hours for HSV-1) than beta- or gamma-herpesviruses (~3 days for HCMV, ~4-5 days for EBV). ICP4 is conserved only among all alpha-herpesviruses, but not in beta- or gamma- herpesviruses. It is tempting to speculate that ICP4 may induce the particular dynamics of the alpha-herpesvirus chromatin, which would in turn result in the increased rate of transcription and consequently shorter replication cycle.

HSV-1 genes are transcribed by the cellular RNA polymerase II complex, which is enriched on HSV-1 genes while depleted from cellular genes in lytic infections (440, 441). Nucleosomes impair accessibility of the RNA polymerase II

complex to promoter DNA (402, 422–424), and the HSV-1 chromatin is far more dynamic and accessible than the cellular one (373). ICP4 may maintain the HSV-1 genomes in this dynamic and highly accessible chromatin, resulting in the RNA polymerase II complexes being sequestered away from the cellular genome and to the HSV-1 genomes (441), thus leading to the activation of HSV-1 transcription and inhibition of cellular transcription.

In summary, we show that the HSV-1 transcription activator ICP4 is sufficient and necessary to enhance histone dynamics. ICP4 preferentially affects the silencing histone H3.1 over the non-silencing variant H3.3, and it does not affect canonical H2A. ICP4 may therefore target silencing histones, preventing them from assembling silencing nucleosomes with HSV-1 genomes, or mobilizing them away from HSV-1 nucleosomes, to activate HSV-1 gene transcription. This mobilization may function to counteract a cellular defense mechanism against dsDNA viruses involving chromatin silencing.

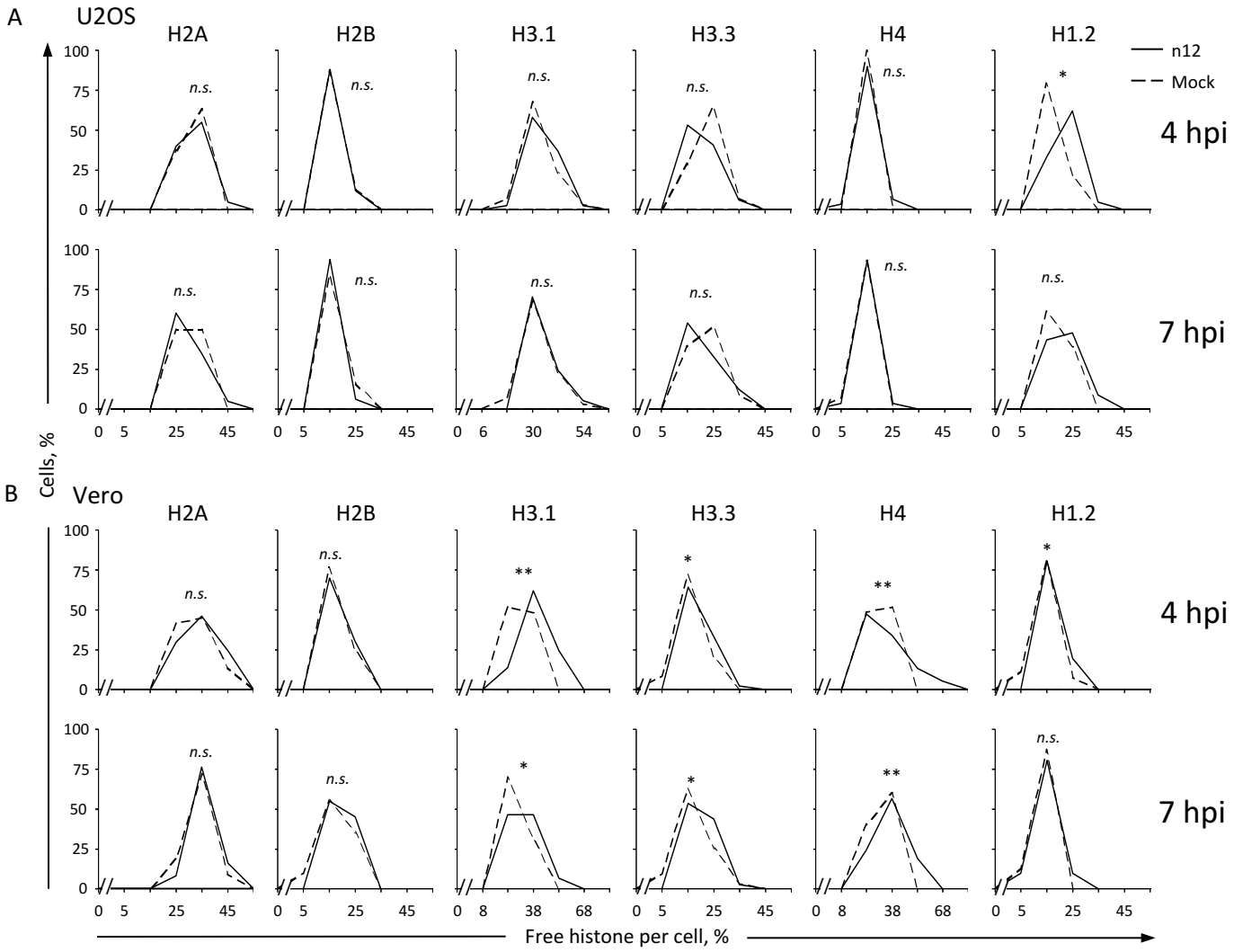

Figure 3.1. **The dynamics of linker and core histones are only minimally altered in the absence of functional ICP4**. U2OS (**A**) or Vero (**B**) cells were transfected with plasmids expressing GFP fused to H2A, H2B, H3.1, H3.3, H4, or H1.2. Transfected cells were mock infected or infected with 30 plaque forming units (PFU) per cell of HSV-1 strain n12 and histone dynamics were examined from 4 to 5 or 7 to 8 hours post infection (hpi) (**4 hpi or 7 hpi**, respectively) by FRAP. Frequency distribution plots showing the percentage of free GFP-H2A, -H2B, -H3.1, -H3.3, -H4, or -H1.2 per individual mock- (dashed line) or n12 (solid line) infected cell at 4 or 7 hpi. **, $P < 0.01$; *, $P < 0.05$; *n.s.,* not significant. n ≥ 20 cells from at least 3 independent experiments, except for U2OS H2A (n = 20 cells from 2 independent experiments). ***Dr. Kristen Conn performed all experiments presented in this figure except for the evaluations of H4 in U2OS cells*.**

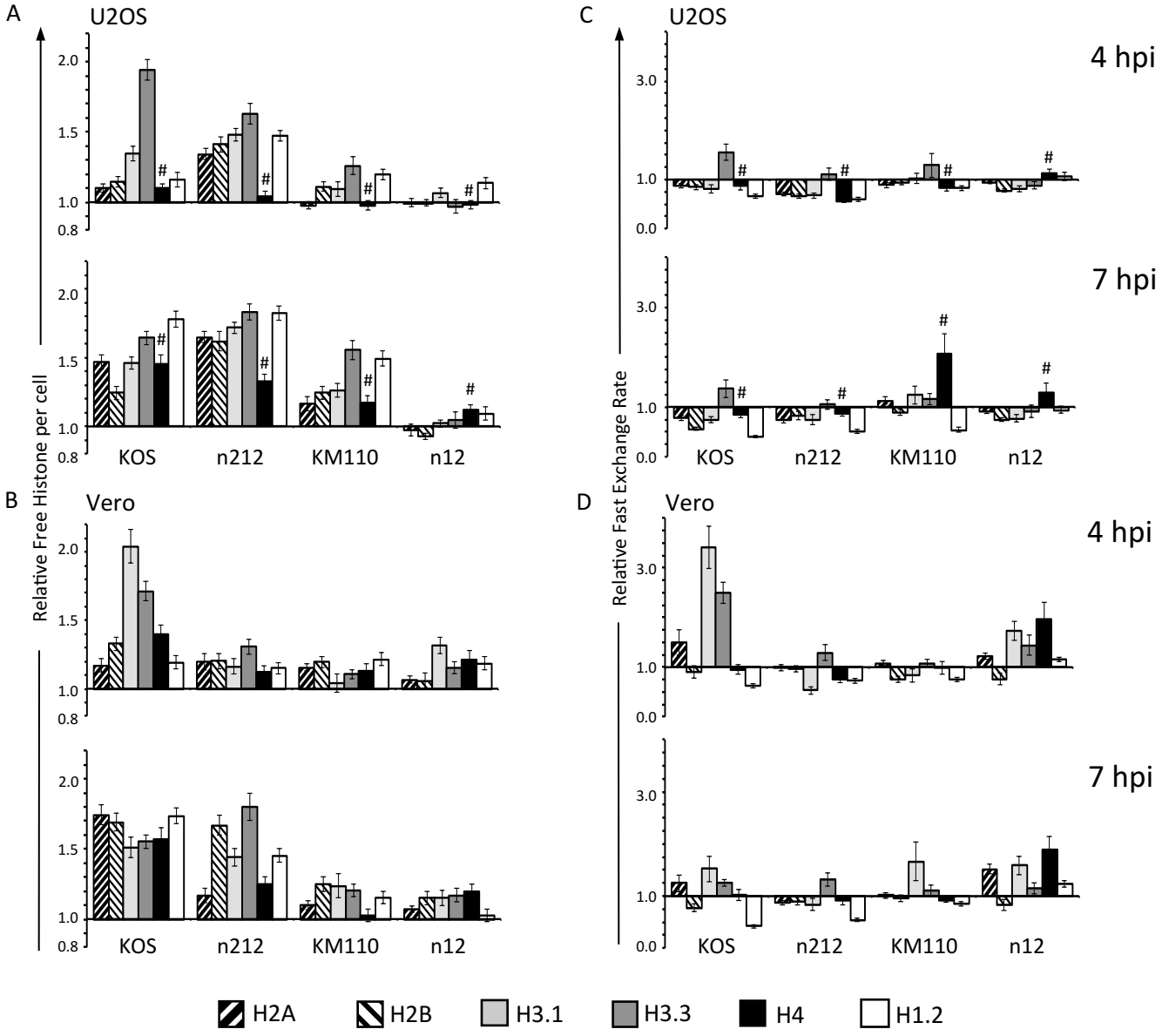

Figure 3.2. **Core and linker histone dynamics during infection with wild-type or mutant HSV-1 strains defective in VP16, ICP0 or ICP4**. U2OS or Vero cells were transfected with plasmids expressing GFP fused to H2A, H2B, H3.1, H3.3, H4, or H1.2. Transfected cells were mock-infected or infected with 30 PFU per cell of HSV-1 strains KOS (wild type), n212 (ICP0 truncation mutant), KM110 (ICP0 and VP16 double truncation mutant), or n12 (ICP4 truncation mutant), or 6 PFU per cell of strain KOS (U2OS cells). Histone dynamics were evaluated from 4 to 5 (**4 hpi**) or 7 to 8 (**7 hpi**) hpi by FRAP. A), B) Bar graphs showing the average levels of free GFP-H2A, -H2B, -H3.1, -H3.3, -H4, or -H1.2 relative to those in mock-infected cells at 4 or 7 hpi. C), D) Bar graphs showing the average initial rates of normalized fluorescence recovery (core histones) or the average T_{50} (H1.2) relative to those in mock-infected cells (set at 1.0) at 4 or 7 hpi. Error bars, SEM.

Dr. Kristen Conn performed all experiments presented in this figure except for those noted with #.

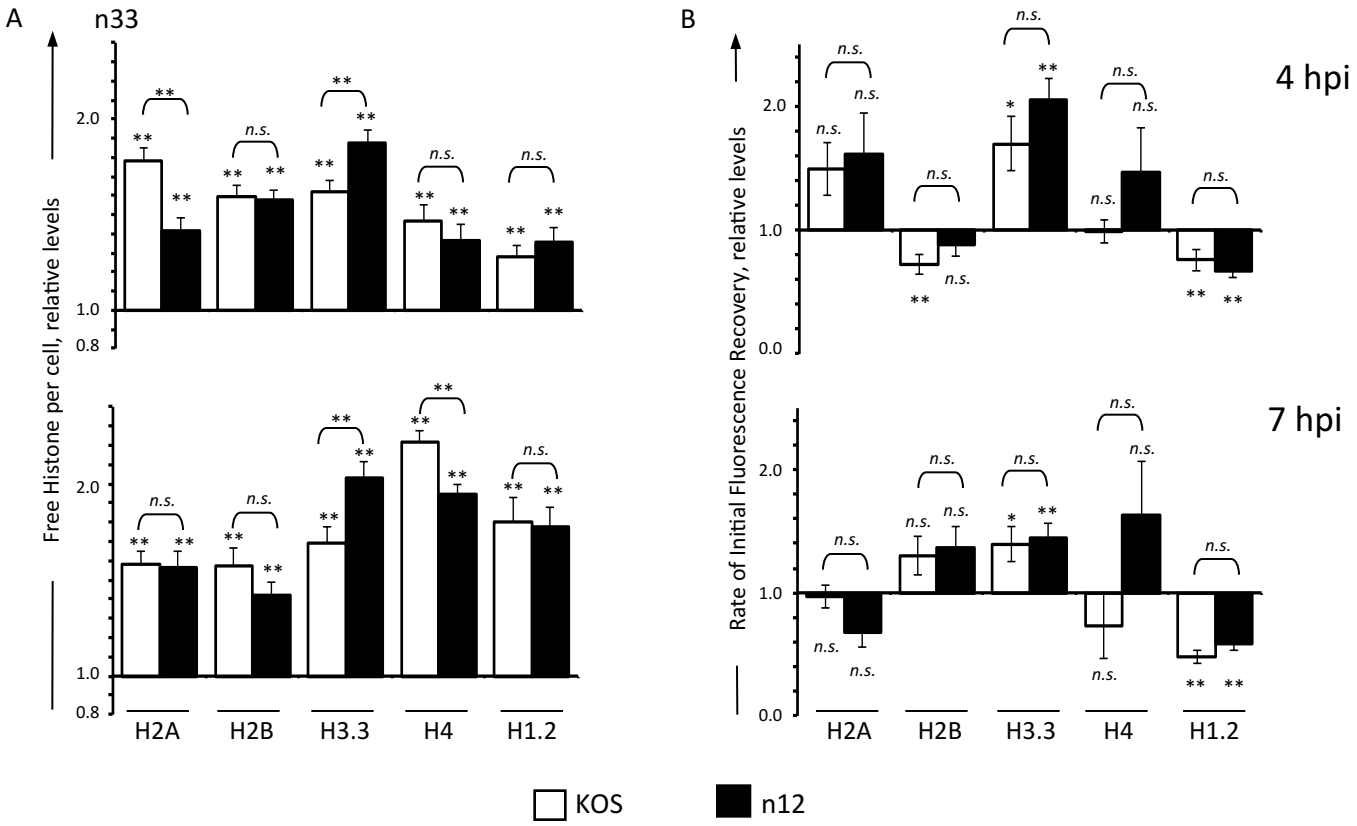

Figure 3.3. **Functional ICP4 enhances histone dynamics during n12 infection**. n-33 cells transfected with plasmids expressing GFP fused to H2A, H2B, H3.3, H4, or H1.2 were mock infected or infected with 30 PFU per cell of HSV-1 strain KOS (□) or n12 (■). Histone dynamics were evaluated from 4 to 5 (**4 hpi**) or 7 to 8 (**7 hpi**) hpi by FRAP. A) Bar graphs showing the average levels of free GFP-H2A, -H2B, -H3.3, -H4, or -H1.2 in KOS- or n12- infected cells relative to those in mock-infected cells (set at 1.0) at 4 or 7 hpi. B) Bar graphs showing the average initial rates of normalized fluorescence recovery (core histones) or the average T_{50} (H1.2) in KOS- or n12-infected cells relative to those in mock-infected cells (set at 1.0) at 4 or 7 hpi. Error bars, SEM. **, $P < 0.01$; *, $P < 0.05$; *n.s.*, not significant. n ≥ 15 cells from at least 2 independent experiments, except GFP-H2A and -H4 n ≥ 8 cells from 1 experiment. ***Dr. Kristen Conn performed all experiments presented in this figure*.**

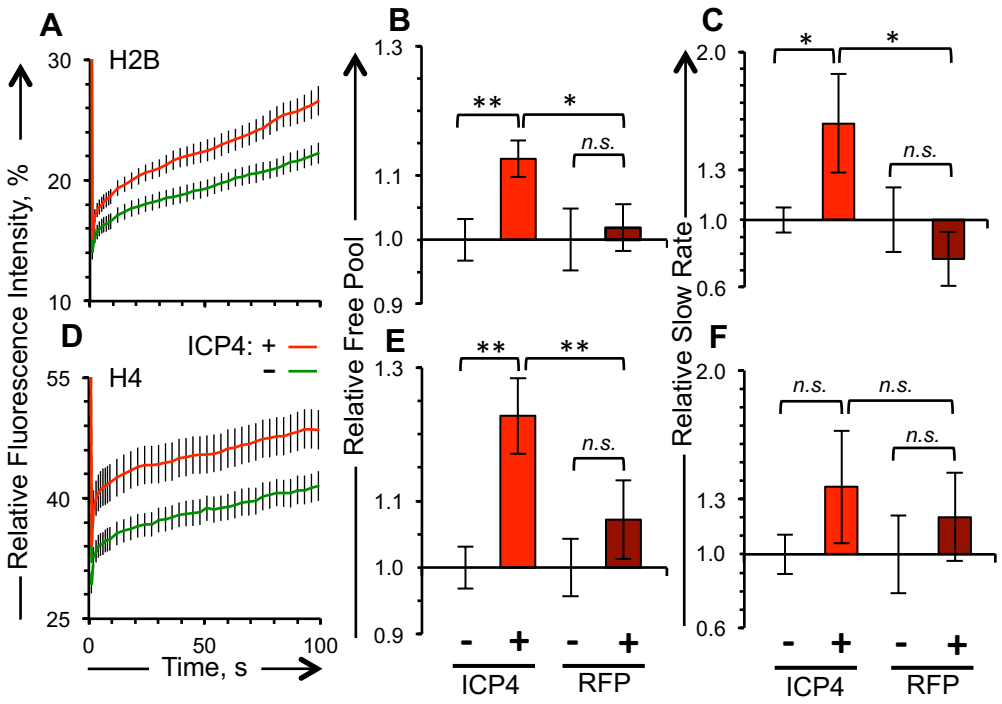

Figure 3.4. The dynamics of H2B and H4, representative of each histone dimer, are enhanced in cells transiently expressing ICP4. Vero cells were co-transfected with plasmids expressing GFP-H2B or -H4 and RFP-ICP4 or RFP, such that approximately half of the cells expressing detectable levels of GFP-histone also express detectable levels of RFP. A), D) Average fluorescence recovery curves for GFP-H2B and -H4, respectively, for cells expressing detectable (red line) or undetectable (green line) levels of RFP-ICP4. B), E) Bar graphs showing the average levels of free GFP-H2B or -H4, respectively, in cells expressing detectable levels of RFP-ICP4 or RFP relative to those in cells expressing undetectable levels of RFP-ICP4 or RFP, respectively. C), F) Bar graphs showing average GFP-H2B or -H4 slow exchange rate in cells expressing detectable levels of RFP-ICP4 or RFP relative to those in cells expressing undetectable levels of RFP-ICP4 or RFP. Error bars, SEM. **, $P < 0.01$; *, $P < 0.05$; *n.s.,* not significant. n ≥ 15 cells from at least 3 independent experiments.

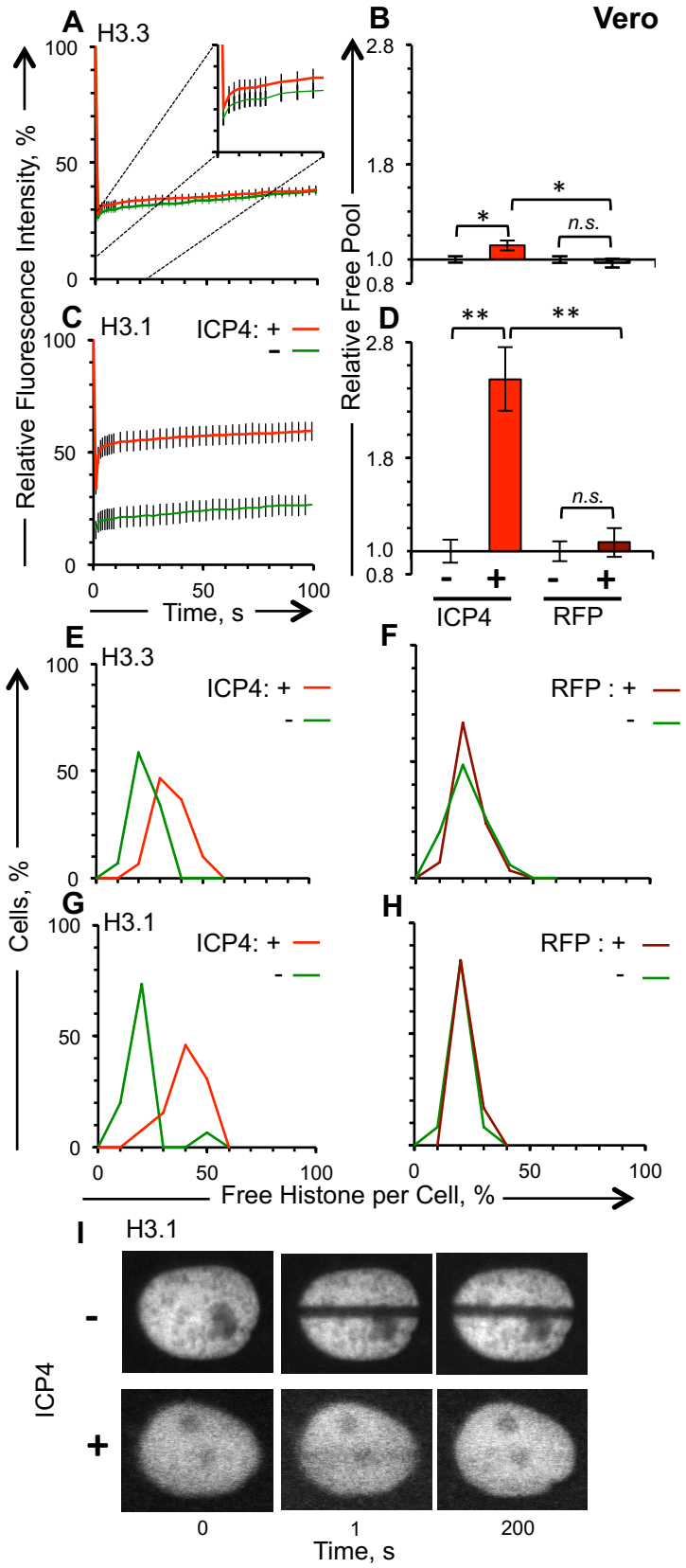
A
H3.3
Relative Fluorescence Intensity, %
100
50
0
B
Vero
Relative Free Pool
2.8
1.8
1.0
0.8
*
*
n.s.
C
H3.1
ICP4: +
-
Time, s
0
50
100
D
**
**
n.s.
- + - +
ICP4
RFP
E
H3.3
ICP4: +
-
F
RFP : +
-
Cells, %
G
H3.1
ICP4: +
-
H
RFP : +
-
Free Histone per Cell, %
I
H3.1
ICP4
-
+
0
1
200
Time, s

Figure 3.5. **H3.1 dynamics are enhanced more than those of H3.3 in Vero cells transiently expressing ICP4.** Vero cells were co-transfected with plasmids expressing GFP-H3.1 or -H3.3 and RFP-ICP4 or RFP, such that approximately half of the cells expressing detectable levels of GFP also express detectable levels of RFP. A), C) Average fluorescence recovery curves for GFP-H3.3 and -H3.1, respectively, for cells expressing detectable (red line) or undetectable (green line) levels of RFP-ICP4. B), D) Bar graphs showing the average levels of free GFP-H3.3 or -H3.1, respectively, in cells expressing detectable levels of RFP-ICP4 or RFP relative to cells expressing undetectable levels of RFP-ICP4 or RFP, respectively. E) Frequency distribution of the free pool of GFP-H3.3 in cells expressing detectable (red line) or undetectable (green line) levels of RFP-ICP4. F) Frequency distribution of the free pool of GFP-H3.3 in cells expressing detectable (dark red line) or undetectable (green line) levels of RFP. G) Frequency distribution of the free pool of H3.1 in cells expressing detectable (red line) or undetectable (green line) levels of RFP-ICP4. H) Frequency distribution of the free pool of GFP-H3.1 in cells expressing detectable (dark red line) or undetectable (green line) levels of RFP. I) Representative images of fluorescent nuclei expressing GFP-H3.1 and detectable or undetectable levels of RFP-ICP4, immediately prior to (T = 0) or after (T = 1) photobleaching, or 200 seconds later. Error bars, SEM. **, $P < 0.01$; *, $P < 0.05$; *n.s.,* not significant. n 15 cells from at least 3 independent experiments.

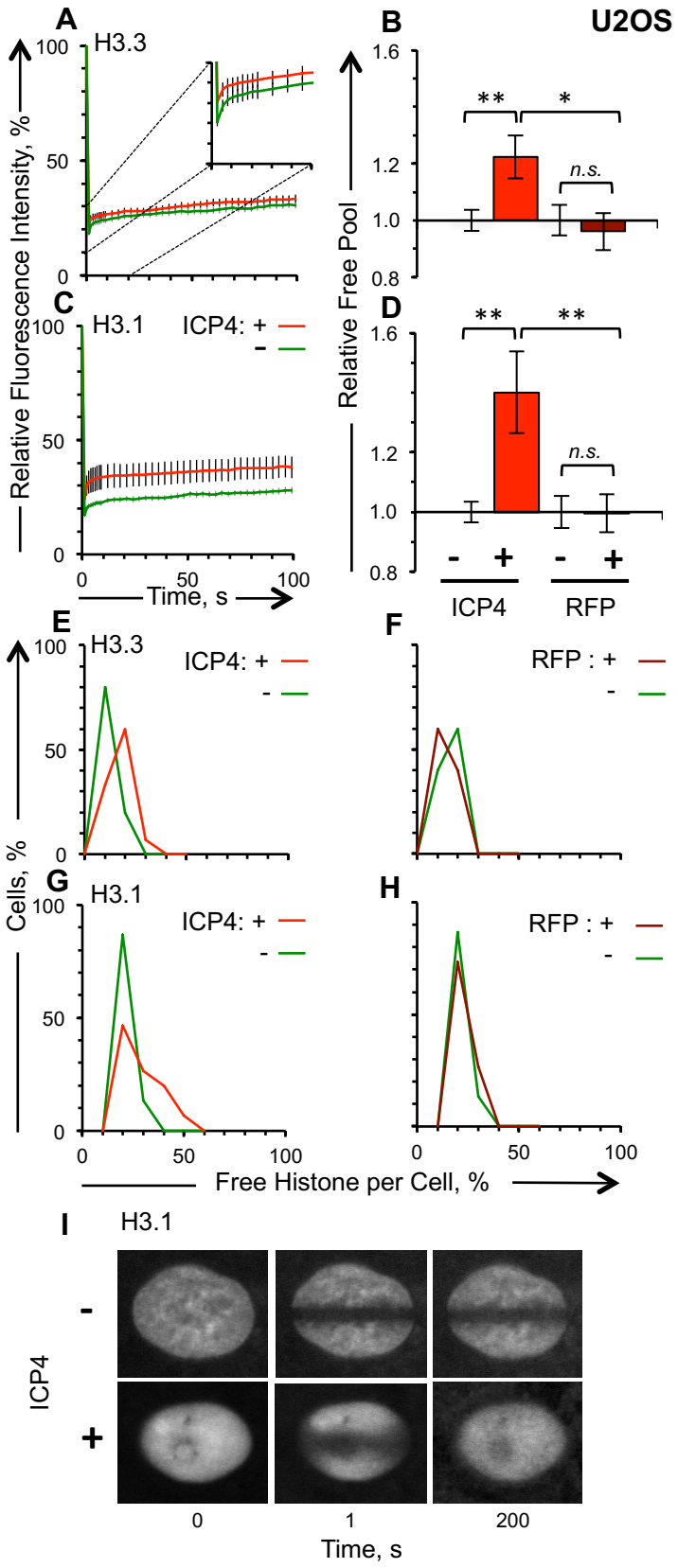
A
H3.3
Relative Fluorescence Intensity, %
100
50
0
B
U2OS
Relative Free Pool
1.6
1.2
1.0
0.8
**
*
n.s.
C
H3.1
ICP4: +
-
Time, s
0
50
100
D
**
**
n.s.
-
+
-
+
ICP4
RFP
E
H3.3
ICP4: +
-
Cells, %
F
RFP : +
-
G
H3.1
ICP4: +
-
H
RFP : +
-
Free Histone per Cell, %
I
H3.1
ICP4
-
+
0
1
200
Time, s

Figure 3.6. **H3.1 dynamics are enhanced more than those of H3.3 in U2OS cells transiently expressing ICP4.** U2OS cells were co-transfected with plasmids expressing GFP-H3.1 or -H3.3 and RFP-ICP4 or RFP, such that approximately half of the cells expressing detectable levels of GFP also express detectable levels of RFP. A), C) Average fluorescence recovery curves for GFP-H3.3 and -H3.1, respectively, for cells expressing detectable (red line) or undetectable (green line) levels of RFP-ICP4. B), D) Bar graphs showing the average levels of free GFP-H3.3 or -H3.1, respectively, in cells expressing detectable levels of RFP-ICP4 or RFP relative to those in cells expressing undetectable levels of RFP-ICP4 or RFP. E) Frequency distribution of the free pool of GFP-H3.3 in cells expressing detectable (redline) or undetectable (greenline) levels of RFP-ICP4. F) Frequency distribution curve of the free pool of GFP-H3.3 in cells expressing detectable (dark red line) or undetectable (green line) levels of RFP. G) Frequency distribution of the free pool of GFP-H3.1 in cells expressing detectable (red line) or undetectable (green line) levels of RFP-ICP4. H) Frequency distribution curve of the free pool of GFP-H3.1 in cells expressing detectable (dark red line) or undetectable (green line) levels of RFP. I) Representative images of fluorescent nuclei expressing GFP-H3.1 and detectable or undetectable levels of RFP-ICP4, immediately prior to (T = 0) or 1 second after (T = 1) photobleaching, or 200 seconds later. Error bars, SEM. **, $P < 0.01$; *, $P < 0.05$; *n.s.*, not significant. n 15 cells from at least 3 independent experiments.

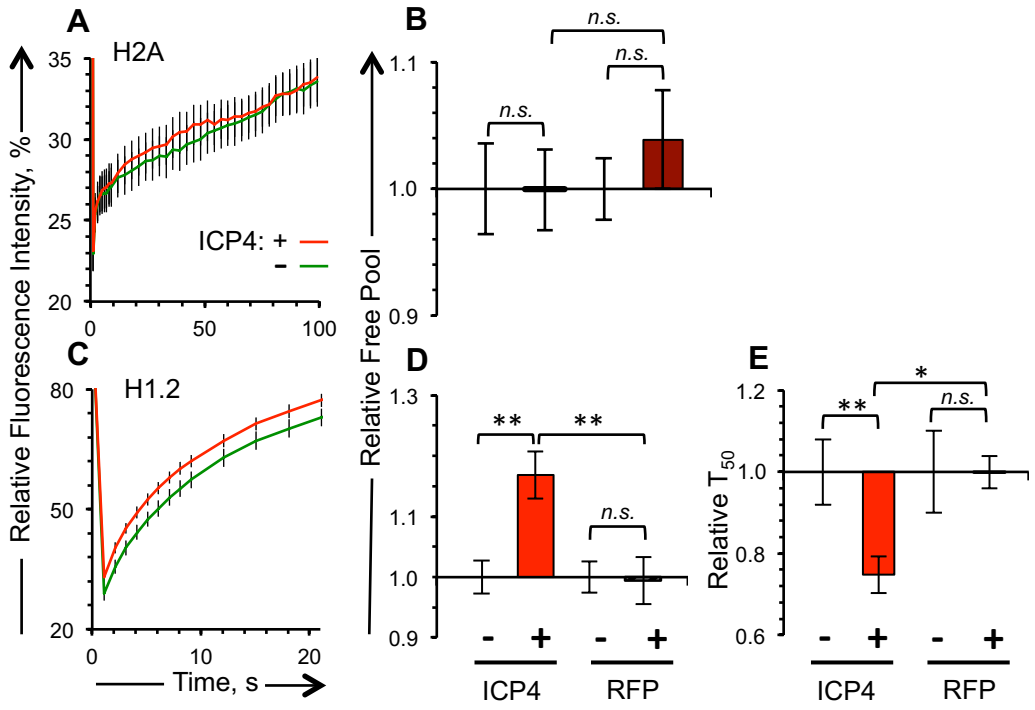

Figure 3.7. The dynamics of H1.2, but not those of canonical H2A, are enhanced in cells transiently expressing ICP4. Vero cells were co-transfected with plasmids expressing GFP-H2A or -H1.2 and RFP-ICP4 or RFP such that approximately half of the cells expressing detectable levels of GFP also express detectable levels of RFP. A), C) Average fluorescence recovery curves for GFP-H2A and -H1.2, respectively, for cells expressing detectable (red line) or undetectable (green line) levels of RFP-ICP4. B), D) Bar graphs showing the average levels of free GFP-H2A or -H1.2, respectively, in cells expressing detectable levels of RFP-ICP4 or RFP relative to those in cells expressing undetectable levels of RFP-ICP4 or RFP, respectively. E) Bar graphs showing the average T_{50} of GFP-H1.2 in cells expressing detectable levels of RFP-ICP4 or RFP relative to those in cells expressing undetectable levels of RFP-ICP4 or RFP. Error bars, SEM. **, $P < 0.01$; *, $P < 0.05$; *n.s.,* not significant. n ≥ 15 cells from at least 3 independent experiments.

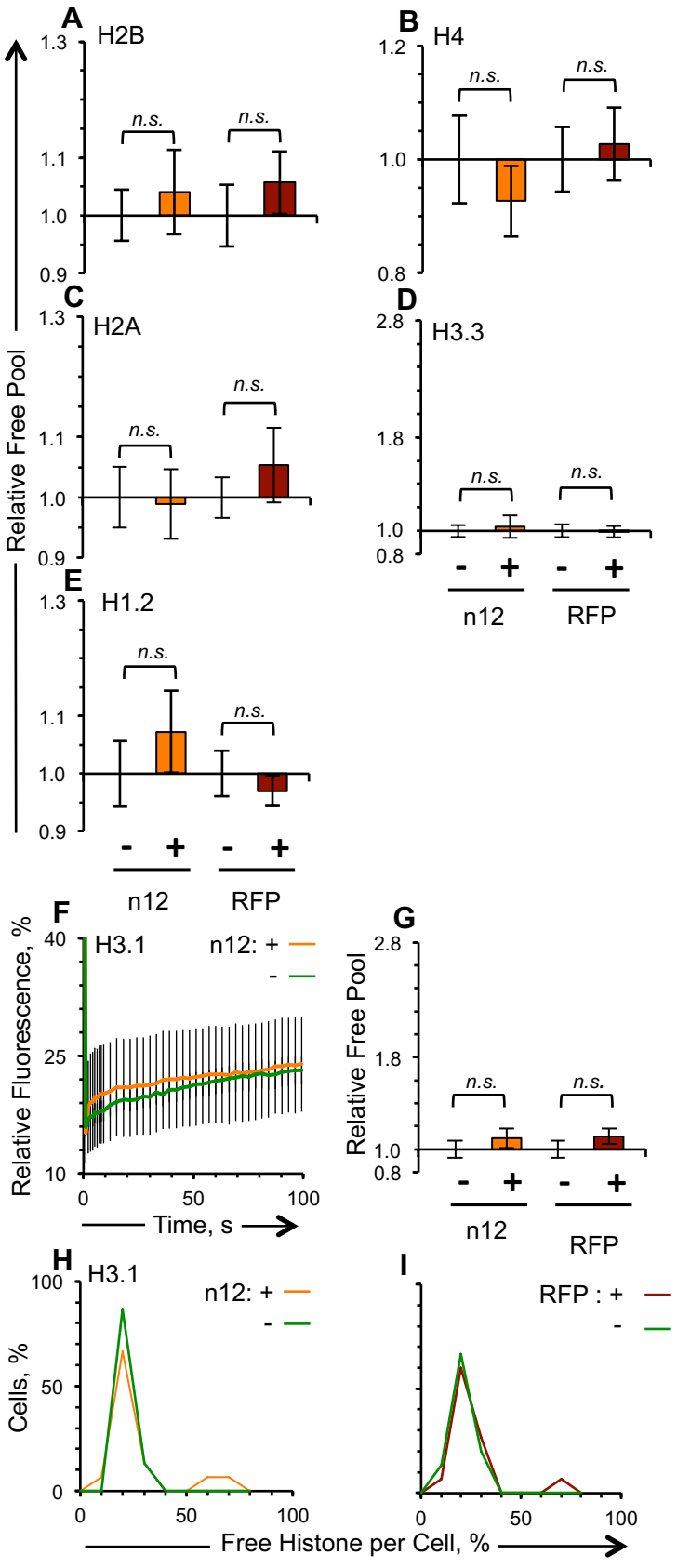
A
H2B
B
H4
C
H2A
D
H3.3
E
H1.2
Relative Free Pool
n.s.
n12
RFP
F
H3.1
n12: +
-
Relative Fluorescence, %
Time, s
G
Relative Free Pool
H
H3.1
n12: +
-
Cells, %
I
RFP : +
-
Free Histone per Cell, %

Figure 3.8. **The dynamics of no histone is altered in cells transiently expressing the truncated, non-functional, ICP4 mutant n12.** Vero cells were co-transfected with plasmids expressing GFP-histones and RFP-n12 or RFP such that approximately half of the cells expressing detectable levels of GFP also express detectable levels of RFP-n12. A-E), G) Bar graphs showing average levels of free GFP-H1.2, -H2A, -H2B, -H3.3, -H4, and -H3.1 in cells expressing detectable levels of RFP-n12 or RFP relative to those in cells expressing undetectable levels of RFP-n12 or RFP, respectively. F) Average fluorescence recovery curves for GFP-H3.1 in cells expressing detectable (orange) or undetectable (green line) levels of RFP-n12. H) Distribution curve of the free pool of GFP-H3.1 in cells expressing detectable (orange line) or undetectable (green line) levels of RFP-n12. I) Distribution curve of the free pool of GFP-H3.1 in cells expressing detectable (dark red line) or undetectable (green line) levels of RFP. Error bars, SEM. **, $P < 0.01$; *, $P < 0.05$; *n.s.*, not significant. $n \geq 15$ cells from at least 3 independent experiments.

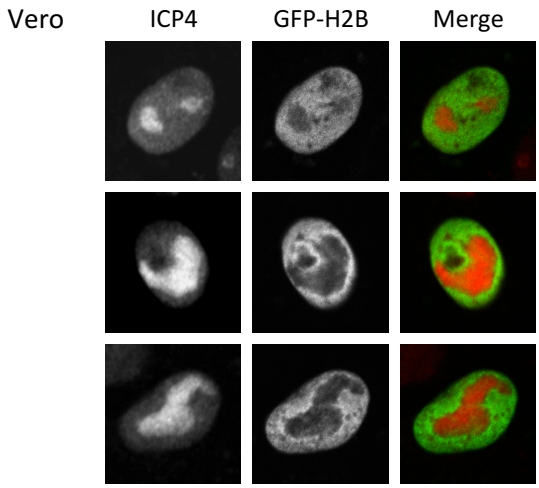

Figure 3.9. The majority of ICP4 localizes in the replication compartments with a small pool of histones. Digital fluorescent micrographs showing Vero cells expressing GFP-H2B, infected with 30 PFU of HSV-1 strain KOS, and stained with anti-ICP4 antibodies. Cells were fixed at 7 hpi and immunostained for ICP4. Single channel and merged images are shown. Note the presence of a small pool of GFP-H2B in the replication compartments.
Dr. Kristen Conn performed this experiment.

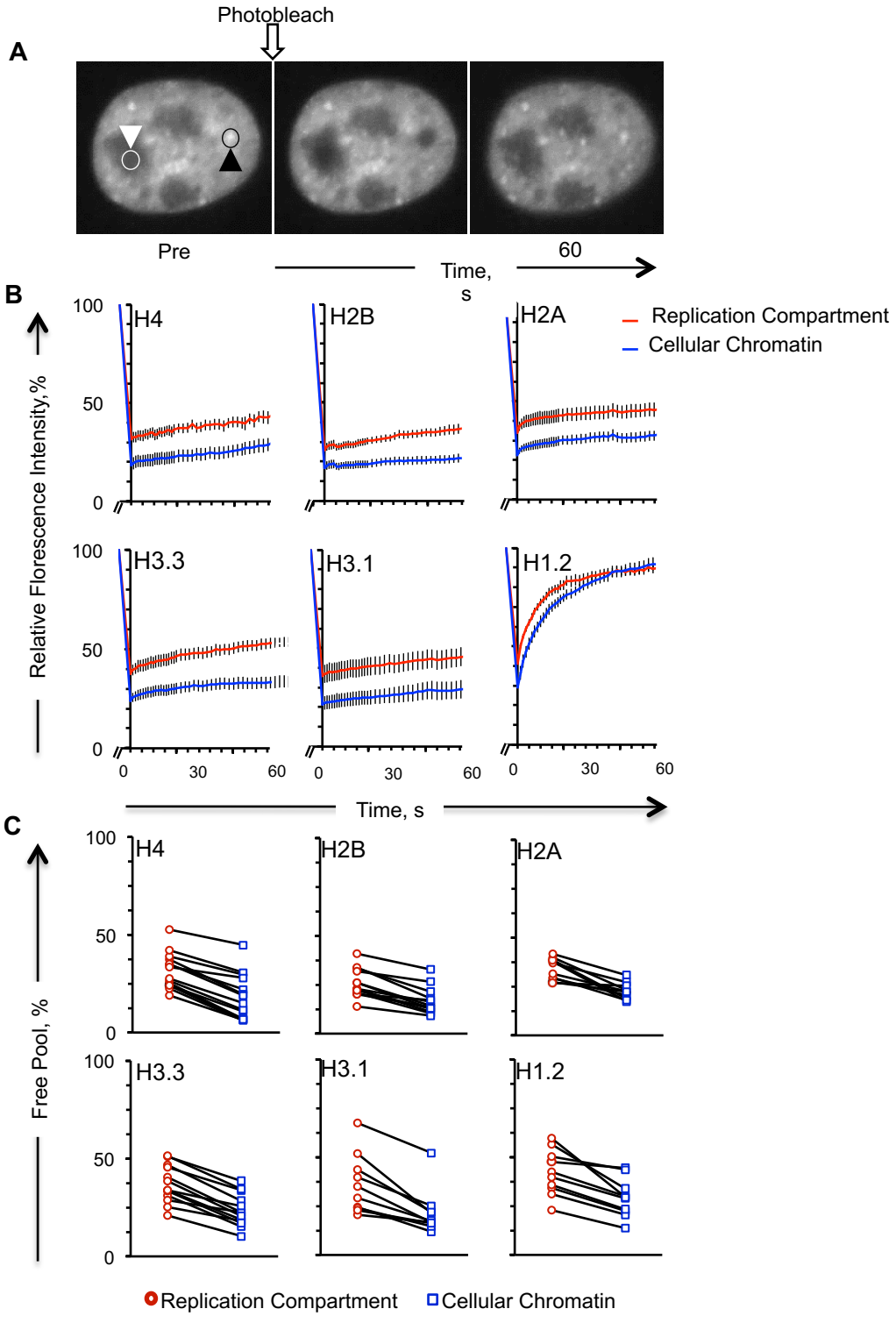
A
Photobleach
Pre
60
Time, s
B
Relative Florescence Intensity,%
H4
H2B
H2A
H3.3
H3.1
H1.2
Replication Compartment
Cellular Chromatin
100
50
0
0
30
60
Time, s
C
Free Pool, %
Replication Compartment
Cellular Chromatin

Figure 3.10. Fluorescence recovery of GFP-tagged histones in HSV-1 replication compartments or cellular chromatin. A) Fluorescence micrographs of the nucleus of an HSV-1 infected Vero cell expressing GFP-H1.2 and undergoing FRAP at 7 to 8 hpi. Left and middle micrographs, immediately prior (pre) or after photobleaching (T = 0), respectively; right micrograph, 60 seconds after photobleaching. White downward arrowhead and white circle, replication compartment region to be photobleached; black upward arrowhead and black circle, cellular chromatin region to be photobleached. Note the presence of a small pool of H1.2 in the replication compartments. B) Line graphs presenting the average ± SEM fluorescence recovery curves of histones GFP-H3.1 (n=10), GFP-H3.3 (n=13), GFP-H4 (n=14), GFP-H2A (n=10), GFP-H2B (n=13), and GFP-H1.2 (n=10) in the replication compartments or cellular chromatin at 7 to 8 h of infection with HSV-1, strain KOS. C) Dot plot presenting the free pools in the replication compartments or the cellular chromatin in each individual cell. Solid lines, same cells.
Michael Bildersheim performed the experiments presented in this figure.

Histone	Cotransfected	RFP	Free Pool (avg ± SEM)		Fast Rate (avg ± SEM)		Slow Rate (avg ± SEM)	
Variant	plasmid	detection	Absolute	Relative	Absolute	Relative	Absolute	Relative
H2B	RFP-ICP4	-	12.64 ± 0.47	1.00 ± 0.03	1.32 ± 0.08	1.00 ± 0.06	0.05 ± 0.01	1.00 ± 0.07
		+	14.12 ± 0.35	1.13 ± 0.03	1.66 ± 0.18	1.28 ± 0.14	0.08 ± 0.015	1.57 ± 0.29
	RFP-n12	-	12.43 ± 1.29	1.00 ± 0.10	1.05 ± 0.12	1.00 ± 0.11	0.09 ± 0.01	1.00 ± 0.15
		+	12.02 ± 0.56	0.96 ± 0.04	1.27 ± 0.10	1.31 ± 0.10	0.06 ± 0.01	0.65 ± 0.09
	free RFP	-	13.02 ± 0.84	1.00 ± 0.05	1.25 ± 0.15	1.00 ± 0.11	0.12 ± 0.05	1.00 ± 0.19
		+	12.89 ± 0.69	1.01 ± 0.04	1.44 ± 0.11	1.27 ± 0.13	0.10 ± 0.04	0.77 ± 0.16
H4	RFP-ICP4	-	29.34 ± 1.20	1.00 ± 0.03	3.24 ± 0.44	1.00 ± 0.14	0.06 ± 0.01	1.00 ± 0.11
		+	34.14 ± 1.70	1.23 ± 0.06	4.69 ± 0.61	1.45 ± 0.19	0.06 ± 0.01	1.37 ± 0.03
	RFP-n12	-	16.83 ± 1.32	1.00 ± 0.08	2.12 ± 0.41	1.00 ± 0.19	0.04 ± 0.01	1.00 ± 0.17
		+	15.53 ± 0.98	0.92 ± 0.06	1.78 ± 0.26	0.84 ± 0.12	0.05 ± 0.01	1.20 ± 0.18
	free RFP	-	23.41 ± 1.22	1.00 ± 0.04	2.16 ± 0.40	1.00 ± 0.18	0.09 ± 0.02	1.00 ± 0.21
		+	25.59 ± 1.28	1.07 ± 0.06	3.79 ± 0.80	1.76 ± 0.37	0.08 ± 0.01	1.20 ± 0.24
H3.1	RFP-ICP4	-	15.40 ± 2.49	1.00 ± 0.10	3.24 ± 1.56	1.00 ± 0.48	0.07 ± 0.01	1.00 ± 0.12
		+	33.66 ± 2.41	2.48 ± 0.28	15.02 ± 1.67	4.63 ± 0.51	0.05 ± 0.01	0.76 ± 0.09
	RFP-n12	-	15.87 ± 1.27	1.00 ± 0.08	0.91 ± 0.17	1.00 ± 0.18	0.05 ± 0.01	1.00 ± 0.19
		+	15.16 ± 3.89	0.95 ± 0.25	1.35 ± 1.87	1.49 ± 2.06	0.04 ± 0.01	0.76 ± 0.17
	free RFP	-	14.21 ± 1.60	1.00 ± 0.09	3.53 ± 1.23	1.00 ± 0.35	0.07 ± 0.01	1.00 ± 0.18
		+	14.95 ± 1.72	1.08 ± 0.12	2.98 ± 0.74	0.84 ± 0.21	0.06 ± 0.01	0.84 ± 0.20
H3.3	RFP-ICP4	-	26.21 ± 1.26	1.00 ± 0.03	2.24 ± 0.19	1.00 ± 0.08	0.08 ± 0.02	1.00 ± 0.14
		+	28.12 ± 1.53	1.11 ± 0.04	2.43 ± 0.21	1.08 ± 0.09	0.06 ± 0.01	0.89 ± 0.14
	RFP-n12	-	14.30 ± 0.87	1.00 ± 0.06	2.28 ± 0.34	1.00 ± 0.15	0.04 ± 0.01	1.00 ± 0.17
		+	15.07 ± 1.53	1.05 ± 0.11	1.56 ± 0.18	0.68 ± 0.08	0.04 ± 0.01	0.97 ± 0.10
	free RFP	-	27.32 ± 1.21	1.00 ± 0.03	2.90 ± 0.23	1.00 ± 0.08	0.07 ± 0.01	1.00 ± 0.21
		+	25.76 ± 1.20	0.97 ± 0.04	2.72 ± 0.19	0.93 ± 0.07	0.06 ± 0.01	0.92 ± 0.19
H2A	RFP-ICP4	-	22.91 ± 1.04	1.00 ± 0.02	2.43 ± 0.19	1.00 ± 0.08	0.07 ± 0.01	1.00 ± 0.16
		+	23.10 ± 1.22	1.00 ± 0.02	2.39 ± 0.26	0.98 ± 0.11	0.06 ± 0.01	0.92 ± 0.21
	RFP-n12	-	12.12 ± 0.77	1.00 ± 0.06	1.37 ± 0.17	1.00 ± 0.13	0.05 ± 0.01	1.00 ± 0.18
		+	11.94 ± 0.75	0.99 ± 0.06	1.44 ± 0.13	1.04 ± 0.10	0.05 ± 0.01	1.01 ± 0.25
	free RFP	-	21.21 ± 0.67	1.00 ± 0.02	2.25 ± 0.17	1.00 ± 0.08	0.07 ± 0.01	1.00 ± 0.10
		+	23.02 ± 1.16	1.02 ± 0.03	2.57 ± 0.19	1.14 ± 0.08	0.06 ± 0.01	0.82 ± 0.13

Table 3.1. Histone dynamics in Vero cells expressing detectable or undetectable levels of RFP-ICP4, RFP-n12, or free RFP.

Histone	Cotransfected	RFP	Free Pool (avg ± SEM)		Fast Rate (avg ± SEM)		Slow Rate (avg ± SEM)	
variant	plasmid	detection	Absolute	Relative	Absolute	Relative	Absolute	Relative
H3.1	RFP-ICP4	-	17.23 ± 0.75	1.00 ± 0.03	2.99 ± 0.51	1.00 ± 0.17	0.05 ± 0.02	1.00 ± 0.30
		+	24.24 ± 2.62	1.40 ± 0.14	5.91 ± 2.14	1.98 ± 0.71	0.04 ± 0.01	0.83 ± 0.18
	free RFP	-	16.21 ± 0.95	1.00 ± 0.05	3.67 ± 0.71	1.00 ± 0.19	0.05 ± 0.01	1.00 ± 0.18
		+	16.09 ± 1.04	1.00 ± 0.06	1.95 ± 0.51	0.53 ± 0.14	0.04 ± 0.01	0.77 ± 0.14
H3.3	RFP-ICP4	-	18.18 ± 0.76	1.00 ± 0.04	3.27 ± 0.74	1.00 ± 0.22	0.06 ± 0.01	1.00 ± 0.15
		+	22.18 ± 1.43	1.22 ± 0.08	1.48 ± 0.37	0.76 ± 0.11	0.05 ± 0.02	1.16 ± 0.26
	free RFP	-	19.94 ± 1.14	1.00 ± 0.05	3.88 ± 1.00	1.00 ± 0.26	0.07 ± 0.01	1.00 ± 0.14
		+	19.18 ± 1.36	0.96 ± 0.07	3.58 ± 0.54	0.92 ± 0.14	0.06 ± 0.01	0.81 ± 0.17

Table 3.2. H3 dynamics in U2OS cells expressing detectable or undetectable levels of RFP-ICP4, RFP-n12, or free RFP.

Chapter 4: The dynamics of H2A.B are enhanced in ICP4-expressing cells, whereas those of macroH2A, H2A.X, and H2A.Z are not.

4.1 Introduction

Cellular double-stranded (ds) DNA is organized in chromatin. The basic unit of chromatin is the core nucleosome, composed of two each of the core histone dimers H2A-H2B and H3-H4 wrapped by 146 base pairs (bp) of dsDNA. Chromatin is dynamic, as histones disassemble from nucleosomes, diffuse through the nucleoplasm in the free pool bound by chaperones, and reassemble nucleosomes at different sites. The dynamics of nucleosomes are altered through many factors, including the incorporation of histone variants in place of the canonical ones.

Whereas canonical histones are synthesized during the S-phase of the cell cycle and are assembled with newly synthesized DNA via DNA replication dependent mechanisms, most variant histones are synthesized independently of the cell cycle and are assembled with DNA via DNA replication independent mechanisms. Several H2A variants exist, including H2A.X, H2A.Z, macroH2A, and H2A.B. H2A.X has the greatest sequence similarity (91%) to canonical H2A, with an additional 13 amino acids on the C-terminal tail. H2A.X assembles more dynamic nucleosomes than canonical H2A in vitro, but is nonetheless less dynamic in the cells (81, 97). H2A.Z has 59% sequence similarity to canonical H2A (179). H2A.Z is enriched in nucleosomes at transcription start sites, and assembles more dynamic nucleosomes than H2A (151, 177, 187, 188, 442). H2A.B has only 48% sequence homology to H2A, lacking the N-terminal lysine residues which are extensively post-translationally modified in canonical H2A and also 15 amino acid residues at the C-terminus. Deletion of the N- or C-terminal tails of canonical H2A increases its dynamics (443). H2A.B assembles the most dynamic nucleosomes of any H2A variant and is the most dynamic H2A in living cells (193, 444). In contrast, macroH2A has an extended C-terminus (the macro domain) and assembles the least dynamic nucleosomes (445). Whereas H2A.B is generally enriched in nucleosomes in transcribed genes, macroH2A is generally enriched in nucleosomes in silenced genes (177).

The nucleoli are discrete highly transcribed nuclear domains. Most GFP-tagged core histones appear to be relatively depleted from the nucleolus. As expected from highly dynamic chromatin, the nucleolus has less DNA density, and higher protein density, than the nucleus (89, 90). Consequently, it contains a higher ratio of histones to DNA than the cellular chromatin (446). Most histones appear to have shorter residency times on nucleolar DNA (Kristen Conn, unpublished results), whereas H2A.B appears to be enriched in the nucleoli (447).

Like the nucleoli, replication compartments are discrete and highly transcribed nuclear domains with apparent general histone depletion. HSV-1 genomes and many HSV-1 proteins, including the essential transcription activator ICP4, localize at replication compartments. The dsDNA genomes of HSV-1 are assembled in highly dynamic chromatin (373), and the dynamics of histones are enhanced in infected cells, and particularly so in the replication compartments (82, 373–375).

ICP4 (in the presence of plasmid DNA) was sufficient to increase the free pools of all canonical core histones except H2A. H2B is in the free pool only as a dimer with canonical H2A or one of its variants. The dynamics of one or more of the H2A variants were thus expected to be enhanced in cells expressing ICP4. ICP4 (in the presence of plasmid DNA) was also sufficient to enhance to dynamics of the H3 variant H3.3 to some extent. However, the dynamics of canonical H3.1 were enhanced more, suggesting that ICP4 preferentially targets H3.1 over H3.3. I propose that, likewise, ICP4 may preferentially target an H2A variant over the others.

4.2 Results

4.2.1 GFP-macroH2A and GFP-H2A.B are incorporated into chromatin.

The only method available to evaluate histone dynamics in live cells is fluorescence recovery after photobleaching (FRAP). For FRAP of histones, a green fluorescent protein (GFP) polypeptide is covalently linked to the histone (78, 80, 82, 374, 375, 443, 448). GFP (~33 kDa) is approximately twice the size of canonical core histones, including canonical H2A (~14 kDa). Histones with GFP fused to the N-terminus are nonetheless still assembled in chromatin. I therefore decided to

construct plasmids encoding H2A.B or macroH2A with N-terminal GFP. H2A.B or macroH2A were fused in frame with GFP with a 5 amino acid linker, as confirmed by sequencing (The Applied Genomics Core, University of Alberta).

Canonical H2A is synthesized during S phase of the cell cycle and incorporated in DNA via replication-dependent mechanisms. In contrast, the H2A variants are synthesized independently of the cell cycle and incorporated in DNA via replication-independent mechanisms. The transient expression of the recombinant GFP-histones is driven by constitutive CMV IE promoters instead. GFP-H2A, GFP-H2A.B, and GFP-macroH2A are thus all expressed at any time of the cell cycle. GFP-H2A.B or –macroH2A, like endogenous H2A.B or macroH2A, are assembled in nucleosomes at any time of the cell cycle. GFP-H2A, like endogenous H2A, is only assembled in newly replicated DNA during S phase of the cell cycle. Whereas newly synthesized GFP-H2A.B or –macroH2A are assembled into chromatin before the cells have replicated, as observed by their discrete distributions, newly synthesized GFP-H2A are not, as observed by their diffuse distribution (Kristen Conn, unpublished observations). At 48 hours post transfection, most cells have undergone two full cycles, and GFP-H2A was assembled in chromatin, as shown by its discrete distribution (Kristen Conn, unpublished observation). The dynamics of GFP-H2A were thus evaluated by FRAP approximately 48 hours after transfection, whereas those GFP-H2A.B or –macroH2A were evaluated as early as 20 hours after transfection.

Like GFP-H2A, the ectopically expressed GFP-H2A.B or –macroH2A localized to the nucleus with discrete distribution consistent with their incorporation into chromatin (Figure 4.1.). Nuclei expressing GFP-H2A.B or –macroH2A show the clear bleached region at the first time point after photobleaching, indicating their incorporation into chromatin. Nuclei expressing GFP-H2A.B or –macroH2A still show a visibly bleached region at 100 s after photobleaching.

GFP-H2A.B was more dynamic than GFP-H2A, which is consistent with its assembling more dynamic nucleosomes. The fluorescence intensity of the bleached region was not clearly different between nuclei expressing GFP-H2A.B or –H2A at one second after photobleaching, (Figure 4.1.). A hundred seconds later, however,

the photobleached region in the nuclei expressing GFP-H2A.B had recovered more fluorescence than that in nuclei expressing GFP-H2A (Figure 4.1.). The average fluorescence recovery curve for GFP-H2A shows that the normalized free pool, which drops to approximately 15% at 1 sec, recovers to only 30% at 100 sec after photobleaching (Figure 4.2.). In contrast, the average fluorescence recovery for GFP-H2A.B, which was greater than 20% at 1 sec, recovered to as much as 70% at 100 sec after photobleaching (Figure 4.2.).

GFP-macroH2A was less dynamic than GFP-H2A, which is consistent with its assembling less dynamic nucleosomes. The fluorescence intensity of the bleached region was lower in nuclei expressing GFP-macroH2A at 1 sec or 100 sec after photobleaching, (Figure 4.1.). The slope of the fluorescence recovery curve of GFP-H2A was steeper than that of GFP-macroH2A, indicating than GFP-H2A recovered more fluorescence in the photobleached region than GFP-macroH2A (Figure 4.2.). At 100 sec after photobleaching, GFP-H2A had recovered approximately 30% of the initial fluorescence in the photobleached region, whereas GFP-macroH2A had recovered only 20%.

Cells expressing higher levels of GFP-H2A or GFP-H4 have no higher levels of GFP-histones in the free pool (82). Likewise, cells expressing higher levels of GFP-macroH2A or –H2A.B have no higher levels of GFP-histones in the free pool than cells expressing lower levels of GFP-macroH2A or –H2A.B (Figure 4.3.).

4.2.2 The dynamics of macroH2A, H2A.X, and H2A.Z are not affected by ICP4.

I optimized the transfection of GFP-macroH2A, -H2A.X, or –H2A.Z and RFP-ICP4, RFP-n12, or free RFP such that approximately half of the cells that expressed detectable levels of GFP also expressed detectable levels of RFP. I then compared the dynamics of the GFP-histones in cells expressing detectable levels of RFP to those in cells expressing undetectable levels of RFP in the same well. The dynamics of the GFP-histones were measured by FRAP.

The distribution of GFP-macroH2A was not different in Vero or U2OS cells expressing detectable or undetectable levels of RFP-ICP4, RFP-n12, or free RFP (Figure 4.4., 4.7.). The free pools, fast exchange rates, or slow exchange rates of

GFP-macroH2A were not significantly different in Vero or U2OS cells expressing detectable or undetectable levels of RFP-ICP4, RFP-n12, or free RFP either (Figure 4.5., 4.6., 4.8.).

The dynamics of GFP-H2A.X were not significantly altered in cells expressing detectable levels of RFP-ICP4, -n12, or free RFP (Figure 4.9.). The free pool, or fast or slow exchange rates of GFP-H2A.X were not altered in cells expressing detectable levels of RFP-ICP4, RFP-n12, or free RFP relative to cells expressing undetectable levels either (Figure 4.10.).

The free pool, fast exchange rate, or slow exchange rate of GFP-H2A.Z was not altered in cells expressing detectable levels of RFP-ICP4, RFP-n12, or free RFP (Figure 4.11., 4.12.).

In summary, ICP4 does not preferentially enhance the dynamics of the most silencing H2A variant, macroH2A. ICP4 neither affects the dynamics of H2A.X nor H2A.Z.

4.2.3 The dynamics of H2A.B are enhanced in cells expressing ICP4.

H2A.B assembles the most dynamic nucleosomes of any H2A variant, and is also the most dynamic H2A variant in the nucleus (449). To test whether the dynamics of H2A.B are affected by ICP4, cells were co-transfected with plasmids encoding GFP-H2A.B and RFP-ICP4. In Vero cells expressing detectable levels of RFP-ICP4, GFP-H2A.B was enriched at the nucleoli, which is where RFP-ICP4 also localizes in transfected cells (Figure 4.13., 4.14.). In contrast, the nuclear distribution of GFP-H2A.B was not different in Vero cells expressing detectable or undetectable levels of RFP-n12 or free RFP (Figure 4.14.). H2A.B had granular distribution in the nucleolus and general chromatin in ICP4-expressing cells, suggesting that ICP4 does not inhibit the assembly of H2A.B into chromatin (Figure 4.15.). The free pool and fast exchange rate of GFP-H2A.B was significantly higher in Vero cells expressing detectable levels of RFP-ICP4 (Figure 4.16, 4.17.C,E). In contrast, the free pool and fast exchange rate of GFP-H2A.B were not significantly different in Vero cells expressing detectable or undetectable levels of RFP-n12 or free RFP.

GFP-H2A.B was also enriched at the nucleoli in U2OS cells expressing detectable levels of RFP-ICP4 (Figure 4.18.). There was no difference in the distribution of GFP-H2A.B in U2OS cells expressing detectable or undetectable levels of free RFP, but there was a partial enrichment of GFP-H2A.B in U2OS cells expressing detectable levels of RFP-n12. The free pool and fast exchange rate of GFP-H2A.B was significantly higher in U2OS cells expressing detectable levels of RFP-ICP4 than in cells expressing undetectable levels (Figure 4.19.). The free pool and fast exchange rate of GFP-H2A.B were also increased in U2OS cells expressing detectable levels of RFP-n12, albeit less so than those in cells expressing RFP-ICP4. Free RFP had no effect on the dynamics of GFP-H2A.B (Figure 4.19.).

4.3 Discussion

H2A with GFP fused to its N- or C-terminus still incorporates into chromatin (443). Whereas H2B and H4 with N-terminal GFP strictly localizes to chromatin, H2B and H4 with C-terminal GFP do not (Kristen Conn, unpublished observations). The N-termini of H2B and H4 are unstructured and extend from the globular domain, whereas their C-termini are folded within the globular domain (30). In contrast, 15 amino acids of the C-terminus of H2A extend from the globular domain (30). The attachment of GFP to the C-terminus of H2B or H4 may thus prevent the proper folding of their globular domains, and assembly of the core nucleosome, whereas it does not affect folding of H2A. As GFP is less likely to affect histone folding when fused to the N-terminus and all other GFP histone fusions had GFP at their N-terminus, I constructed fusion proteins of macroH2A or H2A.B with GFP fused to the N-terminus. MacroH2A is the only H2A variant reported to assemble less dynamic nucleosomes than those containing canonical H2A (176). H2A.B is reported to assemble the most dynamic nucleosomes (193). Consistently, GFP-macroH2A is less dynamic and GFP-H2A.B is more dynamic than GFP-H2A (Figure 4.1.,4.2.).

Whereas H3.1 is assembled in nucleosomes by CAF-1 via DNA-replication dependent mechanisms, H3.3 is assembled in nucleosomes by HIRA or DAXX via DNA-replication independent mechanisms. HIRA assembles H3.3 in nucleosomes

with transcribed DNA, whereas DAXX assembles H3.3 in nucleosomes with telomeric DNA (40, 45, 146, 147, 410, 450). In salt stability assays, with a minimal set of cellular proteins, H3.3-containing nucleosomes are less stable than those containing H3.1 (151). However, H3.3 assembled in nucleosomes at telomeres is less dynamic than H3.3 assembled in nucleosomes with transcribed genes (150). Consistently, genes are silenced when inserted into telomeres (412). H3.3-containing nucleosomes may thus be more or less dynamic than H3.1-containing nucleosomes, depending on whether they are assembled with transcribed genes or telomeres, respectively. ICP4 may prevent the assembly of H3.3 via Daxx in HSV-1 nucleosomes, as they may silence HSV-1 gene transcription. The levels of H3.3 stably associated with HSV-1 genomes decreases in cells knocked down for HIRA, and the genomes are less efficiently transcribed and replicated (371). H3.3 assembled in nucleosomes with HSV-1 genomes via HIRA thus likely supports HSV-1 replication. Knockdown of Daxx increases the transcription and replication efficiency of HSV-1 mutants encoding no functional ICP0 (428). However, ICP0 does not directly interact with Daxx, nor does it cause its degradation (428). Instead, ICP0 promotes the degradation of PML, resulting in the dissociation of PML bodies to where Daxx and HSV-1 genomes both localize (336). HSV-1 may have thus evolved mechanisms to prevent to assembly of H3.3 in less dynamic nucleosomes with HSV-1 genomes via Daxx, while promoting the assembly of H3.3 in more dynamic nucleosomes via HIRA. Likewise, HSV-1 may have evolved ICP4 to prevent the assembly of H3.1 in nucleosomes with HSV-1 genomes, as they are less dynamic than those containing H3.3 (151). We expected then that ICP4 would also preferentially enhance the dynamics of macroH2A, as it assembles the most stable nucleosomes of any H2A variant (176). We found instead that ICP4 enhanced the dynamics of only H2A.B, which assembles the most dynamic nucleosomes (193).

The distribution of H2A.B, but not that of H2A, macroH2A, H2A.X, or H2A.Z, is different in cells expressing detectable or undetectable levels of RFP-ICP4 (Figure 4.4., 4.8., 4.10., 4.11., 4.20, 4.21). H2A.B is more enriched at nucleoli in Vero or U2OS cells expressing detectable RFP-ICP4 (Figure 4.14., 4.18.). RFP-ICP4 localizes to the replication compartments in infected cells, but at the nucleolus in transfected cells.

RFP-ICP4 may thus recruit H2A.B, directly or indirectly, to the nucleolus. Histones in the nucleolus are more dynamic than those in the general chromatin, with nucleolar H2A.B being the most dynamic (Kristen Conn, unpublished results). The recruitment of H2A.B from the less dynamic cellular chromatin to the more dynamic nucleolus would thus be expected to enhance the average nuclear dynamics of H2A.B.

Whereas RFP-ICP4 altered the distribution of H2A.B in both Vero and U2OS cells, RFP-n12 altered to some extent the distribution of H2A.B in only U2OS cells. Nucleolar enrichment of H2A.B in U2OS cells expressing RFP-n12 was less than in those expressing RFP-ICP4. Consistently, RFP-n12 enhanced H2A.B dynamics less than RFP-ICP4 in U2OS cells. U2OS cells are permissive to HSV-1 mutants lacking VP16 and ICP0, without directly complementing their activities. U2OS cells do not express ATRX, whose knockdown enhances the replication of ICP0 mutants in other cell lines (428).

H3.3 is assembled in nucleosomes with HSV-1 genomes immediately upon nuclear entry, whereas H3.1 is only assembled in nucleosomes with HSV-1 genomes after the onset of HSV-1 DNA replication (371). The HSV-1 transcription activators ICP0 and VP16 decrease the stable association of histones with HSV-1 genomes (316, 333). ICP0 and VP16 are present prior to HSV-1 DNA replication, and prior to the assembly of H3.1 in nucleosomes with HSV-1 DNA. Thus, ICP0 and VP16 may preferentially affect nucleosomes containing H3.3, as HSV-1 genomes are only assembled in H3.3-containing nucleosomes when they are both initially expressed. In the absence of ATRX, H3.3 may not be efficiently disassembled from nucleosomes with cell genomes or assembled in nucleosomes with the infecting HSV-1 genomes. Thus, HSV-1 gene transcription may occur efficiently even in the absence of ICP0 or VP16. RFP-n12 is unable to activate transcription, but it contains ICP4 amino acid residues 90 to 275, which are required to activate transcription (342). U2OS cells are deficient in cellular defense mechanisms against HSV-1, allowing replication of HSV-1 ICP0 or VP16 mutants (395, 451). I propose that the deficiency in U2OS cells also allows RFP-n12 to affect H2A.B dynamics.

Though we show that ICP4 preferentially enhances the dynamics of H3.1 and H2A.B, it seems to do so by different mechanisms. GFP-H3.1, which assembles less dynamic nucleosomes, appears to not be efficiently incorporated into chromatin in cells expressing ICP4, suggesting that ICP4 inhibits the assembly of H3.1 in nucleosomes. In contrast, GFP-H2A.B, which assembles the most dynamic nucleosomes and is the only H2A variant affected by ICP4, appears to still be incorporated into chromatin in cells expressing ICP4. Instead, GFP-H2A.B is enriched at the nucleoli, where ICP4 is localized, suggesting possible recruitment by ICP4. I thus propose a model in which ICP4 prevents the assembly of nucleosomes containing the most stable variants, and promotes the assembly of nucleosomes containing the least stable ones. ICP4 has no known enzymatic activity, and therefore it cannot directly modify histones to alter nucleosome dynamics. VP16 is recruited to IE promoters by cellular Oct-1 bound to specific DNA sequences. Likewise, ICP4 could recruit histone modifiers or chromatin remodeling complexes to HSV-1 genomes. I don't favor this model, however, because E or L promoters contain no specific DNA sequences required for ICP4 recruitment, and the DNA-binding activity of ICP4 is not required to activate transcription (353). ICP4 may compete with histones for binding to DNA, decreasing the histones stably associated with HSV-1 genomes. Alternatively, ICP4 may enhance dynamics of histones by binding to dimers or monomers, preventing the assembly of histones in less dynamic nucleosomes with HSV-1 genomes, or promoting the assembly of histones in the more dynamic ones. White Spot Syndrome Virus (WSSV), another nuclear-replicating DNA virus, encodes for a protein named ICP11 which localizes with H3 and H2A.X (452). ICP11 is negatively charged, and may mimic DNA to directly bind histones and prevent their assembly in nucleosomes (452). Like ICP11, ICP4 has negatively charged domains (355). ICP4 may thus enhance dynamics of histones by binding to histone chaperones and preventing them from assembling histones in chaperones. BNRF1 of Epstein-Barr Virus binds to DAXX and H3.3, resulting in increased H3.3 dynamics in cells expressing BNRF1 (435). My results suggest different mechanisms for ICP4 enhancement of the dynamics of H3.1 and H2A.B.

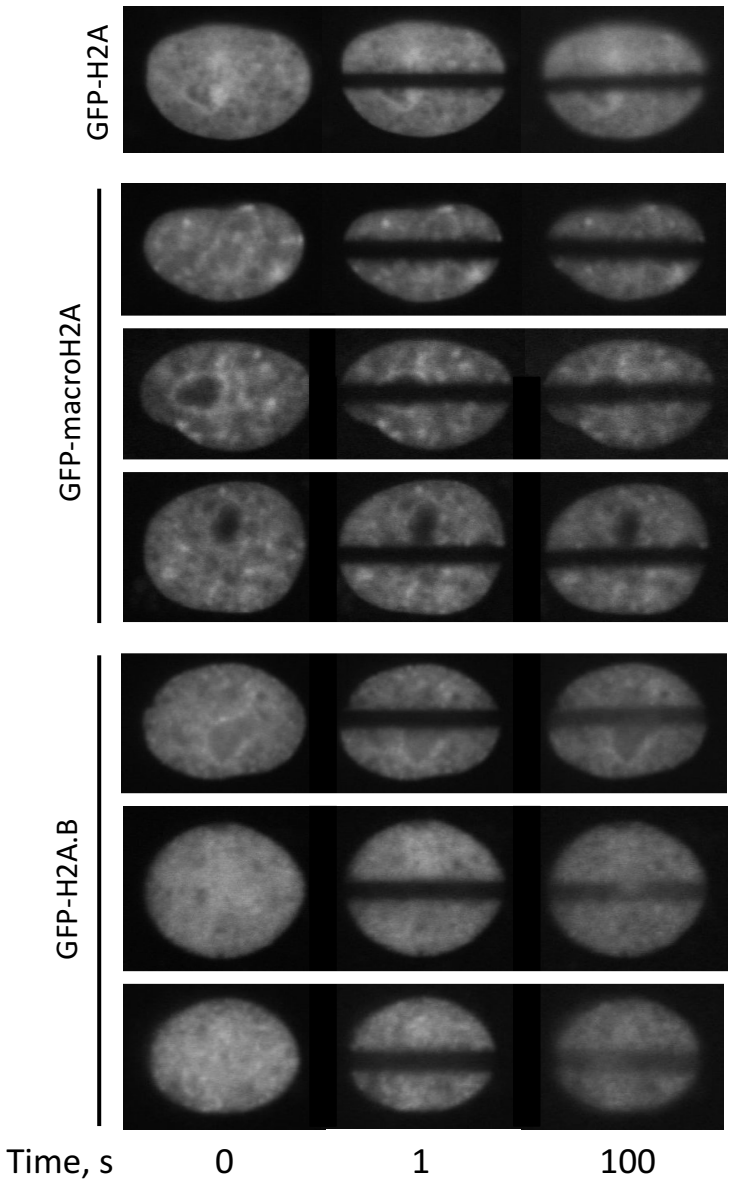

Figure 4.1. GFP-H2A.B and GFP-macroH2A are incorporated in chromatin. Representative fluorescent micrograph images of Vero cells expressing GFP-H2A, -macroH2A, or –H2A.B. The GFP-histones in regions spanning mock-infected nuclei were photobleached. 0 s, immediately prior to photobleaching; 1 s, immediately after photobleaching; 100 s, 100 s after photobleaching.

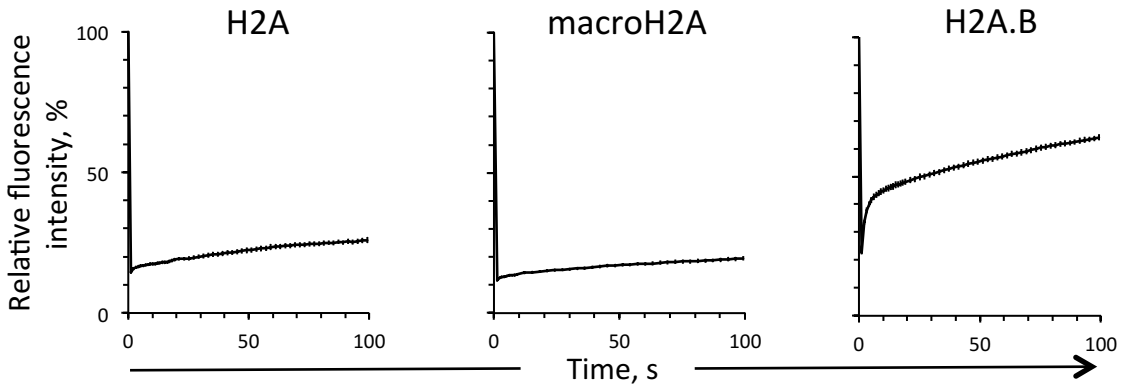

Figure 4.2. H2A.B is more dynamic than canonical H2A, whereas macroH2A is less dynamic. Line graphs representing the average fluorescence recovery curves for GFP-H2A, -H2A.B and –macroH2A in mock-infected cells at 4 hpi. Error bars, SEM.

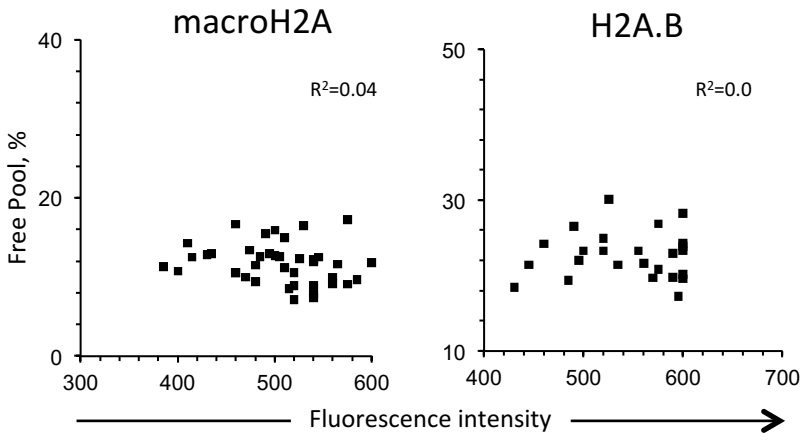

Figure 4.3. The percent of free GFP-H2A.B or –macroH2A per cell does not correlate to its expression levels. Dot plots presenting the level of GFP-H2A.B or -macroH2A in the free pool of each individual cell against its normalized fluorescence intensity. Vero cells were transfected with GFP-H2A.B or -macroH2A, mock-infected, and the dynamics of GFP-H2A.B or -macroH2A were evaluated 4 to 5 hours later.

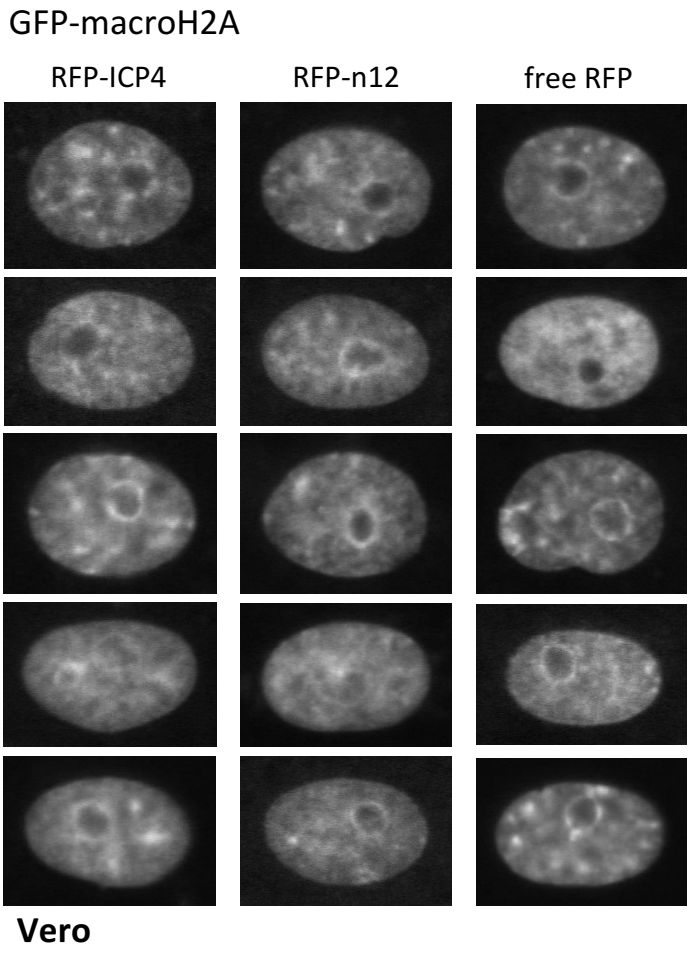

Figure 4.4. ICP4 does not affect the distribution of macroH2A in Vero cells. Representative fluorescent micrograph images of nuclei expressing GFP-macroH2A and detectable levels of RFP-ICP4, RFP-n12, or free RFP.

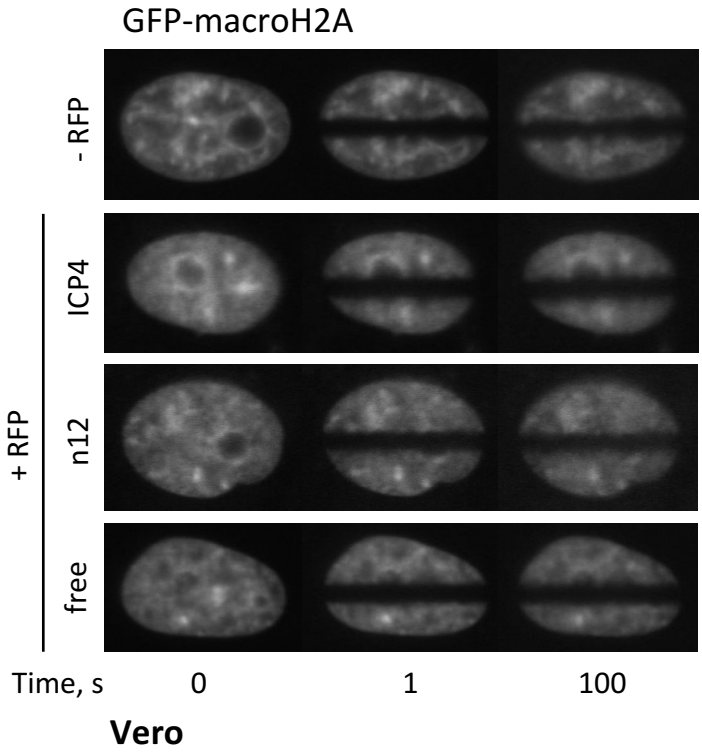

Figure 4.5. The dynamics of macroH2A are not significantly different in Vero cells expressing detectable levels of ICP4. Representative fluorescent micrograph images of nuclei expressing GFP-macroH2A alone, or expressing GFP-macroH2A with RFP-ICP4, RFP-n12, or free RFP. 0 s, immediately prior to photobleaching; 1 s, immediately after photobleaching; 100 s, 100 s after photobleaching.

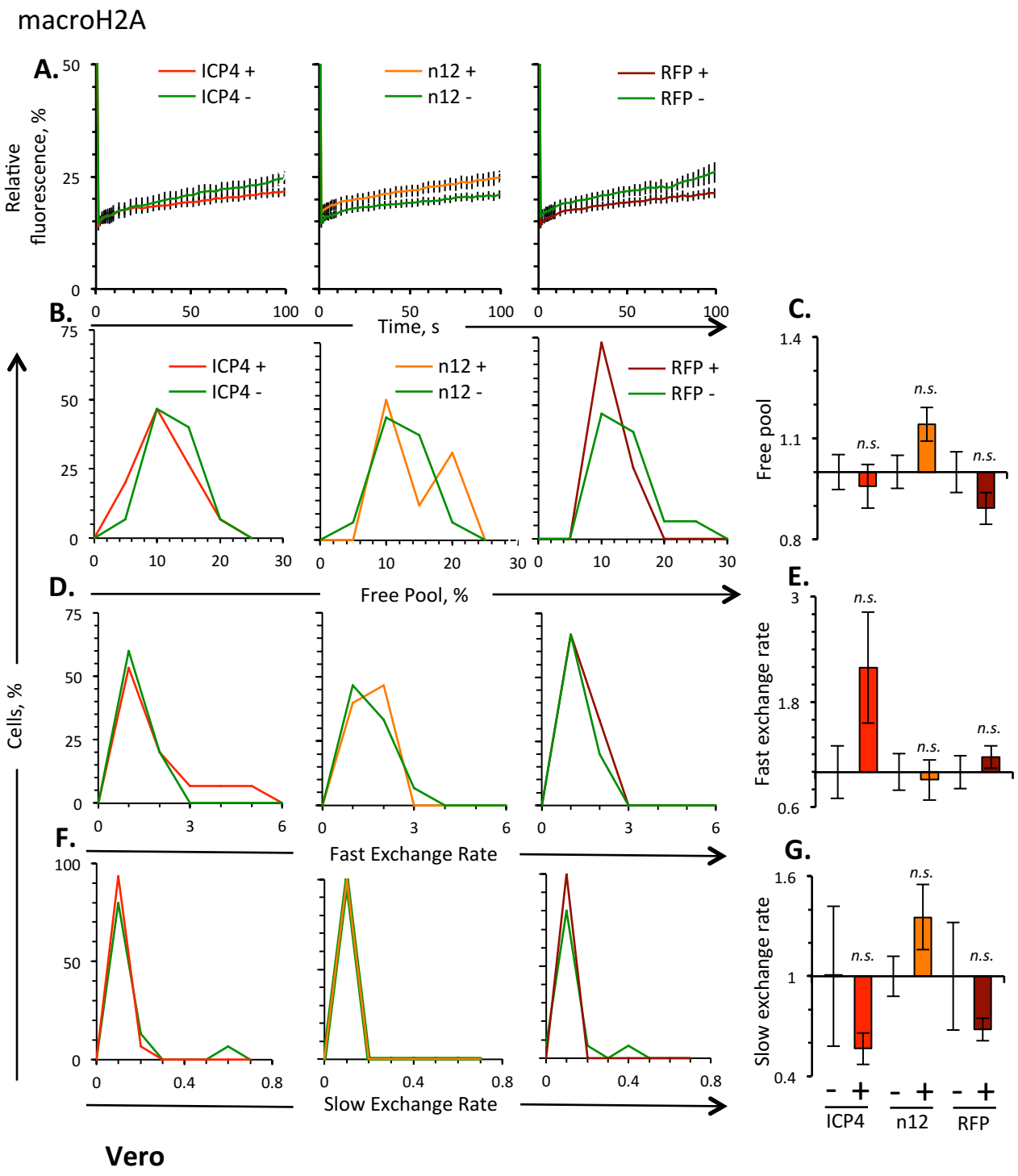
macroH2A
A.
ICP4 +
ICP4 -
n12 +
n12 -
RFP +
RFP -
Relative fluorescence, %
Time, s
B.
C.
Free pool
n.s.
D.
Free Pool, %
E.
Fast exchange rate
F.
Fast Exchange Rate
G.
Slow exchange rate
Slow Exchange Rate
Cells, %
ICP4
n12
RFP
Vero

Figure 4.6. The dynamics of macroH2A are not altered in Vero cells expressing ICP4. Vero cells were transfected with plasmids expressing GFP-macroH2A and RFP-ICP4, RFP-n12, or free RFP, such that approximately half of the cells expressing detectable levels of GFP also expressed detectable levels of RFP. The dynamics of GFP-macroH2A in cells expressing detectable levels of RFP were compared to those in cells in the same well not expressing detectable levels of RFP. A) Average fluorescence recovery curves for GFP-macroH2A in cells expressing undetectable levels (green line) or detectable levels of RFP-ICP4, RFP-n12, or free RFP (red, orange, or dark red line, respectively). B) Frequency distribution graphs of the free pools, fast exchange rates, or slow exchange rates of GFP-macroH2A in cells expressing detectable levels (green line) or detectable levels of RFP-ICP4, RFP-n12, or free RFP (red, orange, or dark red line, respectively). C) Bar graphs showing the average levels of free GFP-macroH2A in cells expressing undetectable levels or detectable levels of RFP-ICP4, RFP-n12, or free RFP. D) Bar graphs showing the average fast exchange rates of GFP-macroH2A in cells expressing undetectable levels or detectable levels of RFP-ICP4, RFP-n12. E) Bar graphs showing the average slow exchange rates of GFP-macroH2A in cells expressing undetectable levels or detectable levels of RFP-ICP4, RFP-n12, or free RFP. Error bars, SEM. *n.s.,* not significant. n ≥ 15 cells from at least 3 independent experiments.

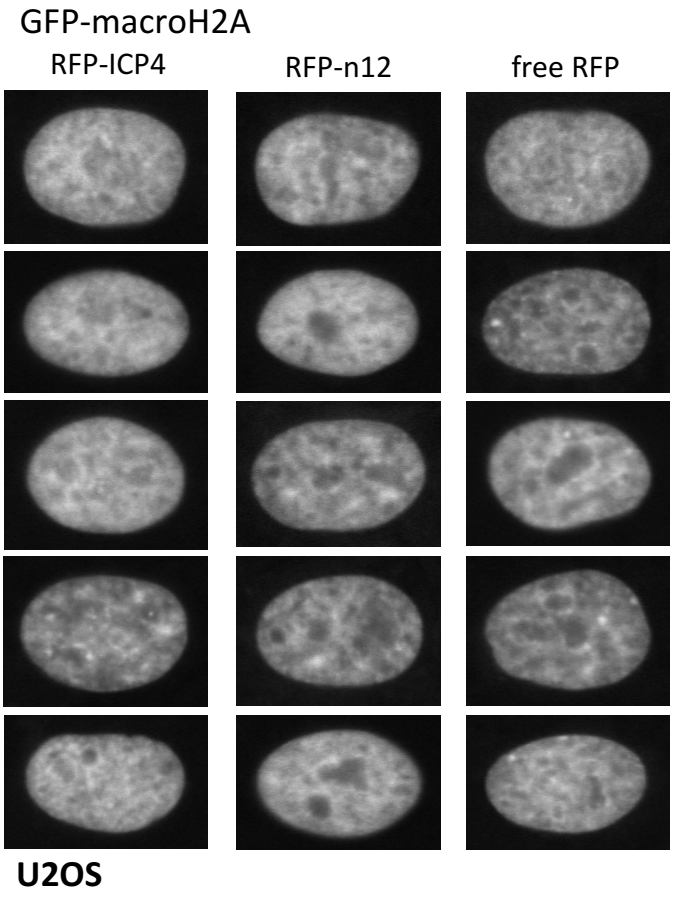

Figure 4.7. ICP4 does not affect the distribution of macroH2A in U2OS cells. Representative fluorescent micrograph images of nuclei expressing GFP-macroH2A and detectable levels of RFP-ICP4, RFP-n12, or free RFP.

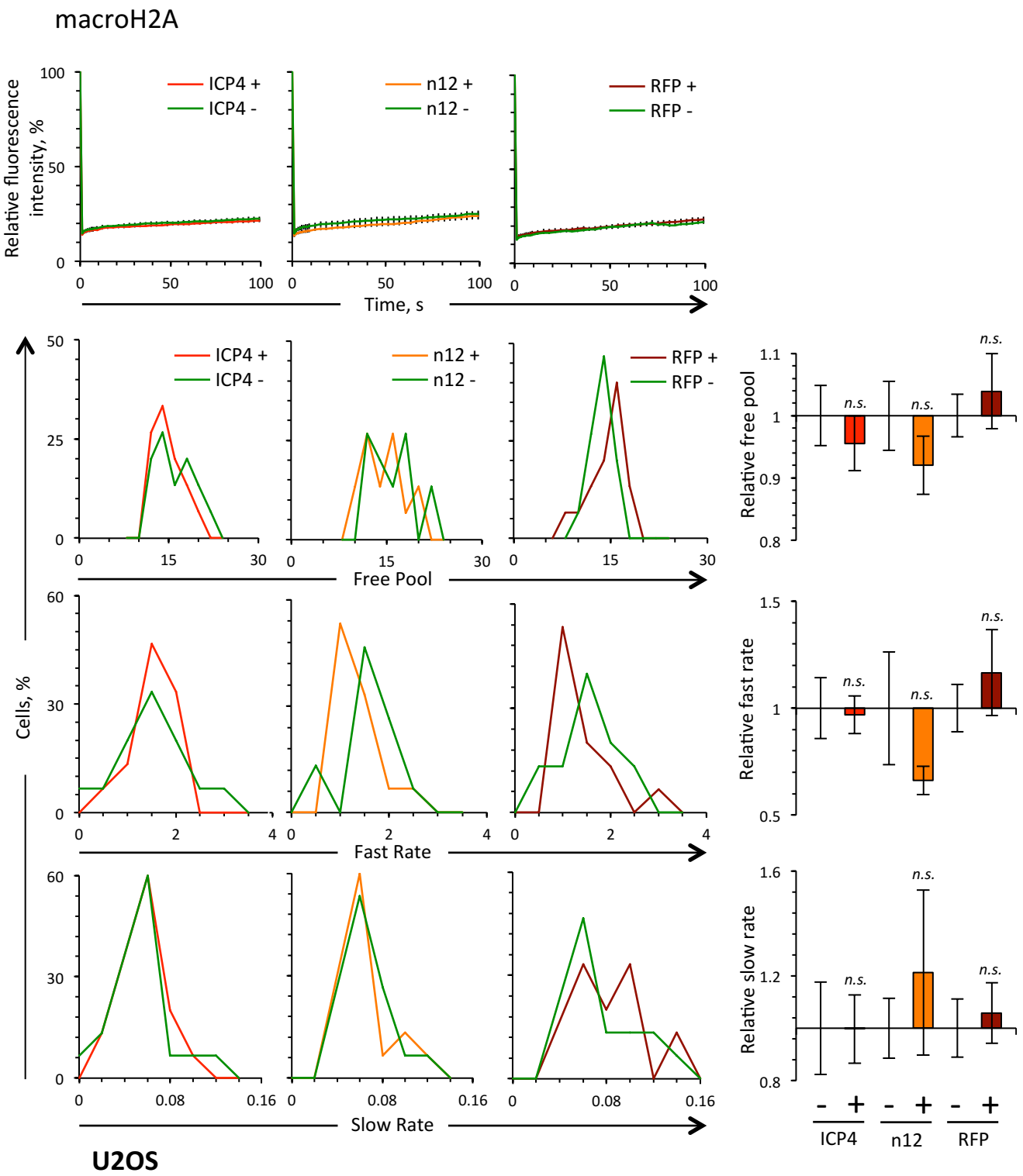
macroH2A
Relative fluorescence intensity, %
ICP4 +
ICP4 -
n12 +
n12 -
RFP +
RFP -
Time, s
Cells, %
Free Pool
Fast Rate
Slow Rate
Relative free pool
Relative fast rate
Relative slow rate
n.s.
- + - + - +
ICP4
n12
RFP
U2OS

Figure 4.8. The dynamics of macroH2A are not altered in U2OS cells expressing ICP4. Vero cells were transfected with plasmids expressing GFP-macroH2A and RFP-ICP4, RFP-n12, or free RFP such that approximately half of the cells expressing detectable levels of GFP also expressed detectable levels of RFP. The dynamics of GFP-macroH2A in cells expressing detectable levels of RFP were compared to those in cells not expressing detectable levels of RFP from the same well. A) Average fluorescence recovery curves for GFP-macroH2A in cells expressing undetectable levels (green line) or detectable levels of RFP-ICP4, RFP-n12, or free RFP (red, orang, or dark red line, respectively). B) Frequency distribution graphs of the free pools, fast exchange rates, or slow exchange rates of GFP-macroH2A in cells expressing undetectable levels (green line) or detectable levels of RFP-ICP4, RFP-n12, or free RFP (red, orange, or dark red line, respectively). C) Bar graphs showing the average levels of free GFP-macroH2A in cells expressing undetectable levels or detectable levels of RFP-ICP4, RFP-n12, or free RFP. D) Bar graphs showing the average fast exchange rates of GFP-macroH2A in cells expressing undetectable levels or detectable levels of RFP-ICP4, RFP-n12, or free RFP. E) Bar graphs showing the average slow exchange rates of GFP-macroH2A in cells expressing undetectable levels or detectable levels of RFP-ICP4, RFP-n12, or free RFP. Error bars, SEM. *n.s.,* not significant. n ≥ 15 cells from at least 3 independent experiments.

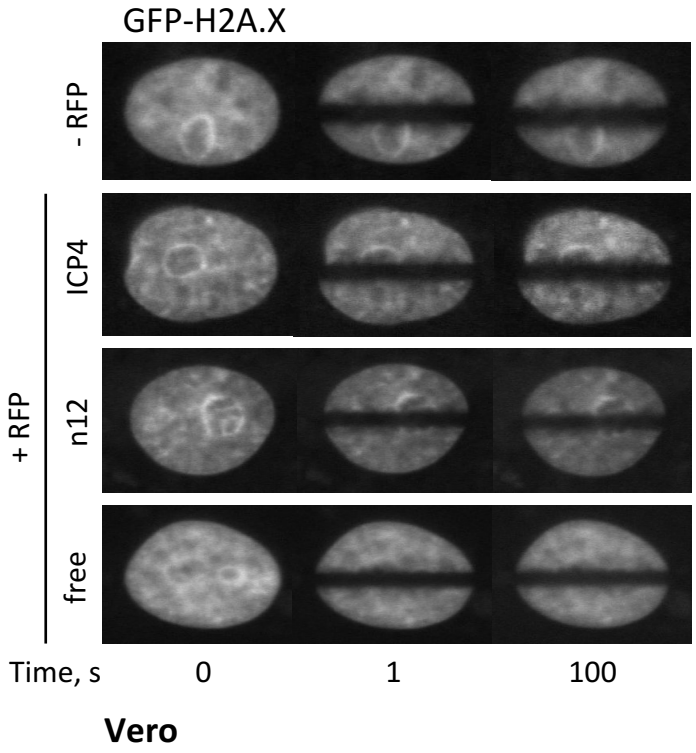

Figure 4.9. The dynamics of H2A.X are not significantly different in cells expressing detectable levels of ICP4. Representative fluorescent micrograph images of nuclei expressing GFP-H2A.X alone, or expressing GFP-H2A.X with RFP-ICP4, RFP-n12, or free RFP. 0 s, immediately prior to photobleaching; 1 s, immediately after photobleaching; 100 s, 100 s after photobleaching.

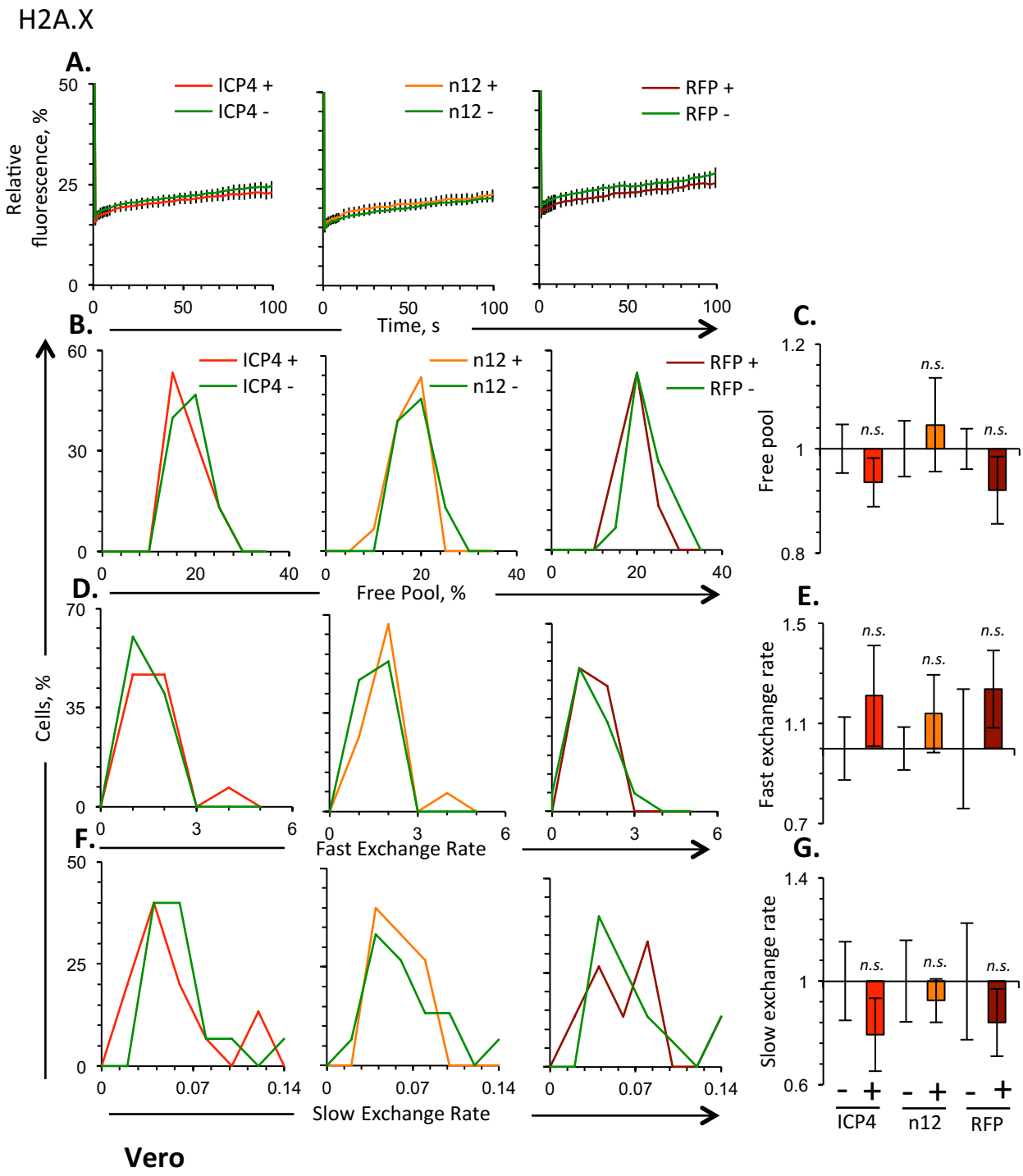
H2A.X
A.
ICP4 +
ICP4 -
n12 +
n12 -
RFP +
RFP -
Relative fluorescence, %
Time, s
B.
Free Pool, %
C.
Free pool
n.s.
D.
Cells, %
E.
Fast exchange rate
F.
Fast Exchange Rate
G.
Slow exchange rate
Slow Exchange Rate
ICP4
n12
RFP
Vero

Figure 4.10. The dynamics of H2A.X are not altered in cells expressing ICP4. Vero cells were transfected with plasmids expressing GFP-H2A.X and RFP-ICP4, RFP-n12, or free RFP such that approximately half of the cells expressing detectable levels of GFP also expressed detectable levels of RFP. The dynamics of GFP-H2A.X in cells expressing detectable levels of RFP were compared to those in cells not expressing detectable levels of RFP from the same well. A) Average fluorescence recovery curves for GFP-H2A.X in cells expressing undetectable levels (green line) or detectable levels of RFP-ICP4, RFP-n12, or free RFP (red, orange, or dark red line, respectively). B) Frequency distribution graphs of the free pools, fast exchange rates, or slow exchange rates of GFP-H2A.X in cells expressing undetectable levels (green line) or detectable levels of RFP-ICP4, RFP-n12, or free RFP (red, orange, or dark red line, respectively). C) Bar graphs showing the average levels of free GFP-H2A.X in cells expressing undetectable levels or detectable levels of RFP-ICP4, RFP-n12. D) Bar graphs showing the average fast exchange rates of GFP-H2A.X in cells expressing undetectable levels or detectable levels of RFP-ICP4, RFP-n12, or free RFP. E) Bar graphs showing the average slow exchange rates of GFP-H2A.X in cells expressing undetectable levels or detectable levels of RFP-ICP4, RFP-n12, or free RFP. Error bars, SEM. $n \geq 10$ cells from at least 2 independent experiments.

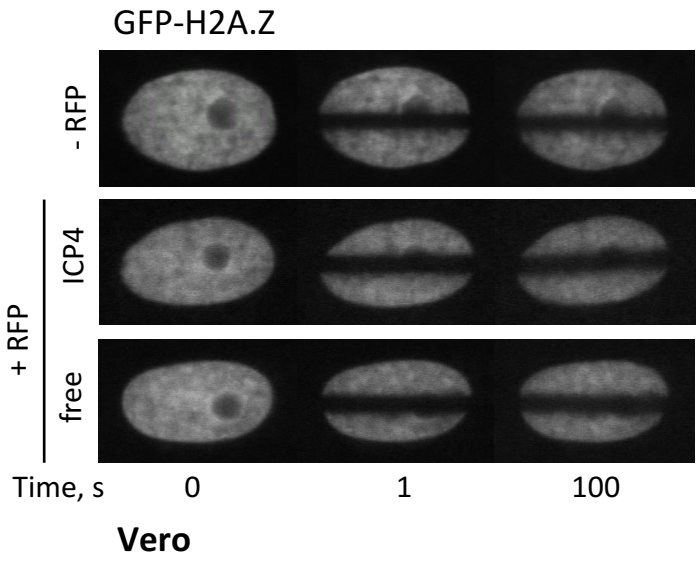

Figure 4.11. The dynamics of H2A.Z are not significantly different in cells expressing detectable levels of ICP4. Representative fluorescent micrograph images of nuclei expressing GFP-H2A.Z alone, or expressing GFP-H2A.Z with RFP-ICP4, or free RFP. 0 s, immediately prior to photobleaching; 1 s, immediately after photobleaching; 100 s, 100 s after photobleaching.

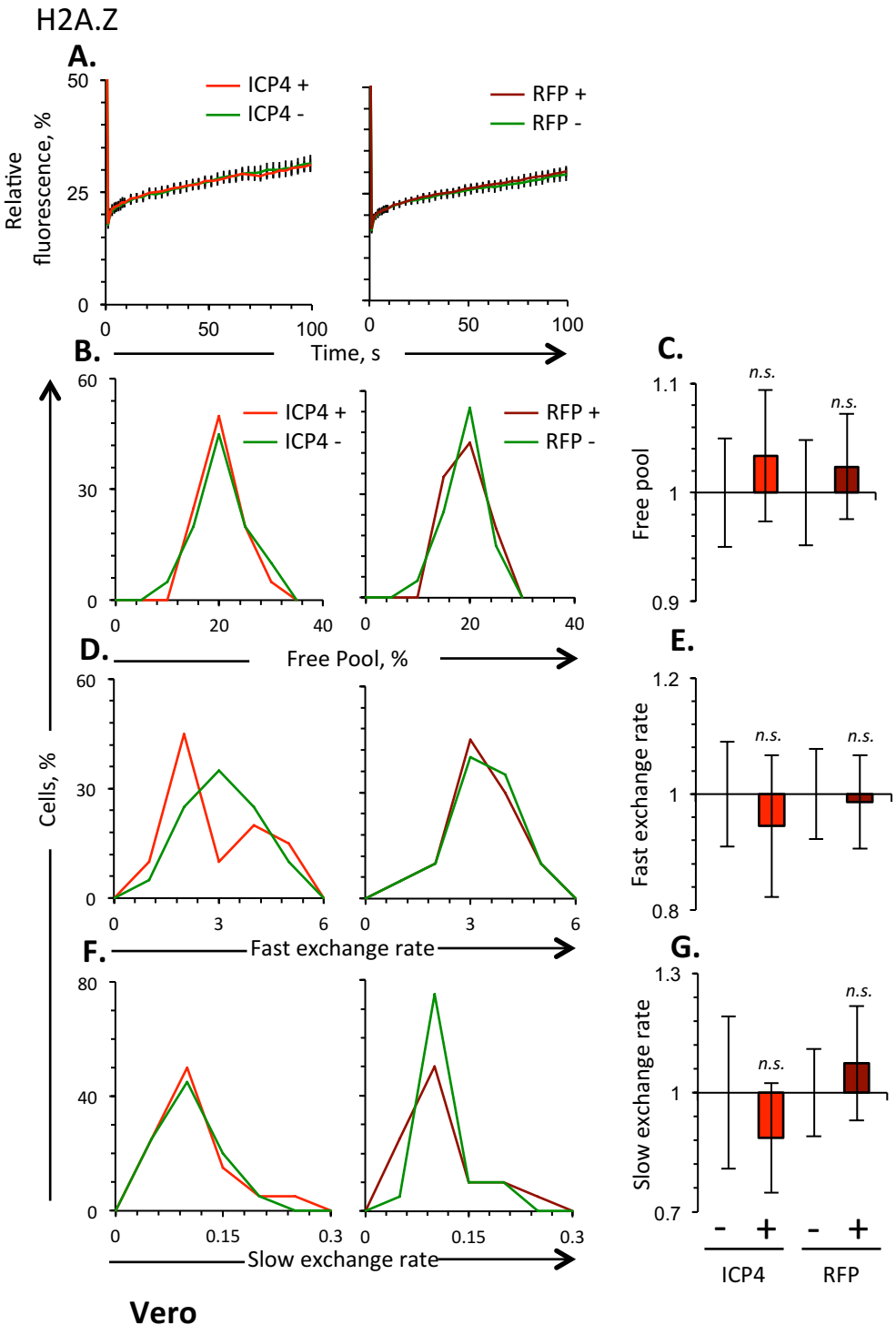
H2A.Z
A.
ICP4 +
ICP4 -
RFP +
RFP -
Relative fluorescence, %
Time, s
B.
C.
Free pool
n.s.
D.
Free Pool, %
Cells, %
E.
Fast exchange rate
F.
G.
Slow exchange rate
ICP4
RFP
Vero

Figure 4.12. The dynamics of H2A.Z are not altered in cells expressing ICP4. Vero cells were transfected with plasmids expressing GFP-H2A.Z and RFP-ICP4 or free RFP such that approximately half of the cells expressing detectable levels of GFP also expressed detectable levels of RFP. The dynamics of GFP-H2A.Z in cells expressing detectable levels of RFP were compared to those in cells not expressing detectable levels of RFP from the same well. A) Average fluorescence recovery curves for GFP-H2A.Z in cells expressing undetectable levels (green line) or detectable levels of RFP-ICP4 or free RFP (red or dark red line, respectively). B) Frequency distribution graphs of the free pools, fast exchange rates, or slow exchange rates of GFP-H2A.Z in cells expressing undetectable levels (green line) or detectable levels of RFP-ICP4 or free RFP (red or dark red line, respectively). C) Bar graphs showing the average levels of free GFP-H2A.Z in cells expressing undetectable levels or detectable levels of RFP-ICP4 or free RFP. D) Bar graphs showing the average fast exchange rates of GFP-H2A.Z in cells expressing undetectable levels or detectable levels of RFP-ICP4 or free RFP. E) Bar graphs showing the average slow exchange rates of GFP-H2A.Z in cells expressing undetectable levels or detectable levels of RFP-ICP4 or free RFP. Error bars, SEM. n ≥ 15 cells from at least 3 independent experiments.

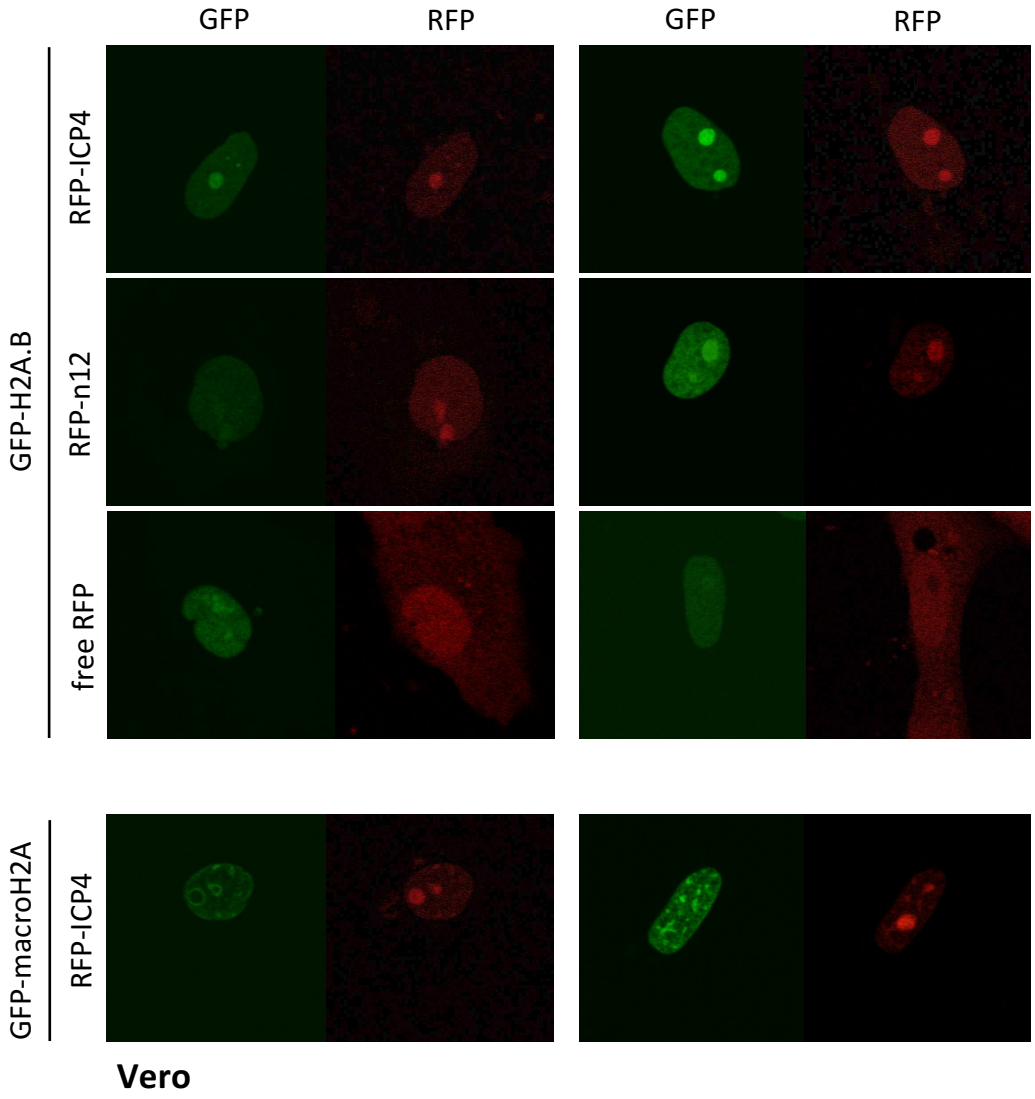

Figure 4.13. H2A.B is localized at the nucleoli with ICP4. Representative fluorescent micrograph images of nuclei expressing GFP-H2A.B or GFP-macroH2A (green filter) and RFP-ICP4, RFP-n12, or free RFP (red filter).

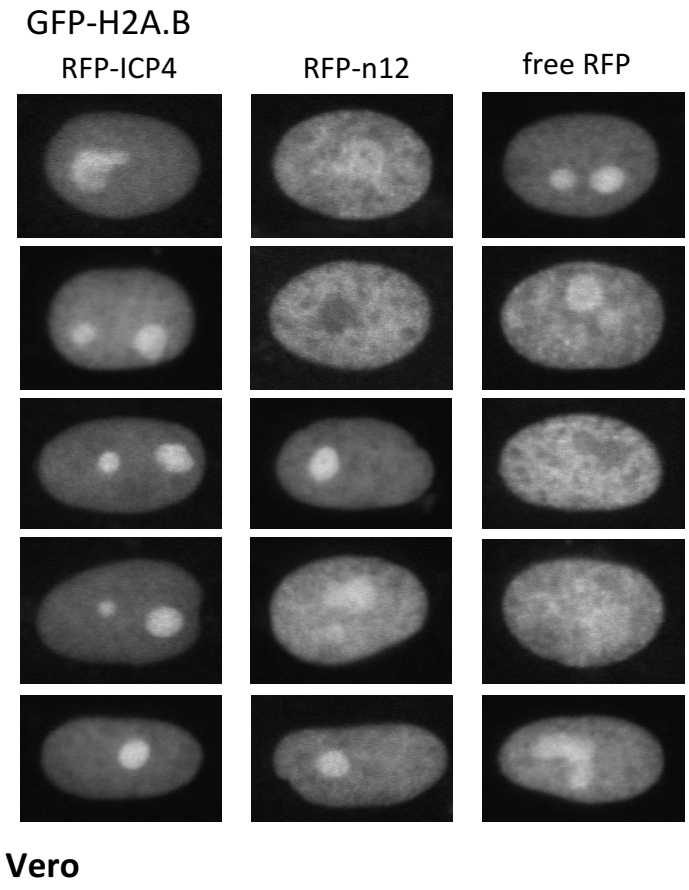

Figure 4.14. H2A.B is enriched in nucleoli in Vero cells expressing detectable levels of ICP4, n12 or free RFP. Fluorescent micrograph images of nuclei expressing GFP-H2A.B and detectable levels of RFP-ICP4, RFP-n12, or free RFP.

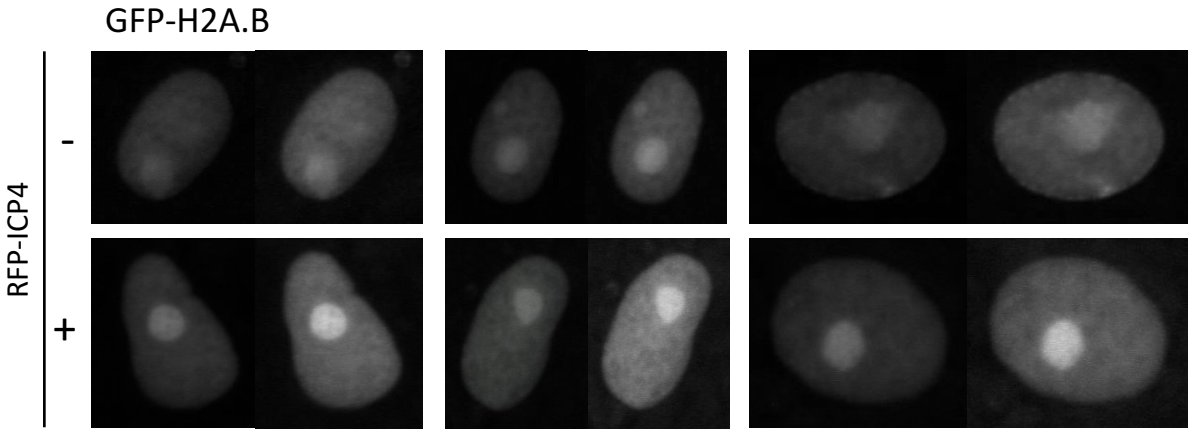

Figure 4.15. H2A.B is incorporated into chromatin in ICP4-expressing cells. Fluorescent micrograph images of nuclei expressing GFP-H2A.B and undetectable levels (-) or detectable levels (+) of RFP-ICP4 at two different exposures. H2A.B has granular distribution in the chromatin and nucleoli of all cells, regardless of ICP4 expression.

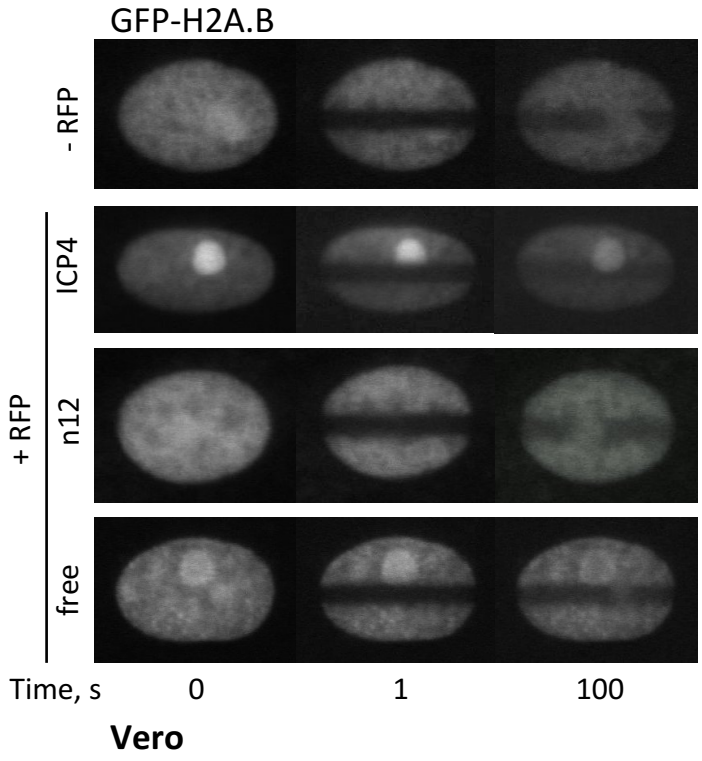

Figure 4.16. The dynamics of H2A.B are greater in Vero cells expressing detectable levels of ICP4. Representative fluorescent micrograph images of nuclei expressing GFP-H2A.B alone, or expressing GFP-H2A.B with RFP-ICP4, RFP-n12, or free RFP. 0 s, immediately prior to photobleaching; 1 s, immediately after photobleaching; 100 s, 100 s after photobleaching.

H2A.B

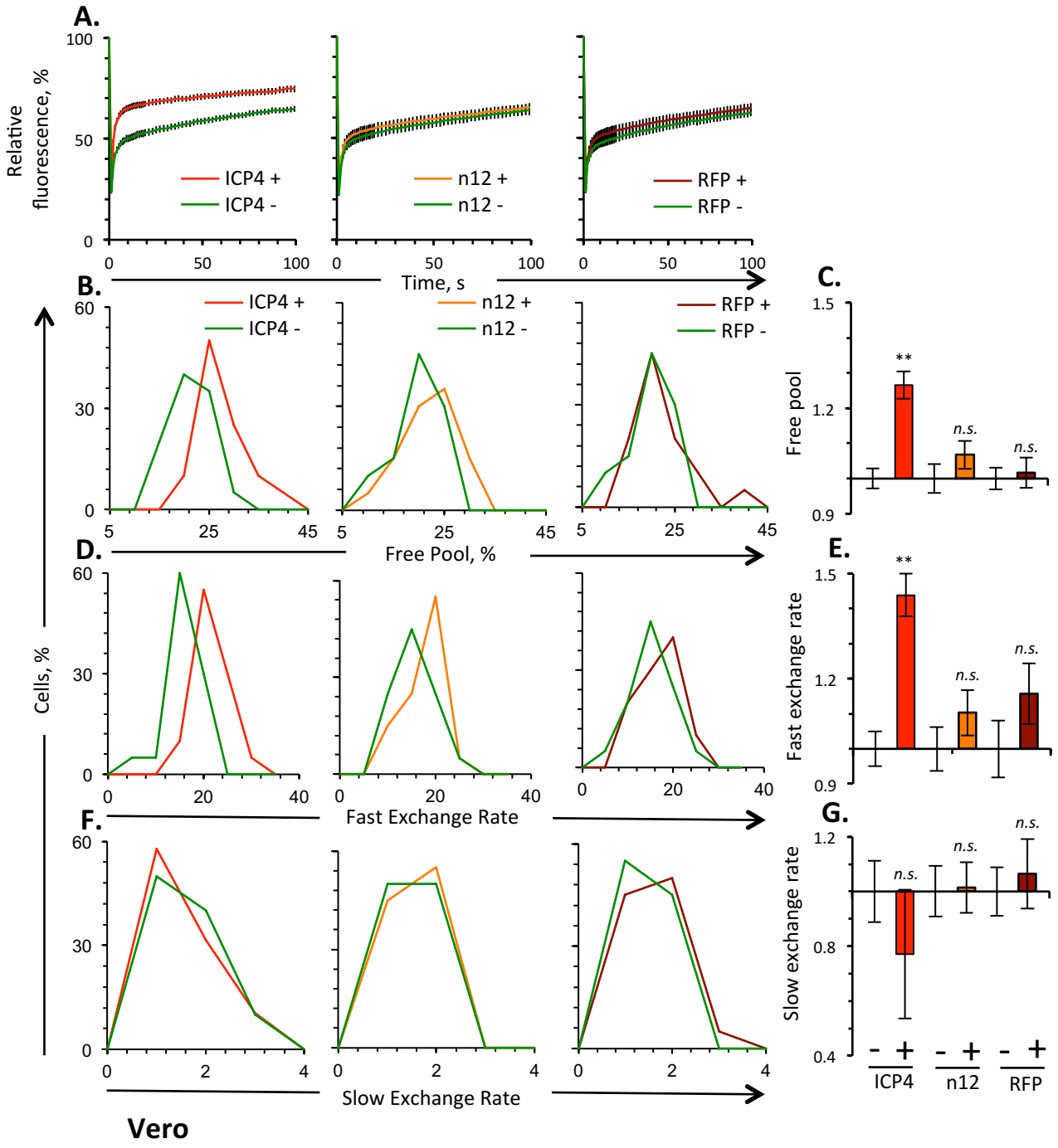
A.
Relative fluorescence, %
ICP4 +
ICP4 -
n12 +
n12 -
RFP +
RFP -
Time, s
B.
C.
Free pool
n.s.
D.
Free Pool, %
E.
Fast exchange rate
F.
Fast Exchange Rate
G.
Slow exchange rate
Slow Exchange Rate
Cells, %
ICP4
n12
RFP
Vero

Figure 4.17. The dynamics of H2A.B are enhanced in Vero cells expressing ICP4. Vero cells were transfected with plasmids expressing GFP-H2A.B and RFP-ICP4, RFP-n12, or free RFP such that approximately half of the cells expressing detectable levels of GFP also expressed detectable levels of RFP. The dynamics of GFP-H2A.B in cells expressing detectable levels of RFP were compared to those in cells not expressing detectable levels of RFP from the same well. A) Average fluorescence recovery curves for GFP-H2A.B in cells expressing undetectable levels (green line) or detectable levels of RFP-ICP4, RFP-n12, or free RFP (red, orange, or dark red line, respectively). B) Frequency distribution graphs of the free pools, fast exchange rates, or slow exchange rates of GFP-H2A.B in cells expressing undetectable levels (green line) or detectable levels of RFP-ICP4, RFP-n12, or free RFP (red, orange, or dark red line, respectively). C) Bar graphs showing the average levels of free GFP-H2A.B in cells expressing undetectable levels or detectable levels of RFP-ICP4, RFP-n12, or free RFP. D) Bar graphs showing the average fast exchange rates of GFP-H2A.B in cells expressing undetectable levels or detectable levels of RFP-ICP4, RFP-n12, or free RFP. E) Bar graphs showing the average slow exchange rates of GFP-H2A.B in cells expressing undetectable levels or detectable levels of RFP-ICP4, RFP-n12, or free RFP. Error bars, SEM. **, $P < 0.01$. $n \geq 15$ cells from at least 3 independent experiments.

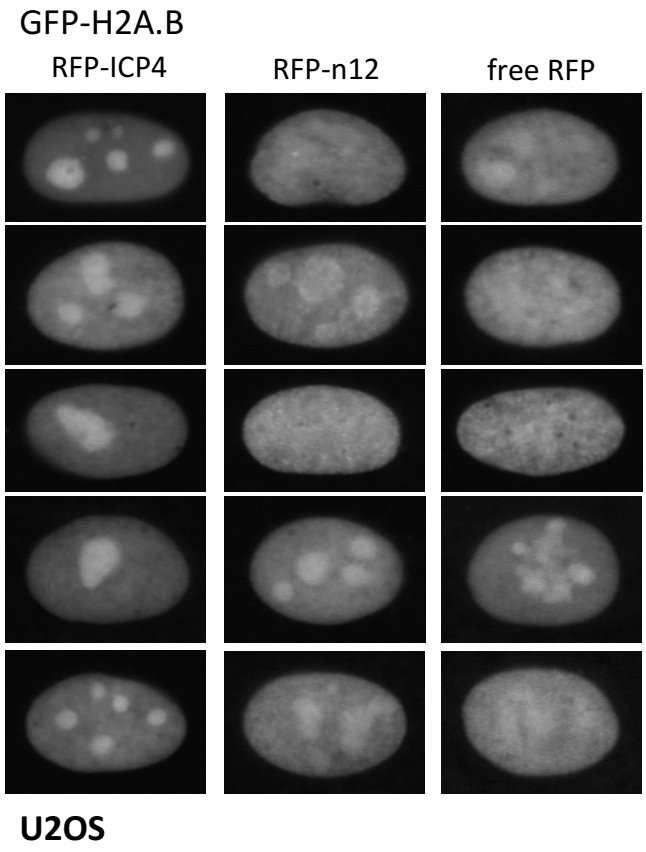

Figure 4.18. H2A.B is enriched in nucleoli in U2OS cells expressing detectable levels of ICP4, n12 or free RFP. Fluorescent micrograph images of nuclei expressing GFP-H2A.B and detectable levels of RFP-ICP4, RFP-n12, or free RFP.

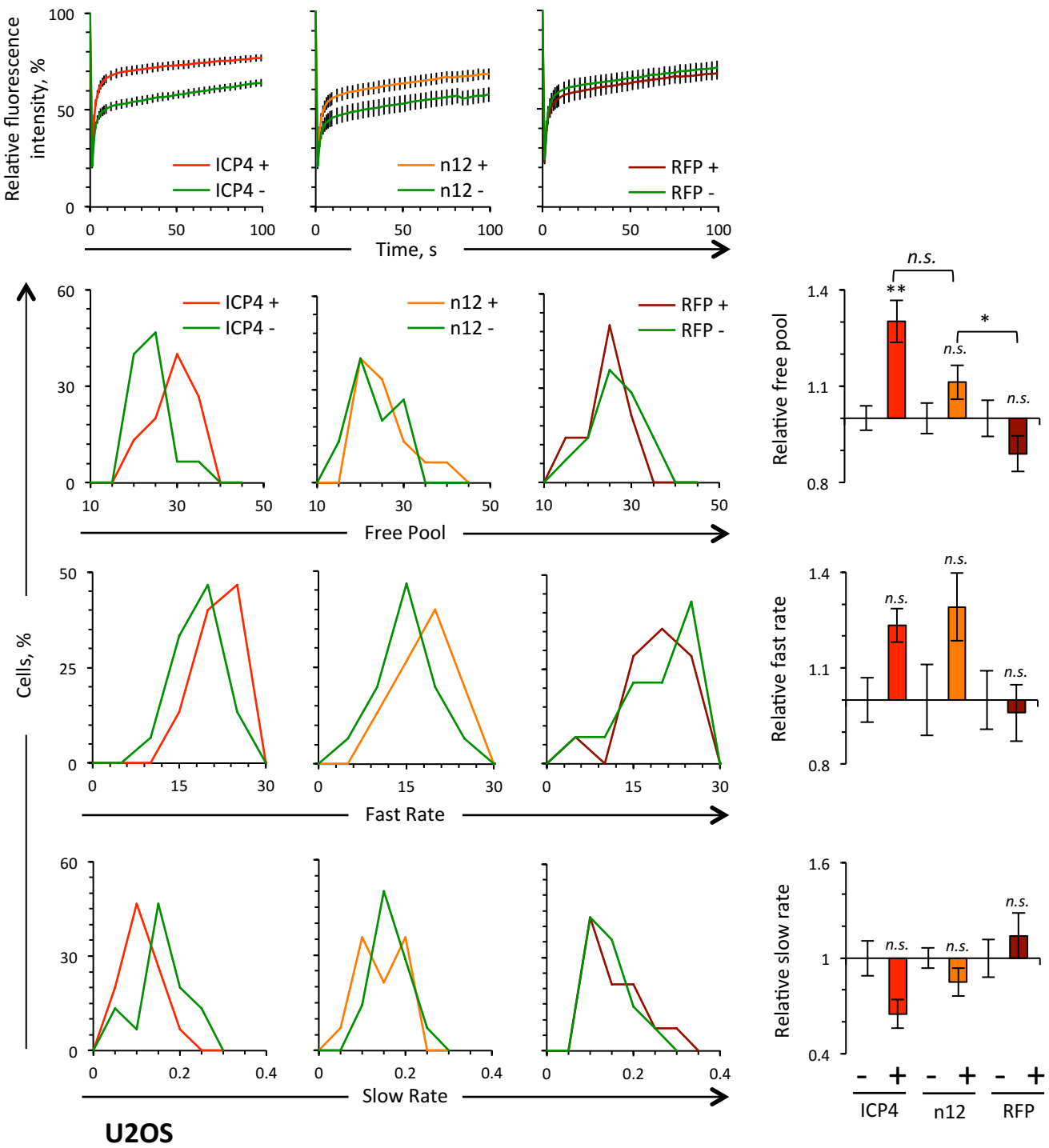
Relative fluorescence intensity, %
ICP4 +
ICP4 -
n12 +
n12 -
RFP +
RFP -
Time, s
Cells, %
Free Pool
Fast Rate
Slow Rate
U2OS
Relative free pool
Relative fast rate
Relative slow rate
n.s.
**
*
ICP4
n12
RFP

Figure 4.19. The dynamics of H2A.B are enhanced in U2OS cells expressing ICP4. U2OS cells were transfected with plasmids expressing GFP-H2A.B and RFP-ICP4, RFP-n12, or free RFP such that approximately half of the cells expressing detectable levels of GFP also expressed detectable levels of RFP. The dynamics of GFP-H2A.B in cells expressing detectable levels of RFP were compared to those in cells not expressing detectable levels of RFP from the same well. A) Average fluorescence recovery curves for GFP-H2A.B in cells expressing undetectable levels (green line) or detectable levels of RFP-ICP4, RFP-n12, or free RFP (red, orange, or dark red line, respectively). B) Frequency distribution graphs of the free pools, fast exchange rates, or slow exchange rates of GFP-H2A.B in cells expressing undetectable levels (green line) or detectable levels of RFP-ICP4, RFP-n12, or free RFP (red, orange, or dark red line, respectively). C) Bar graphs showing the average levels of free GFP-H2A.B in cells expressing undetectable levels or detectable levels of RFP-ICP4, RFP-n12, or free RFP. D) Bar graphs showing the average fast exchange rates of GFP-H2A.B in cells expressing undetectable levels or detectable levels of RFP-ICP4, RFP-n12, or free RFP. E) Bar graphs showing the average slow exchange rates of GFP-H2A.B in cells expressing undetectable levels or detectable levels of RFP-ICP4, RFP-n12, or free RFP. Error bars, SEM. **, $P < 0.01$. $n \geq 15$ cells from at least 3 independent experiments.

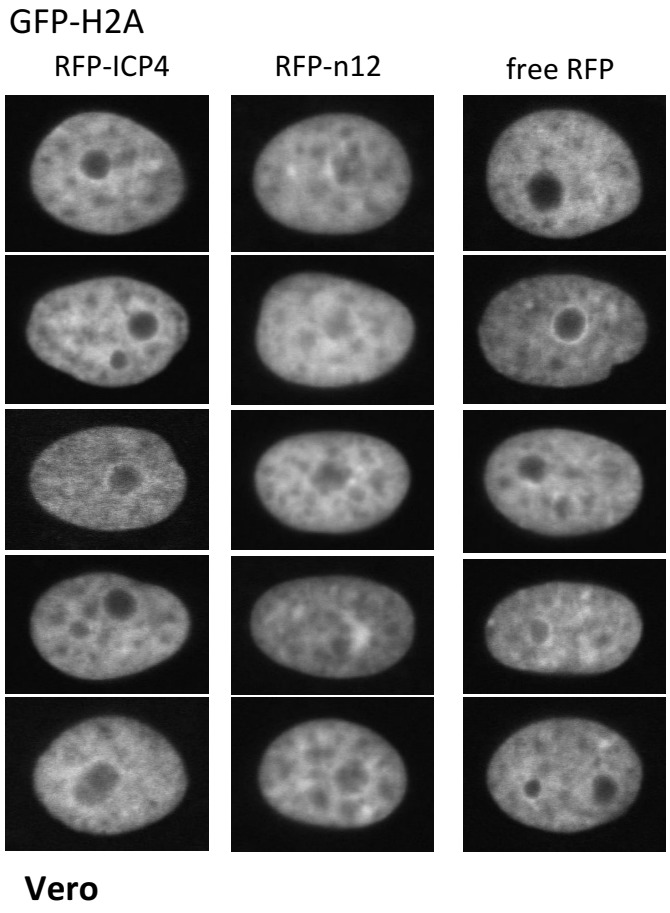

Figure 4.20. ICP4 does not affect the distribution of H2A in Vero cells.
Fluorescent micrograph images of Vero nuclei expressing GFP-H2A and detectable levels of RFP-ICP4, RFP-n12, or free RFP.

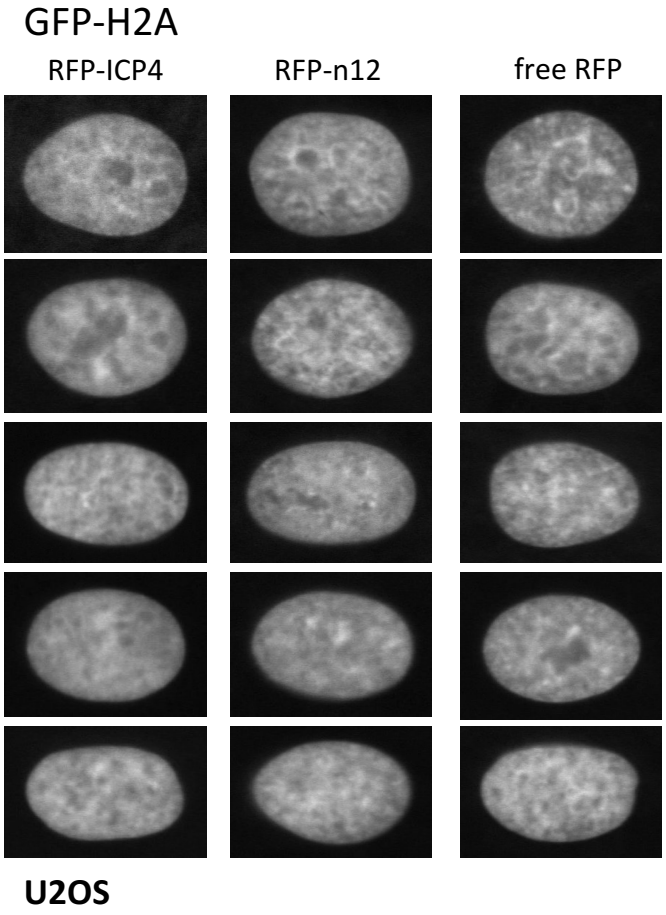

Figure 4.21. ICP4 does not affect the distribution of H2A in U2OS cells.
Fluorescent micrograph images of U2OS nuclei expressing GFP-H2A and detectable levels of RFP-ICP4, RFP-n12, or free RFP.

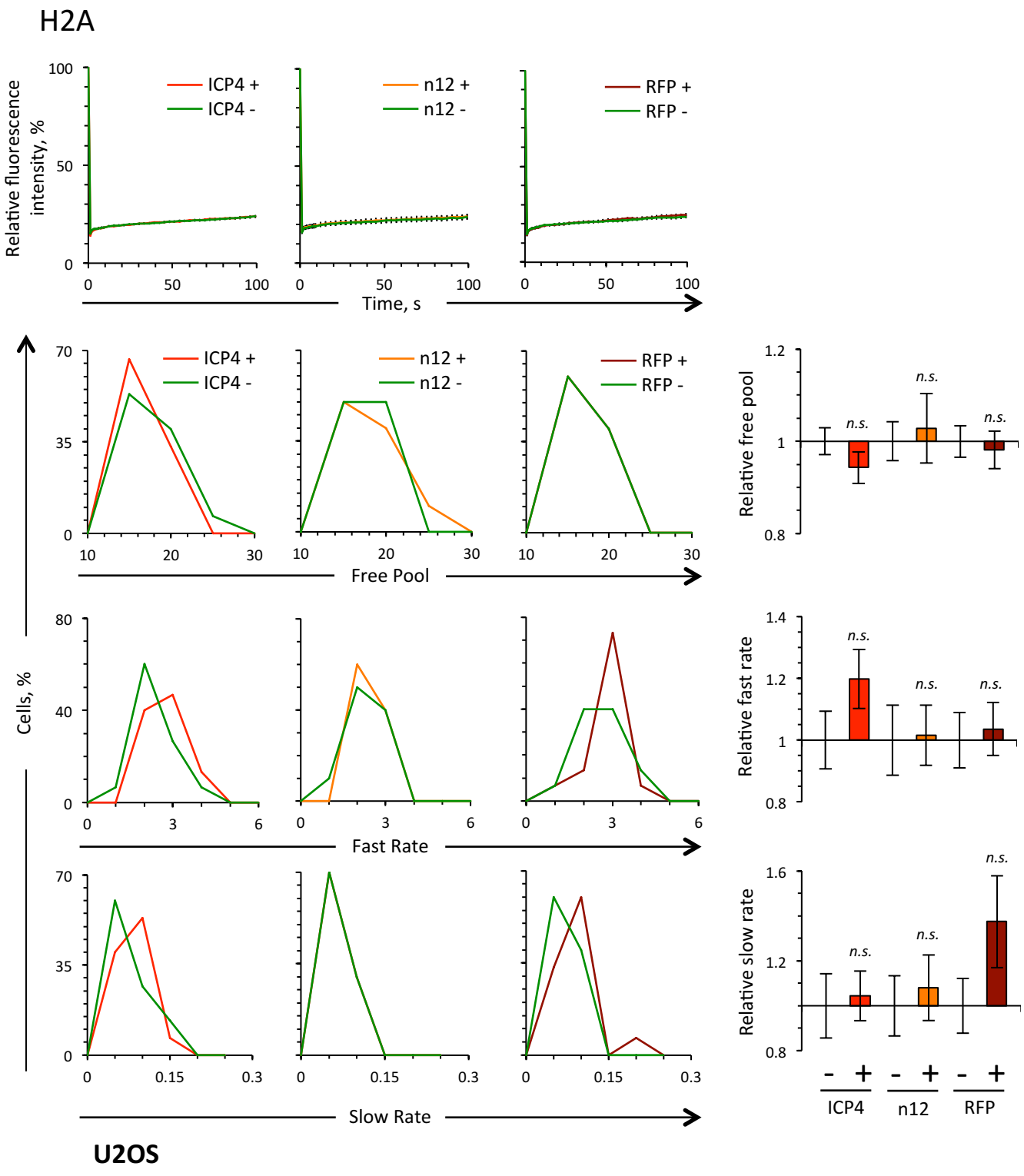
H2A
Relative fluorescence intensity, %
ICP4 +
ICP4 -
n12 +
n12 -
RFP +
RFP -
Time, s
Cells, %
Free Pool
Fast Rate
Slow Rate
Relative free pool
Relative fast rate
Relative slow rate
n.s.
ICP4
n12
RFP
U2OS

Figure 4.22. The dynamics of H2A are not enhanced in U2OS cells expressing ICP4. U2OS cells were transfected with plasmids expressing GFP-H2A and RFP-ICP4, RFP-n12, or free RFP such that approximately half of the cells expressing detectable levels of GFP also expressed detectable levels of RFP. The dynamics of GFP-H2A in cells expressing detectable levels of RFP were compared to those in cells not expressing detectable levels of RFP from the same well. A) Average fluorescence recovery curves for GFP-H2A in cells expressing undetectable levels (green line) or detectable levels of RFP-ICP4, RFP-n12, or free RFP (red, orange, or dark red line, respectively). B) Frequency distribution graphs of the free pools, fast exchange rates, or slow exchange rates of GFP-H2A in cells expressing undetectable levels (green line) or detectable levels of RFP-ICP4, RFP-n12, or free RFP (red, orange, or dark red line, respectively). C) Bar graphs showing the average levels of free GFP-H2A in cells expressing undetectable levels or detectable levels of RFP-ICP4, RFP-n12, or free RFP. D) Bar graphs showing the average fast exchange rates of GFP-H2A in cells expressing undetectable levels or detectable levels of RFP-ICP4, RFP-n12, or free RFP. E) Bar graphs showing the average slow exchange rates of GFP-H2A in cells expressing undetectable levels or detectable levels of RFP-ICP4, RFP-n12, or free RFP. Error bars, SEM. $n \geq 15$ cells from at least 3 independent experiments.

Histone variant	Cotransfected plasmid	RFP detection	Free Pool (avg ± SEM)		Fast Rate (avg ± SEM)		Slow Rate (avg ± SEM)	
			Absolute	Relative	Absolute	Relative	Absolute	Relative
H2A.B	RFP-ICP4	-	23.62 ± 0.88	1.00 ± 0.03	13.20 ± 0.65	1.00 ± 0.05	1.03 ± 0.12	1.00 ± 0.11
		+	29.81 ± 1.06	1.26 ± 0.04	19.00 ± 0.81	1.44 ± 0.06	0.80 ± 0.24	0.77 ± 0.23
	RFP-n12	-	22.66 ± 1.05	1.00 ± 0.04	13.59 ± 0.85	1.00 ± 0.06	1.00 ± 0.09	1.00 ± 0.09
		+	24.29 ± 1.15	1.07 ± 0.04	14.98 ± 0.87	1.19 ± 0.06	1.01 ± 0.09	1.01 ± 0.09
	free RFP	-	23.75 ± 0.87	1.00 ± 0.03	12.38 ± 1.01	1.00 ± 0.08	0.99 ± 0.09	1.00 ± 0.09
		+	24.26 ± 1.30	1.02 ± 0.04	14.33 ± 1.07	1.15 ± 0.09	1.06 ± 0.13	1.06 ± 0.13
macroH2A	RFP-ICP4	-	14.61 ± 0.80	1.00 ± 0.05	0.53 ± 0.16	1.00 ± 0.30	0.08 ± 0.03	1.00 ± 0.42
		+	14.02 ± 0.99	0.96 ± 0.07	1.17 ± 0.34	2.19 ± 0.63	0.04 ± 0.01	0.57 ± 0.09
	RFP-n12	-	14.58 ± 0.89	1.00 ± 0.05	0.84 ± 0.17	1.00 ± 0.21	0.03 ± 0.01	1.00 ± 0.12
		+	16.80 ± 1.14	1.14 ± 0.05	0.77 ± 0.19	0.91 ± 0.23	0.04 ± 0.01	1.34 ± 0.19
	free RFP	-	15.95 ± 1.05	1.00 ± 0.06	0.68 ± 0.13	1.00 ± 0.19	0.07 ± 0.02	1.00 ± 0.32
		+	14.12 ± 0.61	0.89 ± 0.05	0.80 ± 0.09	1.17 ± 0.13	0.05 ± 0.01	0.68 ± 0.07
H2A.X	RFP-ICP4	-	16.73 ± 0.81	1.00 ± 0.05	0.98 ± 0.12	1.00 ± 0.13	0.05 ± 0.01	1.00 ± 0.15
		+	15.66 ± 0.82	0.93 ± 0.05	1.19 ± 0.20	1.21 ± 0.02	0.04 ± 0.01	0.79 ± 0.14
	RFP-n12	-	14.51 ± 0.80	1.00 ± 0.05	1.11 ± 0.10	1.00 ± 0.09	0.05 ± 0.01	1.00 ± 0.16
		+	14.98 ± 1.13	1.04 ± 0.09	1.27 ± 0.17	1.14 ± 0.15	0.05 ± 0.02	0.93 ± 0.08
	free RFP	-	19.94 ± 0.99	1.00 ± 0.04	0.76 ± 0.18	1.00 ± 0.24	0.07 ± 0.02	1.00 ± 0.23
		+	18.21 ± 1.30	0.92 ± 0.06	0.94 ± 0.12	1.24 ± 0.16	0.06 ± 0.01	0.84 ± 0.13
H2A.Z	RFP-ICP4	-	17.83 ± 1.01	1.00 ± 0.06	2.52 ± 0.23	1.00 ± 0.09	0.09 ± 0.02	1.00 ± 0.19
		+	18.16 ± 0.96	1.02 ± 0.05	2.38 ± 0.31	0.95 ± 0.12	0.08 ± 0.01	0.89 ± 0.14
	free RFP	-	16.53 ± 0.80	1.00 ± 0.05	2.76 ± 0.21	1.00 ± 0.08	0.08 ± 0.01	1.00 ± 0.11
		+	16.92 ± 0.80	1.02 ± 0.05	2.73 ± 0.22	0.99 ± 0.09	0.09 ± 0.01	1.07 ± 0.14

Table 4.1. Dynamics of H2A variants in cells expressing detectable or undetectable levels of RFP-ICP4, RFP-n12, or free RFP.

Chapter 5: Depletion of H2A.B from the nucleolus is not sufficient to decrease H2A.B dynamics.

5.1 Introduction

The double-stranded DNA (dsDNA) genomes of herpes simplex virus 1 (HSV-1) are not chromatinized in the virion, but become assembled in highly dynamic chromatin during lytic infection (373). The basic unit of chromatin is the nucleosome, consisting of two each of the core histone dimers H2A-H2B and H3-H4 wrapped by 146 base pairs of dsDNA. H2A and H3, but not H2B or H4, have variants. Unlike the canonical histones, which are assembled in nucleosomes via DNA-replication dependent mechanisms, most variant histones are synthesized at any time during the cell cycle and are assembled in nucleosomes via DNA-replication independent mechanisms. The incorporation of the histone variants in place of the canonical ones often modifies the stability of the nucleosome.

Chromatin is dynamic, as histones disassemble from nucleosomes, diffuse through the nucleus bound by chaperones, and reassemble nucleosomes at different sites (78, 80, 443, 448). Genes that are assembled in more dynamic nucleosomes are transcribed to higher levels than those that are assembled in less dynamic ones (44, 453). H2A variants alter nucleosome dynamics. H2A.B (previously called H2A.Bbd for Barr body deficient) lacks the C-terminal unstructured tail of H2A and assembles more dynamic nucleosomes than canonical H2A (193). MacroH2A contains a macro domain on the C-terminus in addition to the H2A-like domain, and assembles less dynamic nucleosomes than canonical H2A (176). MacroH2A, which increases nucleosome stability, is enriched in nucleosomes with the cellular DNA in silenced genes, whereas H2A.B, which decreases stability, is enriched in nucleosomes with the cellular DNA in transcribed genes (177). A third H2A variant, H2A.X, is reported to assemble less stable nucleosomes than canonical H2A (97).

We, and others, propose a model in which the chromatinization of HSV-1 genomes is a cellular defense mechanism to silence viral gene expression. To counteract silencing, HSV-1 would have evolved mechanisms to increase the dynamics of HSV-1 chromatin. Consistently, all three HSV-1 transcription activators affect the stability or dynamics of chromatin. VP16 reduces the levels of total H3

and acetylated H3 stably associated with immediate-early promoters (316). ICP0 reduces the levels of total H3 and acetylated H3 stably associated with early promoters (333). ICP4 (in the presence of plasmid DNA) enhances the dynamics of histones, even in the absence of HSV-1 DNA or other HSV-1 proteins (454).

Both canonical H3.1, which assembles the least dynamic nucleosomes, and variant H3.3, which assembles the most dynamic nucleosomes, are stably associated with HSV-1 genomes (151, 371). H3.3 is stably associated with HSV-1 DNA immediately upon nuclear entry, whereas H3.1 becomes stably associated with HSV-1 DNA only after the start of HSV-1 DNA replication (371). Consistently, the dynamics of both H3.1 and H3.3 are enhanced in HSV-1 infected cells, but the dynamics of only H3.1 are enhanced to an even greater extent when HSV-1 DNA replication is inhibited (375). When the assembly of H3.3 in HSV-1 nucleosomes is inhibited by the knockdown of its chaperone HIRA, the HSV-1 RNA levels decrease (371). It is possible that the most dynamic nucleosomes containing H3.3 are less restrictive to HSV-1 transcription than the least dynamic ones containing H3.1. Likewise, the most dynamic nucleosomes containing H2A.B may be the least restrictive to HSV-1 transcription, and the least dynamic ones containing macroH2A, the most. Expression of ICP4 (in the presence of plasmid DNA) is sufficient to enhance the dynamics of H3.1 and H3.3. However, the dynamics of H3.1 are enhanced the most. ICP4 may prevent the assembly of H3.1 in chromatin or promptly disrupt H3.1-containing nucleosomes. Surprisingly, however, ICP4 did not enhance the dynamics of macroH2A, but rather those of only H2A.B. A greater amount of H2A.B was localized at the nucleolus in cells expressing ICP4 relative to non-expressing cells. H2A.B in the nucleolus is more dynamic than that in the general chromatin. I thus propose that ICP4 does not enhance the dynamics of the H2A.B in the general cellular chromatin. Instead, the enhancement of H2A.B dynamics is a result of the enrichment of H2A.B in the most dynamic population in ICP4 expressing cells.

The dynamics of H2B, which forms dimers with H2A or one of its variants, are altered in HSV-1 infected cells (82). Whereas the free pools and fast exchange rates of H3.1 increase in HSV-1 infected cells, the free pools of H2B are increased but

its fast exchange rate decreases (82, 414). Here, I show that the dynamics of canonical H2A and its variants are altered in HSV-1 infected cells. Canonical H2A, macroH2A, and H2A.X had faster fast exchange rates in HSV-1, whereas H2A.B had a slower fast exchange rate, most closely mimicking H2B dynamics. The decrease in H2A.B dynamics in HSV-1 infected cells may result from the dissipation of the nucleolus and the consequent displacement of H2A.B from this structure. However, H2A.B dynamics are enhanced in cells infected with an HSV-1 mutant encoding no functional ICP4. The displacement of H2A.B from the nucleolus is thus not sufficient to decrease H2A.B dynamics. HSV-1 may preferentially assemble unstable nucleosomes with H2A.B on HSV-1 DNA, resulting in the observed decrease in H2A.B dynamics in HSV-1 infected cells.

5.2 Results

5.2.1 H2A.B is depleted less than other variants from the replication compartments

The dynamics of only H2A.B, of all H2A.B variants, are enhanced in cells expressing ICP4. Like H3.1, the distribution of H2A.B is changed in cells expressing ICP4. In contrast to H3.1, H2A.B is still incorporated in chromatin. H2A.B is enriched at the nucleolus in uninfected cells, and even more so H2A.B in cells expressing ICP4. ICP4 itself also localizes to the nucleolus. The nucleolus is dissipated in infected cells, and ICP4 localizes to the replication compartments. I proposed that ICP4 recruits H2A.B to the nucleolus in co-transfected cells, and therefore also recruits H2A.B to the replication compartments in infected cells.

MacroH2A and H2A.X, like canonical H2A and the other canonical histones, were mostly depleted from replication compartments in cells infected with wt HSV-1 (Figure 5.1.). In contrast, H2A.B was enriched in the replication compartments. Thus, H2A.B may be recruited to the replication compartments by ICP4 upon dissipation of the nucleolus.

5.2.2 The dynamics of H2A.B are altered in HSV-1 infected cells

The histones in the nucleolus are more dynamic than those in the cellular chromatin. For most histones, those in the replication compartments are even more dynamic than those in the nucleolus of mock-infected cells (Kristen Conn, unpublished observations). H2A.B is the only histone that is more dynamic in the nucleolus than in the replication compartments. I thus proposed that the dynamics of H2A.B are enhanced in ICP4 expressing cells due to the shift of H2A.B from the less dynamic population in the cellular chromatin to the more dynamic population in the nucleolar chromatin. The dynamics of H2A.B would thus decrease in infected cells, as the dissipation of the nucleolus would result in the shift in population of H2A.B in the highly dynamic nucleolus to the comparatively less dynamic cellular chromatin or replication compartments.

Consistent with my expectations, the dynamics of H2A.B decreased in HSV-1 infected cells (Figure 5.2., 5.3.). The fluorescence recovery curve of H2A.B in infected cells is lower than that in mock-infected cells, corresponding to less fluorescence recovery at each time point. The fast exchange rate of H2A.B decreased at both 4 and 7 hpi in infected cells relative to mock-infected cells. However, the free pool of H2A.B still significantly increased at 4 hpi, but not at 7 hpi, in HSV-1 infected cells relative to mock-infected cells.

5.2.3 The dynamics of H2A, macroH2A, and H2A.X are increased in HSV-1 infected cells

Whereas the localization and dynamics of H2A.B are altered in cells expressing ICP4, the localization and dynamics of macroH2A, H2A.X, and canonical H2A are not. MacroH2A, H2A.X, and canonical H2A are not enriched in the nucleolus in uninfected cells, or in replication compartments in infected cells. Unlike H2A.B, the populations of macroH2A, H2A.X, and H2A, in the replication compartments are more dynamic than those in the nucleolus. The dynamics of macroH2A, H2A.X, and canonical H2A would then be expected to be enhanced in HSV-1 infected cells.

In contrast to H2A.B, the dynamics of macroH2A, H2A.X, and H2A increased in infected cells (Figure 5.4., 5.5., 5.6.). The relative fluorescence recovery curves of

macroH2A, H2A.X, and H2A were higher in infected cells than in mock-infected cells, corresponding to greater fluorescence recovery at each time point. The free pools of macroH2A, H2A.X, and H2A increased in HSV-1 infected cells relative to those in mock-infected cells at both 4 and 7 hpi. The fast exchange rates of macroH2A, H2A.X, and H2A, also increased in infected cells. The fast exchange rate of macroH2A, which assembles the least dynamic nucleosomes, increased the most in HSV-1 infected cells. The dynamics of only H2A.B, and no other H2A variant, thus decrease in HSV-1 infected cells.

5.2.4 The dynamics of macroH2A and H2A.B are enhanced in cells infected with an HSV-1 mutant encoding a non-functional ICP4

The dynamics of all canonical core histones are enhanced in cells infected with HSV-1. The dynamics of all canonical core histones are enhanced the least in cells infected with an HSV-1 mutant encoding no functional ICP4, n12. The HSV-1 genome is not replicated in cells infected with n12. Replication compartments thus do not form, but the nucleolus fractures. MacroH2A or H2A.B assembles the least or most dynamics nucleosomes, respectively. The dynamics of macroH2A are enhanced the most in HSV-1 infected cells, whereas those of H2A.B are decreased. I proposed that the decrease in H2A.B dynamics is due to the displacement of H2A.B from the nucleolus and recruitment to the replication compartments. In n12-infected cells, H2A.B is still displaced from the nucleolus, but there are no replication compartments to which it can be recruited.

The dynamics of macroH2A were enhanced in n12-infected cells (Figure 5.7.). The free pool of macroH2A was greater in n12-infected cells relative to mock-infected cells at 4 hpi ($p<0.05$), but not at 7 hpi. The fast exchange rates of macroH2A increased at 4 and 7 hpi. There is no statistical signifance between the increases to fast exchange rates in n12-infected cells relative to wt HSV-1 infected cells at 4 or 7 hpi (Figure 5.8.). Expression of ICP4 is therefore not required to enhance the dynamics of macroH2A in infected cells.

The dynamics of GFP-H2A.B are also enhanced in n12-infected cells (Figure 5.9.). The free pool of GFP-H2A.B increased in n12-infected cells relative to mock-

infected cells at 4 hpi ($p<0.01$), but not at 7 hpi. Whereas the fast exchange rate of H2A.B decreased in cells infected with wt HSV-1 relative to mock-infected cells (Figure 5.3.C,5.8.B), the fast exchange rate of H2A.B increased in n12-infected cells at 4 hpi ($p<0.05$) but not at 7 hpi (Figure 5.8.B, Figure 5.9.C). The fast exchange rates of GFP-H2A.B are significantly different between n12- and wt HSV-1-infected cells at 4 and 7 hpi ($p<0.01$). Thus, the displacement of H2A.B from the nucleolus is in itself not sufficient to decrease the dynamics of H2A.B. Expression of ICP4 is, however, required to decrease H2A.B dynamics. In the absence of functional ICP4, IE genes are overexpressed, E and L genes are not expressed, HSV-1 genomes are not replicated, and replication compartments do not form. The replication of HSV-1 genomes or the formation of the replication compartments may be necessary to decrease H2A.B dynamics. Alternatively, an IE protein may enhance H2A.B dynamics, or an E or L protein may decrease them.

5.3 Discussion

HSV-1 chromatin is far more dynamic than cellular chromatin (373). Consistently, histones are more dynamic in HSV-1 infected cells than in mock-infected cells (82, 374, 375). The free pool of H2B, a surrogate measure for the H2B not assembled in nucleosomes, was increased from 33% at 4 hpi to 69% at 7 hpi in HSV-1 infected cells (82). Similarly, the free pool of H2A, which is only found in dimers with H2B in the free pool, was increased from 32% at 4 hpi to 42% at 7 hpi in HSV-1 infected cells. The fast exchange rate of H2B, a surrogate measure for the dynamics of H2B assembled in unstable nucleosomes, decreased at 4 and even more so at 7 hpi in HSV-1 infected cells relative to mock-infected cells (82). In contrast, the initial velocity of H2A increased at both 4 and 7 hpi in HSV-1 infected cells, though the increase at 4 hpi was nearly 4 times that at 7 hpi. H2A only dimerizes with H2B in the free pool, whereas H2B dimerizes with H2A or one of its many variants. Therefore, the dynamics of H2B are not necessarily expected to follow the same pattern as those of H2A, but would reflect the average of the dynamics of all H2A variants.

The free pools of all H2A variants increased in HSV-1 infected cells at 4 hpi. Whereas the free pools of H2A, H2A.X and macroH2A increased to similar levels, the free pool of H2A.B increased to less than half. Direct comparisons between GFP-histone fusion proteins is not possible. The GFP tag can well have differential effects on the binding affinity for DNA. H2A.B was the only H2A variant that did not increase its free pool in HSV-1 infected cells at 7 hpi. H2A.B was also the only H2A variant with decreased fast exchange rates at 4 or 7 hpi. Nucleosomes containing H2A.B are more dynamic than those containing canonical H2A, macroH2A, or H2A.X, and H2A.B is enriched in nucleosomes containing DNA of highly transcribed cellular genes (177, 193). HSV-1 genes are transcribed by cellular RNA polymerase II, and are thus also expected to be more efficiently transcribed if dynamically chromatinized. Consistently, HSV-1 genomes are more dynamically chromatinized during lytic infections, when most HSV-1 genes are transcribed, than during latent infections, when most HSV-1 genes are not (370, 373, 455). Nucleosome assembly protein I (NAP-1) has been shown to catalyze the exchange between H2A-H2B dimers and H2A.B-H2B dimers in vitro, but it is not yet fully understood how H2A.B is assembled in nucleosomes in vivo (52). HSV-1 may have evolved mechanisms that promote the assembly of nucleosomes containing H2A.B with HSV-1 genomes, or that inhibit the assembly of nucleosomes containing canonical H2A (or the other H2A variants). For example, ICP4 may interact with a specific chaperone of H2A.B that has yet to be identified. The incorporation of H2A.B in nucleosomes would result in dynamic chromatin that allows efficient transcription of HSV-1 genomes.

The fast exchange rate of H2B decreased in cells infected with wt HSV-1, as did that of H2A.B (but not of canonical H2A or any other H2A variant). The amount of total nuclear DNA increases, albeit very little, with the entry of the infecting HSV-1 genomes, and further increases with HSV-1 DNA replication. Core nucleosomes assemble with 146 bp of dsDNA, and are linked by up to 80 bp of dsDNA. The cellular genome has 3 billion bps, providing approximately $1.3x10^7$ nucleosome binding sites. HSV-1 genomes are 152 kbp in length, and thus each HSV-1 genome offers approximately only 675 new nucleosome binding sites. HSV-1 infects at any stage of the cell cycle, and inhibits cellular protein synthesis. The dynamics of all

histones could have been expected to decrease during HSV-1 infection, as the number of histones is constant but the number of binding sites increase (by approximately 0.005% for each HSV-1 genome). However, the dynamics of only H2A.B and H2B decreased. Nucleosomes assembled with canonical H2A are protected from nucleases to 146 bp of DNA, whereas those assembled with H2A.B are protected to 116-130 bp (192, 193, 444). DNA wraps around the nucleosome less stably when the nucleosomes contain H2A.B than when they contain H2A, making the ends more accessible to digestion and likely to other cellular proteins (192, 193, 444). As a result, reconstituted nucleosomes assembled with H2A.B protect DNA to broader bands from nucleases than those assembled with canonical H2A (192). Lytic HSV-1 genomes serially digested with nucleosomes also results in broad DNA bands (373, 456). The DNA bands correspond approximately to mono-, di-, tri-, and poly-nucleosome sizes. However, the composition of HSV-1 nucleosomes has still not been elucidated. HSV-1 nucleosomes may contain H2A.B, resulting in the broadened bands. Consistently, GFP-H2A.B is the most enriched GFP-histone in the HSV-1 replication compartments.

Nucleoli are discrete nuclear regions with the highest levels of transcription in non-infected cells. Whereas H2A, macroH2A, and H2A.X are mostly depleted from the nucleolus, H2A.B is not, consistent with the assembly of H2A.B in highly dynamic nucleosomes with nucleolar DNA. During infection, the nucleolus is disrupted and new novel discrete regions with high levels of transcription are formed, the HSV-1 replication compartments. H2A, macroH2A, and H2A.X are also mostly depleted from replication compartments, whereas H2A.B is not. With the disruption of the nucleoli, H2A.B may translocate to the replication compartments, where it would assemble highly dynamic nucleosomes with HSV-1 genomes. The dynamics of H2A, macroH2A, and H2A would thus increase during HSV-1 infection, as they are disassembled from nucleosomes with cellular DNA but then are not reassembled in nucleosomes with the replicating HSV-1 genomes. In contrast, the dynamics of H2A.B would decrease, as the H2A.B that is disassembled from highly dynamic nucleosomes in the nucleolus is reassembled in comparatively less dynamic nucleosomes with HSV-1 DNA. A mutant HSV-1 encoding a truncated, non-

functional ICP4, n12, does not replicate and therefore does not form replication compartments. However, the nucleoli are still fractured in cells expressing n12, and H2A.B is still displaced from the nucleoli. If the dynamics of H2A.B are increased in ICP4 expressing cells only because they are enriched in the nucleolus, and decreased in HSV-1 infected cells only because they are displaced from the nucleolus, we would also expect the dynamics of H2A.B to decrease in n12-infected cells. However, we find that the dynamics of H2A.B actually increase in n12-infected cells. Thus, the decrease of H2A.B dynamics appears to require the formation of replication compartments. ICP4 inhibits the expression of itself and other IE proteins(366, 457). Whereas E and L proteins are not expressed in the absence of functional ICP4, IE proteins are expressed to higher levels (458). The increase of H2A.B dynamics in n12-infected cells may therefore also result from higher levels of ICP0, which promotes histone removal, for example (333). However, histone free pools were even greater in cells infected with an HSV-1 mutant encoding no functional ICP0 than in cells infected with wild-type HSV-1, suggesting that ICP0 actually induces the degradation of histones in the free pool.

Whereas H2A.B is the most dynamic H2A variant, macroH2A is the least. H2A.B was the only H2A variant with a decreased fast exchange rate in HSV-1 infected cells. In contrast, macroH2A had the greatest increase in its fast exchange rate in HSV-1 infected cells, by 4- or 3-fold at 4 or 7 hpi, respectively, more than twice the increase for canonical H2A. MacroH2A is assembled in nucleosomes with cellular DNA of mostly silenced genes(171, 177). The C-terminal macro domain of macroH2A inhibits the remodeling of nucleosomes by SWI/SNF, and represses transcription initiation(178). The macro domain also interacts with HDAC1, and induces hypoacetylation of all histones in nucleosomes containing macroH2A (174). The HSV-1 transcription activators VP16 recruits SWI/SNF to HSV-1 promoters, and ICP0 dissociates HDAC1 from the REST/CoREST complex(316, 332). As HSV-1 has evolved proteins that counter the activities of macroH2A, we expect the assembly of macroH2A in nucleosomes with HSV-1 genomes to be particularly restrictive to HSV-1 transcription. HSV-1 may thus have evolved mechanisms to prevent the incorporation of macroH2A in HSV-1 nucleosomes, or to promote their dissociation.

MacroH2A that is disassembled from nucleosomes with cellular DNA is thus not stably reassembled in nucleosomes with newly replicated HSV-1 genomes, resulting in the increased dynamics of macroH2A.

The dynamics of H2A.Z or H2A.X, which assemble nucleosomes slightly more or less dynamic, respectively, than canonical H2A, were not enhanced in cells expressing ICP4. The dynamics of macroH2A, which assembles the least dynamic nucleosomes, were not enhanced in cells expressing ICP4 either. The fast exchange rate of macroH2A was increased to statistically the same levels in cells infected with wt or n12 HSV-1. ICP4 expression is therefore not required to enhance macroH2A dynamics. As E and L proteins are not expressed in cells infected with n12 HSV-1, early and late proteins are also not required to enhance macroH2A dynamics.

In conclusion, here I report that the change in H2A variant dynamics during HSV- infection is correlated with the dynamics that each H2A variant provides to nucleosomes. The dynamics of H2A.B, which assembles the most dynamic nucleosomes, are decreased in HSV-1 infected cells relative to mock-infected cells, whereas the dynamics of macroH2A, which assembles the least dynamic nucleosomes, are increased the most among H2A variants. I propose that ICP4 recruits H2A.B to the replication compartments to assemble dynamic nucleosomes with HSV-1 genomes, because they are the least inhibitory to transcription. HSV-1 has developed other mechanisms to preferentially prevent the assembly of nucleosomes with macroH2A because they are the most inhibitory to transcription.

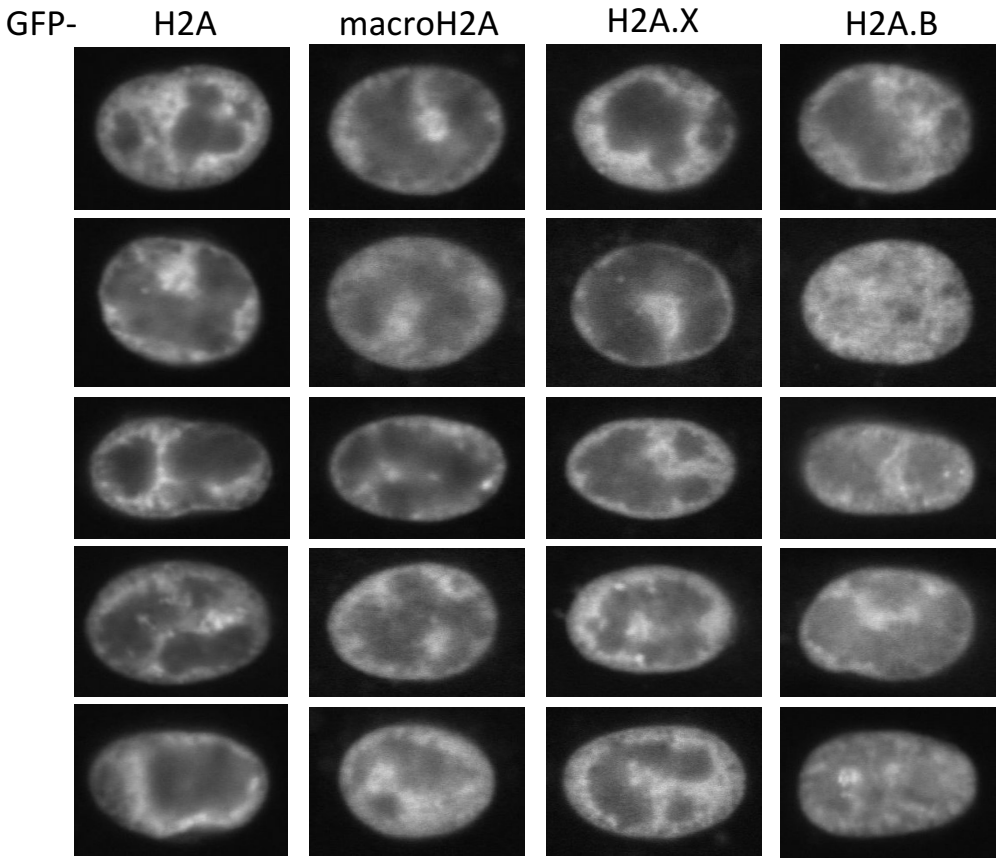

Figure 5.1. H2A.B is more enriched in the replication compartments than H2A, macroH2A, or H2A.X. Representative fluorescent micrograph images of nuclei expressing GFP-H2A, -macroH2A, –H2A.B, or –H2A.X in cells infected with HSV-1 at 7 hpi.

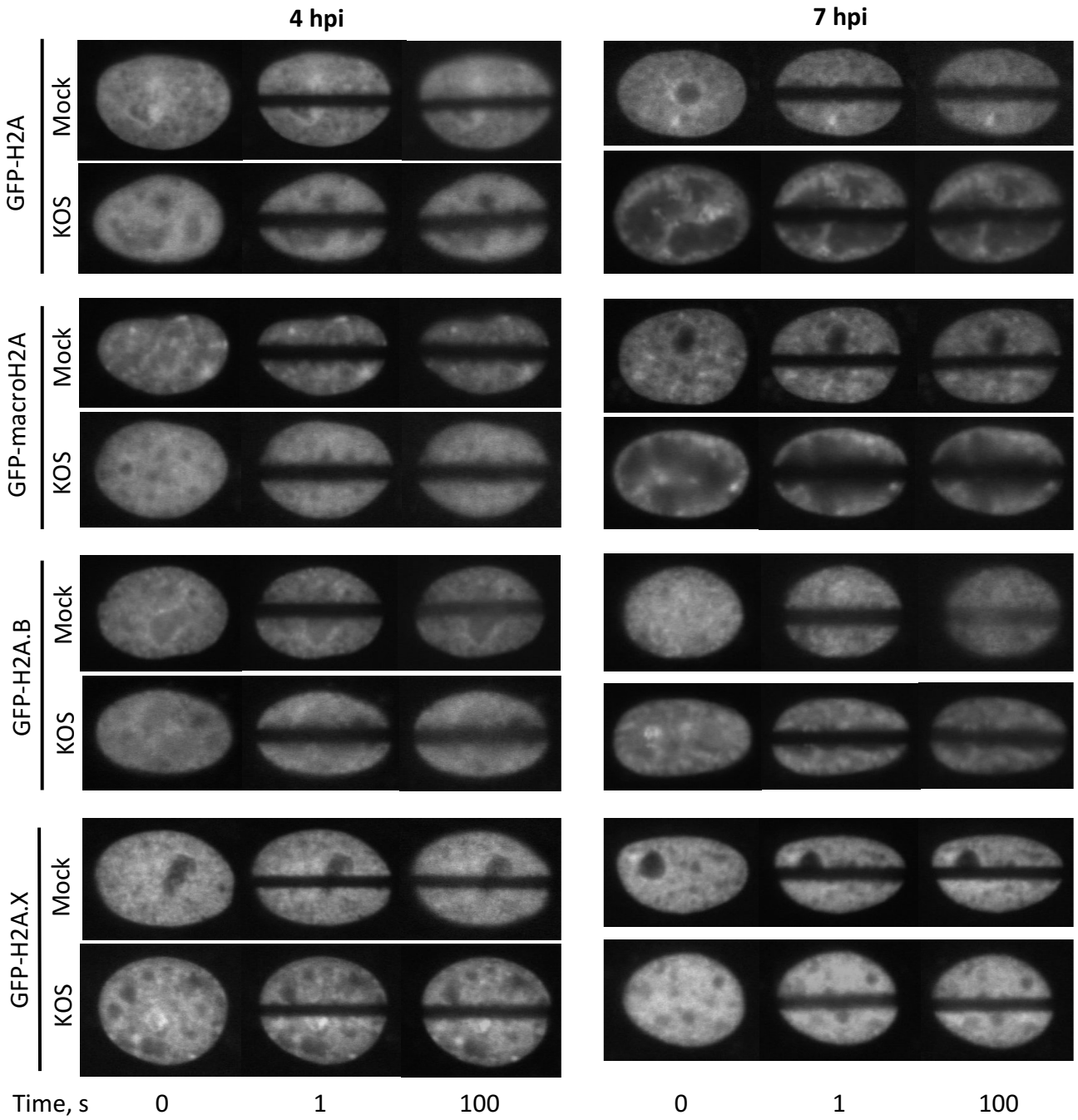

Figure 5.2. The dynamics of H2A, macroH2A, H2A.B, and H2A.X are altered in cells infected with HSV-1. Representative fluorescent micrograph images of nuclei expressing GFP-H2A, -macroH2A, –H2A.B, or –H2A.X and mock-infected (**Mock**) or infected with HSV-1 moi 5 (**KOS**) for 4 or 7 hours. 0 s, immediately prior to photobleaching; 1 s, immediately after photobleaching; 100 s, 100 s after photobleaching.

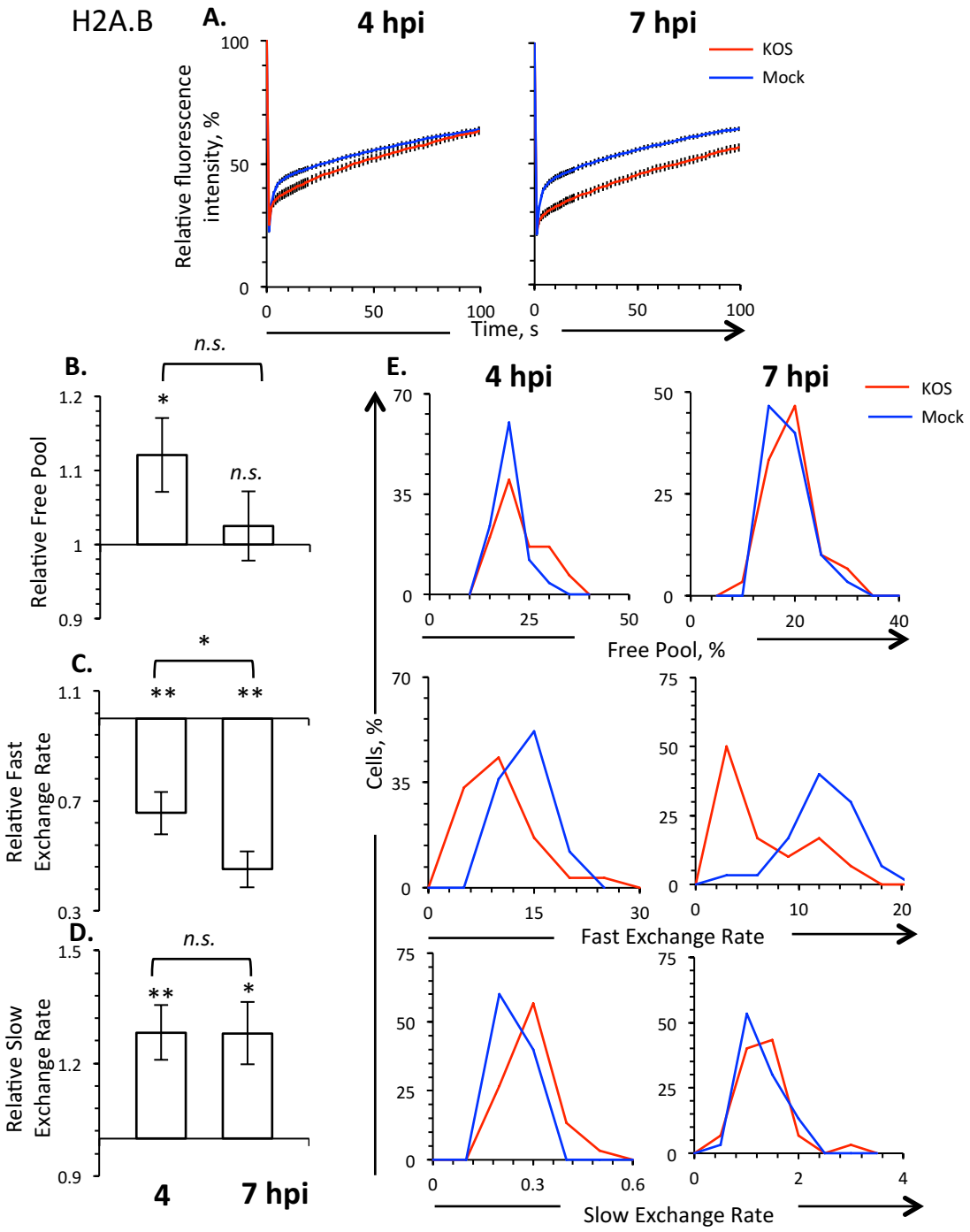
H2A.B
A.
4 hpi
7 hpi
KOS
Mock
Relative fluorescence intensity, %
Time, s
B.
n.s.
Relative Free Pool
C.
Relative Fast Exchange Rate
D.
Relative Slow Exchange Rate
4
7 hpi
E.
4 hpi
7 hpi
KOS
Mock
Cells, %
Free Pool, %
Fast Exchange Rate
Slow Exchange Rate

Figure 5.3. The dynamics of H2A.B decrease in HSV-1 infected cells. Vero cells were transfected with a plasmid expressing GFP-H2A.B. Transfected cells were mock-infected (**Mock**) infected with HSV-1 moi 5 (**KOS**). The dynamics of GFP-H2A.B were evaluated 4 to 5 (**4 hpi**) or 7 to 8 (**7 hpi**) hours later by FRAP. A) Average fluorescence recovery curves for GFP-H2A.B at 4 or 7 hpi in HSV-1- (red line) or mock-infected (blue line) cells. B) Bar graphs showing the average levels of free GFP-H2A.B in HSV-1- relative to mock-infected cells at 4 or 7 hpi. C) Bar graphs showing the average fast exchange rates of GFP-H2A.B in HSV-1- relative to mock-infected cells at 4 or 7 hpi. D) Bar graphs showing the average slow exchange rates of GFP-H2A.B in HSV-1- relative to mock-infected cells at 4 or 7 hpi. E) Frequency distribution graphs of free pools, fast, or slow exchange rates of GFP-H2A.B in HSV-1- (red line) or mock-infected (blue line) cells at 4 or 7 hpi. Error bars, SEM. **, $P < 0.01$; *, $P < 0.05$; *n.s.,* not significant. $n \geq 15$ cells from at least 3 independent experiments.

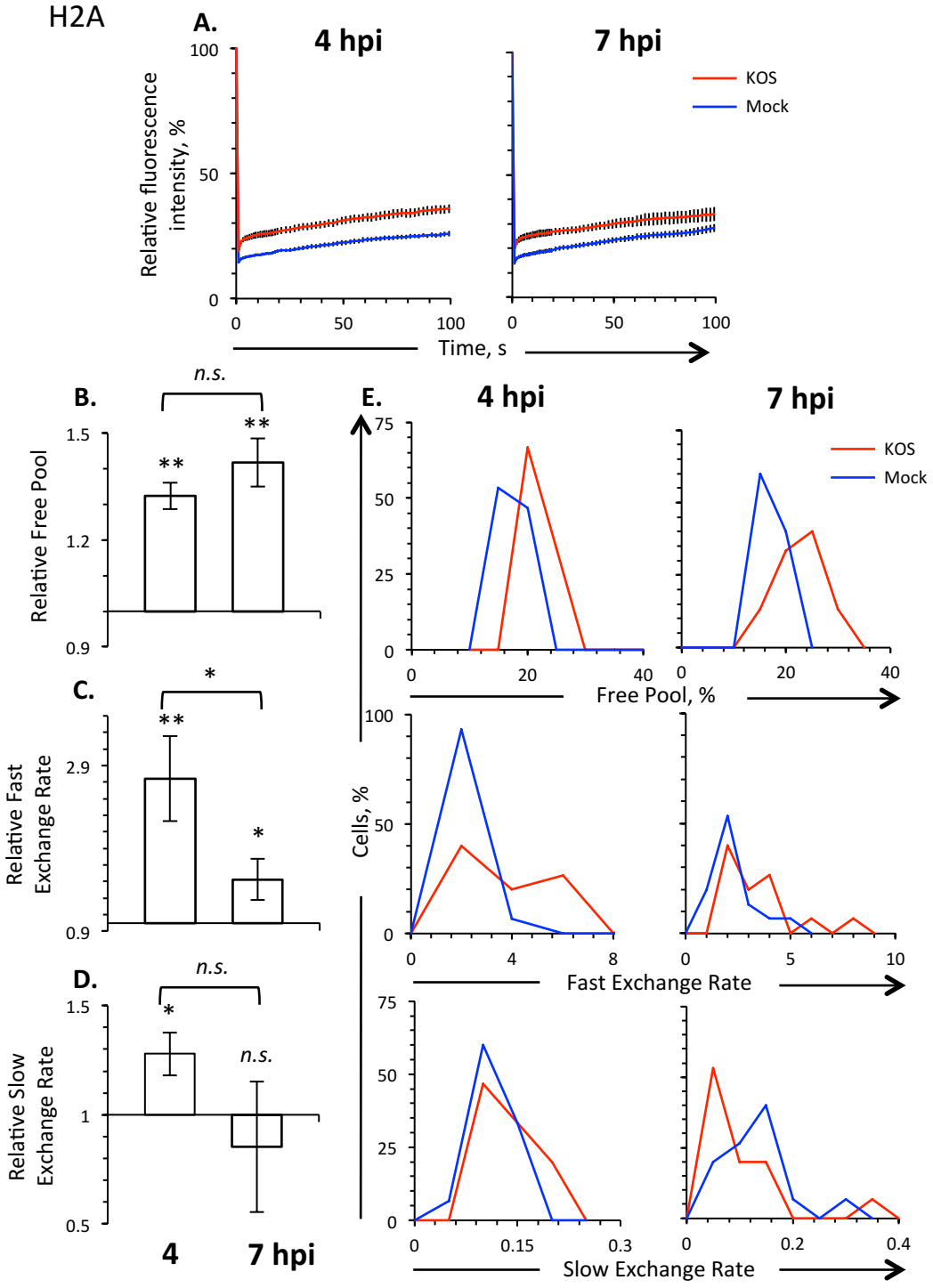
H2A
A.
4 hpi
7 hpi
KOS
Mock
Relative fluorescence intensity, %
Time, s
B.
n.s.
Relative Free Pool
C.
Relative Fast Exchange Rate
D.
Relative Slow Exchange Rate
4
7 hpi
E.
4 hpi
7 hpi
Cells, %
Free Pool, %
Fast Exchange Rate
Slow Exchange Rate

Figure 5.4. The dynamics of H2A are enhanced in HSV-1 infected cells. Vero cells were transfected with a plasmid expressing GFP-H2A. Transfected cells were mock-infected (**Mock**) or infected with HSV-1 moi 5 (**KOS**). The dynamics of GFP-H2A were evaluated 4 to 5 (**4 hpi**) or 7 to 8 (**7 hpi**) hours later by FRAP. A) Average fluorescence recovery curves for GFP-H2A at 4 or 7 hpi in HSV-1- (black line) or mock-infected (grey line) cells. B) Bar graphs showing average levels of free GFP-H2A in HSV-1- relative to mock-infected cells at 4 or 7 hpi. C) Bar graphs showing the average fast exchange rates of GFP-H2A in HSV-1- relative to mock-infected cells at 4 or 7 hpi. D) Bar graphs showing the average slow exchange rates of GFP-H2A in HSV-1- relative to mock-infected cells at 4 or 7 hpi. E) Frequency distribution graphs of free pools, fast, or slow exchange rates of GFP-H2A in HSV-1- (red line) or mock-infected (blue line) cells at 4 or 7 hpi. Error bars, SEM. **, $P < 0.01$; *, $P < 0.05$; *n.s.,* not significant. $n \geq 15$ cells from at least 3 independent experiments.

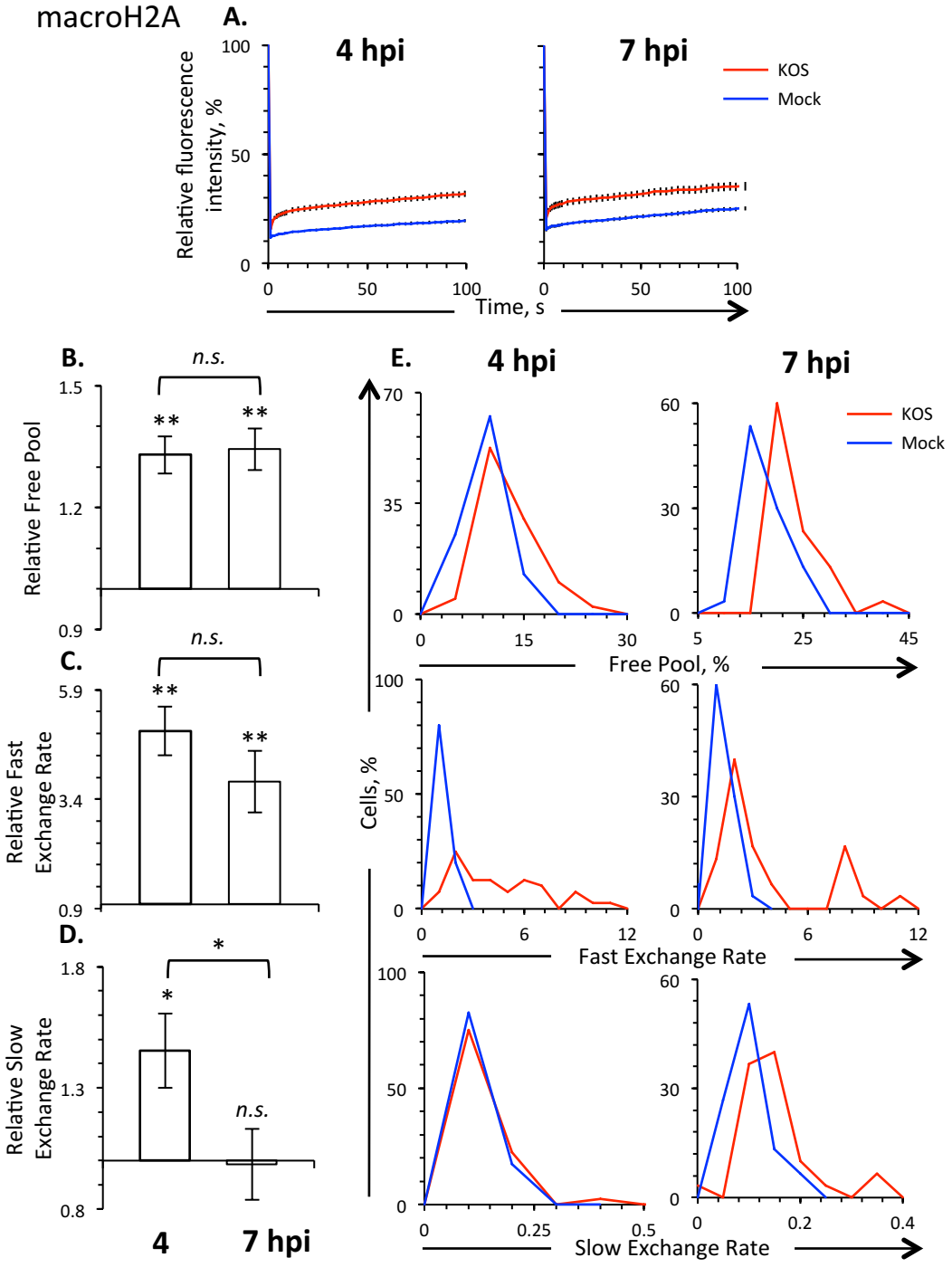
macroH2A
A.
4 hpi
7 hpi
KOS
Mock
Relative fluorescence intensity, %
Time, s
B.
n.s.
Relative Free Pool
C.
Relative Fast Exchange Rate
D.
Relative Slow Exchange Rate
4
7 hpi
E.
4 hpi
7 hpi
Cells, %
Free Pool, %
Fast Exchange Rate
Slow Exchange Rate

Figure 5.5. The dynamics of macroH2A are enhanced in HSV-1 infected cells. Vero cells were transfected with a plasmid expressing GFP-macroH2A. Transfected cells were mock-infected (**Mock**) infected with HSV-1 moi 5 (**KOS**). The dynamics of GFP-macroH2A were evaluated 4 to 5 (**4 hpi**) or 7 to 8 (**7 hpi**) hours later by FRAP. A) Average fluorescence recovery curves for GFP-macroH2A at 4 or 7 hpi in HSV-1- (red line) or mock-infected (blue line) cells. B) Bar graphs showing the average levels of free GFP-macroH2A in HSV-1- relative to mock-infected cells at 4 or 7 hpi. C) Bar graphs showing the average fast exchange rates of GFP-macroH2A in HSV-1- relative to mock-infected cells at 4 or 7 hpi. D) Bar graphs showing the average slow exchange rates of GFP-macroH2A in HSV-1- relative to mock-infected cells at 4 or 7 hpi. E) Frequency distribution graphs of free pools, fast, or slow exchange rates of GFP-macroH2A in HSV-1- (red line) or mock-infected (blue line) cells at 4 or 7 hpi. Error bars, SEM. **, $P < 0.01$; *, $P < 0.05$; *n.s.,* not significant. $n \geq 15$ cells from at least 3 independent experiments.

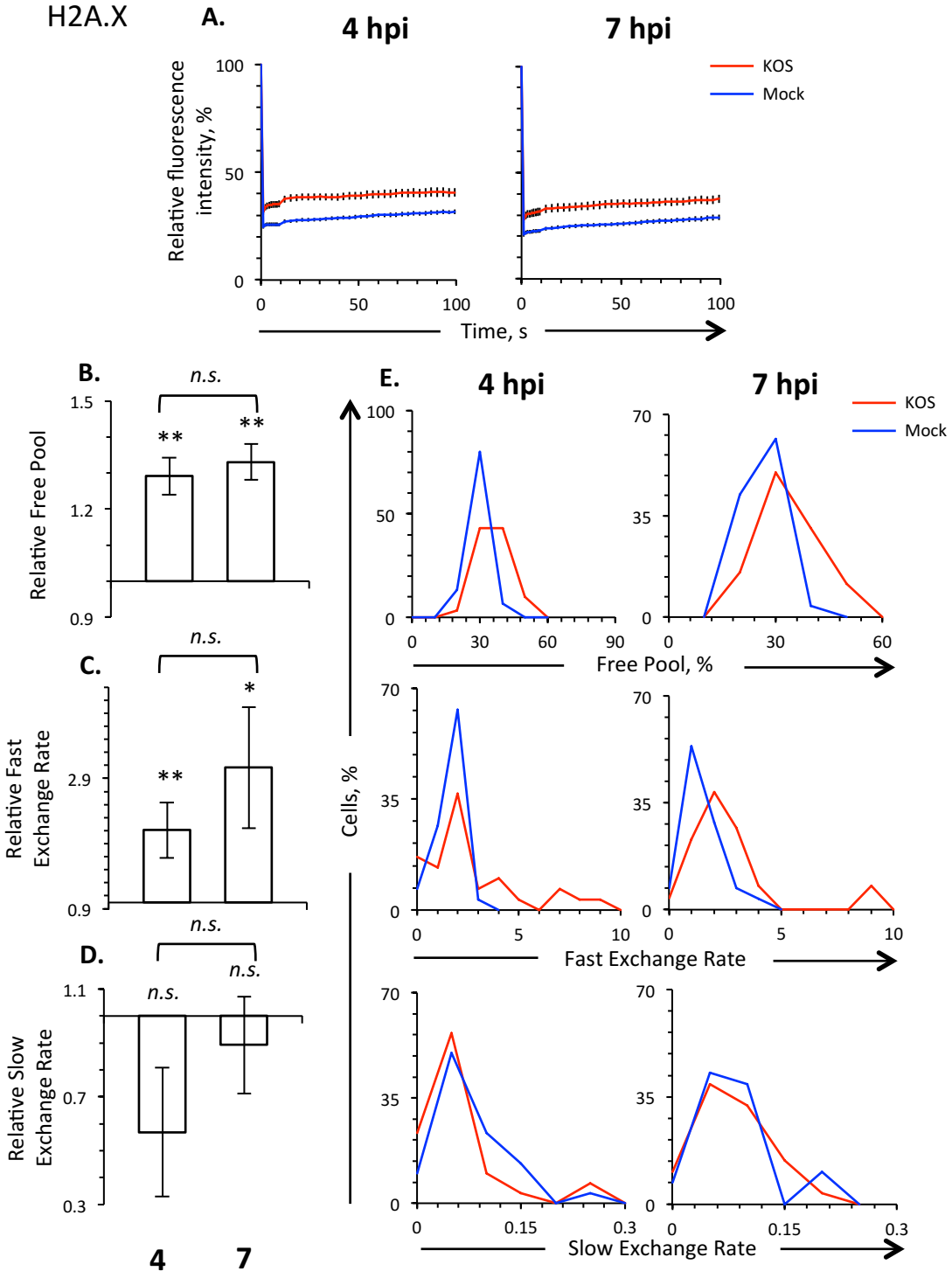
H2A.X
A.
4 hpi
7 hpi
KOS
Mock
Relative fluorescence intensity, %
Time, s
B.
n.s.
Relative Free Pool
C.
Relative Fast Exchange Rate
D.
Relative Slow Exchange Rate
4
7
E.
Cells, %
Free Pool, %
Fast Exchange Rate
Slow Exchange Rate

Figure 5.6. The dynamics of H2A.X are enhanced in HSV-1 infected cells. Vero cells were transfected with a plasmid expressing GFP-H2A.X. Transfected cells were mock-infected (**Mock**) or infected with HSV-1 moi 5 (**KOS**). The dynamics of GFP-H2A.X were evaluated 4 to 5 (**4 hpi**) or 7 to 8 (**7 hpi**) hours later by FRAP. A) Average fluorescence recovery curves for GFP-H2A.X at 4 or 7 hpi in HSV-1- (red line) or mock-infected (blue line) cells. B) Bar graphs showing the average levels of free GFP-H2A.X in HSV-1- relative to mock-infected cells at 4 or 7 hpi. C) Bar graphs showing the average fast exchange rates of GFP-H2A.X in HSV-1- relative to mock-infected cells at 4 or 7 hpi. D) Bar graphs showing the average slow exchange rates of GFP-H2A.X in HSV-1- relative to mock-infected cells at 4 or 7 hpi. E) Frequency distribution graphs of free pools, fast, or slow exchange rates of GFP-H2A.X in HSV-1- (red line) or mock-infected (blue line) cells at 4 or 7 hpi. Error bars, SEM. **, $P < 0.01$; *, $P < 0.05$; *n.s.,* not significant. $n \geq 15$ cells from at least 3 independent experiments.

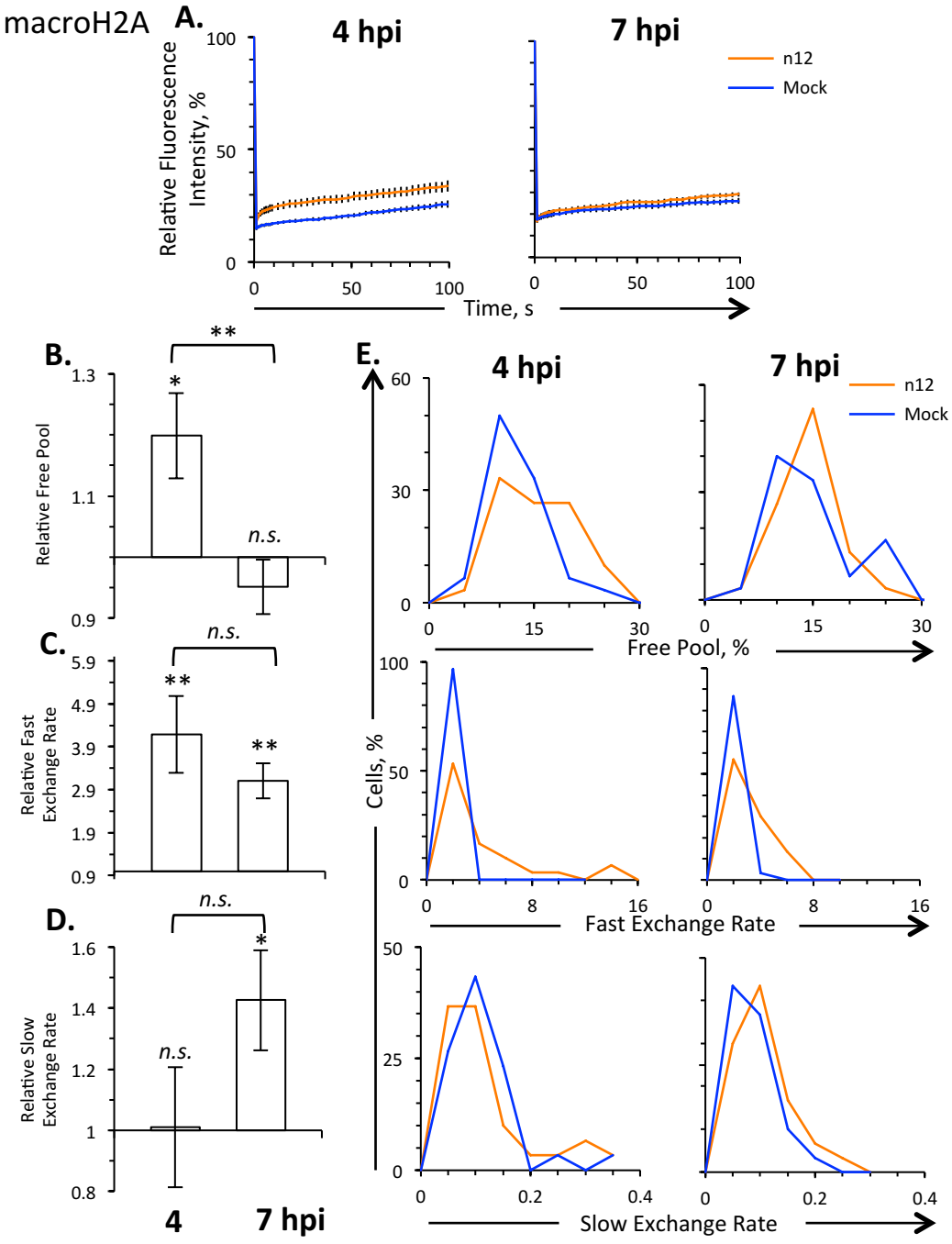
macroH2A
A.
4 hpi
7 hpi
n12
Mock
Relative Fluorescence Intensity, %
Time, s
B.
Relative Free Pool
n.s.
C.
Relative Fast Exchange Rate
D.
Relative Slow Exchange Rate
4
7 hpi
E.
4 hpi
7 hpi
Cells, %
Free Pool, %
Fast Exchange Rate
Slow Exchange Rate

Figure 5.7. The dynamics of macroH2A are enhanced in n12-infected cells. Vero cells were transfected with a plasmid expressing GFP-macroH2A. Transfected cells were mock-infected (**Mock**) or infected with HSV-1 n12 moi 5 (**n12**). The dynamics of GFP-macroH2A were evaluated 4 to 5 (**4 hpi**) or 7 to 8 (**7 hpi**) hours later by FRAP. A) Average fluorescence recovery curves for GFP-macroH2A at 4 or 7 hpi in n12- (orange line) or mock-infected (blue line) cells. B) Bar graphs showing the average levels of free GFP-macroH2A in n12- relative to mock-infected cells at 4 or 7 hpi. C) Bar graphs showing the average fast exchange rates of GFP-macroH2A in n12- relative to mock-infected cells at 4 or 7 hpi. D) Bar graphs showing the average slow exchange rates of GFP-macroH2A in n12- relative to mock-infected cells at 4 or 7 hpi. E) Frequency distribution graphs of free pools, fast, or slow exchange rates of GFP-macroH2A in n12- (orange line) or mock-infected (blue line) cells at 4 or 7 hpi. Error bars, SEM. **, $P < 0.01$; *, $P < 0.05$; *n.s.,* not significant. $n \geq 15$ cells from at least 3 independent experiments.

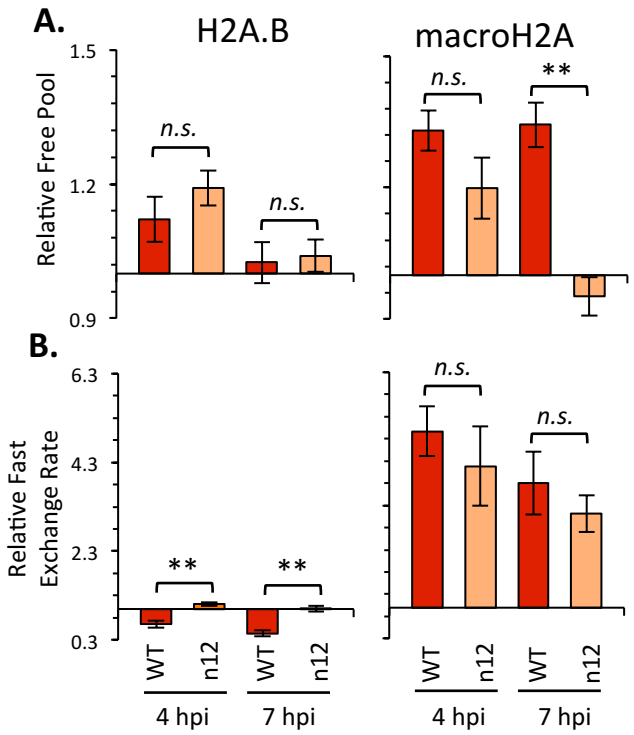

Figure 5.8. The dynamics of macroH2A and H2A.B are differently altered in cells infected with wt or n12 HSV-1. Vero cells were transfected with plasmids expressing GFP-macroH2A or GFP-H2A.B. Transfected cells were infected with 5 moi of n12 (**n12**) or wt (**WT**) HSV-1 and the dynamics of GFP-macroH2A or –H2A.B were evaluated 4 to 5 (**4 hpi**) or 7 to 8 (**7 hpi**) hours later by FRAP. A) Bar graphs showing the average levels of free GFP-macroH2A or –H2A.B in cells infected with n12 or wt HSV-1 relative to mock-infected cells at 4 or 7 hpi. B) Bar graphs showing the average fast exchange rates of GFP-macroH2A or –H2A.B in cells infected with n12 or wt HSV-1 relative to mock-infected cells at 4 or 7 hpi.

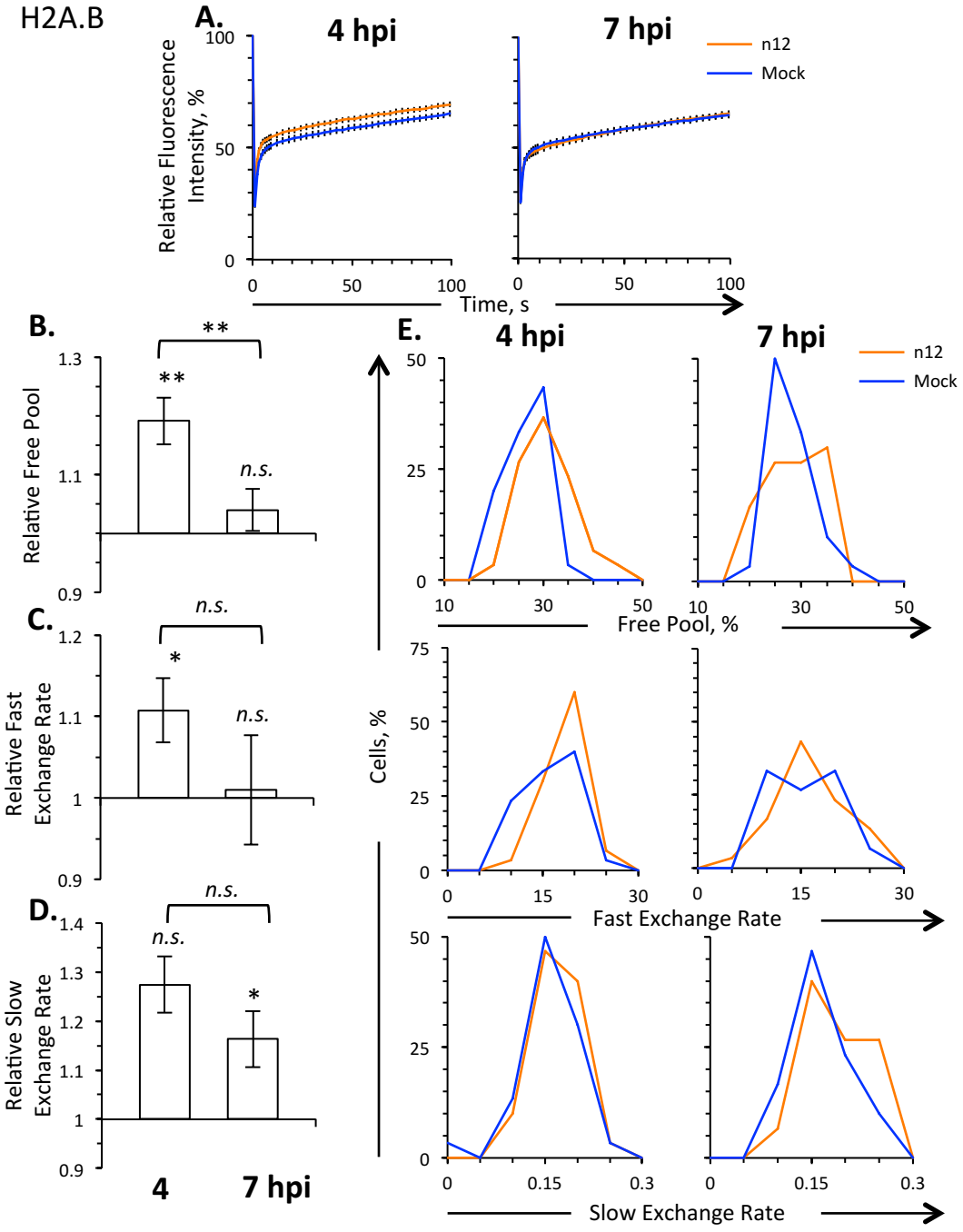
H2A.B
A.
4 hpi
7 hpi
n12
Mock
Relative Fluorescence Intensity, %
Time, s
B.
Relative Free Pool
**
n.s.
C.
Relative Fast Exchange Rate
*
n.s.
D.
Relative Slow Exchange Rate
n.s.
*
4
7 hpi
E.
4 hpi
7 hpi
n12
Mock
Cells, %
Free Pool, %
Fast Exchange Rate
Slow Exchange Rate

Figure 5.9. The dynamics of H2A.B are enhanced in n12-infected cells. Vero cells were transfected with a plasmid expressing GFP-H2A.B. Transfected cells were mock-infected (**Mock**) or infected with HSV-1 n12 moi 5 (**n12**). The dynamics of GFP-macroH2A were evaluated 4 to 5 (**4 hpi**) or 7 to 8 (**7 hpi**) hours later by FRAP. A) Average fluorescence recovery curves for GFP-H2A.B at 4 or 7 hpi in n12- (orange line) or mock-infected (blue line) cells. B) Bar graphs showing the average levels of free GFP-H2A.B in n12- relative to mock-infected cells at 4 or 7 hpi. C) Bar graphs showing the average fast exchange rates of GFP-H2A.B in n12- relative to mock-infected cells at 4 or 7 hpi. D) Bar graphs showing the average slow exchange rates of GFP-H2A.B in n12- relative to mock-infected cells at 4 or 7 hpi. E) Frequency distribution graphs of free pools, fast, or slow exchange rates of GFP-H2A.B in n12- (orange line) or mock-infected (blue line) cells at 4 or 7 hpi. Error bars, SEM. **, $P < 0.01$; *, $P < 0.05$; *n.s.,* not significant. $n \geq 15$ cells from at least 3 independent experiments.

			Free core histone (avg ± SEM)			
Histone	Virus	PFU /	4 hpi		7 hpi	
variant	strain	cell	Absolute	Relative	Absolute	Relative
H2A	-	-	14.44 ± 0.45	1.00 ± 0.03	13.94 ± 0.57	1.00 ± 0.04
	KOS	5	19.10 ± 0.48	1.32 ± 0.04	19.74 ± 0.96	1.42 ± 0.07
H2A.B	-	-	22.68 ± 0.62	1.00 ± 0.02	20.85 ± 0.71	1.00 ± 0.03
	KOS	5	25.25 ± 1.06	1.12 ± 0.05	21.36 ± 0.93	1.02 ± 0.05
H2A.X	-	-	24.49 ± 0.79	1.00 ± 0.03	20.80 ± 0.91	1.00 ± 0.03
	KOS	5	31.60 ± 1.26	1.29 ± 0.05	27.83 ± 1.52	1.33 ± 0.05
macroH2A	-	-	11.71 ± 0.40	1.00 ± 0.03	15.39 ± 0.70	1.00 ± 0.04
	KOS	5	15.45 ± 0.58	1.32 ± 0.05	20.68 ± 0.84	1.34 ± 0.05

Table 5.1. Free pools of H2A variants in mock-infected cells or cells infected with KOS.

			Fast exchange rate (avg ± SEM)			
Histone	Virus	PFU /	4 hpi		7 hpi	
variant	strain	cell	Absolute	Relative	Absolute	Relative
H2A	-	-	1.25 ± 0.10	1.00 ± 0.08	1.93 ± 0.27	1.00 ± 0.14
	KOS	5	3.44 ± 0.64	2.75 ± 0.51	2.94 ± 0.48	1.53 ± 0.25
H2A.B	-	-	10.87 ± 0.86	1.00 ± 0.05	11.03 ± 0.30	1.00 ± 0.05
	KOS	5	7.13 ± 0.84	0.66 ± 0.08	4.96 ± 0.71	0.45 ± 0.07
H2A.X	-	-	1.04 ± 0.11	1.00 ± 0.10	0.93 ± 0.15	1.00 ± 0.15
	KOS	5	2.19 ± 0.44	2.11 ± 0.42	2.08 ± 0.42	4.91 ± 0.93
macroH2A	-	-	0.80 ± 0.04	1.00 ± 0.06	0.88 ± 0.10	1.00 ± 0.12
	KOS	5	3.97 ± 0.45	4.96 ± 0.56	3.34 ± 0.62	3.80 ± 0.70

Table 5.2. Fast exchange rates of H2A variants in mock-infected cells or cells infected with KOS.

			Slow exchange rate (avg ± SEM)			
Histone	Virus	PFU /	4 hpi		7 hpi	
variant	strain	cell	Absolute	Relative	Absolute	Relative
H2A	-	-	0.09 ± 0.01	1.00 ± 0.10	0.11 ± 0.02	1.00 ± 0.15
	KOS	5	0.11 ± 0.01	1.28 ± 0.10	0.09 ± 0.03	0.85 ± 0.30
H2A.B	-	-	0.19 ± 0.01	1.00 ± 0.04	0.20 ± 0.01	1.00 ± 0.05
	KOS	5	0.25 ± 0.01	1.28 ± 0.07	0.26 ± 0.02	1.28 ± 0.08
H2A.X	-	-	0.05 ± 0.01	1.00 ± 0.20	0.06 ± 0.01	1.00 ± 0.17
	KOS	5	0.04 ± 0.01	0.75 ± 0.25	0.05 ± 0.01	0.90 ± 0.18
macroH2A	-	-	0.06 ± 0.01	1.00 ± 0.12	0.08 ± 0.01	1.00 ± 0.10
	KOS	5	0.07 ± 0.01	1.26 ± 0.15	0.08 ± 0.01	0.98 ± 0.15

Table 5.3. Slow exchange rates of H2A variants in mock-infected cells or cells infected with KOS.

			Free core histone (avg ± SEM)			
Histone	Virus	PFU /	4 hpi		7 hpi	
variant	strain	cell	Absolute	Relative	Absolute	Relative
H2A.B	-	-	23.90 ± 0.76	1.00 ± 0.03	25.27 ± 0.70	1.00 ± 0.03
	n12	5	28.47 ± 0.95	1.19 ± 0.04	26.27 ± 0.90	1.04 ± 0.04
macroH2A	-	-	14.95 ± 0.78	1.00 ± 0.05	17.52 ± 1.08	1.00 ± 0.06
	n12	5	17.92 ± 1.05	1.20 ± 0.07	16.67 ± 0.78	0.95 ± 0.04

Table 5.4. Free pools of H2A.B or macroH2A in mock-infected cells or cells infected with n12.

			Fast exchange rate (avg ± SEM)			
Histone	Virus	PFU /	4 hpi		7 hpi	
variant	strain	cell	Absolute	Relative	Absolute	Relative
H2A.B	-	-	14.00 ± 0.70	1.00 ± 0.05	13.46 ± 0.77	1.00 ± 0.06
	n12	5	15.51 ± 0.55	1.11 ± 0.04	13.59 ± 0.90	1.01 ± 0.07
macroH2A	-	-	0.71 ± 0.11	1.00 ± 0.15	0.71 ± 0.11	1.00 ± 0.15
	n12	5	2.93 ± 0.63	4.18 ± 0.89	2.22 ± 0.29	3.11 ± 0.41

Table 5.5. Fast exchange rates of H2A.B or macroH2A in mock-infected cells or cells infected with n12.

			Slow exchange rate (avg ± SEM)			
Histone	Virus	PFU /	4 hpi		7 hpi	
variant	strain	cell	Absolute	Relative	Absolute	Relative
H2A.B	-	-	0.11 ± 0.03	1.00 ± 0.25	0.14 ± 0.01	1.00 ± 0.07
	n12	5	0.14 ± 0.01	1.27 ± 0.06	0.17 ± 0.01	1.16 ± 0.06
macroH2A	-	-	0.10 ± 0.02	1.00 ± 0.20	0.06 ± 0.01	1.00 ± 0.12
	n12	5	0.10 ± 0.02	1.00 ± 0.20	0.08 ± 0.01	1.43 ± 0.16

Table 5.6. Slow exchange rates of H2A.B or macroH2A in mock-infected cells or cells infected with n12.

Chapter 6: Discussion

The work presented in this study demonstrates that ICP4 is largely responsible for the increased histone dynamics during HSV-1 infection. ICP4 (in the presence of plasmid DNA) was sufficient to enhance the dynamics of most, but not all, core histones. The dynamics of canonical H3.1 and variant H3.3 were both enhanced in cells expressing ICP4, but to different extents (Figure 3.5., 3.6). ICP4 appeared to prevent the incorporation of H3.1 in chromatin, as observed by diffuse distribution of H3.1 in ICP4-expressing cells, and its free pool was doubled. The dynamics of H2A.B, but not those of canonical H2A or any other H2A variant, were enhanced in ICP4-expressing cells (Figure 4.6., 4.8., 4.10., 4.12., 4.17., 4.19.). H2A.B co-localized with ICP4 at the nucleolus in transfected cells or at replication compartments in infected cells (Figure 4.13., 5.1.). The dynamics of H2A.B, but not those of any other H2A variant, decreased in HSV-1 infected cells (Figure 5.3., 5.4., 5.5., 5.6.). The dynamics of H2A.B increased in cells infected with an HSV-1 mutant encoding no functional ICP4 (Figure 5.9.).

ICP4 is the only essential HSV-1 transcription activator, but its mechanisms of action are the least understood among all three HSV-1 transcription activators. ICP4 is a large protein of 1298 amino acids, a molecular weight of 175 kDa, and a stokes radius of about 90 angstroms (342). ICP4 interacts with over 200 proteins, including all of the components of TFIID and over half of the components of the mediator complex (360). ICP4 has thus been suggested to activate transcription by a 'gene-looping' model. In this model, a homodimer of ICP4 bound to the promoter DNA of E or L genes interacts with the mediator complex and other proteins to provide a structural link between the promoter and terminator regions. After transcribing a gene, RNA pol II is proximal to the promoter and re-initiation is thus more efficient, resulting in increased transcription kinetics. If ICP4 activated transcription by gene-looping, we would expect at least basal levels of E or L RNA in the absence of ICP4. However, there is only detectable IE RNAs and no detectable E or L RNAs, or viral replication, in the absence of functional ICP4 (459). Unlike most cellular genes, most HSV-1 genes have no introns. As a result, HSV-1 genes are generally shorter, with also shorter distances between promoter and terminator

regions. Gene-looping occurs in genes as short as 1 kbp, and is used by other viruses such as HIV-1 (460, 461). However, transcription inhibition resulted in the loss of gene-looping, suggesting that transcription causes gene-looping as opposed to being a consequence of it (461). According to the gene-looping model, ICP4 would have to bind to DNA to activate transcription. However, ICP4 binds to specific DNA sequences to actually inhibit transcription of its own gene and other IE genes (352). ICP4 forms multiple hydrogen bonds with its specific DNA sequence to strengthen the interaction (352). E and L genes have no specific DNA sequences recognized by ICP4, and ICP4 mutants unable to bind DNA but which retain the ability to dimerize still activate transcription (353). Therefore, ICP4 activates transcription by mechanisms that require no direct binding to DNA.

The HSV-1 nuclear DNA amounts to 0.6 or 6% of the total nuclear DNA at 4 or 7 hpi, respectively (Miyao Hu, unpublished results), and histone synthesis is inhibited in HSV-1 infected cells (462). The number of histone binding sites thus increases in HSV-1 infected cells, whereas the number of histone molecules does not. As a result, we expected that the free pool of histones would decrease in HSV-1 infected cells. Instead, the free pool of histones increased in HSV-1 infected cells (82, 374, 414).

The histone free pools were still enhanced in the absence of DNA replication or L gene expression, but not so much in cells infected with UV-inactivated HSV-1. Therefore, IE or E proteins enhanced histone dynamics. We proposed a model in which the chromatinization of HSV-1 genomes is a cellular defense mechanism to silence HSV-1 gene expression. To counteract silencing, HSV-1 would have evolved proteins that prevent or disrupt the silencing chromatinization of HSV-1 genomes. These proteins would be transcription activators. Consistent with this model, all three HSV-1 transcription activators interact with histone modifying and chromatin remodeling complexes. VP16 recruits the histone acetyltransferases p300/CBP and the chromatin remodeler SWI/SNF to IE promoters (315), and the IE promoters stably associated with histones in the absence of functional VP16 (316). ICP0 dissociates HDAC from the CoREST complex (332), and E promoters stably associated with histones in the absence of functional ICP0 (333). ICP4 interacts

with the histone acetyltransferase CLOCK and many components of the SWI/SNF, NURD, and Ino80 chromatin remodeling complexes (360, 365).

To test whether any of the three transcription activators are required to enhance dynamics, we evaluated histone dynamics in Vero or U2OS cells infected with HSV-1 mutants in ICP0, VP16, or ICP4 (Figure 3.2.). The HSV-1 mutant in ICP0, n212, enhanced histone free pools even more than wild-type HSV-1 in U2OS cells, which are permissive to mutants in ICP0 without complementing any known ICP0 activity (451), suggesting that ICP0 promotes the degradation of histones in the free pool. The free pools of histones were barely enhanced in n212-infected Vero cells at 4 hpi, but were enhanced at 7 hpi, consistent with the delayed kinetics of n212 in Vero cells. The HSV-1 mutant encoding no functional ICP0 or VP16, KM110, barely enhanced the histone free pools in U2OS cells at 4 hpi, but did enhance them at 7 hpi, consistent with the delayed kinetics of KM110 in U2OS cells. In contrast, the histone free pools were barely enhanced in KM110-infected Vero cells at either 4 or 7 hpi. Only 6% of Vero cells infected with KM110 express detectable levels of ICP4 whereas 74% of U2OS cells infected with KM110 do so (374). Thus, Vero cells infected with KM110 express little of all three HSV-1 transcription activators and are deficient for replication (395). An HSV-1 mutant in ICP4, n12, enhanced histone dynamics the least. The histone free pools were barely enhanced in n12-infected U2OS or Vero cells. ICP4 inhibits the expression of itself, as well as that of the other IE genes. As a result, ICP0 is overexpressed in cells infected with an HSV-1 mutant encoding no functional ICP4. Overexpression of ICP0 in n12-infected cells thus did not increase the histone free pools. To test whether the n12 deficit was due to the nonsense mutation within the ICP4 gene, or to another unknown mutation within the virus, histone dynamics were evaluated in n33 cells, which express HSV-2 ICP4 and complement n12. Histone free pools were enhanced in n12-infected n33 cells. We proposed that ICP4 directly enhances histone dynamics. Alternatively, ICP4 may activate the transcription of an E protein, which then enhances histone dynamics.

To test if ICP4 itself enhanced histone dynamics, I constructed a plasmid encoding full length ICP4 fused in frame to RFP. I also constructed a plasmid encoding the truncated n12 ICP4, consisting of only the N-terminal 251 amino acids,

fused in frame to RFP. I optimized the co-transfection of RFP-ICP4, RFP-n12, or free RFP with GFP-histones such that approximately half of the cells expressing detectable levels of GFP also expressed detectable levels of RFP. I thus compared the histone dynamics in cells expressing detectable levels of RFP to those in cells expressing undetectable levels of RFP under otherwise identical conditions.

H2B and H4, which have no variants and represent the H2B-H2A and H3-H4 dimers, were more dynamic in cells expressing detectable than undetectable levels of ICP4 (Figure 3.4.). Canonical H3.1 and variant H3.3, both of which assemble dimers with H4, were also more dynamic in cells expressing detectable levels of ICP4 (Figure 3.5., 3.6.). The histones incorporated into chromatin produce a granular distribution of the tagged fluorescence, which is consistent with more or less compacted chromatin. H3.1 had this granular distribution in cells expressing no detectable ICP4, but had instead a diffuse distribution in cells expressing detectable ICP4 (Figure 3.5.I, 3.6.I). The free pool of H3.1 also doubled in ICP4-expressing Vero cells, suggesting that ICP4 may prevent the incorporation of H3.1 in chromatin (Figure 3.5.D, Table 3.1.). In contrast, H3.3 still had granular distribution in ICP4-expressing Vero cells, and its free pool increased by only 11% (Figure 3.5.B, Table 3.1.). H3.3 assembles nucleosomes with HSV-1 genomes immediately upon nuclear entry, whereas H3.1 only assembles nucleosomes with HSV-1 genomes after the onset of HSV-1 DNA replication (371). In the absence of HSV-1 DNA replication, H3.1 is not assembled in HSV-1 nucleosomes (371). H3.1 is likely assembled in nucleosomes with HSV-1 genomes via DNA-replication dependent mechanisms, as it assembled in nucleosomes with cellular DNA. Alternatively, the incorporation of H3.1 in HSV-1 nucleosomes may require L gene expression. IE or E genes are transcribed before HSV-1 DNA replication, and thus the promoters of IE or E genes are assembled in nucleosomes with H3.3 before they are transcribed. If H3.1 is assembled in HSV-1 nucleosomes via DNA-replication dependent mechanisms, then the promoters of L genes, which are transcribed after HSV-1 DNA replication, may be assembled in nucleosomes with either H3.1 or H3.3. The tegument protein VP16 would then disrupt H3.3-containing nucleosomes to activate IE gene expression. Upon its expression, ICP4 may disrupt the H3.3-containing nucleosomes on E

promoters to activate E gene expression. As the HSV-1 genomes replicate, ICP4 may preferentially prevent the assembly of H3.1 into nucleosomes with the replicating genomes, as nucleosomes containing H3.1 are expected to be more silencing than those containing H3.3.

The dynamics of canonical H2A were not enhanced in ICP4-expressing cells (Figure 3.7.A,B). As those of H2B were, we expected that the dynamics of at least one H2A variant to also be enhanced. We expected that ICP4 would preferentially target the silencing H2A variant macroH2A, just as it preferentially targets H3.1. To test if the dynamics of any H2A variant histone were enhanced by ICP4, I first constructed plasmids expressing full-length macroH2A or H2A.B fused in frame to GFP. Histones with GFP tagged on the N-terminus are still incorporated into chromatin, whereas those with GFP tagged on the C-terminus sometimes are not. I thus cloned N-terminal GFP tags fused to macroH2A or H2A.B.

ICP4 enhanced the dynamics of only the most activating variant, H2A.B (Figure 4.17., 4.19.). Whereas canonical H2A and the other H2A variants are usually depleted in the nucleolus, H2A.B is usually enriched. Histones in the nucleolus are more dynamic than those in the cellular chromatin. In ICP4-transiently expressing cells, there is a greater enrichment of H2A.B in the nucleolus, where ICP4 itself localizes in the absence of viral DNA or other viral proteins. The dynamics of H2A.B are thus likely enhanced in ICP4-expressing cells due to a shift of H2A.B to the most dynamic population.

Whereas the nucleolus is disassembled in cells infected with wild-type HSV-1, it is fragmented in cells infected with n12. ICP4 is not required to deplete H2A.B from nucleoli, as H2A.B was still depleted from the fragmented nucleoli in n12-infected cells. H2A.B is relatively enriched in the HSV-1 replication compartments relative to the other histones. The population of H2A.B previously localized to the nucleolus may thus re-localize to the replication compartments when the nucleolus is disassembled. Replications compartments do not form in n12-infected cells. The population of H2A.B that is displaced from the nucleolus therefore must diffuse into the general chromatin.

All H2A variants are more dynamic in the nucleolus than in the general chromatin in mock-infected cells, and all H2A variants are more dynamic in the replication compartments than in the general chromatin of infected cells. However, H2A.B is the only H2A variant that is more dynamic in the nucleolus than in the replication compartments (Kristen Conn, unpublished observations). Whereas the dynamics of macroH2A, H2A.X, and H2A were all enhanced in cells infected with wild-type HSV-1, those of H2A.B decreased (Figure 5.3.). In contrast, the dynamics of H2A.B increased in n12-infected cells (Figure 5.9.). Expression of ICP4 is therefore required to decrease the dynamics of H2A.B. ICP4 may be required to recruit H2A.B into the replication compartments. However, ICP4 may be required only because it is required for the formation of the replication compartments.

H3.3 and H3.1 are both assembled in nucleosomes with HSV-1 genomes, but with different kinetics (371). It is not yet known if any of the H2A variants are assembled in nucleosomes with HSV-1 genomes. H2A.B is enriched in nucleosomes on transcriptionally active cellular genes (177, 447), and also appear to be enriched in the highly dynamic nucleosomes of the nucleoli. H2A.B may also be enriched in nucleosomes on HSV-1 genomes, as HSV-1 genes are highly transcribed. Consistent with this hypothesis, H2A.B is enriched in replication compartments relative to canonical H2A or any other H2A variants, and the dynamics of only H2A.B are decreased in infected cells (Figure 5.1.,5.3.). H2A.B also appears to have a granular distribution, expected for histones incorporated into chromatin, within the replication compartments, though less so than in the cellular chromatin, consistent with replication compartments having a more uniform distribution of protein and DNA than cellular chromatin (463). Nucleosomes containing canonical H2A are stably wrapped by 146 bp of dsDNA. In contrast, nucleosomes containing canonical H2A.B are stably wrapped by as little as 116 bp of dsDNA (192, 193, 444). DNA wraps around H2A.B-containing nucleosomes less stably than it does around H2A-containing nucleosomes, resulting in more accessible entry and exit DNA (192). As a result, reconstituted nucleosomes assembled with H2A.B protect DNA to broader bands from nucleases than those assembled with canonical H2A (192). MCN digested HSV-1 chromatin also results in broad DNA bands, corresponding to

approximately mono-, di-, tri-, and poly-nucleosome sizes (373, 456). The composition of HSV-1 nucleosomes is not yet known. HSV-1 nucleosomes may be assembled preferentially with H2A.B and HSV-1 nucleosomal DNA may thus be less protected from nuclease digestion, resulting in the broad DNA bands smaller than 146 bp when digested.

The dynamics of H3.1 and H2A.B were preferentially enhanced in ICP4-expressing cells, and the distribution was altered. H3.1 had a diffuse distribution in ICP4-expressing cells, whereas H2A.B was enriched at the nucleolus. ICP4 may thus alter the dynamics of H3.1 and H2A by different mechanisms. The diffuse distribution of H3.1 suggests that ICP4 prevents its assembly in nucleosomes. In contrast, H2A.B co-localizes with ICP4 at the nucleoli or the replication compartments of transfected or infected cells, respectively. BNRF1 binds directly to Daxx. BNRF1 disrupts the interaction between Daxx and ATRX1, but not between Daxx and H3.3. BNRF1 thus inhibits the assembly of H3.3 in nucleosomes, increasing the H3.3 free pool. H2A.B is assembled in nucleosomes by the non-specific chaperone NAP-1 in vitro, but whether an H2A.B specific chaperone exists is not yet known. ICP4 may bind directly to a specific chaperone without competing for binding with H2A.B, accounting for the co-localization of H2A.B and ICP4. In contrast, ICP4 and H3.1 do not co-localize, and ICP4 thus does not form a complex with CAF-1 and H3.1.

Only alpha herpesviruses encode homologs of ICP4. Alpha herpesviruses also happen to have more dynamic chromatin and faster replication cycles than beta or gamma herpesviruses (386, 388, 390, 391). I have shown that ICP4 is the main HSV-1 protein enhancing HSV-1 chromatin dynamics. It is thus likely that ICP4 maintains the HSV-1 genomes in the highly dynamic state, which in turn results in the faster replication cycle. We, and other labs, propose that the stable chromatinization of viral genomes is a cellular defense mechanism to silence viral gene expression. All nuclear-replicating dsDNA viruses would then be inhibited by chromatinization. Consistent with this model, many viruses have evolved mechanisms that prevent the stable chromatinization of their genomes. We have shown that BNRF1, of the gamma herpesvirus EBV, enhances the dynamics of H3.3

through direct binding to Daxx (435). Other groups have shown that IE1, of the beta herpesvirus CMV, reduces the amount of histones stably associated with CMV genomes (388). Nuclear-replicating dsDNA viruses from other families have also evolved mechanism to prevent the stable chromatinization of their genomes. For example, adenovirus E1B-55K promotes the proteosomal degradation of Daxx (464). ICP4 may just happen to be one of the more efficient destabilizers of chromatin.

Though the stable chromatinization of HSV-1 genomes is expected to inhibit HSV-1 replication, the dynamic chromatinization of HSV-1 genomes may actually promote it. Consistent with this idea, the knockdown of the chaperone HIRA, which assembles dynamic nucleosomes containing H3.3, actually reduces HSV-1 RNA levels (371). IFI16 is a sensor that induces the production of interferon-β upon recognition of dsDNA, including HSV-1 genomes (432, 465). IFI16 knockdown increased expression of HSV-1 genes, which are not chromatinized in the virion, but had no effect on SV40 genes, which are chromatinized in the virion, suggesting that IFI16 distinguishes foreign dsDNAs by the lack of chromatinization (466). Nucleosomes inhibit IFI16 oligomerization, and likely prevent the induction of the IFI16 signalling cascade (429). Upon its expression, ICP0 degrades IFI16 in infected cells (432). However, ICP0 is not expressed immediately upon nuclear entry of HSV-1 genomes. It may thus be beneficial for HSV-1 genomes to assemble in dynamic nucleosomes prior to ICP0 expression, as a mechanism to evade IFI16-induced cellular responses.

Chapter 7: Future Directions

H2A.B dynamics are decreased in cells infected with wild-type HSV-1, but enhanced in cells infected with a mutant HSV-1 encoding no functional ICP4, n12. The expression of ICP4 is thus required to decrease H2A.B dynamics. In the absence of ICP4, replication compartments do not form. I propose that the H2A.B displaced from the dissipated nucleoli in cells infected with wild-type HSV-1 are mobilized to the replication compartments. H2A.B is then assembled in nucleosomes with HSV-1 genomes, resulting in the observed decrease of H2A.B dynamics in HSV-1-infected cells. In n12-infected cells, H2A.B is still displaced from the nucleoli, but H2A.B is not assembled into HSV-1 genomes. More H2A.B remains in the free pool, resulting in the observed increase of H2A.B dynamics in n12-infected cells. To test whether the formation of replication compartments is essential to decrease histone dynamics, I would evaluate H2A.B dynamics in cells infected with wild-type HSV-1 and treated with phosphonoacetic acid (PAA). PAA is an inhibitor of the HSV-1 DNA polymerase (467). As a result, IE and E genes are expressed in PAA-treated and infected cells, but HSV-1 genomes do not replicate, L genes are not expressed, and replication compartments are not formed. Under my hypothesis, H2A.B dynamics will increase in PAA-treated infected cells, as the replication compartments are required for their decrease. Alternatively, H2A.B dynamics may be unchanged or even more decreased in PAA-treated cells. HSV-1 DNA replication was not required to enhance the dynamics of H2B, H3.1, or H3.3 (82, 375). The dynamics of H3.1 were actually greater in PAA-treated cells than in untreated cells, as H3.1 is likely still disassembled from the cellular chromatin and not being reassembled in nucleosomes with the replicated HSV-1 genomes (375). If H2A.B dynamics are still decreased in PAA-treated cells, then expression of ICP4 or another IE or E protein is required to decrease histone dynamics.

In cells expressing undetectable levels of ICP4, H2A.B is enriched in the nucleolus. Even more H2A.B is enriched in the nucleolus in cells expressing detectable levels of ICP4. The nucleolar H2A.B has granular distribution in cells expressing undetectable or detectable levels of ICP4, with regions of low or high H2A.B density, consistent with its assembly into chromatin. Nucleolar H2A.B is also

less dynamic than linker histones or non-nucleosomal DNA-binding proteins, consistent with its assembly into chromatin (Kristen Conn, unpublished observations). Transcriptionally inactive nucleolar chromatin is regularly chromatinized, whereas transcriptionally active nucleolar chromatin appears to be mostly depleted of nucleosomes in electron microscopy (88). However, active nucleolar chromatin still produces a nucleosomal ladder when digested with nucleases, suggesting that it is in highly dynamic chromatin (93). As the active nucleolar chromatin is less stably associated with histones, the regions of the nucleolus with low H2A.B density may mark the active nucleolar chromatin. Recently, it has been demonstrated that H2A.B binds RNA in vitro (468). The nucleolus has higher amounts of RNA than the general nucleus (89, 90). H2A.B may be thus be enriched in the nucleolus because it is binding to the rRNA. If H2A.B is associated with the rRNA then the regions with high H2A.B density may mark the active nucleolar chromatin. To test if H2A.B is enriched or depleted from the active nucleolar chromatin, I would evaluate the co-localization of H2A.B and UBF, a transcription factor of Pol I that is associated with active but not inactive nucleolar chromatin (469, 470). Alternatively, I may label the rRNA transcripts using a run-on assay with BrU (470). If H2A.B is depleted from nucleolar regions that are enriched with UBF or BrU, it would suggest that H2A.B does not assemble the unstable chromatin with active rDNA.

Both H3.1 and H3.3 have been found to stably interact with HSV-1 genomes via ChIP (371). H3.3 initially interacts with the incoming HSV-1 genomes, but H3.1 interacts with the HSV-1 genomes after HSV-1 DNA replication, consistent with H3.1 or H3.3 being assembled in nucleosomes via DNA-replication independent or dependent mechanisms, respectively (371). The stable interaction identified via ChIP is thus likely due to the organization of HSV-1 genomes in chromatin. The other canonical core histones, H2A, H2B, and H4 have also been found to stably interact with HSV-1 genomes via ChIP (317). However, it is not yet known whether any H2A variant stably interacts with HSV-1 genomes. H2A.B is enriched in cellular transcribed genes, and appears to also be enriched in replication compartments (177). HSV-1 genomes also release broader bands when digested with MCN, similar

to those released by cellular genes assembled with H2A.B (193, 456). To test if H2A.B or another H2A variant is preferentially assembled in HSV-1 chromatin, I have constructed cell lines stably expressing plasmids encoding H2A.B, macroH2A, H2A, or H2B fused in frame with a FLAG tag. The N-terminus of histones is unstructured and extends from the core nucleosome. The FLAG tags were thus attached to the N-terminus of all histones, so that it less likely to affect folding and more likely to be recognized by the specific antibodies. Using ChIP and quantitative PCR with primers against HSV-1 promoters of each class, I would then quantify the amount of HSV-1 DNA bound to each histone. I expect that the H2A variants will be enriched on the HSV-1 genome at early times post infection, but that the levels of H2A will increase with HSV-1 DNA replication. HSV-1 genomes are stably associated with approximately 90% less H2B than cellular genes (317). Thus, I expect that at any time, there will also be less canonical or H2A variants stably associated with the HSV-1 genomes than with cellular DNA. Under my hypothesis, I expect that there would be more H2A.B than canonical H2A or macroH2A that interacts with HSV-1 DNA at any time.

I propose that ICP4 activates transcription by preventing or disrupting the stable chromatinization of HSV-1 genomes. Under my hypothesis, the domains of ICP4 that are essential to enhance histone dynamics would be the same ones that are essential to activate transcription. Many mutants of ICP4 have already been constructed and characterized. I have already shown that a mutant of ICP4 encoding only the N-terminal 251 amino acids, which is unable to activate transcription, is also unable to activate transcription. To determine which domains are essential for enhancing histone dynamics, I would construct plasmids encoding previously characterized mutants of ICP4 fused in frame with RFP. I would then evaluate histone dynamics in cells expressing these mutant ICP4 constructs. I would select mutants that specifically affect the transactivation abilities of ICP4. One mutant encoding only the N-terminal 774 amino acids is able to repress transcription, and activate the E genes, but is unable to activate the L genes (361). The further deletion of amino acids 143-210 results in a mutant that is able to repress transcription, but not activate E or L gene expression (458). To test if ICP4

must bind DNA to enhance histone dynamics, I would also test a mutant of ICP4 that is unable to bind DNA, but still activates transcription (353). If this mutant still enhanced histone dynamics, then ICP4 does not enhance histone dynamics by binding DNA.

ICP4 interacts with over 200 proteins in infected cells (360). ICP4 enhances histone dynamics in the absence of any other HSV-1 protein. The proteins required to enhance histone dynamics must therefore interact with ICP4 in uninfected cells. Once the domains of ICP4 that are required to enhance histone dynamics are identified, I would find the cellular proteins that are used by ICP4 to enhance histone dynamics. I would construct plasmids encoding full length ICP4 or the mutant of ICP4 lacking the minimal domain required for histone mobilization fused in frame to a tag such as TAP (360). I would identify the proteins that interact with the full length or mutant ICP4 using LC-MS/MS, and confirm the interactions with Western Blot. My proteins of interest would be those that interact with the full length ICP4, but not the mutant ICP4. I would also focus on cellular proteins that are involved in chromatin assembly or remodeling, such as chaperones or chromatin remodeling complexes. These experiments would lead to the characterization of the mechanisms by which ICP4 enhances histone dynamics, and perhaps activates transcription.

The chromatinization of viral DNA may be a cellular defense mechanism against only HSV-1, all herpesviruses, or all nuclear-replicating dsDNA viruses. Any virus that is targeted by this cellular defense mechanism would also be expected to have evolved mechanisms to counteract it. I have already shown that transient expression of BNRF1, of the gamma herpesvirus EBV, enhances H3.3 dynamics (435). However, it has not yet been shown that the dynamics of histones are enhanced in cells infected with any gamma or beta herpesvirus. The genomes of adenovirus, another nuclear-replicating dsDNA virus, are also assembled in chromatin (471). Influenza viruses are RNA viruses that replicate in the nucleus, whereas pox viruses are DNA viruses that replicate in the cytoplasm. The genomes of influenza or pox viruses are not chromatinized. I would evaluate histone

dynamics in cells infected with these different viruses. With these experiments, I may identify a novel cellular defense mechanisms against a broad group of viruses.

References

1. Bader C, Crumpacker CS, Schnipper LE et al. The natural history of recurrent facial-oral infection with herpes simplex virus. J Infect Dis. 1978;138:897-905.
2. Reeves WC, Corey L, Adams HG, Vontver LA, Holmes KK. Risk of recurrence after first episodes of genital herpes. Relation to HSV type and antibody response. N Engl J Med. 1981;305:315-319.
3. Ribes JA, Steele AD, Seabolt JP, Baker DJ. Six-Year Study of the Incidence of Herpes in Genital and Nongenital Cultures in a Central Kentucky Medical Center Patient Population. Journal of Clinical Microbiology. 2001;39:3321-3325.
4. STERN H, ELEK SD, MILLAR DM, ANDERSON HF. Herpetic whitlow, a form of cross-infection in hospitals. Lancet. 1959;2:871-874.
5. Becker TM, Kodsi R, Bailey P, Lee F, Levandowski R, Nahmias AJ. Grappling with herpes: herpes gladiatorum. Am J Sports Med. 1988;16:665-669.
6. Baringer JR. Recovery of herpes simplex virus from human sacral ganglions. N Engl J Med. 1974;291:828-830.
7. Cook ML, Bastone VB, Stevens JG. Evidence that neurons harbor latent herpes simplex virus. Infect Immun. 1974;9:946-951.
8. Blondeau JM, Aoki FY, Glavin GB. Stress-induced reactivation of latent herpes simplex virus infection in rat lumbar dorsal root ganglia. J Psychosom Res. 1993;37:843-849.
9. Schmidt DD, Zyzanski S, Ellner J, Kumar ML, Arno J. Stress as a precipitating factor in subjects with recurrent herpes labialis. J Fam Pract. 1985;20:359-366.
10. Dawson CR, Togni B. Herpes simplex eye infections: clinical manifestations, pathogenesis and management. Surv Ophthalmol. 1976;21:121-135.
11. Bradshaw MJ, Venkatesan A. Herpes Simplex Virus-1 Encephalitis in Adults: Pathophysiology, Diagnosis, and Management. Neurotherapeutics. 2016;13:493-508.
12. Venkatesan A. Epidemiology and outcomes of acute encephalitis. Curr Opin Neurol. 2015;28:277-282.
13. Zarafonetis CJ, Smadel JE. Fatal Herpes Simplex Encephalitis in Man. Am J Pathol. 1944;20:429-445.
14. Pinninti SG, Kimberlin DW. Neonatal herpes simplex virus infections. Pediatr Clin North Am. 2013;60:351-365.
15. Looker KJ, Magaret AS, May MT et al. Global and Regional Estimates of Prevalent and Incident Herpes Simplex Virus Type 1 Infections in 2012. PLoS One. 2015;10:e0140765.
16. Singh AE, Romanowski B, Wong T et al. Herpes simplex virus seroprevalence and risk factors in 2 Canadian sexually transmitted disease clinics. Sex Transm Dis. 2005;32:95-100.
17. Elion GB, Furman PA, Fyfe JA, de Miranda P, Beauchamp L, Schaeffer HJ. Selectivity of action of an antiherpetic agent, 9-(2-hydroxyethoxymethyl) guanine. Proc Natl Acad Sci U S A. 1977;74:5716-5720.
18. Elion GB. Mechanism of action and selectivity of acyclovir. Am J Med. 1982;73:7-13.

19. Piret J, Boivin G. Resistance of herpes simplex viruses to nucleoside analogues: mechanisms, prevalence, and management. Antimicrob Agents Chemother. 2011;55:459-472.
20. Coen DM, Schaffer PA. Two distinct loci confer resistance to acycloguanosine in herpes simplex virus type 1. Proc Natl Acad Sci U S A. 1980;77:2265-2269.
21. Field HJ, Darby G, Wildy P. Isolation and characterization of acyclovir-resistant mutants of herpes simplex virus. J Gen Virol. 1980;49:115-124.
22. Loret S, Guay G, Lippé R. Comprehensive characterization of extracellular herpes simplex virus type 1 virions. J Virol. 2008;82:8605-8618.
23. Wolfstein A, Nagel CH, Radtke K, Döhner K, Allan VJ, Sodeik B. The inner tegument promotes herpes simplex virus capsid motility along microtubules in vitro. Traffic. 2006;7:227-237.
24. Newcomb WW, Jones LM, Dee A, Chaudhry F, Brown JC. Role of a reducing environment in disassembly of the herpesvirus tegument. Virology. 2012;431:71-79.
25. Gibson W, Roizman B. Proteins specified by herpes simplex virus. 8. Characterization and composition of multiple capsid forms of subtypes 1 and 2. J Virol. 1972;10:1044-1052.
26. Schrag JD, Prasad BV, Rixon FJ, Chiu W. Three-dimensional structure of the HSV1 nucleocapsid. Cell. 1989;56:651-660.
27. Pignatti PF, Cassai E. Analysis of herpes simplex virus nucleoprotein complexes extracted from infected cells. J Virol. 1980;36:816-828.
28. Gibson W, Roizman B. Compartmentalization of spermine and spermidine in the herpes simplex virion. Proc Natl Acad Sci U S A. 1971;68:2818-2821.
29. Mahiet C, Ergani A, Huot N et al. Structural variability of the herpes simplex virus 1 genome in vitro and in vivo. J Virol. 2012;86:8592-8601.
30. Luger K, Mäder AW, Richmond RK, Sargent DF, Richmond TJ. Crystal structure of the nucleosome core particle at 2.8 A resolution. Nature. 1997;389:251-260.
31. Gross DS, Garrard WT. Nuclease hypersensitive sites in chromatin. Annu Rev Biochem. 1988;57:159-197.
32. Zhou J, Fan JY, Rangasamy D, Tremethick DJ. The nucleosome surface regulates chromatin compaction and couples it with transcriptional repression. Nat Struct Mol Biol. 2007;14:1070-1076.
33. International HGSC. Finishing the euchromatic sequence of the human genome. Nature. 2004;431:931-945.
34. Wu RS, Tsai S, Bonner WM. Patterns of histone variant synthesis can distinguish G0 from G1 cells. Cell. 1982;31:367-374.
35. Campos EI, Fillingham J, Li G et al. The program for processing newly synthesized histones H3.1 and H4. Nat Struct Mol Biol. 2010;17:1343-1351.
36. Cook AJ, Gurard-Levin ZA, Vassias I, Almouzni G. A specific function for the histone chaperone NASP to fine-tune a reservoir of soluble H3-H4 in the histone supply chain. Mol Cell. 2011;44:918-927.
37. Agez M, Chen J, Guerois R et al. Structure of the histone chaperone ASF1 bound to the histone H3 C-terminal helix and functional insights. Structure. 2007;15:191-199.
38. Jasencakova Z, Scharf AN, Ask K et al. Replication stress interferes with histone

recycling and predeposition marking of new histones. Mol Cell. 2010;37:736-743.
39. Mello JA, Silljé HH, Roche DM, Kirschner DB, Nigg EA, Almouzni G. Human Asf1 and CAF-1 interact and synergize in a repair-coupled nucleosome assembly pathway. EMBO Rep. 2002;3:329-334.
40. Tagami H, Ray-Gallet D, Almouzni G, Nakatani Y. Histone H3.1 and H3.3 complexes mediate nucleosome assembly pathways dependent or independent of DNA synthesis. Cell. 2004;116:51-61.
41. Shibahara K, Stillman B. Replication-dependent marking of DNA by PCNA facilitates CAF-1-coupled inheritance of chromatin. Cell. 1999;96:575-585.
42. Smith S, Stillman B. Purification and characterization of CAF-I, a human cell factor required for chromatin assembly during DNA replication in vitro. Cell. 1989;58:15-25.
43. Mosammaparast N, Ewart CS, Pemberton LF. A role for nucleosome assembly protein 1 in the nuclear transport of histones H2A and H2B. EMBO J. 2002;21:6527-6538.
44. Lorch Y, LaPointe JW, Kornberg RD. Nucleosomes inhibit the initiation of transcription but allow chain elongation with the displacement of histones. Cell. 1987;49:203-210.
45. Ahmad K, Henikoff S. The histone variant H3.3 marks active chromatin by replication-independent nucleosome assembly. Mol Cell. 2002;9:1191-1200.
46. Daury L, Chailleux C, Bonvallet J, Trouche D. Histone H3.3 deposition at E2F-regulated genes is linked to transcription. EMBO Rep. 2006;7:66-71.
47. Zhang R, Poustovoitov MV, Ye X et al. Formation of MacroH2A-containing senescence-associated heterochromatin foci and senescence driven by ASF1a and HIRA. Dev Cell. 2005;8:19-30.
48. Tang Y, Poustovoitov MV, Zhao K et al. Structure of a human ASF1a-HIRA complex and insights into specificity of histone chaperone complex assembly. Nat Struct Mol Biol. 2006;13:921-929.
49. Straube K, Blackwell JS, Pemberton LF. Nap1 and Chz1 have separate Htz1 nuclear import and assembly functions. Traffic. 2010;11:185-197.
50. Luk E, Vu ND, Patteson K et al. Chz1, a nuclear chaperone for histone H2AZ. Mol Cell. 2007;25:357-368.
51. Mizuguchi G, Shen X, Landry J, Wu WH, Sen S, Wu C. ATP-driven exchange of histone H2AZ variant catalyzed by SWR1 chromatin remodeling complex. Science. 2004;303:343-348.
52. Okuwaki M, Kato K, Shimahara H, Tate S, Nagata K. Assembly and disassembly of nucleosome core particles containing histone variants by human nucleosome assembly protein I. Mol Cell Biol. 2005;25:10639-10651.
53. Heo K, Kim H, Choi SH et al. FACT-mediated exchange of histone variant H2AX regulated by phosphorylation of H2AX and ADP-ribosylation of Spt16. Mol Cell. 2008;30:86-97.
54. Kwon H, Imbalzano AN, Khavari PA, Kingston RE, Green MR. Nucleosome disruption and enhancement of activator binding by a human SW1/SNF complex. Nature. 1994;370:477-481.
55. Cairns BR, Lorch Y, Li Y et al. RSC, an essential, abundant chromatin-

remodeling complex. Cell. 1996;87:1249-1260.
56. Flowers S, Nagl NG, Beck GR, Moran E. Antagonistic roles for BRM and BRG1 SWI/SNF complexes in differentiation. J Biol Chem. 2009;284:10067-10075.
57. Kadam S, Emerson BM. Transcriptional specificity of human SWI/SNF BRG1 and BRM chromatin remodeling complexes. Mol Cell. 2003;11:377-389.
58. Szerlong H, Hinata K, Viswanathan R, Erdjument-Bromage H, Tempst P, Cairns BR. The HSA domain binds nuclear actin-related proteins to regulate chromatin-remodeling ATPases. Nat Struct Mol Biol. 2008;15:469-476.
59. Hassan AH, Awad S, Al-Natour Z, Othman S, Mustafa F, Rizvi TA. Selective recognition of acetylated histones by bromodomains in transcriptional co-activators. Biochem J. 2007;402:125-133.
60. Shen W, Xu C, Huang W et al. Solution structure of human Brg1 bromodomain and its specific binding to acetylated histone tails. Biochemistry. 2007;46:2100-2110.
61. Kasten M, Szerlong H, Erdjument-Bromage H, Tempst P, Werner M, Cairns BR. Tandem bromodomains in the chromatin remodeler RSC recognize acetylated histone H3 Lys14. EMBO J. 2004;23:1348-1359.
62. Carey M, Li B, Workman JL. RSC exploits histone acetylation to abrogate the nucleosomal block to RNA polymerase II elongation. Mol Cell. 2006;24:481-487.
63. Dechassa ML, Sabri A, Pondugula S et al. SWI/SNF has intrinsic nucleosome disassembly activity that is dependent on adjacent nucleosomes. Mol Cell. 2010;38:590-602.
64. Kassabov SR, Zhang B, Persinger J, Bartholomew B. SWI/SNF unwraps, slides, and rewraps the nucleosome. Mol Cell. 2003;11:391-403.
65. Gao H, Lukin K, Ramírez J, Fields S, Lopez D, Hagman J. Opposing effects of SWI/SNF and Mi-2/NuRD chromatin remodeling complexes on epigenetic reprogramming by EBF and Pax5. Proc Natl Acad Sci U S A. 2009;106:11258-11263.
66. Musselman CA, Mansfield RE, Garske AL et al. Binding of the CHD4 PHD2 finger to histone H3 is modulated by covalent modifications. Biochem J. 2009;423:179-187.
67. Mansfield RE, Musselman CA, Kwan AH et al. Plant homeodomain (PHD) fingers of CHD4 are histone H3-binding modules with preference for unmodified H3K4 and methylated H3K9. J Biol Chem. 2011;286:11779-11791.
68. Ramírez J, Dege C, Kutateladze TG, Hagman J. MBD2 and multiple domains of CHD4 are required for transcriptional repression by Mi-2/NuRD complexes. Mol Cell Biol. 2012;32:5078-5088.
69. Wang HB, Zhang Y. Mi2, an auto-antigen for dermatomyositis, is an ATP-dependent nucleosome remodeling factor. Nucleic Acids Res. 2001;29:2517-2521.
70. Xie W, Ling T, Zhou Y et al. The chromatin remodeling complex NuRD establishes the poised state of rRNA genes characterized by bivalent histone modifications and altered nucleosome positions. Proc Natl Acad Sci U S A. 2012;109:8161-8166.
71. Zhao Z, Dammert MA, Grummt I, Bierhoff H. lncRNA-Induced Nucleosome

Repositioning Reinforces Transcriptional Repression of rRNA Genes upon Hypotonic Stress. Cell Rep. 2016;14:1876-1882.
72. Grüne T, Brzeski J, Eberharter A et al. Crystal structure and functional analysis of a nucleosome recognition module of the remodeling factor ISWI. Mol Cell. 2003;12:449-460.
73. Wiechens N, Singh V, Gkikopoulos T, Schofield P, Rocha S, Owen-Hughes T. The Chromatin Remodelling Enzymes SNF2H and SNF2L Position Nucleosomes adjacent to CTCF and Other Transcription Factors. PLoS Genet. 2016;12:e1005940.
74. Chen L, Cai Y, Jin J et al. Subunit organization of the human INO80 chromatin remodeling complex: an evolutionarily conserved core complex catalyzes ATP-dependent nucleosome remodeling. J Biol Chem. 2011;286:11283-11289.
75. Lever MA, Th'ng JP, Sun X, Hendzel MJ. Rapid exchange of histone H1.1 on chromatin in living human cells. Nature. 2000;408:873-876.
76. Misteli T, Gunjan A, Hock R, Bustin M, Brown DT. Dynamic binding of histone H1 to chromatin in living cells. Nature. 2000;408:877-881.
77. Carrero G, McDonald D, Crawford E, de Vries G, Hendzel MJ. Using FRAP and mathematical modeling to determine the in vivo kinetics of nuclear proteins. Methods. 2003;29:14-28.
78. Kimura H. Histone dynamics in living cells revealed by photobleaching. DNA Repair (Amst). 2005;4:939-950.
79. Th'ng JP, Sung R, Ye M, Hendzel MJ. H1 family histones in the nucleus. Control of binding and localization by the C-terminal domain. J Biol Chem. 2005;280:27809-27814.
80. Kimura H, Cook PR. Kinetics of core histones in living human cells: little exchange of H3 and H4 and some rapid exchange of H2B. J Cell Biol. 2001;153:1341-1353.
81. Siino JS, Nazarov IB, Svetlova MP et al. Photobleaching of GFP-labeled H2AX in chromatin: H2AX has low diffusional mobility in the nucleus. Biochem Biophys Res Commun. 2002;297:1318-1323.
82. Conn KL, Hendzel MJ, Schang LM. Core histones H2B and H4 are mobilized during infection with herpes simplex virus 1. J Virol. 2011;85:13234-13252.
83. Belotserkovskaya R, Oh S, Bondarenko VA, Orphanides G, Studitsky VM, Reinberg D. FACT facilitates transcription-dependent nucleosome alteration. Science. 2003;301:1090-1093.
84. Park YJ, Chodaparambil JV, Bao Y, McBryant SJ, Luger K. Nucleosome assembly protein 1 exchanges histone H2A-H2B dimers and assists nucleosome sliding. J Biol Chem. 2005;280:1817-1825.
85. Campoy FJ, Meehan RR, McKay S, Nixon J, Bird A. Binding of Histone H1 to DNA Is Indifferent to Methylation at CpG Sequences. Journal of Biological Chemistry. 1995;270:26473-26481.
86. Nightingale K, Wolffe AP. Methylation at CpG sequences does not influence histone H1 binding to a nucleosome including a Xenopus borealis 5 S rRNA gene. J Biol Chem. 1995;270:4197-4200.
87. Gilbert N, Thomson I, Boyle S, Allan J, Ramsahoye B, Bickmore WA. DNA methylation affects nuclear organization, histone modifications, and linker

histone binding but not chromatin compaction. J Cell Biol. 2007;177:401-411.
88. Trendelenburg MF, McKinnell RG. Transcriptionally active and inactive regions of nucleolar chromatin in amplified nucleoli of fully grown oocytes of hibernating frogs, Rana pipiens (Amphibia, Anura). A quantitative electron microscopic study. Differentiation. 1979;15:73-95.
89. MAGGIO R, SIEKEVITZ P, PALADE GE. STUDIES ON ISOLATED NUCLEI. II. ISOLATION AND CHEMICAL CHARACTERIZATION OF NUCLEOLAR AND NUCLEOPLASMIC SUBFRACTIONS. J Cell Biol. 1963;18:293-312.
90. Merriam RW, Koch WE. The Relative Concentration of Solids in the Nucleolus, Nucleus, and Cytoplasm of the Developing Nerve Cell of the Chick. J Biophys Biochem Cytol. 1960;7:151-160.
91. Thompson WF, Flavell RB. DNase I sensitivity of ribosomal RNA genes in chromatin and nucleolar dominance in wheat. J Mol Biol. 1988;204:535-548.
92. Conconi A, Widmer RM, Koller T, Sogo JM. Two different chromatin structures coexist in ribosomal RNA genes throughout the cell cycle. Cell. 1989;57:753-761.
93. Jones HS, Kawauchi J, Braglia P, Alen CM, Kent NA, Proudfoot NJ. RNA polymerase I in yeast transcribes dynamic nucleosomal rDNA. Nat Struct Mol Biol. 2007;14:123-130.
94. Santoro R, Li J, Grummt I. The nucleolar remodeling complex NoRC mediates heterochromatin formation and silencing of ribosomal gene transcription. Nat Genet. 2002;32:393-396.
95. Rickards B, Flint SJ, Cole MD, LeRoy G. Nucleolin is required for RNA polymerase I transcription in vivo. Mol Cell Biol. 2007;27:937-948.
96. Iwasaki W, Miya Y, Horikoshi N et al. Contribution of histone N-terminal tails to the structure and stability of nucleosomes. FEBS Open Bio. 2013;3:363-369.
97. Li A, Yu Y, Lee SC, Ishibashi T, Lees-Miller SP, Ausió J. Phosphorylation of histone H2A.X by DNA-dependent protein kinase is not affected by core histone acetylation, but it alters nucleosome stability and histone H1 binding. J Biol Chem. 2010;285:17778-17788.
98. Stucki M, Clapperton JA, Mohammad D, Yaffe MB, Smerdon SJ, Jackson SP. MDC1 directly binds phosphorylated histone H2AX to regulate cellular responses to DNA double-strand breaks. Cell. 2005;123:1213-1226.
99. Gansen A, Hieb AR, Böhm V, Tóth K, Langowski J. Closing the gap between single molecule and bulk FRET analysis of nucleosomes. PLoS One. 2013;8:e57018.
100. Di Cerbo V, Mohn, F, Ryan, DP, et al. Acetylation of histone H3 at lysine 64 regulates nucleosome dynamics and facilitates transcription
. eLIFE. 2014;e01632
101. Chen J, Ghazawi FM, Li Q. Interplay of bromodomain and histone acetylation in the regulation of p300-dependent genes. Epigenetics. 2014;5:509-515.
102. Duan MR, Smerdon MJ. Histone H3 lysine 14 (H3K14) acetylation facilitates DNA repair in a positioned nucleosome by stabilizing the binding of the chromatin Remodeler RSC (Remodels Structure of Chromatin). J Biol Chem. 2014;289:8353-8363.
103. Berger SL. Histone modifications in transcriptional regulation. Curr Opin Genet

Dev. 2002;12:142-148.
104. Bode J, Henco K, Wingender E. Modulation of the nucleosome structure by histone acetylation. Eur J Biochem. 1980;110:143-152.
105. Hebbes TR, Clayton AL, Thorne AW, Crane-Robinson C. Core histone hyperacetylation co-maps with generalized DNase I sensitivity in the chicken beta-globin chromosomal domain. EMBO J. 1994;13:1823-1830.
106. Krajewski WA, Becker PB. Reconstitution of hyperacetylated, DNase I-sensitive chromatin characterized by high conformational flexibility of nucleosomal DNA. Proc Natl Acad Sci U S A. 1998;95:1540-1545.
107. Garcia-Ramirez M, Rocchini C, Ausio J. Modulation of chromatin folding by histone acetylation. J Biol Chem. 1995;270:17923-17928.
108. Tse C, Sera T, Wolffe AP, Hansen JC. Disruption of higher-order folding by core histone acetylation dramatically enhances transcription of nucleosomal arrays by RNA polymerase III. Mol Cell Biol. 1998;18:4629-4638.
109. Wang X, Hayes JJ. Acetylation mimics within individual core histone tail domains indicate distinct roles in regulating the stability of higher-order chromatin structure. Mol Cell Biol. 2008;28:227-236.
110. Dobson ME, Ingram VM. In vitro transcription of chromatin containing histones hyperacetylated in vivo. Nucleic Acids Res. 1980;8:4201-4219.
111. Hebbes TR, Thorne AW, Crane-Robinson C. A direct link between core histone acetylation and transcriptionally active chromatin. EMBO J. 1988;7:1395-1402.
112. Tjeertes JV, Miller KM, Jackson SP. Screen for DNA-damage-responsive histone modifications identifies H3K9Ac and H3K56Ac in human cells. EMBO J. 2009;28:1878-1889.
113. Kim J, Lee J, Lee TH. Lysine Acetylation Facilitates Spontaneous DNA Dynamics in the Nucleosome. J Phys Chem B. 2015;119:15001-15005.
114. Wang Y, Kallgren SP, Reddy BD et al. Histone H3 lysine 14 acetylation is required for activation of a DNA damage checkpoint in fission yeast. J Biol Chem. 2012;287:4386-4393.
115. Wang H, Huang ZQ, Xia L et al. Methylation of histone H4 at arginine 3 facilitating transcriptional activation by nuclear hormone receptor. Science. 2001;293:853-857.
116. Huang S, Litt M, Felsenfeld G. Methylation of histone H4 by arginine methyltransferase PRMT1 is essential in vivo for many subsequent histone modifications. Genes Dev. 2005;19:1885-1893.
117. Hyllus D, Stein C, Schnabel K et al. PRMT6-mediated methylation of R2 in histone H3 antagonizes H3 K4 trimethylation. Genes Dev. 2007;21:3369-3380.
118. Feng Q, Wang H, Ng HH et al. Methylation of H3-lysine 79 is mediated by a new family of HMTases without a SET domain. Curr Biol. 2002;12:1052-1058.
119. Jones B, Su H, Bhat A et al. The histone H3K79 methyltransferase Dot1L is essential for mammalian development and heterochromatin structure. PLoS Genet. 2008;4:e1000190.
120. Ng HH, Ciccone DN, Morshead KB, Oettinger MA, Struhl K. Lysine-79 of histone H3 is hypomethylated at silenced loci in yeast and mammalian cells: a potential mechanism for position-effect variegation. Proc Natl Acad Sci U S A. 2003;100:1820-1825.

121. Santos-Rosa H, Schneider R, Bannister AJ et al. Active genes are tri-methylated at K4 of histone H3. Nature. 2002;419:407-411.
122. Bernstein BE, Humphrey EL, Erlich RL et al. Methylation of histone H3 Lys 4 in coding regions of active genes. Proc Natl Acad Sci U S A. 2002;99:8695-8700.
123. Rea S, Eisenhaber F, O'Carroll D et al. Regulation of chromatin structure by site-specific histone H3 methyltransferases. Nature. 2000;406:593-599.
124. Lachner M, O'Carroll D, Rea S, Mechtler K, Jenuwein T. Methylation of histone H3 lysine 9 creates a binding site for HP1 proteins. Nature. 2001;410:116-120.
125. Shi Y, Lan F, Matson C et al. Histone demethylation mediated by the nuclear amine oxidase homolog LSD1. Cell. 2004;119:941-953.
126. Tsukada Y, Fang J, Erdjument-Bromage H et al. Histone demethylation by a family of JmjC domain-containing proteins. Nature. 2006;439:811-816.
127. Whetstine JR, Nottke A, Lan F et al. Reversal of histone lysine trimethylation by the JMJD2 family of histone demethylases. Cell. 2006;125:467-481.
128. Cloos PA, Christensen J, Agger K et al. The putative oncogene GASC1 demethylates tri- and dimethylated lysine 9 on histone H3. Nature. 2006;442:307-311.
129. Kysela B, Chovanec M, Jeggo PA. Phosphorylation of linker histones by DNA-dependent protein kinase is required for DNA ligase IV-dependent ligation in the presence of histone H1. Proc Natl Acad Sci U S A. 2005;102:1877-1882.
130. Contreras A, Hale TK, Stenoien DL, Rosen JM, Mancini MA, Herrera RE. The Dynamic Mobility of Histone H1 Is Regulated by Cyclin/CDK Phosphorylation. Molecular and Cellular Biology. 2003;23:8626-8636.
131. Rogakou EP, Pilch DR, Orr AH, Ivanova VS, Bonner WM. DNA Double-stranded Breaks Induce Histone H2AX Phosphorylation on Serine 139. Journal of Biological Chemistry. 1998;273:5858-5868.
132. Lo WS, Trievel RC, Rojas JR et al. Phosphorylation of serine 10 in histone H3 is functionally linked in vitro and in vivo to Gcn5-mediated acetylation at lysine 14. Mol Cell. 2000;5:917-926.
133. Lau PN, Cheung P. Histone code pathway involving H3 S28 phosphorylation and K27 acetylation activates transcription and antagonizes polycomb silencing. Proc Natl Acad Sci U S A. 2011;108:2801-2806.
134. Hans F, Dimitrov S. Histone H3 phosphorylation and cell division. Oncogene. 2001;20:3021-3027.
135. Hendzel MJ, Wei Y, Mancini MA et al. Mitosis-specific phosphorylation of histone H3 initiates primarily within pericentromeric heterochromatin during G2 and spreads in an ordered fashion coincident with mitotic chromosome condensation. Chromosoma. 1997;106:348-360.
136. Nickel BE, Allis CD, Davie JR. Ubiquitinated histone H2B is preferentially located in transcriptionally active chromatin. Biochemistry. 1989;28:958-963.
137. Parlow MH, Haas AL, Lough J. Enrichment of ubiquitinated histone H2A in a low salt extract of micrococcal nuclease-digested myotube nuclei. J Biol Chem. 1990;265:7507-7512.
138. Dawson BA, Herman T, Haas AL, Lough J. Affinity isolation of active murine erythroleukemia cell chromatin: uniform distribution of ubiquitinated histone H2A between active and inactive fractions. J Cell Biochem. 1991;46:166-173.

139. Li W, Nagaraja S, Delcuve GP, Hendzel MJ, Davie JR. Effects of histone acetylation, ubiquitination and variants on nucleosome stability. Biochem J. 1993;296:737-744.
140. Chandrasekharan MB, Huang F, Sun ZW. Ubiquitination of histone H2B regulates chromatin dynamics by enhancing nucleosome stability. Proc Natl Acad Sci U S A. 2009;106:16686-16691.
141. Machida S, Sekine S, Nishiyama Y, Horikoshi N, Kurumizaka H. Structural and biochemical analyses of monoubiquitinated human histones H2B and H4. Open Biol. 2016;6
142. Niikura Y, Kitagawa R, Ogi H, Abdulle R, Pagala V, Kitagawa K. CENP-A K124 Ubiquitylation Is Required for CENP-A Deposition at the Centromere. Dev Cell. 2015;32:589-603.
143. Wang H, Zhai L, Xu J et al. Histone H3 and H4 ubiquitylation by the CUL4-DDB-ROC1 ubiquitin ligase facilitates cellular response to DNA damage. Mol Cell. 2006;22:383-394.
144. Jang CW, Shibata Y, Starmer J, Yee D, Magnuson T. Histone H3.3 maintains genome integrity during mammalian development. Genes Dev. 2015;29:1377-1392.
145. Galvani A, Courbeyrette R, Agez M, Ochsenbein F, Mann C, Thuret JY. In vivo study of the nucleosome assembly functions of ASF1 histone chaperones in human cells. Mol Cell Biol. 2008;28:3672-3685.
146. Lewis PW, Elsaesser SJ, Noh KM, Stadler SC, Allis CD. Daxx is an H3.3-specific histone chaperone and cooperates with ATRX in replication-independent chromatin assembly at telomeres. Proc Natl Acad Sci U S A. 2010;107:14075-14080.
147. Drané P, Ouararhni K, Depaux A, Shuaib M, Hamiche A. The death-associated protein DAXX is a novel histone chaperone involved in the replication-independent deposition of H3.3. Genes Dev. 2010;24:1253-1265.
148. McKittrick E, Gafken PR, Ahmad K, Henikoff S. Histone H3.3 is enriched in covalent modifications associated with active chromatin. Proc Natl Acad Sci U S A. 2004;101:1525-1530.
149. Udugama M, M Chang FT, Chan FL et al. Histone variant H3.3 provides the heterochromatic H3 lysine 9 tri-methylation mark at telomeres. Nucleic Acids Res. 2015;43:10227-10237.
150. Kraushaar DC, Jin W, Maunakea A, Abraham B, Ha M, Zhao K. Genome-wide incorporation dynamics reveal distinct categories of turnover for the histone variant H3.3. Genome Biol. 2013;14:R121.
151. Jin C, Felsenfeld G. Nucleosome stability mediated by histone variants H3.3 and H2A.Z. Genes Dev. 2007;21:1519-1529.
152. Sullivan KF, Hechenberger M, Masri K. Human CENP-A contains a histone H3 related histone fold domain that is required for targeting to the centromere. J Cell Biol. 1994;127:581-592.
153. Earnshaw WC, Rothfield N. Identification of a family of human centromere proteins using autoimmune sera from patients with scleroderma. Chromosoma. 1985;91:313-321.
154. Palmer DK, O'Day K, Wener MH, Andrews BS, Margolis RL. A 17-kD centromere

protein (CENP-A) copurifies with nucleosome core particles and with histones. J Cell Biol. 1987;104:805-815.
155. Howman EV, Fowler KJ, Newson AJ et al. Early disruption of centromeric chromatin organization in centromere protein A (Cenpa) null mice. Proc Natl Acad Sci U S A. 2000;97:1148-1153.
156. Dunleavy EM, Roche D, Tagami H et al. HJURP is a cell-cycle-dependent maintenance and deposition factor of CENP-A at centromeres. Cell. 2009;137:485-497.
157. Bassett EA, DeNizio J, Barnhart-Dailey MC et al. HJURP uses distinct CENP-A surfaces to recognize and to stabilize CENP-A/histone H4 for centromere assembly. Dev Cell. 2012;22:749-762.
158. Hasson D, Panchenko T, Salimian KJ et al. The octamer is the major form of CENP-A nucleosomes at human centromeres. Nat Struct Mol Biol. 2013;20:687-695.
159. Dimitriadis EK, Weber C, Gill RK, Diekmann S, Dalal Y. Tetrameric organization of vertebrate centromeric nucleosomes. Proc Natl Acad Sci U S A. 2010;107:20317-20322.
160. Black BE, Brock MA, Bédard S, Woods VL, Cleveland DW. An epigenetic mark generated by the incorporation of CENP-A into centromeric nucleosomes. Proc Natl Acad Sci U S A. 2007;104:5008-5013.
161. Arimura Y, Shirayama K, Horikoshi N et al. Crystal structure and stable property of the cancer-associated heterotypic nucleosome containing CENP-A and H3.3. Sci Rep. 2014;4:7115.
162. Tachiwana H, Kagawa W, Shiga T et al. Crystal structure of the human centromeric nucleosome containing CENP-A. Nature. 2011;476:232-235.
163. Roulland Y, Ouararhni K, Naidenov M et al. The Flexible Ends of CENP-A Nucleosome Are Required for Mitotic Fidelity. Mol Cell. 2016;63:674-685.
164. Mannironi C, Bonner WM, Hatch CL. H2A.X. a histone isoprotein with a conserved C-terminal sequence, is encoded by a novel mRNA with both DNA replication type and polyA 3' processing signals. Nucleic Acids Res. 1989;17:9113-9126.
165. Celeste A, Petersen S, Romanienko PJ et al. Genomic instability in mice lacking histone H2AX. Science. 2002;296:922-927.
166. Burma S, Chen BP, Murphy M, Kurimasa A, Chen DJ. ATM phosphorylates histone H2AX in response to DNA double-strand breaks. J Biol Chem. 2001;276:42462-42467.
167. Stiff T, O'Driscoll M, Rief N, Iwabuchi K, Löbrich M, Jeggo PA. ATM and DNA-PK function redundantly to phosphorylate H2AX after exposure to ionizing radiation. Cancer Res. 2004;64:2390-2396.
168. Pehrson, Fried V. MacroH2A, a core histone containing a large nonhistone region. Science. 1992;257:1398-1400.
169. Costanzi C, Pehrson JR. MACROH2A2, a new member of the MARCOH2A core histone family. J Biol Chem. 2001;276:21776-21784.
170. Rasmussen TP, Huang T, Mastrangelo MA, Loring J, Panning B, Jaenisch R. Messenger RNAs encoding mouse histone macroH2A1 isoforms are expressed at similar levels in male and female cells and result from alternative splicing.

Nucleic Acids Res. 1999;27:3685-3689.
171. Costanzi C, Pehrson JR. Histone macroH2A1 is concentrated in the inactive X chromosome of female mammals. Nature. 1998;393:599-601.
172. Chadwick BP, Valley CM, Willard HF. Histone variant macroH2A contains two distinct macrochromatin domains capable of directing macroH2A to the inactive X chromosome. Nucleic Acids Res. 2001;29:2699-2705.
173. Pehrson JR, Changolkar LN, Costanzi C, Leu NA. Mice without macroH2A histone variants. Mol Cell Biol. 2014;34:4523-4533.
174. Chakravarthy S, Gundimella SK, Caron C et al. Structural characterization of the histone variant macroH2A. Mol Cell Biol. 2005;25:7616-7624.
175. Chakravarthy S, Luger K. The Histone Variant Macro-H2A Preferentially Forms "Hybrid Nucleosomes". Journal of Biological Chemistry. 2006;281:25522-25531.
176. Bowerman S, Wereszczynski J. Effects of MacroH2A and H2A.Z on Nucleosome Dynamics as Elucidated by Molecular Dynamics Simulations. Biophys J. 2016;110:327-337.
177. Tolstorukov MY, Goldman JA, Gilbert C, Ogryzko V, Kingston RE, Park PJ. Histone variant H2A.Bbd is associated with active transcription and mRNA processing in human cells. Mol Cell. 2012;47:596-607.
178. Doyen CM, An W, Angelov D et al. Mechanism of polymerase II transcription repression by the histone variant macroH2A. Mol Cell Biol. 2006;26:1156-1164.
179. Hatch CL, Bonner WM. Sequence of cDNAs for mammalian H2A.Z, an evolutionarily diverged but highly conserved basal histone H2A isoprotein species. Nucleic Acids Res. 1988;16:1113-1124.
180. Hatch CL, Bonner WM. The human histone H2A.Z gene. Sequence and regulation. J Biol Chem. 1990;265:15211-15218.
181. van Daal A, Elgin SC. A histone variant, H2AvD, is essential in Drosophila melanogaster. Mol Biol Cell. 1992;3:593-602.
182. Faast R, Thonglairoam V, Schulz TC et al. Histone variant H2A.Z is required for early mammalian development. Curr Biol. 2001;11:1183-1187.
183. Raisner RM, Hartley PD, Meneghini MD et al. Histone variant H2A.Z marks the 5' ends of both active and inactive genes in euchromatin. Cell. 2005;123:233-248.
184. Zhang H, Roberts DN, Cairns BR. Genome-wide dynamics of Htz1, a histone H2A variant that poises repressed/basal promoters for activation through histone loss. Cell. 2005;123:219-231.
185. Kobor MS, Venkatasubrahmanyam S, Meneghini MD et al. A protein complex containing the conserved Swi2/Snf2-related ATPase Swr1p deposits histone variant H2A.Z into euchromatin. PLoS Biol. 2004;2:E131.
186. Papamichos-Chronakis M, Watanabe S, Rando OJ, Peterson CL. Global regulation of H2A.Z localization by the INO80 chromatin-remodeling enzyme is essential for genome integrity. Cell. 2011;144:200-213.
187. Placek BJ, Harrison LN, Villers BM, Gloss LM. The H2A.Z/H2B dimer is unstable compared to the dimer containing the major H2A isoform. Protein Sci. 2005;14:514-522.

188. Suto RK, Clarkson MJ, Tremethick DJ, Luger K. Crystal structure of a nucleosome core particle containing the variant histone H2A.Z. Nat Struct Biol. 2000;7:1121-1124.
189. Chadwick BP, Willard HF. A novel chromatin protein, distantly related to histone H2A, is largely excluded from the inactive X chromosome. J Cell Biol. 2001;152:375-384.
190. Gautier T, Abbott DW, Molla A, Verdel A, Ausio J, Dimitrov S. Histone variant H2ABbd confers lower stability to the nucleosome. EMBO Rep. 2004;5:715-720.
191. Eirín-López JM, Ishibashi T, Ausió J. H2A.Bbd: a quickly evolving hypervariable mammalian histone that destabilizes nucleosomes in an acetylation-independent way. FASEB J. 2008;22:316-326.
192. Bao Y, Konesky K, Park YJ et al. Nucleosomes containing the histone variant H2A.Bbd organize only 118 base pairs of DNA. EMBO J. 2004;23:3314-3324.
193. Doyen CM, Montel F, Gautier T et al. Dissection of the unusual structural and functional properties of the variant H2A.Bbd nucleosome. EMBO J. 2006;25:4234-4244.
194. Shukla MS, Syed SH, Goutte-Gattat D et al. The docking domain of histone H2A is required for H1 binding and RSC-mediated nucleosome remodeling. Nucleic Acids Res. 2011;39:2559-2570.
195. Shaw ML, Williams EJ, Hawes S, Saffery R. Characterisation of histone variant distribution in human embryonic stem cells by transfection of in vitro transcribed mRNA. Mol Reprod Dev. 2009;76:1128-1142.
196. Yang C, Bolotin E, Jiang T, Sladek FM, Martinez E. Prevalence of the initiator over the TATA box in human and yeast genes and identification of DNA motifs enriched in human TATA-less core promoters. Gene. 2007;389:52-65.
197. Lagrange T, Kapanidis AN, Tang H, Reinberg D, Ebright RH. New core promoter element in RNA polymerase II-dependent transcription: sequence-specific DNA binding by transcription factor IIB. Genes Dev. 1998;12:34-44.
198. Burke TW, Kadonaga JT. Drosophila TFIID binds to a conserved downstream basal promoter element that is present in many TATA-box-deficient promoters. Genes & Development. 1996;10:711-724.
199. Burke TW, Kadonaga JT. The downstream core promoter element, DPE, is conserved from Drosophila to humans and is recognized by TAFII60 of Drosophila. Genes Dev. 1997;11:3020-3031.
200. Gershenzon NI, Ioshikhes IP. Synergy of human Pol II core promoter elements revealed by statistical sequence analysis. Bioinformatics. 2005;21:1295-1300.
201. Price DH, Sluder AE, Greenleaf AL. Dynamic interaction between a Drosophila transcription factor and RNA polymerase II. Mol Cell Biol. 1989;9:1465-1475.
202. Robert F, Douziech M, Forget D et al. Wrapping of promoter DNA around the RNA polymerase II initiation complex induced by TFIIF. Mol Cell. 1998;2:341-351.
203. Sopta M, Carthew RW, Greenblatt J. Isolation of three proteins that bind to mammalian RNA polymerase II. J Biol Chem. 1985;260:10353-10360.
204. Flores O, Lu H, Killeen M, Greenblatt J, Burton ZF, Reinberg D. The small subunit of transcription factor IIF recruits RNA polymerase II into the

preinitiation complex. Proc Natl Acad Sci U S A. 1991;88:9999-10003.
205. Mittler G, Kremmer E, Timmers HT, Meisterernst M. Novel critical role of a human Mediator complex for basal RNA polymerase II transcription. EMBO Rep. 2001;2:808-813.
206. Baek HJ, Malik S, Qin J, Roeder RG. Requirement of TRAP/Mediator for Both Activator-Independent and Activator-Dependent Transcription in Conjunction with TFIID-Associated TAFIIs. Molecular and Cellular Biology. 2002;22:2842-2852.
207. Chen XF, Lehmann L, Lin JJ et al. Mediator and SAGA have distinct roles in Pol II preinitiation complex assembly and function. Cell Rep. 2012;2:1061-1067.
208. Johnson KM, Wang J, Smallwood A, Arayata C, Carey M. TFIID and human mediator coactivator complexes assemble cooperatively on promoter DNA. Genes Dev. 2002;16:1852-1863.
209. Johnson KM, Carey M. Assembly of a Mediator/TFIID/TFIIA Complex Bypasses the Need for an Activator. Current Biology. 2003;13:772-777.
210. Plaschka C, Larivière L, Wenzeck L et al. Architecture of the RNA polymerase II-Mediator core initiation complex. Nature. 2015;518:376-380.
211. Holstege FC, van der Vliet PC, Timmers HT. Opening of an RNA polymerase II promoter occurs in two distinct steps and requires the basal transcription factors IIE and IIH. EMBO J. 1996;15:1666-1677.
212. Schultz P, Fribourg S, Poterszman A, Mallouh V, Moras D, Egly JM. Molecular structure of human TFIIH. Cell. 2000;102:599-607.
213. Moreland RJ, Tirode F, Yan Q, Conaway JW, Egly J-M, Conaway RC. A Role for the TFIIH XPB DNA Helicase in Promoter Escape by RNA Polymerase II. Journal of Biological Chemistry. 1999;274:22127-22130.
214. Rossignol M, Kolb-Cheynel I, Egly JM. Substrate specificity of the cdk-activating kinase (CAK) is altered upon association with TFIIH. EMBO J. 1997;16:1628-1637.
215. Wong KH, Jin Y, Struhl K. TFIIH phosphorylation of the Pol II CTD stimulates mediator dissociation from the preinitiation complex and promoter escape. Mol Cell. 2014;54:601-612.
216. Zawel L, Kumar KP, Reinberg D. Recycling of the general transcription factors during RNA polymerase II transcription. Genes & Development. 1995;9:1479-1490.
217. Komarnitsky P. Different phosphorylated forms of RNA polymerase II and associated mRNA processing factors during transcription. Genes & Development. 2000;14:2452-2460.
218. Kim YK, Bourgeois CF, Isel C, Churcher MJ, Karn J. Phosphorylation of the RNA Polymerase II Carboxyl-Terminal Domain by CDK9 Is Directly Responsible for Human Immunodeficiency Virus Type 1 Tat-Activated Transcriptional Elongation. Molecular and Cellular Biology. 2002;22:4622-4637.
219. McCracken S, Fong N, Yankulov K et al. The C-terminal domain of RNA polymerase II couples mRNA processing to transcription. Nature. 1997;385:357-361.
220. Murthy KG, Manley JL. The 160-kD subunit of human cleavage-polyadenylation specificity factor coordinates pre-mRNA 3'-end formation. Genes &

Development. 1995;9:2672-2683.
221. MacDonald CC, Wilusz J, Shenk T. The 64-kilodalton subunit of the CstF polyadenylation factor binds to pre-mRNAs downstream of the cleavage site and influences cleavage site location. Mol Cell Biol. 1994;14:6647-6654.
222. RYAN K. Evidence that polyadenylation factor CPSF-73 is the mRNA 3' processing endonuclease. RNA. 2004;10:565-573.
223. Wahle E. Purification and characterization of a mammalian polyadenylate polymerase involved in the 3' end processing of messenger RNA precursors. J Biol Chem. 1991;266:3131-3139.
224. West S, Gromak N, Proudfoot NJ. Human 5' --> 3' exonuclease Xrn2 promotes transcription termination at co-transcriptional cleavage sites. Nature. 2004;432:522-525.
225. Knezetic JA, Luse DS. The presence of nucleosomes on a DNA template prevents initiation by RNA polymerase II in vitro. Cell. 1986;45:95-104.
226. Kireeva ML, Walter W, Tchernajenko V, Bondarenko V, Kashlev M, Studitsky VM. Nucleosome remodeling induced by RNA polymerase II: loss of the H2A/H2B dimer during transcription. Mol Cell. 2002;9:541-552.
227. Kireeva ML, Hancock B, Cremona GH, Walter W, Studitsky VM, Kashlev M. Nature of the nucleosomal barrier to RNA polymerase II. Mol Cell. 2005;18:97-108.
228. Guermah M, Palhan VB, Tackett AJ, Chait BT, Roeder RG. Synergistic functions of SII and p300 in productive activator-dependent transcription of chromatin templates. Cell. 2006;125:275-286.
229. Orphanides G, LeRoy G, Chang CH, Luse DS, Reinberg D. FACT, a factor that facilitates transcript elongation through nucleosomes. Cell. 1998;92:105-116.
230. Bell AC, West AG, Felsenfeld G. The protein CTCF is required for the enhancer blocking activity of vertebrate insulators. Cell. 1999;98:387-396.
231. Renda M, Baglivo I, Burgess-Beusse B et al. Critical DNA binding interactions of the insulator protein CTCF: a small number of zinc fingers mediate strong binding, and a single finger-DNA interaction controls binding at imprinted loci. J Biol Chem. 2007;282:33336-33345.
232. Mukhopadhyay R, Yu W, Whitehead J et al. The binding sites for the chromatin insulator protein CTCF map to DNA methylation-free domains genome-wide. Genome Res. 2004;14:1594-1602.
233. Lutz M, Burke LJ, Barreto G et al. Transcriptional repression by the insulator protein CTCF involves histone deacetylases. Nucleic Acids Res. 2000;28:1707-1713.
234. Ding H, Rimsky S, Batson S, Bustin M, Hansen U. Stimulation of RNA polymerase II elongation by chromosomal protein HMG-14. Science. 1994;265:796-799.
235. Paranjape SM, Krumm A, Kadonaga JT. HMG17 is a chromatin-specific transcriptional coactivator that increases the efficiency of transcription initiation. Genes & Development. 1995;9:1978-1991.
236. Herold BC, WuDunn D, Soltys N, Spear PG. Glycoprotein C of herpes simplex virus type 1 plays a principal role in the adsorption of virus to cells and in infectivity. J Virol. 1991;65:1090-1098.

237. Rux AH, Lou H, Lambris JD, Friedman HM, Eisenberg RJ, Cohen GH. Kinetic analysis of glycoprotein C of herpes simplex virus types 1 and 2 binding to heparin, heparan sulfate, and complement component C3b. Virology. 2002;294:324-332.
238. Whitbeck JC, Peng C, Lou H et al. Glycoprotein D of herpes simplex virus (HSV) binds directly to HVEM, a member of the tumor necrosis factor receptor superfamily and a mediator of HSV entry. J Virol. 1997;71:6083-6093.
239. Krummenacher C, Rux AH, Whitbeck JC et al. The first immunoglobulin-like domain of HveC is sufficient to bind herpes simplex virus gD with full affinity, while the third domain is involved in oligomerization of HveC. J Virol. 1999;73:8127-8137.
240. Shukla D, Liu J, Blaiklock P et al. A novel role for 3-O-sulfated heparan sulfate in herpes simplex virus 1 entry. Cell. 1999;99:13-22.
241. Karaba AH, Kopp SJ, Longnecker R. Herpesvirus entry mediator and nectin-1 mediate herpes simplex virus 1 infection of the murine cornea. J Virol. 2011;85:10041-10047.
242. Krummenacher C, Supekar VM, Whitbeck JC et al. Structure of unliganded HSV gD reveals a mechanism for receptor-mediated activation of virus entry. EMBO J. 2005;24:4144-4153.
243. Atanasiu D, Whitbeck JC, Cairns TM, Reilly B, Cohen GH, Eisenberg RJ. Bimolecular complementation reveals that glycoproteins gB and gH/gL of herpes simplex virus interact with each other during cell fusion. Proc Natl Acad Sci U S A. 2007;104:18718-18723.
244. Rogalin HB, Heldwein EE. Interplay between the Herpes Simplex Virus 1 gB Cytodomain and the gH Cytotail during Cell-Cell Fusion. J Virol. 2015;89:12262-12272.
245. Stow ND. Localization of an origin of DNA replication within the TRS/IRS repeated region of the herpes simplex virus type 1 genome. EMBO J. 1982;1:863-867.
246. Polvino-Bodnar M, Orberg PK, Schaffer PA. Herpes simplex virus type 1 oriL is not required for virus replication or for the establishment and reactivation of latent infection in mice. J Virol. 1987;61:3528-3535.
247. Igarashi K, Fawl R, Roller RJ, Roizman B. Construction and properties of a recombinant herpes simplex virus 1 lacking both S-component origins of DNA synthesis. J Virol. 1993;67:2123-2132.
248. Stow ND, McMonagle EC. Characterization of the TRS/IRS origin of DNA replication of herpes simplex virus type 1. Virology. 1983;130:427-438.
249. Weller SK, Spadaro A, Schaffer JE, Murray AW, Maxam AM, Schaffer PA. Cloning, sequencing, and functional analysis of oriL, a herpes simplex virus type 1 origin of DNA synthesis. Mol Cell Biol. 1985;5:930-942.
250. Wu CA, Nelson NJ, McGeoch DJ, Challberg MD. Identification of Herpes Simplex Virus type 1 genes required for origin-dependent DNA synthesis. Virol J. 1988;62:435-443.
251. Weir HM, Calder JM, Stow ND. Binding of the herpes simplex virus type 1 UL9 gene product to an origin of viral DNA replication. Nucleic Acids Res. 1989;17:1409-1425.

252. Aslani A, Macao B, Simonsson S, Elias P. Complementary intrastrand base pairing during initiation of Herpes simplex virus type 1 DNA replication. Proc Natl Acad Sci U S A. 2001;98:7194-7199.
253. Elias P, Lehman IR. Interaction of origin binding protein with an origin of replication of herpes simplex virus 1. Proc Natl Acad Sci U S A. 1988;85:2959-2963.
254. Makhov AM, Boehmer PE, Lehman IR, Griffith JD. The herpes simplex virus type 1 origin-binding protein carries out origin specific DNA unwinding and forms stem-loop structures. EMBO J. 1996;15:1742-1750.
255. Boehmer PE, Craigie MC, Stow ND, Lehman IR. Association of origin binding protein and single strand DNA-binding protein, ICP8, during herpes simplex virus type 1 DNA replication in vivo. J Biol Chem. 1994;269:29329-29334.
256. Aslani A, Olsson M, Elias P. ATP-dependent unwinding of a minimal origin of DNA replication by the origin-binding protein and the single-strand DNA-binding protein ICP8 from herpes simplex virus type I. J Biol Chem. 2002;277:41204-41212.
257. Boehmer PE. The Herpes Simplex Virus Type-1 Single-strand DNA-binding Protein, ICP8, Increases the Processivity of the UL9 Protein DNA Helicase. Journal of Biological Chemistry. 1998;273:2676-2683.
258. Chen Y, Bai P, Mackay S et al. Herpes simplex virus type 1 helicase-primase: DNA binding and consequent protein oligomerization and primase activation. J Virol. 2011;85:968-978.
259. Carrington-Lawrence SD, Weller SK. Recruitment of Polymerase to Herpes Simplex Virus Type 1 Replication Foci in Cells Expressing Mutant Primase (UL52) Proteins. Journal of Virology. 2003;77:4237-4247.
260. Digard P, Bebrin WR, Weisshart K, Coen DM. The extreme C terminus of herpes simplex virus DNA polymerase is crucial for functional interaction with processivity factor UL42 and for viral replication. J Virol. 1993;67:398-406.
261. Monahan SJ, Grinstead LA, Olivieri W, Parris DS. Interaction between the herpes simplex virus type 1 origin-binding and DNA polymerase accessory proteins. Virology. 1998;241:122-130.
262. Newcomb WW, Juhas RM, Thomsen DR et al. The UL6 gene product forms the portal for entry of DNA into the herpes simplex virus capsid. J Virol. 2001;75:10923-10932.
263. Newcomb WW, Trus BL, Booy FP, Steven AC, Wall JS, Brown JC. Structure of the herpes simplex virus capsid. Molecular composition of the pentons and the triplexes. J Mol Biol. 1993;232:499-511.
264. Thomsen DR, Roof LL, Homa FL. Assembly of herpes simplex virus (HSV) intermediate capsids in insect cells infected with recombinant baculoviruses expressing HSV capsid proteins. J Virol. 1994;68:2442-2457.
265. White CA, Stow ND, Patel AH, Hughes M, Preston VG. Herpes Simplex Virus Type 1 Portal Protein UL6 Interacts with the Putative Terminase Subunits UL15 and UL28. Journal of Virology. 2003;77:6351-6358.
266. Adelman K, Salmon B, Baines JD. Herpes simplex virus DNA packaging sequences adopt novel structures that are specifically recognized by a component of the cleavage and packaging machinery. Proc Natl Acad Sci U S A.

2001;98:3086-3091.
267. Deiss LP, Chou J, Frenkel N. Functional domains within the a sequence involved in the cleavage-packaging of herpes simplex virus DNA. J Virol. 1986;59:605-618.
268. Yu D, Weller SK. Genetic analysis of the UL 15 gene locus for the putative terminase of herpes simplex virus type 1. Virology. 1998;243:32-44.
269. Cockrell SK, Sanchez ME, Erazo A, Homa FL. Role of the UL25 protein in herpes simplex virus DNA encapsidation. J Virol. 2009;83:47-57.
270. Reynolds AE, Ryckman BJ, Baines JD, Zhou Y, Liang L, Roller RJ. UL31 and UL34 Proteins of Herpes Simplex Virus Type 1 Form a Complex That Accumulates at the Nuclear Rim and Is Required for Envelopment of Nucleocapsids. Journal of Virology. 2001;75:8803-8817.
271. Bigalke JM, Heldwein EE. Structural basis of membrane budding by the nuclear egress complex of herpesviruses. EMBO J. 2015;34:2921-2936.
272. Yang K, Baines JD. Selection of HSV capsids for envelopment involves interaction between capsid surface components pUL31, pUL17, and pUL25. Proc Natl Acad Sci U S A. 2011;108:14276-14281.
273. Johnson DC, Spear PG. Monensin inhibits the processing of herpes simplex virus glycoproteins, their transport to the cell surface, and the egress of virions from infected cells. J Virol. 1982;43:1102-1112.
274. Dasgupta A, Wilson DW. Evaluation of the primary effect of brefeldin A treatment upon herpes simplex virus assembly. J Gen Virol. 2001;82:1561-1567.
275. Komuro M, Tajima M, Kato K. Transformation of Golgi membrane into the envelope of herpes simplex virus in rat anterior pituitary cells. Eur J Cell Biol. 1989;50:398-406.
276. Turcotte S, Letellier J, Lippé R. Herpes simplex virus type 1 capsids transit by the trans-Golgi network, where viral glycoproteins accumulate independently of capsid egress. J Virol. 2005;79:8847-8860.
277. Jambunathan N, Chouljenko D, Desai P et al. Herpes simplex virus 1 protein UL37 interacts with viral glycoprotein gK and membrane protein UL20 and functions in cytoplasmic virion envelopment. J Virol. 2014;88:5927-5935.
278. Farnsworth A, Goldsmith K, Johnson DC. Herpes Simplex Virus Glycoproteins gD and gE/gI Serve Essential but Redundant Functions during Acquisition of the Virion Envelope in the Cytoplasm. Journal of Virology. 2003;77:8481-8494.
279. Johnson DC, Wisner TW, Wright CC. Herpes simplex virus glycoproteins gB and gD function in a redundant fashion to promote secondary envelopment. J Virol. 2011;85:4910-4926.
280. Hogue IB, Scherer J, Enquist LW. Exocytosis of Alphaherpesvirus Virions, Light Particles, and Glycoproteins Uses Constitutive Secretory Mechanisms. MBio. 2016;7
281. Sears AE, Hukkanen V, Labow MA, Levine AJ, Roizman B. Expression of the herpes simplex virus 1 alpha transinducing factor (VP16) does not induce reactivation of latent virus or prevent the establishment of latency in mice. J Virol. 1991;65:2929-2935.
282. Wilcox CL, Smith RL, Everett RD, Mysofski D. The herpes simplex virus type 1

immediate-early protein ICP0 is necessary for the efficient establishment of latent infection. J Virol. 1997;71:6777-6785.
283. Sedarati F, Margolis TP, Stevens JG. Latent infection can be established with drastically restricted transcription and replication of the HSV-1 genome. Virology. 1993;192:687-691.
284. Coen DM, Kosz-Vnenchak M, Jacobson JG et al. Thymidine kinase-negative herpes simplex virus mutants establish latency in mouse trigeminal ganglia but do not reactivate. Proc Natl Acad Sci U S A. 1989;86:4736-4740.
285. Thompson RL, Sawtell NM. Replication of herpes simplex virus type 1 within trigeminal ganglia is required for high frequency but not high viral genome copy number latency. J Virol. 2000;74:965-974.
286. Spivack JG, Fraser NW. Detection of herpes simplex virus type 1 transcripts during latent infection in mice. J Virol. 1987;61:3841-3847.
287. Rock DL, Nesburn AB, Ghiasi H et al. Detection of latency-related viral RNAs in trigeminal ganglia of rabbits latently infected with herpes simplex virus type 1. J Virol. 1987;61:3820-3826.
288. Spivack JG, Fraser NW. Expression of herpes simplex virus type 1 latency-associated transcripts in the trigeminal ganglia of mice during acute infection and reactivation of latent infection. J Virol. 1988;62:1479-1485.
289. Perng GC, Slanina SM, Yukht A, Ghiasi H, Nesburn AB, Wechsler SL. The latency-associated transcript gene enhances establishment of herpes simplex virus type 1 latency in rabbits. J Virol. 2000;74:1885-1891.
290. Thompson RL, Sawtell NM. The herpes simplex virus type 1 latency-associated transcript gene regulates the establishment of latency. J Virol. 1997;71:5432-5440.
291. Sedarati F, Izumi KM, Wagner EK, Stevens JG. Herpes simplex virus type 1 latency-associated transcription plays no role in establishment or maintenance of a latent infection in murine sensory neurons. J Virol. 1989;63:4455-4458.
292. Javier RT, Stevens JG, Dissette VB, Wagner EK. A herpes simplex virus transcript abundant in latently infected neurons is dispensable for establishment of the latent state. Virology. 1988;166:254-257.
293. Lock M, Miller C, Fraser NW. Analysis of protein expression from within the region encoding the 2.0-kilobase latency-associated transcript of herpes simplex virus type 1. J Virol. 2001;75:3413-3426.
294. Mador N, Goldenberg D, Cohen O, Panet A, Steiner I. Herpes simplex virus type 1 latency-associated transcripts suppress viral replication and reduce immediate-early gene mRNA levels in a neuronal cell line. J Virol. 1998;72:5067-5075.
295. Umbach JL, Kramer MF, Jurak I, Karnowski HW, Coen DM, Cullen BR. MicroRNAs expressed by herpes simplex virus 1 during latent infection regulate viral mRNAs. Nature. 2008;454:780-783.
296. Jiang X, Brown D, Osorio N et al. A herpes simplex virus type 1 mutant disrupted for microRNA H2 with increased neurovirulence and rate of reactivation. J Neurovirol. 2015;21:199-209.
297. Flores O, Nakayama S, Whisnant AW, Javanbakht H, Cullen BR, Bloom DC. Mutational inactivation of herpes simplex virus 1 microRNAs identifies viral

mRNA targets and reveals phenotypic effects in culture. J Virol. 2013;87:6589-6603.
298. Halford WP, Gebhardt BM, Carr DJ. Mechanisms of herpes simplex virus type 1 reactivation. J Virol. 1996;70:5051-5060.
299. Wilcox CL, Smith RL, Freed CR, Johnson EM. Nerve growth factor-dependence of herpes simplex virus latency in peripheral sympathetic and sensory neurons in vitro. J Neurosci. 1990;10:1268-1275.
300. Danaher RJ, Jacob RJ, Steiner MR, Allen WR, Hill JM, Miller CS. Histone deacetylase inhibitors induce reactivation of herpes simplex virus type 1 in a latency-associated transcript-independent manner in neuronal cells. J Neurovirol. 2005;11:306-317.
301. Smith RL, Pizer LI, Johnson EM, Wilcox CL. Activation of second-messenger pathways reactivates latent herpes simplex virus in neuronal cultures. Virology. 1992;188:311-318.
302. Kristie TM, Vogel JL, Sears AE. Nuclear localization of the C1 factor (host cell factor) in sensory neurons correlates with reactivation of herpes simplex virus from latency. Proc Natl Acad Sci U S A. 1999;96:1229-1233.
303. Narayanan A, Nogueira ML, Ruyechan WT, Kristie TM. Combinatorial Transcription of Herpes Simplex Virus and Varicella Zoster Virus Immediate Early Genes Is Strictly Determined by the Cellular Coactivator HCF-1. Journal of Biological Chemistry. 2005;280:1369-1375.
304. Halford WP, Schaffer PA. ICP0 is required for efficient reactivation of herpes simplex virus type 1 from neuronal latency. J Virol. 2001;75:3240-3249.
305. Miller CS, Danaher RJ, Jacob RJ. ICP0 is not required for efficient stress-induced reactivation of herpes simplex virus type 1 from cultured quiescently infected neuronal cells. J Virol. 2006;80:3360-3368.
306. Kim JY, Mandarino A, Chao MV, Mohr I, Wilson AC. Transient reversal of episome silencing precedes VP16-dependent transcription during reactivation of latent HSV-1 in neurons. PLoS Pathog. 2012;8:e1002540.
307. Steiner I, Spivack JG, Lirette RP et al. Herpes simplex virus type 1 latency-associated transcripts are evidently not essential for latent infection. EMBO J. 1989;8:505-511.
308. Perng GC, Dunkel EC, Geary PA et al. The latency-associated transcript gene of herpes simplex virus type 1 (HSV-1) is required for efficient in vivo spontaneous reactivation of HSV-1 from latency. J Virol. 1994;68:8045-8055.
309. BenMohamed L, Osorio N, Srivastava R, Khan AA, Simpson JL, Wechsler SL. Decreased reactivation of a herpes simplex virus type 1 (HSV-1) latency-associated transcript (LAT) mutant using the in vivo mouse UV-B model of induced reactivation. J Neurovirol. 2015;21:508-517.
310. Kristie TM, Sharp PA. Purification of the cellular C1 factor required for the stable recognition of the Oct-1 homeodomain by the herpes simplex virus alpha-trans-induction factor (VP16). J Biol Chem. 1993;268:6525-6534.
311. Simmen KA, Newell A, Robinson M et al. Protein interactions in the herpes simplex virus type 1 VP16-induced complex: VP16 peptide inhibition and mutational analysis of host cell factor requirements. J Virol. 1997;71:3886-3894.

312. Gerster T, Roeder RG. A herpesvirus trans-activating protein interacts with transcription factor OTF-1 and other cellular proteins. Proc Natl Acad Sci U S A. 1988;85:6347-6351.
313. Walker S, Hayes S, O'Hare P. Site-specific conformational alteration of the Oct-1 POU domain-DNA complex as the basis for differential recognition by Vmw65 (VP16). Cell. 1994;79:841-852.
314. LaBoissière S, Walker S, O'Hare P. Concerted activity of host cell factor subregions in promoting stable VP16 complex assembly and preventing interference by the acidic activation domain. Mol Cell Biol. 1997;17:7108-7118.
315. Memedula S, Belmont AS. Sequential recruitment of HAT and SWI/SNF components to condensed chromatin by VP16. Curr Biol. 2003;13:241-246.
316. Herrera FJ, Triezenberg SJ. VP16-dependent association of chromatin-modifying coactivators and underrepresentation of histones at immediate-early gene promoters during herpes simplex virus infection. J Virol. 2004;78:9689-9696.
317. Kutluay SB, Triezenberg SJ. Regulation of histone deposition on the herpes simplex virus type 1 genome during lytic infection. J Virol. 2009;83:5835-5845.
318. Kutluay SB, DeVos SL, Klomp JE, Triezenberg SJ. Transcriptional coactivators are not required for herpes simplex virus type 1 immediate-early gene expression in vitro. J Virol. 2009;83:3436-3449.
319. Liang Y, Vogel JL, Narayanan A, Peng H, Kristie TM. Inhibition of the histone demethylase LSD1 blocks alpha-herpesvirus lytic replication and reactivation from latency. Nat Med. 2009;15:1312-1317.
320. Narayanan A, Ruyechan WT, Kristie TM. The coactivator host cell factor-1 mediates Set1 and MLL1 H3K4 trimethylation at herpesvirus immediate early promoters for initiation of infection. Proc Natl Acad Sci U S A. 2007;104:10835-10840.
321. Metzger E, Wissmann M, Yin N et al. LSD1 demethylates repressive histone marks to promote androgen-receptor-dependent transcription. Nature. 2005;437:436-439.
322. Liang Y, Quenelle D, Vogel JL, Mascaro C, Ortega A, Kristie TM. A novel selective LSD1/KDM1A inhibitor epigenetically blocks herpes simplex virus lytic replication and reactivation from latency. MBio. 2013;4:e00558-12.
323. Huang J, Kent JR, Placek B et al. Trimethylation of histone H3 lysine 4 by Set1 in the lytic infection of human herpes simplex virus 1. J Virol. 2006;80:5740-5746.
324. Sadowski I, Ma J, Triezenberg S, Ptashne M. GAL4-VP16 is an unusually potent transcriptional activator. Nature. 1988;335:563-564.
325. Tumbar T, Sudlow G, Belmont AS. Large-scale chromatin unfolding and remodeling induced by VP16 acidic activation domain. J Cell Biol. 1999;145:1341-1354.
326. Stow ND, Stow EC. Isolation and characterization of a herpes simplex virus type 1 mutant containing a deletion within the gene encoding the immediate early polypeptide Vmw110. J Gen Virol. 1986;67:2571-2585.
327. Sacks WR, Schaffer PA. Deletion mutants in the gene encoding the herpes

simplex virus type 1 immediate-early protein ICP0 exhibit impaired growth in cell culture. J Virol. 1987;61:829-839.
328. Everett RD. Trans activation of transcription by herpes virus products: requirement for two HSV-1 immediate-early polypeptides for maximum activity. EMBO J. 1984;3:3135-3141.
329. Gelman IH, Silverstein S. Identification of immediate early genes from herpes simplex virus that transactivate the virus thymidine kinase gene. Proc Natl Acad Sci U S A. 1985;82:5265-5269.
330. Kawaguchi Y, Tanaka M, Yokoymama A et al. Herpes simplex virus 1 alpha regulatory protein ICP0 functionally interacts with cellular transcription factor BMAL1. Proc Natl Acad Sci U S A. 2001;98:1877-1882.
331. Gu H, Liang Y, Mandel G, Roizman B. Components of the REST/CoREST/histone deacetylase repressor complex are disrupted, modified, and translocated in HSV-1-infected cells. Proc Natl Acad Sci U S A. 2005;102:7571-7576.
332. Gu H, Roizman B. Herpes simplex virus-infected cell protein 0 blocks the silencing of viral DNA by dissociating histone deacetylases from the CoREST-REST complex. Proc Natl Acad Sci U S A. 2007;104:17134-17139.
333. Cliffe AR, Knipe DM. Herpes simplex virus ICP0 promotes both histone removal and acetylation on viral DNA during lytic infection. J Virol. 2008;82:12030-12038.
334. Lee JS, Raja P, Knipe DM. Herpesviral ICP0 Protein Promotes Two Waves of Heterochromatin Removal on an Early Viral Promoter during Lytic Infection. MBio. 2016;7:e02007-15.
335. Everett RD, Rechter S, Papior P, Tavalai N, Stamminger T, Orr A. PML contributes to a cellular mechanism of repression of herpes simplex virus type 1 infection that is inactivated by ICP0. J Virol. 2006;80:7995-8005.
336. Everett RD, Freemont P, Saitoh H et al. The disruption of ND10 during herpes simplex virus infection correlates with the Vmw110- and proteasome-dependent loss of several PML isoforms. J Virol. 1998;72:6581-6591.
337. Van Sant C, Hagglund R, Lopez P, Roizman B. The infected cell protein 0 of herpes simplex virus 1 dynamically interacts with proteasomes, binds and activates the cdc34 E2 ubiquitin-conjugating enzyme, and possesses in vitro E3 ubiquitin ligase activity. Proc Natl Acad Sci U S A. 2001;98:8815-8820.
338. Boutell C, Sadis S, Everett RD. Herpes Simplex Virus Type 1 Immediate-Early Protein ICP0 and Its Isolated RING Finger Domain Act as Ubiquitin E3 Ligases In Vitro. Journal of Virology. 2002;76:841-850.
339. Lomonte P, Sullivan KF, Everett RD. Degradation of nucleosome-associated centromeric histone H3-like protein CENP-A induced by herpes simplex virus type 1 protein ICP0. J Biol Chem. 2001;276:5829-5835.
340. Parkinson J, Lees-Miller SP, Everett RD. Herpes simplex virus type 1 immediate-early protein vmw110 induces the proteasome-dependent degradation of the catalytic subunit of DNA-dependent protein kinase. J Virol. 1999;73:650-657.
341. Courtney RJ, Benyesh-Melnick M. Isolation and characterization of a large molecular-weight polypeptide of herpes simplex virus type 1. Virology. 1974;62:539-551.

342. Shepard AA, Tolentino P, DeLuca NA. trans-dominant inhibition of herpes simplex virus transcriptional regulatory protein ICP4 by heterodimer formation. J Virol. 1990;64:3916-3926.
343. Wyrwicz LS, Rychlewski L. Fold recognition insights into function of herpes ICP4 protein. Acta Biochim Pol. 2007;54:551-559.
344. Metzler DW, Wilcox KW. Isolation of herpes simplex virus regulatory protein ICP4 as a homodimeric complex. J Virol. 1985;55:329-337.
345. Gallinari P, Wiebauer K, Nardi MC, Jiricny J. Localization of a 34-amino-acid segment implicated in dimerization of the herpes simplex virus type 1 ICP4 polypeptide by a dimerization trap. J Virol. 1994;68:3809-3820.
346. Tyler JK, Everett RD. The DNA binding domains of the varicella-zoster virus gene 62 and herpes simplex virus type 1 ICP4 transactivator proteins heterodimerize and bind to DNA. Nucleic Acids Res. 1994;22:711-721.
347. Shepard AA, DeLuca NA. Intragenic complementation among partial peptides of herpes simplex virus regulatory protein ICP4. J Virol. 1989;63:1203-1211.
348. Faber SW, Wilcox KW. Association of the herpes simplex virus regulatory protein ICP4 with specific nucleotide sequences in DNA. Nucleic Acids Res. 1986;14:6067-6083.
349. Kristie TM, Roizman B. Alpha 4, the major regulatory protein of herpes simplex virus type 1, is stably and specifically associated with promoter-regulatory domains of alpha genes and of selected other viral genes. Proc Natl Acad Sci U S A. 1986;83:3218-3222.
350. Kristie TM, Roizman B. DNA-binding site of major regulatory protein alpha 4 specifically associated with promoter-regulatory domains of alpha genes of herpes simplex virus type 1. Proc Natl Acad Sci U S A. 1986;83:4700-4704.
351. Lium EK, Panagiotidis CA, Wen X, Silverstein S. Repression of the alpha0 gene by ICP4 during a productive herpes simplex virus infection. J Virol. 1996;70:3488-3496.
352. Tunnicliffe RB, Lockhart-Cairns MP, Levy C et al. The herpes viral transcription factor ICP4 forms a novel DNA recognition complex. Nucleic Acids Res. 2017
353. Shepard AA, DeLuca NA. A second-site revertant of a defective herpes simplex virus ICP4 protein with restored regulatory activities and impaired DNA-binding properties. J Virol. 1991;65:787-795.
354. Xia K, Knipe DM, DeLuca NA. Role of protein kinase A and the serine-rich region of herpes simplex virus type 1 ICP4 in viral replication. J Virol. 1996;70:1050-1060.
355. Advani SJ, Hagglund R, Weichselbaum RR, Roizman B. Posttranslational Processing of Infected Cell Proteins 0 and 4 of Herpes Simplex Virus 1 Is Sequential and Reflects the Subcellular Compartment in Which the Proteins Localize. Journal of Virology. 2001;75:7904-7912.
356. Schang LM, Phillips J, Schaffer PA. Requirement for cellular cyclin-dependent kinases in herpes simplex virus replication and transcription. J Virol. 1998;72:5626-5637.
357. Schang LM, Rosenberg A, Schaffer PA. Roscovitine, a specific inhibitor of cellular cyclin-dependent kinases, inhibits herpes simplex virus DNA synthesis in the presence of viral early proteins. J Virol. 2000;74:2107-2120.

358. Paterson T, Everett RD. A prominent serine-rich region in Vmw175, the major transcriptional regulator protein of herpes simplex virus type 1, is not essential for virus growth in tissue culture. J Gen Virol. 1990;71:1775-1783.
359. Papavassiliou AG, Wilcox KW, Silverstein SJ. The interaction of ICP4 with cell/infected-cell factors and its state of phosphorylation modulate differential recognition of leader sequences in herpes simplex virus DNA. EMBO J. 1991;10:397-406.
360. Wagner LM, DeLuca NA. Temporal association of herpes simplex virus ICP4 with cellular complexes functioning at multiple steps in PolII transcription. PLoS One. 2013;8:e78242.
361. DeLuca NA, Schaffer PA. Physical and functional domains of the herpes simplex virus transcriptional regulatory protein ICP4. J Virol. 1988;62:732-743.
362. Yao F, Schaffer PA. Physical interaction between the herpes simplex virus type 1 immediate-early regulatory proteins ICP0 and ICP4. J Virol. 1994;68:8158-8168.
363. Panagiotidis CA, Lium EK, Silverstein SJ. Physical and functional interactions between herpes simplex virus immediate-early proteins ICP4 and ICP27. J Virol. 1997;71:1547-1557.
364. Carrozza MJ, DeLuca NA. Interaction of the viral activator protein ICP4 with TFIID through TAF250. Mol Cell Biol. 1996;16:3085-3093.
365. Kalamvoki M, Roizman B. The histone acetyltransferase CLOCK is an essential component of the herpes simplex virus 1 transcriptome that includes TFIID, ICP4, ICP27, and ICP22. J Virol. 2011;85:9472-9477.
366. Michael N, Roizman B. Repression of the herpes simplex virus 1 alpha 4 gene by its gene product occurs within the context of the viral genome and is associated with all three identified cognate sites. Proc Natl Acad Sci U S A. 1993;90:2286-2290.
367. Smith CA, Bates P, Rivera-Gonzalez R, Gu B, DeLuca NA. ICP4, the major transcriptional regulatory protein of herpes simplex virus type 1, forms a tripartite complex with TATA-binding protein and TFIIB. J Virol. 1993;67:4676-4687.
368. Gu B, Kuddus R, DeLuca NA. Repression of activator-mediated transcription by herpes simplex virus ICP4 via a mechanism involving interactions with the basal transcription factors TATA-binding protein and TFIIB. Mol Cell Biol. 1995;15:3618-3626.
369. Kuddus R, Gu B, DeLuca NA. Relationship between TATA-binding protein and herpes simplex virus type 1 ICP4 DNA-binding sites in complex formation and repression of transcription. J Virol. 1995;69:5568-5575.
370. Deshmane SL, Fraser NW. During latency, herpes simplex virus type 1 DNA is associated with nucleosomes in a chromatin structure. J Virol. 1989;63:943-947.
371. Placek BJ, Huang J, Kent JR et al. The histone variant H3.3 regulates gene expression during lytic infection with herpes simplex virus type 1. J Virol. 2009;83:1416-1421.
372. Kubat NJ, Amelio AL, Giordani NV, Bloom DC. The herpes simplex virus type 1 latency-associated transcript (LAT) enhancer/rcr is hyperacetylated during

latency independently of LAT transcription. J Virol. 2004;78:12508-12518.
373. Lacasse JJ, Schang LM. During lytic infections, herpes simplex virus type 1 DNA is in complexes with the properties of unstable nucleosomes. J Virol. 2010;84:1920-1933.
374. Conn KL, Hendzel MJ, Schang LM. Linker histones are mobilized during infection with herpes simplex virus type 1. J Virol. 2008;82:8629-8646.
375. Conn KL, Hendzel MJ, Schang LM. The differential mobilization of histones H3.1 and H3.3 by herpes simplex virus 1 relates histone dynamics to the assembly of viral chromatin. PLoS Pathog. 2013;9:e1003695.
376. Weintraub H, Groudine M. Chromosomal subunits in active genes have an altered conformation. Science. 1976;193:848-856.
377. Coleman HM, Connor V, Cheng ZS, Grey F, Preston CM, Efstathiou S. Histone modifications associated with herpes simplex virus type 1 genomes during quiescence and following ICP0-mediated de-repression. J Gen Virol. 2008;89:68-77.
378. Kubat NJ, Tran RK, McAnany P, Bloom DC. Specific Histone Tail Modification and Not DNA Methylation Is a Determinant of Herpes Simplex Virus Type 1 Latent Gene Expression. Journal of Virology. 2004;78:1139-1149.
379. Amelio AL, Giordani NV, Kubat NJ, O'neil JE, Bloom DC. Deacetylation of the herpes simplex virus type 1 latency-associated transcript (LAT) enhancer and a decrease in LAT abundance precede an increase in ICP0 transcriptional permissiveness at early times postexplant. J Virol. 2006;80:2063-2068.
380. Creech CC, Neumann DM. Changes to euchromatin on LAT and ICP4 following reactivation are more prevalent in an efficiently reactivating strain of HSV-1. PLoS One. 2010;5:e15416.
381. Liang Y, Vogel JL, Arbuckle JH et al. Targeting the JMJD2 histone demethylases to epigenetically control herpesvirus infection and reactivation from latency. Sci Transl Med. 2013;5:167ra5.
382. Kalamvoki M, Roizman B. Circadian CLOCK histone acetyl transferase localizes at ND10 nuclear bodies and enables herpes simplex virus gene expression. Proc Natl Acad Sci U S A. 2010;107:17721-17726.
383. Bryant KF, Colgrove RC, Knipe DM. Cellular SNF2H chromatin-remodeling factor promotes herpes simplex virus 1 immediate-early gene expression and replication. MBio. 2011;2:e00330-10.
384. Oh J, Ruskoski N, Fraser NW. Chromatin assembly on herpes simplex virus 1 DNA early during a lytic infection is Asf1a dependent. J Virol. 2012;86:12313-12321.
385. Johnson KE, Bottero V, Flaherty S, Dutta S, Singh VV, Chandran B. IFI16 restricts HSV-1 replication by accumulating on the hsv-1 genome, repressing HSV-1 gene expression, and directly or indirectly modulating histone modifications. PLoS Pathog. 2014;10:e1004503.
386. Nitzsche A, Paulus C, Nevels M. Temporal dynamics of cytomegalovirus chromatin assembly in productively infected human cells. J Virol. 2008;82:11167-11180.
387. Nevels M, Paulus C, Shenk T. Human cytomegalovirus immediate-early 1 protein facilitates viral replication by antagonizing histone deacetylation. Proc

Natl Acad Sci U S A. 2004;101:17234-17239.
388. Zalckvar E, Paulus C, Tillo D et al. Nucleosome maps of the human cytomegalovirus genome reveal a temporal switch in chromatin organization linked to a major IE protein. Proc Natl Acad Sci U S A. 2013;110:13126-13131.
389. Dyson PJ, Farrell PJ. Chromatin structure of Epstein-Barr virus. J Gen Virol. 1985;66:1931-1940.
390. Shaw JE, Levinger LF, Carter CW. Nucleosomal structure of Epstein-Barr virus DNA in transformed cell lines. J Virol. 1979;29:657-665.
391. Murata T, Kondo Y, Sugimoto A et al. Epigenetic histone modification of Epstein-Barr virus BZLF1 promoter during latency and reactivation in Raji cells. J Virol. 2012;86:4752-4761.
392. Toth Z, Maglinte DT, Lee SH et al. Epigenetic analysis of KSHV latent and lytic genomes. PLoS Pathog. 2010;6:e1001013.
393. Smith KO. Relationship between the envelope and the infectivity of herpes simplex virus. Proc Soc Exp Biol Med. 1964;115:814-816.
394. Cai WZ, Schaffer PA. Herpes simplex virus type 1 ICP0 plays a critical role in the de novo synthesis of infectious virus following transfection of viral DNA. J Virol. 1989;63:4579-4589.
395. Mossman KL, Smiley JR. Truncation of the C-terminal acidic transcriptional activation domain of herpes simplex virus VP16 renders expression of the immediate-early genes almost entirely dependent on ICP0. J Virol. 1999;73:9726-9733.
396. Hill JM, Quenelle DC, Cardin RD et al. Inhibition of LSD1 reduces herpesvirus infection, shedding, and recurrence by promoting epigenetic suppression of viral genomes. Sci Transl Med. 2014;6:265ra169.
397. apRhys CM, Ciufo DM, O'Neill EA, Kelly TJ, Hayward GS. Overlapping octamer and TAATGARAT motifs in the VF65-response elements in herpes simplex virus immediate-early promoters represent independent binding sites for cellular nuclear factor III. J Virol. 1989;63:2798-2812.
398. Kristie TM, Roizman B. Host cell proteins bind to the cis-acting site required for virion-mediated induction of herpes simplex virus 1 alpha genes. Proc Natl Acad Sci U S A. 1987;84:71-75.
399. Xiao P, Capone JP. A cellular factor binds to the herpes simplex virus type 1 transactivator Vmw65 and is required for Vmw65-dependent protein-DNA complex assembly with Oct-1. Mol Cell Biol. 1990;10:4974-4977.
400. Zhou G, Te D, Roizman B. The CoREST/REST repressor is both necessary and inimical for expression of herpes simplex virus genes. MBio. 2011;2:e00313-10.
401. Resnick J, Boyd BA, Haffey ML. DNA binding by the herpes simplex virus type 1 ICP4 protein is necessary for efficient down regulation of the ICP0 promoter. J Virol. 1989;63:2497-2503.
402. Aygün O, Mehta S, Grewal SI. HDAC-mediated suppression of histone turnover promotes epigenetic stability of heterochromatin. Nat Struct Mol Biol. 2013;20:547-554.
403. Hieb AR, Gansen A, Böhm V, Langowski J. The conformational state of the nucleosome entry-exit site modulates TATA box-specific TBP binding. Nucleic

Acids Res. 2014;42:7561-7576.
404. Kuo MH, Brownell JE, Sobel RE et al. Transcription-linked acetylation by Gcn5p of histones H3 and H4 at specific lysines. Nature. 1996;383:269-272.
405. Daujat S, Weiss T, Mohn F et al. H3K64 trimethylation marks heterochromatin and is dynamically remodeled during developmental reprogramming. Nat Struct Mol Biol. 2009;16:777-781.
406. Jack AP, Bussemer S, Hahn M et al. H3K56me3 is a novel, conserved heterochromatic mark that largely but not completely overlaps with H3K9me3 in both regulation and localization. PLoS One. 2013;8:e51765.
407. Litt MD, Simpson M, Gaszner M, Allis CD, Felsenfeld G. Correlation between histone lysine methylation and developmental changes at the chicken beta-globin locus. Science. 2001;293:2453-2455.
408. Zheng Y, Tipton JD, Thomas PM, Kelleher NL, Sweet SM. Site-specific human histone H3 methylation stability: fast K4me3 turnover. Proteomics. 2014;14:2190-2199.
409. Elsässer SJ, Huang H, Lewis PW, Chin JW, Allis CD, Patel DJ. DAXX envelops a histone H3.3-H4 dimer for H3.3-specific recognition. Nature. 2012;491:560-565.
410. Goldberg AD, Banaszynski LA, Noh KM et al. Distinct factors control histone variant H3.3 localization at specific genomic regions. Cell. 2010;140:678-691.
411. Ray-Gallet D, Quivy JP, Scamps C, Martini EM, Lipinski M, Almouzni G. HIRA is critical for a nucleosome assembly pathway independent of DNA synthesis. Mol Cell. 2002;9:1091-1100.
412. Koering CE, Pollice A, Zibella MP et al. Human telomeric position effect is determined by chromosomal context and telomeric chromatin integrity. EMBO Rep. 2002;3:1055-1061.
413. Smith CA, Schaffer PA. Mutants defective in herpes simplex virus type 2 ICP4: isolation and preliminary characterization. J Virol. 1987;61:1092-1097.
414. Conn KL, Schang LM. Chromatin dynamics during lytic infection with herpes simplex virus 1. Viruses. 2013;5:1758-1786.
415. Knipe DM. Nuclear sensing of viral DNA, epigenetic regulation of herpes simplex virus infection, and innate immunity. Virology. 2015;479-480:153-159.
416. Kristie TM. Dynamic modulation of HSV chromatin drives initiation of infection and provides targets for epigenetic therapies. Virology. 2015;479-480:555-561.
417. Bloom DC, Giordani NV, Kwiatkowski DL. Epigenetic regulation of latent HSV-1 gene expression. Biochim Biophys Acta. 2010;1799:246-256.
418. Knipe DM, Lieberman PM, Jung JU et al. Snapshots: chromatin control of viral infection. Virology. 2013;435:141-156.
419. Lieberman PM. Keeping it quiet: chromatin control of gammaherpesvirus latency. Nat Rev Microbiol. 2013;11:863-875.
420. Lu X, Triezenberg SJ. Chromatin assembly on herpes simplex virus genomes during lytic infection. Biochim Biophys Acta. 2010;1799:217-222.
421. Roizman B. The checkpoints of viral gene expression in productive and latent infection: the role of the HDAC/CoREST/LSD1/REST repressor complex. J

Virol. 2011;85:7474-7482.
422. Almer A, Rudolph H, Hinnen A, Hörz W. Removal of positioned nucleosomes from the yeast PHO5 promoter upon PHO5 induction releases additional upstream activating DNA elements. EMBO J. 1986;5:2689-2696.
423. Dion MF, Kaplan T, Kim M, Buratowski S, Friedman N, Rando OJ. Dynamics of replication-independent histone turnover in budding yeast. Science. 2007;315:1405-1408.
424. Mao C, Brown CR, Griesenbeck J, Boeger H. Occlusion of regulatory sequences by promoter nucleosomes in vivo. PLoS One. 2011;6:e17521.
425. Ferenczy MW, DeLuca NA. Epigenetic modulation of gene expression from quiescent herpes simplex virus genomes. J Virol. 2009;83:8514-8524.
426. Monier K, Armas JC, Etteldorf S, Ghazal P, Sullivan KF. Annexation of the interchromosomal space during viral infection. Nat Cell Biol. 2000;2:661-665.
427. Glass M, Everett RD. Components of promyelocytic leukemia nuclear bodies (ND10) act cooperatively to repress herpesvirus infection. J Virol. 2013;87:2174-2185.
428. Lukashchuk V, Everett RD. Regulation of ICP0-null mutant herpes simplex virus type 1 infection by ND10 components ATRX and hDaxx. J Virol. 2010;84:4026-4040.
429. Stratmann SA, Morrone SR, van Oijen AM, Sohn J. The innate immune sensor IFI16 recognizes foreign DNA in the nucleus by scanning along the duplex. eLIFE. 2015
430. Johnson KE, Chikoti L, Chandran B. Herpes simplex virus 1 infection induces activation and subsequent inhibition of the IFI16 and NLRP3 inflammasomes. J Virol. 2013;87:5005-5018.
431. Cuchet-Lourenço D, Anderson G, Sloan E, Orr A, Everett RD. The viral ubiquitin ligase ICP0 is neither sufficient nor necessary for degradation of the cellular DNA sensor IFI16 during herpes simplex virus 1 infection. J Virol. 2013;87:13422-13432.
432. Orzalli MH, DeLuca NA, Knipe DM. Nuclear IFI16 induction of IRF-3 signaling during herpesviral infection and degradation of IFI16 by the viral ICP0 protein. Proc Natl Acad Sci U S A. 2012;109:E3008-17.
433. Cheung P, Panning B, Smiley JR. Herpes simplex virus immediate-early proteins ICP0 and ICP4 activate the endogenous human alpha-globin gene in nonerythroid cells. J Virol. 1997;71:1784-1793.
434. LaBoissière S, O'Hare P. Analysis of HCF, the cellular cofactor of VP16, in herpes simplex virus-infected cells. J Virol. 2000;74:99-109.
435. Tsai K, Chan L, Gibeault R et al. Viral reprogramming of the Daxx histone H3.3 chaperone during early Epstein-Barr virus infection. J Virol. 2014;88:14350-14363.
436. Muggeridge MI, Fraser NW. Chromosomal organization of the herpes simplex virus genome during acute infection of the mouse central nervous system. J Virol. 1986;59:764-767.
437. Nitzsche A, Steinhäusser C, Mücke K, Paulus C, Nevels M. Histone H3 lysine 4 methylation marks postreplicative human cytomegalovirus chromatin. J Virol. 2012;86:9817-9827.

438. Arvey A, Tempera I, Lieberman PM. Interpreting the Epstein-Barr Virus (EBV) epigenome using high-throughput data. Viruses. 2013;5:1042-1054.
439. Oh J, Sanders IF, Chen EZ et al. Genome wide nucleosome mapping for HSV-1 shows nucleosomes are deposited at preferred positions during lytic infection. PLoS One. 2015;10:e0117471.
440. Costanzo F, Campadelli-Fiume G, Foa-Tomasi L, Cassai E. Evidence that herpes simplex virus DNA is transcribed by cellular RNA polymerase B. J Virol. 1977;21:996-1001.
441. Abrisch RG, Eidem TM, Yakovchuk P, Kugel JF, Goodrich JA. Infection by Herpes Simplex Virus 1 Causes Near-Complete Loss of RNA Polymerase II Occupancy on the Host Cell Genome. J Virol. 2016;90:2503-2513.
442. Abbott DW, Ivanova VS, Wang X, Bonner WM, Ausió J. Characterization of the stability and folding of H2A.Z chromatin particles: implications for transcriptional activation. J Biol Chem. 2001;276:41945-41949.
443. Higashi T, Matsunaga S, Isobe K et al. Histone H2A mobility is regulated by its tails and acetylation of core histone tails. Biochem Biophys Res Commun. 2007;357:627-632.
444. Arimura Y, Kimura H, Oda T et al. Structural basis of a nucleosome containing histone H2A.B/H2A.Bbd that transiently associates with reorganized chromatin. Sci Rep. 2013;3:3510.
445. Abbott DW, Laszczak M, Lewis JD et al. Structural characterization of macroH2A containing chromatin. Biochemistry. 2004;43:1352-1359.
446. Grogan DE, Desjardins R, Busch H. Nucleolar proteins of rat liver and Walker tumor. Cancer Res. 1966;26:775-779.
447. Chadwick BP, Willard HF. Histone H2A variants and the inactive X chromosome: identification of a second macroH2A variant. Hum Mol Genet. 2001;10:1101-1113.
448. Kanda T, Sullivan KF, Wahl GM. Histone-GFP fusion protein enables sensitive analysis of chromosome dynamics in living mammalian cells. Curr Biol. 1998;8:377-385.
449. Bönisch C, Schneider K, Pünzeler S et al. H2A.Z.2.2 is an alternatively spliced histone H2A.Z variant that causes severe nucleosome destabilization. Nucleic Acids Res. 2012;40:5951-5964.
450. Schwartz BE, Ahmad K. Transcriptional activation triggers deposition and removal of the histone variant H3.3. Genes Dev. 2005;19:804-814.
451. Yao F, Schaffer PA. An activity specified by the osteosarcoma line U2OS can substitute functionally for ICP0, a major regulatory protein of herpes simplex virus type 1. J Virol. 1995;69:6249-6258.
452. Wang HC, Ko TP, Lee YM et al. White spot syndrome virus protein ICP11: A histone-binding DNA mimic that disrupts nucleosome assembly. Proc Natl Acad Sci U S A. 2008;105:20758-20763.
453. O'Neill TE, Roberge M, Bradbury EM. Nucleosome arrays inhibit both initiation and elongation of transcripts by bacteriophage T7 RNA polymerase. J Mol Biol. 1992;223:67-78.
454. Gibeault RL, Conn KL, Bildersheim MD, Schang LM. An Essential Viral Transcription Activator Modulates Chromatin Dynamics. PLoS Pathog.

2016;12:e1005842.
455. Leinbach SS, Summers WC. The structure of herpes simplex virus type 1 DNA as probed by micrococcal nuclease digestion. J Gen Virol. 1980;51:45-59.
456. Lacasse JJ, Schang LM. Herpes simplex virus 1 DNA is in unstable nucleosomes throughout the lytic infection cycle, and the instability of the nucleosomes is independent of DNA replication. J Virol. 2012;86:11287-11300.
457. Michael N, Roizman B. Binding of the herpes simplex virus major regulatory protein to viral DNA. Proc Natl Acad Sci U S A. 1989;86:9808-9812.
458. Shepard AA, Imbalzano AN, DeLuca NA. Separation of primary structural components conferring autoregulation, transactivation, and DNA-binding properties to the herpes simplex virus transcriptional regulatory protein ICP4. J Virol. 1989;63:3714-3728.
459. Watson RJ, Clements JB. Characterization of transcription-deficient temperature-sensitive mutants of herpes simplex virus type 1. Virology. 1978;91:364-379.
460. Singh BN, Hampsey M. A transcription-independent role for TFIIB in gene looping. Mol Cell. 2007;27:806-816.
461. Perkins KJ, Lusic M, Mitar I, Giacca M, Proudfoot NJ. Transcription-dependent gene looping of the HIV-1 provirus is dictated by recognition of pre-mRNA processing signals. Mol Cell. 2008;29:56-68.
462. Yager DR, Bachenheimer SL. Synthesis and metabolism of cellular transcripts in HSV-1 infected cells. Virus Genes. 1988;1:135-148.
463. Spencer CA, Kruhlak MJ, Jenkins HL, Sun X, Bazett-Jones DP. Mitotic Transcription Repression in Vivo in the Absence of Nucleosomal Chromatin Condensation. J Cell Biol. 2000;150:13-26.
464. Schreiner S, Wimmer P, Sirma H et al. Proteasome-dependent degradation of Daxx by the viral E1B-55K protein in human adenovirus-infected cells. J Virol. 2010;84:7029-7038.
465. Unterholzner L, Keating SE, Baran M et al. IFI16 is an innate immune sensor for intracellular DNA. Nat Immunol. 2010;11:997-1004.
466. Orzalli MH, Conwell SE, Berrios C, DeCaprio JA, Knipe DM. Nuclear interferon-inducible protein 16 promotes silencing of herpesviral and transfected DNA. Proc Natl Acad Sci U S A. 2013;110:E4492-501.
467. Mao JC, Robishaw EE, Overby LR. Inhibition of DNA polymerase from herpes simplex virus-infected wi-38 cells by phosphonoacetic Acid. J Virol. 1975;15:1281-1283.
468. Soboleva TA, Parker BJ, Nekrasov M et al. A new link between transcriptional initiation and pre-mRNA splicing: The RNA binding histone variant H2A.B. PLoS Genet. 2017;13:e1006633.
469. Zillner K, Komatsu J, Filarsky K, Kalepu R, Bensimon A, Németh A. Active human nucleolar organizer regions are interspersed with inactive rDNA repeats in normal and tumor cells. Epigenomics. 2015;7:363-378.
470. Roussel P, André C, Comai L, Hernandez-Verdun D. The rDNA transcription machinery is assembled during mitosis in active NORs and absent in inactive NORs. J Cell Biol. 1996;133:235-246.
471. Komatsu T, Haruki H, Nagata K. Cellular and viral chromatin proteins are

positive factors in the regulation of adenovirus gene expression. Nucleic Acids Res. 2011;39:889-901.

Appendix 1: The dynamics of H3.3 are enhanced in cells expressing functional BNRF1

A1.1 Introduction

Epstein-Barr Virus (EBV) is a nuclear-replicating double-stranded (ds) DNA virus. Like those of most other nuclear-replicating viruses, EBV genomes localize next to the promyelocytic leukemia nuclear bodies (PML-NBs, also called ND10s) during lytic infections (1). PML-NBs contain many proteins, including the promyelocytic nuclear protein (PML), ATP-dependent helicase (ATRX), and the transcriptional regulator Sp100. The death-associated protein 6 (Daxx) is recruited to the PML-NBs by sumoylated PML (2). Daxx and ATRX localize together at both the PML-NBs or in heterochromatin, and alter chromatin structure (3–5). Daxx also specifically interacts with the H3 variant H3.3 and, together with ATRX, assembles H3.3 in the silencing stable nucleosomes at telomeres (5). Daxx, ATRX, and Sp100 repress transcription of viral genomes (6–9). To counteract repression, viruses have evolved different mechanisms to degrade or dissociate PML-NBs. For example, ICP0, an immediate early protein of herpes simplex virus 1 (HSV-1), induces the dissociation and proteasomal degradation of PML and Sp100 (10–12).

EBV genomes, as those of other herpesviruses, are not chromatinized in the virion but become chromatinized in the nucleus (13, 14). Transcribed cellular genes are more accessible to nuclease digestion than silenced cellular genes, suggesting that transcribed genes are assembled in more dynamic chromatin (15, 16). Transcribed EBV genes are also more accessible to nuclease digestion than silenced EBV genes (17). Consistently, EBV genomes are more dynamically chromatinized during lytic infection, when most EBV genes are expressed, than during latent infection, when most EBV genes are not expressed (13, 14). Transcribed EBV genes, like transcribed cellular genes, are also enriched in acetylated H3 (18–20). Therefore, transcription of EBV genes appears to be regulated in part by chromatin.

The gamma herpesviruses encode for proteins that share homology with the cellular formylglycineamind-ribotideamidotransferase enzyme (FGARAT). These proteins dissociate or degrade PML-NB proteins. ORF75, the FGARAT homolog of Karposi's sarcoma herpes virus (KSHV), dissociates PML proteins and promotes

degradation of ATRX (21). ORF3, the FGARAT homolog of herpesvirus saimiri (HVS), promotes the proteasomal degradation of Sp100 (22). The FGARAT homolog in EBV is named BNRF1. BNRF1 has no enzymatic activity and is not required for EBV replication (23). However, EBV mutants in BNRF1 are less efficient in their ability to establish latent infections in B cells (23). BNRF1 contains a Daxx-interacting domain (DID) between amino acids 360 and 600 (24). BNRF1 competes with ATRX for binding to Daxx, resulting in the dispersion of ATRX from PML-NBs (24). The Daxx-BNRF1 interaction increases EBV transcription (24).

A Daxx/ATRX complex assembles stable nucleosomes containing H3.3. We proposed that BNRF1 binds to Daxx dissociating ATRX, thus preventing the assembly of stable H3.3-containing nucleosomes with EBV DNA. BNRF1 forms a complex with Daxx and a tetramer of H3.3/H4, which is consistent with our hypothesis. Higher levels of H3.3, Daxx, and ATRX were stably associated with EBV promoters higher when BNRF1 was knocked down. I show here that transient expression of wild type BNRF1, but not of a mutant BNRF1 unable to bind Daxx, enhanced the dynamics of H3.3. In contrast, the dynamics of H2B, which does not interact with Daxx, were not affected.

A1.2 Results

A1.2.1 WT BNRF1, but not the d26 or dATPase mutants, enhances H3.3 dynamics

BNRF1 interacts with Daxx and dissociates ATRX. A BNRF1 mutant lacking residues 550-600 (d26) is unable to interact with Daxx or dissociate the ATRX/Daxx interaction. A second BNRF1 mutant lacking the region with homology to aminoimidazole ribonucleotide synthetase (dATPase) retains the ability to interact with Daxx. BNRF1 binds to the histone binding domain of Daxx, and the laboratory of Dr. Lieberman thus expected to prevent H3.3-Daxx interactions. Instead, they found that BNRF1 forms a complex with Daxx and an H3.3-H4 tetramer. They also found that an EBV mutant lacking BNRF1 had higher levels of H3.3 on EBV promoters. Together, these results suggested the possibility that BNRF1 may

participate in chromatin remodeling. We thus asked whether BNRF1 was sufficient to enhance histone dynamics.

To test whether BNRF1 was sufficient to enhance histone dynamics, I evaluated the dynamics of H3.3 using fluorescence recovery after photobleaching (FRAP). I co-transfected cells with a plasmid encoding H3.3 fused in frame with green fluorescent protein (GFP-H3.3) and plasmids encoding wild type or d26 or dATPase mutant BNRF1 fused in frame with red fluorescent protein (RFP-BNRF1, -d26, or –dATPase), such that approximately half of the cells expressing detectable levels of GFP also expressed detectable levels of RFP. GFP-H3.3 was photobleached in a region of the fluorescent nucleus. Fluorescence is recovered in the bleached region as bleached histones within the region exchange with fluorescent histones from outside the region. Fluorescence is normalized to total nuclear fluorescence to account for differences in expression levels. The normalized fluorescence immediately prior to photobleaching is set as 100%. The relative fluorescence at the first time point after photobleaching (T=1 s) is surrogate measure of the free pool of histones, as only histones not assembled in nucleosomes diffuse in or out of the free pool during and immediately after photobleaching. The slope of the fluorescence recovery from 25 to 100 s after photobleaching is a surrogate measure of the slow exchange rate, or the exchange of histones assembled in less dynamic chromatin such as heterochromatin.

Cells expressing detectable levels of WT RFP-BNRF1 had significantly faster fluorescence recovery in the photobleached region than cells expressing undetectable levels. Cells expressing detectable levels of RFP-d26, RFP-dATPase, or free RFP, in contrast, did not. The dynamics of GFP-H3.3 in cells that co-expressed detectable levels of WT or mutant RFP-BNRF1 or free RFP was normalized to their dynamics in the cells on the same coverslip expressing detectable levels of GFP-H3.3 only. The free pool of H3.3 was 34 +/- 10% greater in cells that expressed detectable than undetectable levels of RFP-BNRF1 ($p<0.01$). In contrast, the free pools of GFP-H3.3 were not different in cells expressing detectable or undetectable levels of RFP-d26, RFP-dATPase, or free RFP. The slow exchange rate of GFP-H3.3 was 90 +/- 43% faster in cells expressing detectable than undetectable levels of RFP-BNRF1

($p<0.05$). The slow exchange rate was not significantly different in cells expressing detectable or undetectable levels of RFP-d26, RFP-dATPase, or free RFP. The variability in the slow exchange rates, however, did not allow to statistically test whether WT or mutant forms of BNRF1 differ in their abilities to modulate it.

WT BNRF1 expression is thus sufficient to enhance H3.3 dynamics in the absence of EBV DNA or any other EBV protein. In contrast, the d26 mutant, which is unable to bind Daxx or displace ATRX, and the dATPase mutant, which is unable to hydrolyze ATP, were unable to enhance H3.3 dynamics. Therefore, BNRF1 must contain both the d26 domain and an active ATPase domain to enhance H3.3 dynamics.

A1.2.2 WT BNRF1 does not enhance the dynamics of H2B

Daxx is a specific chaperone for H3.3-H4, and does not bind H2B-H2A. BNRF1 enhances the dynamics of H3.3, perhaps by binding to Daxx and preventing the assembly of H3.3 in nucleosomes. Alternatively, BNRF1 may promote the disassembly of nucleosomes containing H3.3. Nucleosomes are disassembled in a step-wise process - H2B-H2A dimers are removed from the histone octamer prior to the removal of H3-H4 (25, 26). If BNRF1 promotes the disassembly of nucleosomes, we would thus expect that the dynamics of H2B and H2A would also be enhanced in cells expressing BNRF1. I evaluated the dynamics of H2B in cells expressing BNRF1, as H2B has no variants and is thus representative of total pool of H2B-H2A dimers.

I co-transfected cells with GFP-H2B and RFP-BNRF1, RFP-d26, or free RFP, such that approximately half of the cells expressing detectable levels of GFP also expressed detectable levels of RFP. I evaluated histone dynamics by FRAP in cells expressing detectable or undetectable levels of RFP. The fluorescence recovery curves of H2B were not significantly affected in cells expressing detectable levels of RFP-BNRF1. The free pool or slow exchange rate of H2B were not changed in cells expressing detectable levels of RFP-BNRF1. As expected, the fluorescence recovery curves, free pools, or slow exchange rates were not affected in cells expressing detectable levels of RFP-d26 or free RFP. Expression of BNRF1 is thus not sufficient to enhance the dynamics of H2B.

A1.3 Discussion

EBV gene transcription is regulated, in part, through chromatin remodeling (27). Chromatin silences lytic genes during EBV latency, and latent genes during lytic infection (13, 14, 17). Whereas silenced EBV genes are regularly chromatinized, transcribed EBV genes are assembled into highly dynamic nucleosomes (17). Nuclear-replicating dsDNA viruses have evolved many different mechanisms to maintain their genomes in highly dynamic chromatin, highlighting the importance of chromatin dynamics for efficient viral replication. For example, all three HSV-1 transcription activators modulate HSV-1 chromatin dynamics, by different mechanisms. Unlike HSV-1, which establishes latency in non-replicating cells, EBV establishes latency in replicating cells. EBV episomes are replicated by the cellular DNA polymerase and maintained in daughter cells. Stable chromatinization of the entire EBV genome could thus also prevent episome maintenance during latent infection.

Like those of most other nuclear-replicating viruses, EBV genomes localize next to PML-NBs (1), localization which inhibits viral replication. To counteract this cellular silencing mechanism, viruses have evolved mechanisms to dissociate and degrade components of PML-NBs. For gamma herpesviruses, the dissociation of PML-NBs is accomplished in part by their FGARAT homolog proteins (21, 22). Consistently, the FGARAT homolog of EBV, BNRF1, binds to Daxx and dissociates the repressive chromatin remodeller ATRX from PML-NBs (24).

The histone variant H3.3 differs from canonical H3.1 by only five amino acids residues, but this is sufficient for the differential binding of H3.3 and H3.1 by different chaperones. H3.3 is assembled in nucleosomes of permissive chromatin by the chaperone HIRA (28). H3.3 is also assembled in nucleosomes in telomeres and pericentric repeats as repressive chromatin by Daxx and ATRX (5, 29, 30). Whether H3.3 forms unstable or stable nucleosomes is thus dependent, in part, on the chaperone that assembles it, although the mechanisms that result in these differences remain mostly unknown.

BNRF1 interacts with the histone binding domain of Daxx (31). We proposed that BNRF1 binding to Daxx competes with the binding of H3.3, which would

prevent the assembly of H3.3 in repressive nucleosomes with EBV DNA. Instead, the laboratory of Dr. Lieberman found that BNRF1 forms a complex with Daxx and an H3.3-H4 tetramer (31). However, an EBV mutant in BNRF1 had higher levels of H3.3 stably associated with EBV promoters, suggesting that BNRF1 promotes the disassembly, or prevents the assembly, of H3.3 in nucleosomes with EBV DNA (31). To test if BNRF1 expression was sufficient to promote the disassembly or prevent the assembly of H3.3 in nucleosomes in the absence of EBV DNA or other EBV proteins, I evaluated the dynamics of H3.3 in cells transiently expressing BNRF1. The free pool and slow exchange rate of H3.3 were greater in cells expressing detectable levels of RFP-BNRF1. The d26 mutant of BNRF1, which does not interact with Daxx or displace ATRX, did not affect the free pool or slow exchange rate of H3.3, suggesting that the BNRF1-Daxx interaction is required to enhance H3.3 dynamics. The dATPase mutant of BNRF1 also failed to affect the dynamics of H3.3. Though this domain of BNRF1 has no known function, and is not required for binding to Daxx or H3.3, it may perhaps enhance the affinity of BNRF1 for Daxx. Alternatively, the dATPase domain may mediate the interaction of BNRF1 with another protein.

The removal of H2B-H2A precedes the removal of H3-H4 in the disassembly of nucleosomes (25, 26). If BNRF1 promotes the disassembly of nucleosomes, we would thus expect that the dynamics of H2B and H2A would also be enhanced in cells expressing BNRF1. H2B encodes no variants, and is thus representative of the total levels of H2B-H2A dimers in the nucleus. The dynamics of H2B were not affected in cells expressing wild type or d26 BNRF1. These results suggest that BNRF1 prevents the assembly of H3.3-H4 tetramers in the nucleosome, as opposed to promoting their disassembly. I propose a model in which BNRF1 binds to a complex of Daxx-H3.3-H4 and prevents the dissociation of H3.3-H4 from Daxx. As a result, H3.3 is not assembled in nucleosomes, increasing the levels of H3.3 in the free pools. BNRF1 is one of the most abundant tegument proteins, which may ensure that high levels of BNRF1 are present immediately upon infection to prevent the assembly of repressive chromatin with EBV genomes. Alternatively, EBV

nucleosomes may be assembled differently from cellular ones, or be composed of a different ratio of histones or other unknown proteins.

In conclusion, BNRF1 expression is sufficient to enhance the global dynamics of H3.3, but not those of H2B. EBV genomes, which localize nearby PML-NBs, are restricted by a cellular silencing mechanism that forms repressive chromatin containing H3.3 by Daxx and ATRX. To counteract silencing, BNRF1 dissociates ATRX from Daxx and forms a complex with Daxx and H3.3-H4. BNRF1 likely holds H3.3 in the free pool with Daxx, subsequently preventing the assembly of H3.3 in silencing nucleosomes with EBV genomes.

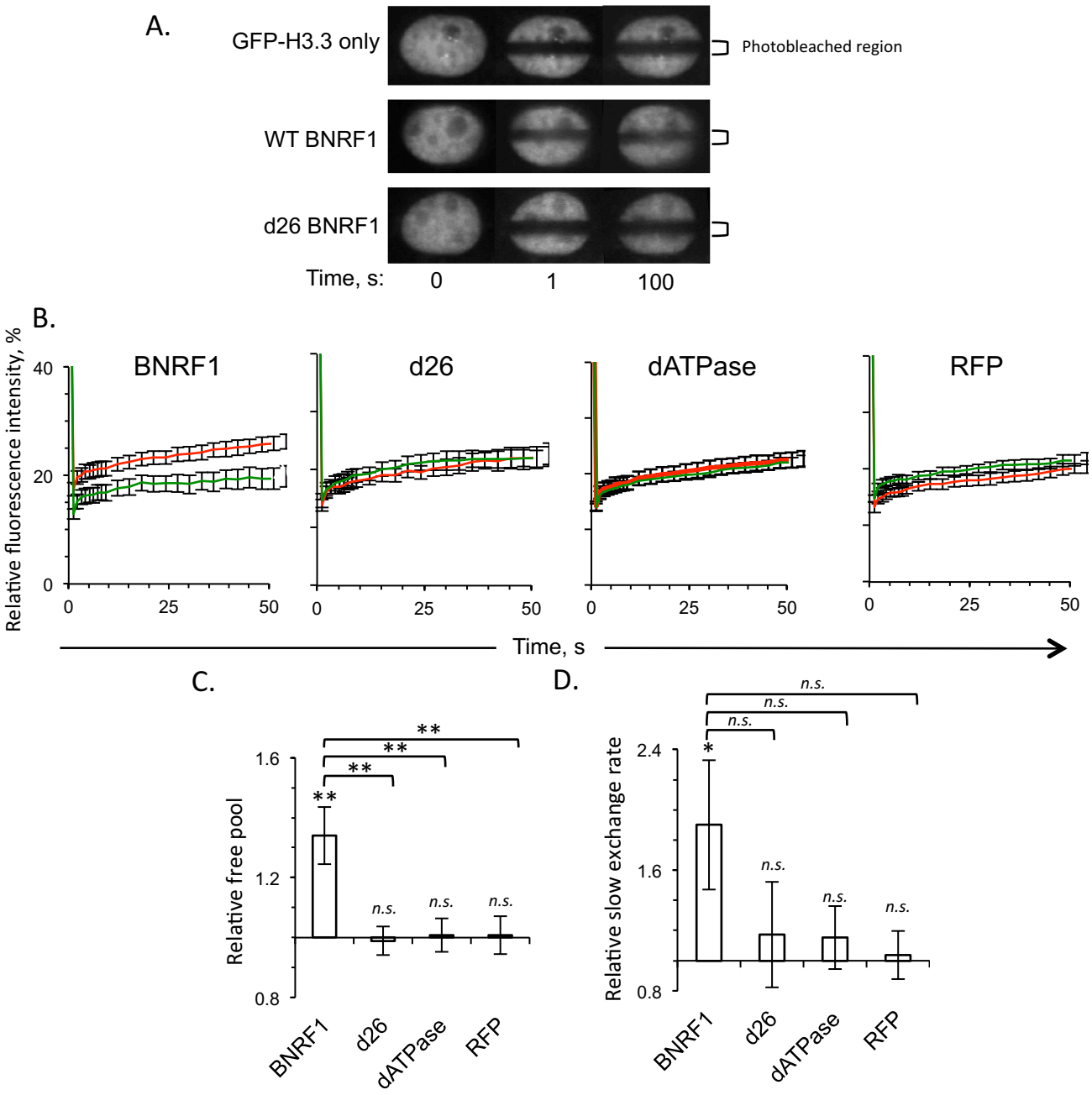
A.
GFP-H3.3 only
WT BNRF1
d26 BNRF1
Photobleached region
Time, s:
0
1
100
B.
Relative fluorescence intensity, %
BNRF1
d26
dATPase
RFP
Time, s
C.
Relative free pool
n.s.
D.
Relative slow exchange rate
n.s.
BNRF1
d26
dATPase
RFP

Figure A1.1. WT BNRF1, but not the d26 or dATPase BNRF1 mutants, enhances the dynamics of H3.1. A) Photomicrographs of nuclei expressing detectable levels of only GFP-H3.3, or of GFP-H3.3 and RFP-ICP4 or RFP-d26, at three different time points. T= 0 s, immediately prior to photobleaching; T= 1 s, immediately after photobleaching. The relative fluorescence of the photobleached region at T = 1 s is representative of the histone free pool. B) Average fluorescence recovery curves of histone H3.3 in cells expressing detectable or undetectable levels of RFP-BNRF1. Error bars, SEM. Red lines, cells expressing detectable levels of GFP-H3.3 and WT, d26, or dATPase RFP-BNRF1, or free RFP. Green lines, cells expressing detectable levels of only GFP-H3.3. C) Bar graphs showing the free pools of GFP-H3.3 in cells expressing detectable levels of WT, d26, or dATPase RFP-BNRF1, or free RFP, relative to the levels in cells expressing undetectable levels on the same coverslip. Error bars, SEM; * $p < 0.05$; ** $p < 0.01$; *n.s.,* $p>0.05$. D) Bar graphs showing the average slow exchange rates of GFP-H3.3 in cells expressing detectable levels of WT, d26, or dATPase RFP-BNRF1, or free RFP, relative to cells expressing undetectable levels on the same coverslip. Error bars, SEM; * $p < 0.05$; ** $p < 0.01$; *n.s.,* $p>0.05$.

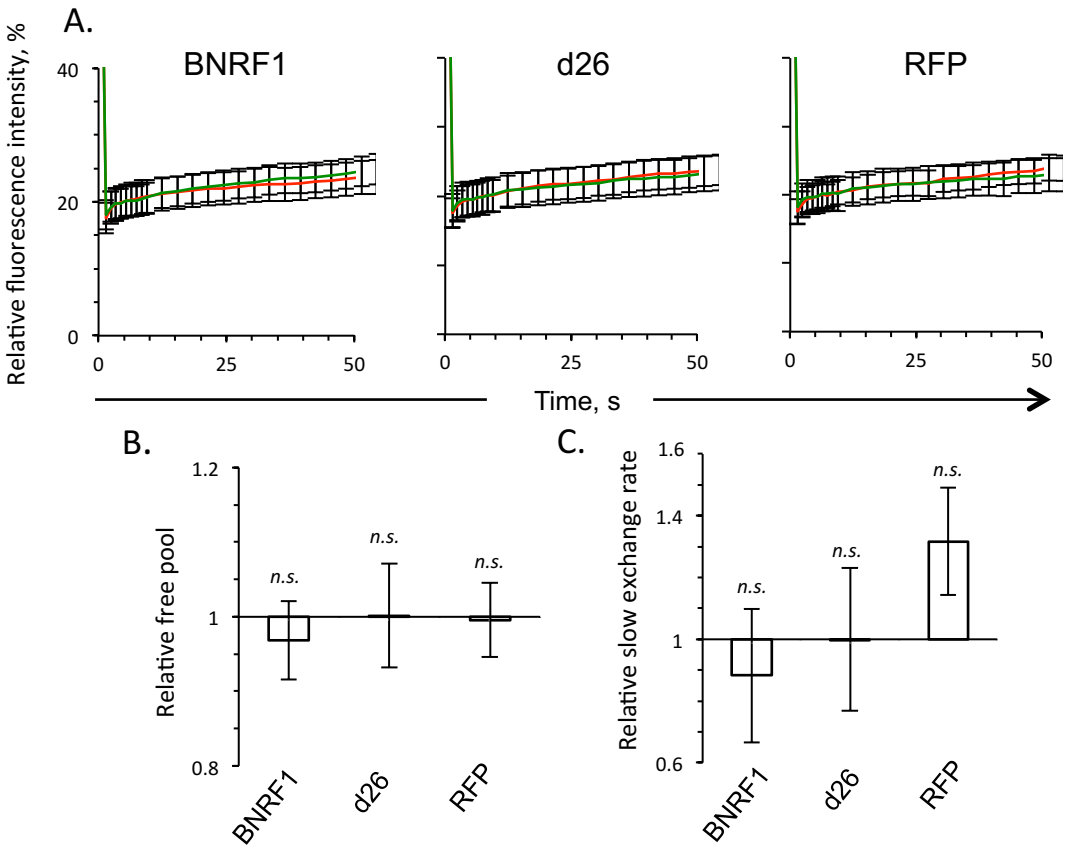

Figure A1.2. Neither WT nor d26 BNRF1 enhance the dynamics of H2B A. Average fluorescence recovery curves of histone H2B in cells expressing detectable or undetectable levels of RFP-BNRF1, RFP-d26, or free RFP. Error bars, SEM. Red lines, cells expressing detectable levels of RFP-BNRF1, RFP-d26, or free RFP. Green lines, cells expressing undetectable levels of RFP-BNRF1, RFP-d26, or free RFP. B) Bar graphs showing the average free pools of GFP-H2B in cells expressing detectable levels of RFP-BNRF1, RFP-d26, or free RFP, relative to the levels in cells expressing undetectable levels on the same coverslip. Error bars, SEM; *n.s.*, p>0.05. C) Bar graphs showing the average slow exchange rate of H2B in cells expressing detectable levels of RFP-BNRF1, RFP-d26, or free RFP, relative to cells expressing undetectable levels on the same coverslip. Error bars, SEM; *n.s.*, p>0.05.

A1.4 References

1. Bell P, Lieberman PM, Maul GG. Lytic but not latent replication of epstein-barr virus is associated with PML and induces sequential release of nuclear domain 10 proteins. J Virol. 2000;74:11800-11810.
2. Ishov AM, Sotnikov AG, Negorev D et al. PML is critical for ND10 formation and recruits the PML-interacting protein daxx to this nuclear structure when modified by SUMO-1. J Cell Biol. 1999;147:221-234.
3. Ishov AM, Vladimirova OV, Maul GG. Heterochromatin and ND10 are cell-cycle regulated and phosphorylation-dependent alternate nuclear sites of the transcription repressor Daxx and SWI/SNF protein ATRX. J Cell Sci. 2004;117:3807-3820.
4. Xue Y, Gibbons R, Yan Z et al. The ATRX syndrome protein forms a chromatin-remodeling complex with Daxx and localizes in promyelocytic leukemia nuclear bodies. Proc Natl Acad Sci U S A. 2003;100:10635-10640.
5. Lewis PW, Elsaesser SJ, Noh KM, Stadler SC, Allis CD. Daxx is an H3.3-specific histone chaperone and cooperates with ATRX in replication-independent chromatin assembly at telomeres. Proc Natl Acad Sci U S A. 2010;107:14075-14080.
6. Lukashchuk V, Everett RD. Regulation of ICP0-null mutant herpes simplex virus type 1 infection by ND10 components ATRX and hDaxx. J Virol. 2010;84:4026-4040.
7. Negorev DG, Vladimirova OV, Ivanov A, Rauscher F, Maul GG. Differential role of Sp100 isoforms in interferon-mediated repression of herpes simplex virus type 1 immediate-early protein expression. J Virol. 2006;80:8019-8029.
8. Woodhall DL, Groves IJ, Reeves MB, Wilkinson G, Sinclair JH. Human Daxx-mediated repression of human cytomegalovirus gene expression correlates with a repressive chromatin structure around the major immediate early promoter. J Biol Chem. 2006;281:37652-37660.
9. Glass M, Everett RD. Components of promyelocytic leukemia nuclear bodies (ND10) act cooperatively to repress herpesvirus infection. J Virol. 2013;87:2174-2185.
10. Chelbi-Alix MK, de Thé H. Herpes virus induced proteasome-dependent degradation of the nuclear bodies-associated PML and Sp100 proteins. Oncogene. 1999;18:935-941.
11. Cuchet-Lourenço D, Vanni E, Glass M, Orr A, Everett RD. Herpes simplex virus 1 ubiquitin ligase ICP0 interacts with PML isoform I and induces its SUMO-independent degradation. J Virol. 2012;86:11209-11222.
12. Perusina Lanfranca M, Mostafa HH, Davido DJ. Two overlapping regions within the N-terminal half of the herpes simplex virus 1 E3 ubiquitin ligase ICP0 facilitate the degradation and dissociation of PML and dissociation of Sp100 from ND10. J Virol. 2013;87:13287-13296.
13. Dyson PJ, Farrell PJ. Chromatin structure of Epstein-Barr virus. J Gen Virol. 1985;66:1931-1940.
14. Shaw JE, Levinger LF, Carter CW. Nucleosomal structure of Epstein-Barr virus DNA in transformed cell lines. J Virol. 1979;29:657-665.
15. Hebbes TR, Clayton AL, Thorne AW, Crane-Robinson C. Core histone

hyperacetylation co-maps with generalized DNase I sensitivity in the chicken beta-globin chromosomal domain. EMBO J. 1994;13:1823-1830.
16. Weintraub H, Groudine M. Chromosomal subunits in active genes have an altered conformation. Science. 1976;193:848-856.
17. Wensing B, Stühler A, Jenkins P, Hollyoake M, Karstegl CE, Farrell PJ. Variant chromatin structure of the oriP region of Epstein-Barr virus and regulation of EBER1 expression by upstream sequences and oriP. J Virol. 2001;75:6235-6241.
18. Berger SL. Histone modifications in transcriptional regulation. Curr Opin Genet Dev. 2002;12:142-148.
19. Alazard N, Gruffat H, Hiriart E, Sergeant A, Manet E. Differential Hyperacetylation of Histones H3 and H4 upon Promoter-Specific Recruitment of EBNA2 in Epstein-Barr Virus Chromatin. Journal of Virology. 2003;77:8166-8172.
20. Gerle B, Koroknai A, Fejer G et al. Acetylated histone H3 and H4 mark the upregulated LMP2A promoter of Epstein-Barr virus in lymphoid cells. J Virol. 2007;81:13242-13247.
21. Full F, Jungnickl D, Reuter N et al. Kaposi's Sarcoma Associated Herpesvirus Tegument Protein ORF75 Is Essential for Viral Lytic Replication and Plays a Critical Role in the Antagonization of ND10-Instituted Intrinsic Immunity. PLoS Pathog. 2014;10:e1003863.
22. Full F, Reuter N, Zielke K, Stamminger T, Ensser A. Herpesvirus saimiri antagonizes nuclear domain 10-instituted intrinsic immunity via an ORF3-mediated selective degradation of cellular protein Sp100. J Virol. 2012;86:3541-3553.
23. Feederle R, Neuhierl B, Baldwin G et al. Epstein-Barr virus BNRF1 protein allows efficient transfer from the endosomal compartment to the nucleus of primary B lymphocytes. J Virol. 2006;80:9435-9443.
24. Tsai K, Thikmyanova N, Wojcechowskyj JA, Delecluse HJ, Lieberman PM. EBV tegument protein BNRF1 disrupts DAXX-ATRX to activate viral early gene transcription. PLoS Pathog. 2011;7:e1002376.
25. Smith S, Stillman B. Stepwise assembly of chromatin during DNA replication in vitro. EMBO J. 1991;10:971-980.
26. Lorch Y, Maier-Davis B, Kornberg RD. Chromatin remodeling by nucleosome disassembly in vitro. Proc Natl Acad Sci U S A. 2006;103:3090-3093.
27. Lieberman PM. Chromatin Structure of Epstein-Barr Virus Latent Episomes. Curr Top Microbiol Immunol. 2015;390:71-102.
28. Tagami H, Ray-Gallet D, Almouzni G, Nakatani Y. Histone H3.1 and H3.3 complexes mediate nucleosome assembly pathways dependent or independent of DNA synthesis. Cell. 2004;116:51-61.
29. Drané P, Ouararhni K, Depaux A, Shuaib M, Hamiche A. The death-associated protein DAXX is a novel histone chaperone involved in the replication-independent deposition of H3.3. Genes Dev. 2010;24:1253-1265.
30. Goldberg AD, Banaszynski LA, Noh KM et al. Distinct factors control histone variant H3.3 localization at specific genomic regions. Cell. 2010;140:678-691.
31. Tsai K, Chan L, Gibeault R et al. Viral reprogramming of the Daxx histone H3.3

chaperone during early Epstein-Barr virus infection. J Virol. 2014;88:14350-14363.